AD-A169 928 DEVELOPMENT OF FINITE ACTIVE CONTROL ELEMENTS FOR LARGE FLEXIBLE SPACE ST.. (U) MASSACHUSETTS INST OF TECH CAMBRIDGE MA SPACE SYSTEMS LAB D W MILLER ET AL. 1/3

UNCLASSIFIED 02 JUN 85 MIT-SSL-6-85 AFOSR-TR-86-0480 F/G 20/11 NL

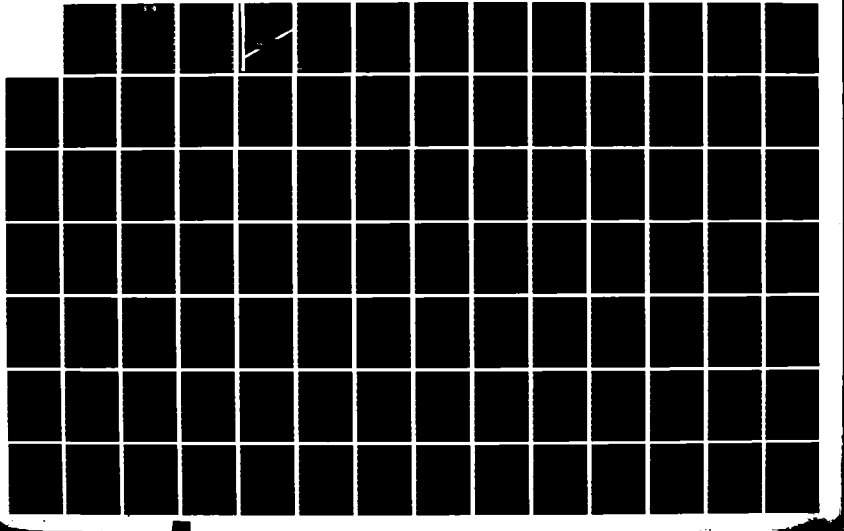

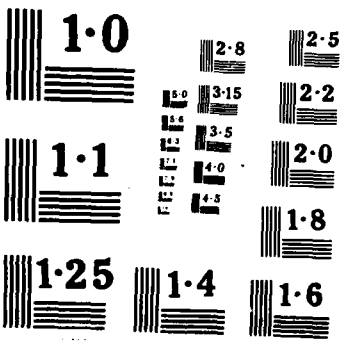
1·0
1·1
1·25
1·4
1·6
1·8
2·0
2·2
2·5
2·8
3·15
3·5
4·0
4·5
5·0

unclassified

SECURITY CLASSIFICATION OF THIS PAGE

REPORT DOCUMENTATION PAGE

1a. REPORT SECURITY CLASSIFICATION: unclassified	1b. RESTRICTIVE MARKINGS
2a. SECURITY CLASSIFICATION AUTHORITY	3. DISTRIBUTION/AVAILABILITY OF REPORT: unclassified/unlimited
2b. DECLASSIFICATION/DOWNGRADING SCHEDULE	
4. PERFORMING ORGANIZATION REPORT NUMBER(S): MIT-SSL #6-85	5. MONITORING ORGANIZATION REPORT NUMBER(S): AFOSR-TR- 86-0480
6a. NAME OF PERFORMING ORGANIZATION: Space Systems Lab., MIT Dept. Aero. and Astro. / 6b. OFFICE SYMBOL (If applicable)	7a. NAME OF MONITORING ORGANIZATION: AFOSR
6c. ADDRESS (City, State and ZIP Code): 37-361, MIT Cambridge, MA 02139	7b. ADDRESS (City, State and ZIP Code): Bolling AFB Washington, DC 20332-6448
8a. NAME OF FUNDING SPONSORING ORGANIZATION: AFOSR / 8b. OFFICE SYMBOL (If applicable)	9. PROCUREMENT INSTRUMENT IDENTIFICATION NUMBER: contract #F49620-83-K-0026
8c. ADDRESS (City, State and ZIP Code): Bolling AFB Washington, DC 20332-6448	PROGRAM ELEMENT NO.: 61102 F / PROJECT NO.: 2302 / TASK NO.: B1 / WORK UNIT NO.:
11. TITLE (Include Security Classification): (see reverse)	
12. PERSONAL AUTHOR(S): Miller, David Wesley Crawley, Edward Francis	
13a. TYPE OF REPORT: annual / 13b. TIME COVERED: FROM 83/3/15 TO 84/5/14	14. DATE OF REPORT (Yr., Mo., Day): 85/2/6 / 15. PAGE COUNT: 224
16. SUPPLEMENTARY NOTATION: DTIC FILE COPY	
17. COSATI CODES: FIELD / GROUP / SUB GR	18. SUBJECT TERMS (Continue on reverse if necessary and identify by block number): active control; distributed, hierarchic control; flexible space structures; distributed processing; active damping.

AD-A169 928

19. ABSTRACT (Continue on reverse if necessary and identify by block number)

Four main objectives were achieved through the research presented in this report. First, a quasi free-free beam, simulating a flexible space structure, was equipped with inertial proof-mass actuators and sensors capable, in principle, of functioning in the space environment, i.e., space-realizable. Secondly, tuning rules were derived which determine the optimal actuator passive stiffness and damping which minimizes the control effort required while increasing the modal damping in the structure. Thirdly, active control using two local and one component level processor was demonstrated. Lastly, multi-input, single output collocated feedback tests were performed.

Optimal passive vibration absorber designs were derived to provide maximum structural damping. Theoretically, the addition of an absorber mass equaling 0.5% of structural mass can result in a single mode structural damping ratio of 5%. Analysis of multimode damping using a single absorber indicated that the absorber stiffness should be tuned to the lowest mode in order to maximize the achievable damping in all the modes. (see reverse)

20. DISTRIBUTION AVAILABILITY OF ABSTRACT: UNCLASSIFIED/UNLIMITED ☒ SAME AS RPT ☐ DTIC USERS ☐	21. ABSTRACT SECURITY CLASSIFICATION: UNCLASSIFIED
22a. NAME OF RESPONSIBLE INDIVIDUAL: Dr. Anthony Amos	22b. TELEPHONE NUMBER (Include Area Code): 202-767-4937 / 22c. OFFICE SYMBOL: AFOSR/NA

DD FORM 1473, 83 APR EDITION OF 1 JAN 73 IS OBSOLETE

unclassified

SECURITY CLASSIFICATION OF THIS PAGE

11) Development of Finite Active Control Elements for Large Flexible Space Structures.

19) Passive actuator components and active feedback gains were derived simultaneously and sequentially yielding identical results whose passive components equal those of the passive vibration absorber.

Passive absorber and active feedback damping tests were performed. A single mode damping ratio of 4.2% was achieved by adding 2.3% of structural mass: 77% of which corresponds to 'dead' absorber mass. Multi-input, single-output control provided damping ratios ranging from 2% to 3%. This functioning collocated control element, composed of actuators, sensors and local and component level processors, constitutes the first stage of research and experimentation into distributed, hierarchic active control of elastic structural behavior.

DEVELOPMENT OF FINITE ACTIVE CONTROL ELEMENTS FOR LARGE FLEXIBLE SPACE STRUCTURES

David W. Miller

Edward F. Crawley

MIT-SSL #6-85

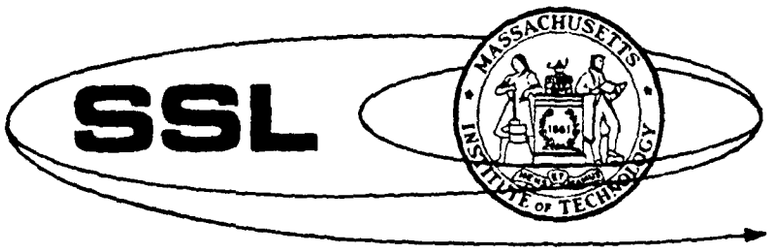

SPACE SYSTEMS LABORATORY
DEPT. OF AERONAUTICS AND ASTRONAUTICS
MASSACHUSETTS INSTITUTE OF TECHNOLOGY
CAMBRIDGE, MA 02139

DEVELOPMENT OF
FINITE ACTIVE CONTROL ELEMENTS FOR
LARGE FLEXIBLE SPACE STRUCTURES

David W. Miller

Edward F. Crawley

MIT-SSL #6-85

TABLE OF CONTENTS

Report Documentation Page . . . . . p. 1
Table of Contents . . . . . p. 3
List of Tables . . . . . p. 5
List of Figures . . . . . p. 7

1.0 Research Overview . . . . . p. 11

2.0 Design Optimization of Passive Vibration Absorbers and Inertial Actuators . . . . . p. 18

2.1 Tuning a Single DOF Passive Vibration Absorber to a Single DOF Structural Model . . p. 24

2.1.1 Steady State Design Criterion . . . . p. 25

2.1.2 Pole Placement Design Criterion . . . p. 34

2.1.3 Weighted Quadratic Cost Design Criterion . . . . . p. 38

2.2 Tuning a Single DOF Passive Vibration Absorber to a Two DOF Structural Model . . . p. 40

2.3 Single Structural DOF with a Single DOF Active Control Actuator . . . . . p. 50

2.4 Conclusions . . . . . p. 56

3.0 Control Processor Architecture . . . . . p. 58

3.1 Architecture for a Distributed Hierarchy of Control . . . . . p. 60

3.2 Compatible Hardware Design Options . . . . . p. 64

3.3 Present Processing Capability . . . . . p. 67

3.4 Second Generation Processing Network . . . . p. 69

4.0 Experimental Hardware and Software Design . . . . p. 71

4.1 Test Article . . . . . p. 71

4.2 Actuator Implementation . . . . . p. 73

4.3 Sensor Implementation . . . . . p. 77

4.4 Signal Processing Implementation . . . . . p. 79

5.0 Control Experiments . . . . . p. 87

5.1 Design Considerations for Experimental Phase . . . . . p. 88

5.2 Single Input, Single Output (SISO) Collocated Controller . . . . . p. 97

5.3 Multiple Input, Single Output (MISO) Controller . . . . . p. 98

5.4 Tests Using Passive Vibration Absorbers . . . p. 100

5.5 Damping Using Active Actuators and Vibration Absorbers . . . . . p. 106

6.0 Conclusions . . . . . p. 107

References . . . . . p. 111

A.0 Appendix A: Optimizing the Passive Parameters of Passive Vibration Absorbers and Active Control Actuators . . . . . p. 113

A.1 System Models . . . . . p. 114

A.2 Quadratic Cost Optimization of Parameters . . p. 119

A.3 Results and Evaluation . . . . . p. 124

A.4 Conclusion . . . . . p. 128

B.0 Appendix B: Information Transport in Structures . . . . . p. 129

B.1 Discretization of Local Elastic Behavior . . p. 132

B.2 Wave Propagation Model Formulation . . . . . p. 140

LIST OF TABLES

2.1 p. 145 Eigenvectors for Two DOF Model for a Mass Ratio of β = 0.02.
2.2 p. 145 Parameter Values for Tuning to the Low and High Mode of a Two Mode Structural Model.
2.3 p. 146 Eigenvectors and Frequencies for Different Absorber Frequency Ratios. (Three DOF Model).
2.4 p. 147 Actuator Design Cases Studied in Chapter 2 and Appendix A.

4.1 p. 148 Modal Characteristics of a Free-Free Beam.
4.2 p. 149 Force Actuator Specifications and Components.
4.3 p. 150 Sensor Specifications.
4.4 p. 150 Signal Processing Equipment Specifications.

5.1 p. 151 Open and Closed-Loop Characteristics of Controlled Modes
5.2 p. 151 Analytic Results for Optimally Tuned Vibration Absorber
5.3 p. 151 Experimental Vibration Absorber Results for Eighth Mode Using a Tip Absorber at Various Frequency Ratios.
5.4 p. 152 Summary of Experimental Vibration Absorber Results for Modes Tested.

A.1 p. 153 Parameter Optimization: Initial Conditions.
A.2 p. 153 Quadratic Cost Versus Frequency Ratio and Nondimensional Damper.
A.3 p. 153 Optimal Passive Parameters.
A.4 p. 154 "COARSE" Quadratic Cost Table. Cost Map, System 1p (Passive Vibration Absorber).
A.5 p. 154 "COARSE" Quadratic Cost Table. Cost Map, System 1a (Control Actuator).
A.6 p. 154 "COARSE" Quadratic Cost Table. Cost Map, System 20p (Passive Vibration Absorber).
A.7 p. 155 "COARSE" Quadratic Cost Table. Cost Map, System 20a (Control Actuator).
A.8 p. 155 "COARSE" Quadratic Cost Table. Cost Map, System 20p (Passive Vibration Absorber).
A.9 p. 155 "COARSE" Quadratic Cost Table. Cost Map, System 20a (Control Actuator).
A.10 p. 156 "COARSE" Quadratic Cost Table. Cost Map, System 20p (Passive Vibration Absorber).
A.11 p. 156 "COARSE" Quadratic Cost Table. Cost Map, System 20a (Control Actuator).
A.12 p. 156 "COARSE" Quadratic Cost Table. Cost Map, System 2Ip (Passive Vibration Absorber).
A.13 p. 157 "COARSE" Quadratic Cost Table. Cost Map, System 2Ia (Control Actuator).
A.14 p. 157 "FINE" Quadratic Cost Table. Cost Map, System 1p (Passive Vibration Absorber).
A.15 p. 157 "FINE" Quadratic Cost Table. Cost Map, System 1a (Control Actuator).

A.16 p. 158 "FINE" Quadratic Cost Table. Cost Map, System 20p (Passive Vibration Absorber).
A.17 p. 158 "FINE" Quadratic Cost Table. Cost Map, System 20a (Control Actuator).
A.18 p. 158 "FINE" Quadratic Cost Table. Cost Map, System 20p (Passive Vibration Absorber).
A.19 p. 159 "FINE" Quadratic Cost Table. Cost Map, System 20a (Control Actuator).
A.20 p. 159 "FINE" Quadratic Cost Table. Cost Map, System 20p (Passive Vibration Absorber).
A.21 p. 159 "FINE" Quadratic Cost Table. Cost Map, System 20a (Control Actuator).
A.22 p. 160 "FINE" Quadratic Cost Table. Cost Map, System 2Ip (Passive Vibration Absorber).
A.23 p. 160 "FINE" Quadratic Cost Table. Cost Map, System 2Ia (Control Actuator).

B.1 p. 161 Fourth Derivative Finite Difference Operators.

LIST OF FIGURES

2.1 p. 162 Inertial Dampers.
A. Passive Inertial Vibration Absorber.
B. Electromagnetic, Inertial-Reaction Actuator with Passive Components.

2.2 p. 163 Single Degree of Freedom Actuator Coupled to a Single Degree of Freedom Representation of a Structural Mode.

2.3 p. 164 Magnitude of Response (X/Δ_{ST}) Versus Nondimensional Frequency (ω/p_o) for a Typical Value of Mass and Frequency Ratio.

2.4 p. 165 Magnitude of Response (X/Δ_{ST}) Versus Nondimensional Frequency (ω/p_o) for the Optimal Choice of Frequency Ratio Given a Mass Ratio of 0.02.

2.5 p. 166 Nondimensional Natural Frequencies (γ) of the Two System Modes as a Function of Absorber Frequency Ratio (δ).

2.6 p. 167 Magnitude of Response (X/Δ_{ST}) Versus Nondimensional Frequency (ω/p_o) for the Optimal Choice of Frequency Ratio Given a Mass Ratio of 0.2 (Compare with Fig. 2.4).

2.7 p. 168 S-Plane Representation of the Poles of the Vibration Absorber as a Function of Increasing Damper Value.

2.8 p. 169 Comparison of Optimal Steady-State and Pole Placement Design Characteristics.
A. Peak Magnitude of Response (X/Δ_{ST}) Versus Nondimensional Frequency (ω/p_o).
B. Time Response to Initial Velocity.

2.9 p. 170 Single DOF Actuator Coupled to a Two DOF Structural Representation.

2.10 p. 171 Magnitude of Response (X/Δ_{ST}) Versus Nondimensional Frequency (ω/p_o) for an Absorber Tuned to the Lower Structural Mode (Curve 1) and Tuned to Both Modes (Curve 2).

2.11 p. 172 Magnitude of Response (X/Δ_{ST}) Versus Nondimensional Frequency (ω/p_o) for an Absorber Tuned to the Higher Structural Mode (Curve 1) and Somewhat Tuned to Both Modes (Curve 2).
A. Response of All System Modes.
B. Detail in the Vicinity of the Low Modal Frequency.
C. Detail in the Vicinity of the Higher Modal Frequency.

2.12 p. 174 Relative Modal Motions of Mass Elements for Different Structure/Absorber Frequency Ratios.

2.13 p. 175 Comparison of the Frequency Response of Several Options of Active, Passive and Active/Passive,

Simultaneous Design.
A. Passive Components
B. Active Components
2.14 p. 176 Root Locus Plot of the System Poles for Various Mass Ratios Obtained From the Different Optimal Formulations.
3.1 p. 177 Hierarchic Processing Network.
3.2 p. 178 Levels of Modeling and Information Feedback in a Distributed, Hierarchic Control Format.
3.3 p. 179 Options for the Selection of Bandwidths and Interactions of the Various Levels of Control.
A. Control Option Providing Extended Bandwidth in the Low Authority Controller.
B. Overlapping Low and High Authority Control.
3.4 p. 180 Single Bus Hardware Arrangement for Multiprocessor, Hierarchic Architecture.
3.5 p. 180 Multibus Hardware Arrangement for Multiprocessor, Hierarchic Architecture.
3.6 p. 181 Interrupt Flow Chart for Single Bus System.
3.7 p. 182 Interrupt Flow Chart for Multibus System.
3.8 p. 183 First Generation Processing Hardware.
3.9 p. 184 First Generation Control Software Flow Chart.
3.10 p. 185 Second Generation Processing System.
4.1 p. 186 Experimental Hardware Configuration.
4.2 p. 187 Swinging Parallelogram Beam Suspension.
4.3 p. 188 Electromagnetic, Inertial-Reaction Actuator Configurations.
A. Torque Configuration.
B. Force Configuration
C. Side View.
4.4 p. 189 Models of Actuator Configurations Coupled to a Single DOF Structural Representation.
A. Model of a Single DOF Torque Actuator Controlling a Single Rotational Mode of a Structure.
B. Model of a Single DOF Force Actuator Controlling a Single Translational Mode of a Structure.
4.5 p. 189 Block Diagram of a Digital Double Integrator.
A. Open-Loop Configuration.
B. Closed-Loop Configuration.
4.6 p. 190 Frequency Response of Stabilized Double Integrator.
4.7 p. 191 Block Diagram of Total Integration and Filtering System.
4.8 p. 192 Frequency Responses of Single and Double Integrating and Filtering Systems.
5.1 p. 193 Actuator Effectiveness as a Function of Position on the Beam as Indicated by:
A. The Sum of the Squares of the Controlled Mode Shapes.
B. The Product of the Squares of the Controlled Mode Shapes.
5.2 p. 194 Root Locus of the Two DOF Model when Rate Feedback is Used.

A. Purely Beam Rate Feedback with no Passive Damper ($\mu = 0$).
B. Beam Rate Feedback with the Passive Actuator Damper Included ($\mu > 0$).
C. Stabilization of Case B through Additional Actuator Rate Feedback.

5.3 p. 195 Experimental Instability Introduced by High Gain Beam Rate Feedback (See Fig. 5.2b).

5.4 p. 196 Experimental Transient Decay of Seventh Mode.
A. Open-Loop.
B. Closed-Loop.

5.5 p. 197 Experimental Transient Decay of Eighth Mode.
A. Open-Loop.
B. Closed-Loop.

5.6 p. 198 Experimental Transient Decay of Ninth Mode.
A. Open-Loop.
B. Closed-Loop.

5.7 p. 199 Experimental Transient Decay of Tenth Mode.
A. Open-Loop.
B. Closed-Loop.

5.8 p. 200 Experimental Transient Decay of Eleventh Mode.
A. Open-Loop.
B. Closed-Loop.

5.9 p. 201 Experimental Transient Decay of Twelfth Mode.
A. Open-Loop.
B. Closed-Loop.

5.10 p. 202 Experimental Transient Decay of Thirteenth Mode.
A. Open-Loop.
B. Closed-Loop.

5.11 p. 203 Experimental Transient Decay of Fourteenth Mode.
A. Open-Loop.
B. Closed-Loop.

5.12 p. 204 Experimental Forced Response Versus Sinusoidal Excitation for Open and Closed-Loop Controller.
A. Open-Loop.
B. Closed-Loop.

5.13 p. 205 Experimental Passive Tuning of Vibration Absorber to the Eighth Mode.
A. Actuator Frequency is 2.60 Hz.
B. Actuator Frequency is 3.31 Hz.
C. Actuator Frequency is 4.50 Hz.
D. Actuator Frequency is 5.68 Hz.
E. Actuator Frequency is 5.93 Hz.

5.14 p. 208 Experimental Passive Tuning to the Seventh Mode.

5.15 p. 208 Experimental Passive Tuning to the Ninth Mode.

5.16 p. 209 Experimental Forced Response Versus Sinusoidal Excitation for Untuned and Tuned Absorbers.
A. Open-Loop.
B. Closed-Loop.

5.17 p. 210 Comparison of Experimental Results and Theoretical Predictions.
A. Minimum Achieved Damper Settings Near Optimal Frequency Ratios.
B. Comparison of Experimental and Predicted

Damping Ratios.
5.18 p. 211 Optimal Damper Characteristics Versus Mass Ratio.
5.19 p. 212 Comparison of Damping Tests Performed on the Ninth Mode.
A. Free Decay.
B. Passively Tuned Decay.
C. Actively Controlled Decay.
D. Actively Controlled and Passively Tuned Decay.
A.1 p. 213 Damper Models.
A. Passive Absorber.
B. Actuator.
A.2 p. 214 Structural Representations Coupled to One DOF Absorber.
A. System 1 : One Mode Structure with Absorber.
B. System 20: Two Mode Structure with Absorber on Outer Mass.
C. System 21: Two Mode Structure with Absorber on Inner Mass.
A.3 p. 215 Closed-Loop Poles of System 1 Optimized for $Z_o = \{0\ 1\ 0\ 0\}^T$.
A.4 p. 216 Closed-Loop Poles of System 20 Optimized for $Z_o = \{0\ 1\ 0\ 1.62\ 0\ 0\}^T$.
A.5 p. 217 Closed-Loop Poles of System 20 Optimized for $Z_o = \{0\ -1.62\ 0\ 2.62\ 0\ 0\}^T$.
A.6 p. 218 Closed-Loop Poles of System 20 Optimized for $Z_o = \{0\ -0.618\ 0\ 2.62\ 0\ 0\}^T$.
A.7 p. 219 Closed-Loop Poles of System 21 Optimized for $Z_o = \{0\ -0.618\ 0\ 2.62\ 0\ 0\}^T$.
B.1 p. 220 Structural Discretization.
B.2 p. 221 Bandedness in Discrete Representations of Elastic Structures.
A. Bandedness in Fourth Derivative, Finite Difference Operators.
B. Comparison of Bandedness in Finite Difference Operators and Flexibility Influence Coefficients.
B.3 p. 222 A Finite Beam Element
B.4 p. 222 Stiffness Terms Derived Using a Flexibility Influence Coefficient Formulation.
B.5 p. 223 Bandedness in Finite Element Representation of Structural Stiffness as Illustrated by:
A. Adjacent Terms Corresponding to Unit Displacement.
B. Adjacent Terms Corresponding to Unit Rotation.
B.6 p. 224 Characteristic Wave Propagation Length Versus Damping.
B.7 p. 224 Ratio of Characteristic Length of Propagation and Structural Length Versus Damping in Structural Modes.

1.0 RESEARCH OVERVIEW

The long term goal of this research is to develop techniques by which the dynamic elastic behavior of large space structures can be effectively modified to meet mission specifications primarily through the incorporation of machine intelligence. By providing active structural control, through the means of widely distributed sensing and actuation, several beneficial characteristics can be attained. This report discusses these benefits and presents solutions to some of the problems encountered in practical implementation of structural control.

Numerous space structures may require some form of active control. The lack of structural stiffness and foundation promotes the occurance of large amplitude structural vibrations. Because of the lack of energy dissipation mechanisms prevalent on earth, these motions are detrimental to the performance of precision pointing equipment and maintenance of a micro-gravity environment. Malfunctioning of critical station-keeping and communication systems might also occur due to large and persistant vibration levels.

Active structural control is one possible solution to both reducing the magnitude of vibration levels and dissipating the associated energy (References 1,2 and 7). The sensors, processors and actuators comprise the closed-loop controller for the structure, or plant. This closed-loop controller would introduce a variable set of state-dependent forces into the dynamics of the

structure. The designer can tailor the dynamics of the plant through the proper selection and configuration of these control components.

The modifications of particular interest are those that are unattainable through passive techniques. Not only Hookean, but non-Hookean behavior can be induced in the structure. This allows the designer versatility in modifying the dynamics by techniques such as time-varying gains, dynamic compensations and noncollocated state feedback. In addition, structural response can be easily modified during construction, and in the event of mission redefinition or component failure. Futhermore, many actuators contain devices which are capable of dissipating energy in the space environment. While these benefits of active control warrant its further investigation, the implementation of a structural controller, capable of functioning in space, presents several unique problems that must be addressed.

One problem involves designing a space-realizable, closed-loop control system for experimental testing and later for orbital application. To be space-realizable, all control components must be capable of functioning in the space environment. In such a system, all sensing and actuation must be performed independent of the laboratory frame. For this reason, only inertial or relative motion actuators and sensors can be considered.

Modeling of large space structures presents a second difficulty. Their large and extremely flexible nature presents a couple of problems. First, generating Linear Quadratic Regulator

feedback controllers or dynamic state estimators requires an accurate model of the structure. Because the number of structural modes is potentially infinite, a very large order model would be required. This model, even if generated by one of the sophisticated techniques available today, will inaccurately represent the higher frequency modes. Since implicitly both output feedback and state estimation schemes require accurate models to insure predictable closed-loop response and explicitly state estimation schemes require accurate models to generate state information, these inaccurate structural representations will likely cause these feedback schemes to become unstable when implemented on the actual structure. For this reason an alternative approach to the modeling and control problem should be investigated.

Secondly, a large space structure may, depending on the geometric properties of the structure, have modes that are close in frequency. This can pose a problem in the rolloff region of the controller where the phase and gain margins become critical. In addition, such close frequency spacing can make accurate model generation and identification more difficult.

The goal of this research is to develop a control technique, which can be readily used for any structural design application, that relies on limited knowledge of basic structural behavior and incorporates space-realizable components. This would reduce the dependency on accurate high order models which are inherent to the application in question.

Schemes will be investigated which provide control robustness

(model insensitivity) as well as accurate low order modeling. Possible solutions to the actuation, sensing, modeling and processing speed problems will also be discussed. Actuators and sensors that operate on inertial elements are chosen to eliminate interaction with, or reference to, the laboratory (earth) frame.

The control methodology under consideration uses hierarchic control, through distributed processing, to perform low and high authority control. Simple distributed processing allows control algorithms to be processed simultaneously by several processors. This enables a higher net processing rate than use of a single equivalent processor, and in turn, allows increased controller bandwidth and therefore the control of higher frequency modes. By arrangement of the processors in a pyramidal, hierarchic command structure, additional benefits are derived. By using hierarchic control, different control tasks are logically distributed among the processors.

The logic behind this hierarchic control is to distribute the control function in a way so as to reflect the fundamental dynamic behavior of the structure. Three levels of processors are envisioned. These levels are refered to as the zero or local level, the one or component level and the two or global level processors. These three levels of processing parallel the three levels of detail in the modeling of the passive structure: the fundamental local material properties; the internal element behavior; and the global behavior of a Finite Element Structural model; respectively. The zero or local level processors carry out high speed, localized low authority (almost collocated) control

using a limited number of local sensors and a single actuator.

The one or component level controller uses the information and actuators associated with several adjacent, local level controllers to perform higher authority, noncollocated control on the disturbances of wavelength up to the length of the element. The increased length over which the actuators and sensors, under the control of the element processor, act allows improved observation and control of longer wavelength (lower frequency) modes. The term controlled element refers to a portion of the structure that is controlled by one component level processor and its associated local level processors.

The two or global level would perform three main tasks. First, it would act as the high authority controller for the lowest modes since these modes are of the longest wavelength, are the most likely to be excited and are usually most critical to mission objectives. Secondly, a global level processor for systems identification and a global processor for failure detection and control reconfiguration could be added at this level. A detailed discussion of a portion of the global level can be found in Reference 4. Note that these are the only processors that have the capability to observe and influence the structure along its entire length.

The size of the control task allocated to each level, i.e. the number of sensor signals it processes, is inversely proportional to each level's required control rate. The local or zero level controller processes a limited amount of local sensor information to generate a control command for an actuator

controlling short wavelength, high frequency waves. At higher levels, more noncollocated information is used to generate commands to more than one actuator, thus requiring longer processing delays and slower control rates. Since these higher levels control lower frequency waves, this represents an ideal marriage of processor task and controller level bandwidth. In this framework of hierarchic control, the development of the 'Finite Control Element' will be discussed.

The contents of this report detail the initial research into the experimental implementation of 'Finite Control Elements' and its application to low authority control. A discussion of the analytic formulation of the hierarchic approach can be found in Reference 14. The questions involved in the implementation of the Finite Control Element include: actuator selection; actuator design optimization; sensor selection; selection and integration of the zero and one level microprocessors; and determination of the level of achievable control.

Chapter 2 discusses design of an inertial actuator and a passive vibration absorber. Several Electromagnetic, Inertial-Reaction Actuator configurations are presented. Tuning laws are derived to determine actuator designs best suited for both passive damping and active control. In this chapter, actuator design options are investigated which provide effort-efficient active control.

Chapter 3 gives a more detailed explanation of the processing hierarchy and its implementation. The details of the data links between the first two levels of controllers and the microprocessor

configuration used in the experimental phase are discussed.

Chapter 4 discusses the design of the experimental test apparatus. The actuators and sensors are chosen so as to provide a space-realizable experiment (i.e. capable, in principle, of functioning in space). Test article design, actuator construction, sensor selection and signal processing development are discussed.

Chapter 5 encompasses the experiments that have been performed to date. First, some preliminary research is presented to illustrate the goals and direction of the laboratory investigation. Next, the results of several tests are compared to expected results to demonstrate the capabilities of the system. Finally, the limitations of the controller are discussed along with planned future improvements.

Appendix A presents actuator optimization and state feedback control law generation using weighted quadratic cost and Linear Quadratic Regulator formulations. This appendix approaches the same problem as is presented in Chapter 2; but from a control theory perspective.

Appendix B presents some of the initial research into the concept of Finite Control Elements. This appendix studies techniques through which fundamental structural behavior can be exploited in a control environment. Model generation for transverse motion is developed. Ways in which the computational burden and dependency on model accuracy can be reduced are used to set guidelines for the development of control algorithms, sensor selection, actuator selection and actuator placement.

2.0 DESIGN OPTIMIZATION OF PASSIVE VIBRATION ABSORBERS AND INERTIAL ACTUATORS

This chapter discusses design considerations for two devices intended to modify structural behavior. The first type uses passive mechanisms to dissipate vibrational energy. The second type employs active feedback to alter the characteristics of a particular structure. The passive device will be hereafter refered to as a passive vibration absorber. The device that operates in conjunction with active feedback is termed a control actuator. In the following sections, one device of each type is selected and analyzed with respect to its ability to modify structural response. For each of these two types, a device is selected which is capable of operating in the space environment: i.e. it is space-realizable. The ultimate goal of analyzing both a passive vibration absorber and active control actuator is to determine whether the corresponding concepts can be incorporated into one device, which would combine the attributes of each, and therefore could achieve structural damping performance exceeding that of either device taken separately.

Many types of control actuators are available for demonstration purposes in the laboratory. However, to demonstrate a space-realizable controller, the forces on the structure must be created without reacting against the laboratory frame of reference. In other words, the controller must, at least in concept, be functional in space. Several catagories of

space-realizable actuators are available. Expendable gas jet thrusters can be used to control elastic modes by accelerating expendable mass. Intrastructural actuators, such as piezoelectric crystals or hydraulic pistons, can generate control forces by pushing against adjacent parts of the structure. Captive mass actuators can influence a structure by reacting against nonexpendable mass or stored momentum. Captive mass actuators include inertial actuators and Control Moment Gyros. Inertial actuators operate on a principle of momentum exchange between masses and the structure. Examples of inertial actuators are pivoting, proof-mass actuators and momentum wheels. Control Moment Gyros (CMG's) react against stored angular momentum. Each of these actuators influences the plant in proportion to some commanded control signal.

Several types of space-realizable vibration absorbers can be used to passively dissipate structural energy. Viscoelastic coatings and distributed friction dampers can be used to dissipate vibrational energy directly as heat. Intrastructural dampers and lossy joints generate damping forces proportional to the relative velocity between adjacent elements of a structure. Captive mass, inertial vibration absorbers dissipate relative motion between the structure and a proof mass. Each of these devices can be used to modify the passive plant dynamics.

From amongst these various concepts for space-realizable control actuators and passive vibration absorbers, this chapter discusses the design of passive, inertial vibration absorbers and inertial control actuators. Because of the functional

similarities in their models, the possibility is created of incorporating both concepts into one device. An Electromagnetic, Inertial-Reaction Actuator is defined as a device that electromagnetically accelerates a captive mass, hereafter refered to as a proof mass. By creating an action on the proof-mass, an equal and opposite reaction is exerted on the structure. The Electromagnetic, Inertial-Reaction Actuators may also have a passive spring and damper. The passive, inertial vibration absorber also uses a captive mass to create a relative velocity across some damping mechanism located between the structure and the attached mass. Figure 2.1 illustrates the similarity between the models used for the analysis of the Electromagnetic, Inertial-Reaction actuator and passive, inertial vibration absorber. The difference between the two devices is that, while only collocated state information affects the behavior of the passive absorber, noncollocated state feedback can be used to drive the actuator's motor.

Both the actuator and absorber can be modelled as spring-mass-damper assemblies (Fig. 2.1). The mass element is the proof mass, which can represent either a translational mass or rotational inertia. The spring element is a centering spring which prevents the proof-mass from developing a bias displacement. The damper corresponds to an adjustable viscous damper and, in addition, represents the armature friction and other passive damping sources in the mechanism.

In the actuator model, the values of these passive parameters can be selected to help reduce the amount of control effort needed

to achieve a desired system performance. The presence of these passive components also enables the actuator to possess the characteristics of a passive vibration absorber.

In the case of the vibration absorber, the parameters may be chosen such that the structure is damped most effectively. Understanding the limiting cases helps clarify what is meant by effective. If the device in Figure 2.1a is attached to an undamped structure and the damper is removed, the assembly contains no damping. Alternately, if the damper is set infinitely strong, the proof mass is locked to the structure and again no damping is introduced into the structural mode. Since the structure is undamped in both limiting cases, there must exist, between the limiting cases, an optimal set of vibration absorber parameters which introduce the greatest degree of damping into the structure.

The principle question of interest in this chapter is as follows: is the design of the optimal passive, inertial vibration absorber identical to the design of the optimal passive components of an optimized Electromagnetic, Inertial-Reaction actuator design. If so, the classical vibration absorber analysis, presented in the next section, can be used to design the optimized, inertial reaction control actuator.

Section 2.1 discusses three design procedures in which an inertial vibration absorber, modeled in Figure 2.1a, is used to damp a single structural mode. These procedures differ in their definition of desired performance for the absorber/structure assembly. The absorber parameters are selected to achieve some

desired optimal performance in each of the three cases. This process of selecting passive absorber parameters will hereafter be refered to as tuning. The three resulting absorber designs are then compared and evaluated.

The first design procedure analyzes the use of a vibration absorber to alter the steady-state response of a single structural mode (Section 2.1.1). The optimal steady-state solution results in the passive vibration absorber design which minimizes the steady-state response of one structural mode subjected to a broad band disturbance. This absorber minimizes the maximum steady-state response of the structure, using a minimax criterion.

In the second design procedure, the optimal pole placement solution yields a set of absorber parameters which place the system poles as far left in the complex S-plane as possible (Section 2.1.2). By attaching a single degree of freedom (DOF) absorber to a structure modeled with one mode, the complete model results in a structural motion which exhibits two modes, each represented by a pair of complex conjugate S-plane poles. The objective is to choose absorber parameters which place these poles as far left in the S-plane as possible.

The third, or final design procedure for the passive inertial vibration absorber requires that a set of absorber parameters be determined such that a structural response to a specified initial condition minimizes the value of a particular quadratic cost function (Section 2.1.3). The cost function of interest is composed of weighted quadratic penalties on the response of various portions of the structure. For example, the penalty could

be placed primarily on a particular system mode, or all of the modes could be evenly penalized. Since energy is typically the quantity penalized, a cost function composed of the weighted sum of the squares of the state variables is used. This penalty function is integrated forward in time from some initial time and state vector to some arbitrary final time (usually infinity) to yield a total cost. The vibration absorber is then designed to minimize the value of this total cost.

Section 2.2 extends the steady-state, vibration absorber problem to that of an absorber attached to a structural model containing two modes. This is done to provide a means for extrapolating the absorber design rules of Section 2.1 to the design rules for an absorber that is to be used to damp a multiple degree of freedom structure.

Section 2.3 details the design procedure for the active, inertial-reaction control actuator. In this section, quadratic penalties on control effort are added to the quadratic cost function of state developed in Section 2.1.3, and a set of passive actuator parameters and active feedback gains are derived simultaneously. The passive portion of this simultaneous design analysis and the passive absorber of Section 2.1 are compared. If the passive vibration absorber design is similar to the passive portion of the active control actuator design, the optimal passive absorber can be used as the passive component of an optimal control actuator.

2.1 TUNING A SINGLE DOF PASSIVE VIBRATION ABSORBER TO A SINGLE DOF STRUCTURAL MODEL

This section develops design rules for selecting the parameters of a passive vibration absorber. Rules are developed for designing absorbers based on three design criteria: best steady-state; optimal pole placement; and minimum weighted quadratic cost performance. The three resulting designs are then compared.

Since a modal representation of a structure yields decoupled, ordinary differential equations expressed in generalized coordinates, a single mode was deamed the simplest model which can represent typical structural behavior. In each of the three analyses, the rules are developed for tuning the absorber model shown in Fig. 2.1a to a structural model containing a single structural mode. Figure 2.2 is the resulting model analyzed with a single DOF absorber and a single structural mode: where K_1 and M_1 are the modal stiffness and modal mass; respectively. Note that throughout this section, the possibility of introducing active feedback control through the electromagnetic force labled F_E is ignored. The passive absorber spring (K_2), damper (C) and mass (M_2) are the only parameters which may be varied. The rules for selecting these parameters are developed below.

2.1.1 STEADY-STATE DESIGN CRITERION

The first of the three design criteria for designing a passive vibration absorber is that of the optimal steady-state response. Under the optimal steady-state criterion, the optimal absorber parameters are those parameters which minimize the maximum response of the structure when it is subjected to a broad band disturbance. The choice of absorber parameters alters the transfer function of the system. This solution is often refered to as the 'Classical Tuned Spring-Mass-Damper Vibration Absorber.' This solution yields a set of passive absorber parameters which equate and minimize the structure's two peak resonant amplitudes. This procedure is detailed in Reference 12 and reviewed here for completeness. A closed form solution from a control point of view is presented in Reference 9.

The approach used in the classical 'Vibration Absorber' problem calls for modifying the transfer function which relates the disturbance on the structure (P in Fig. 2.2) to the response of the structure (X_1 in Fig. 2.2) through selection of the passive absorber parameters. Assuming a sinusoidal disturbance and motion, the transfer function from P to X_1 (Eq. 2.2) is obtained from the equations of motion

$$m_1\ddot{x}_1 + c\dot{x}_1 + (k_1+k_2)x_1 - c\dot{x}_2 - k_2x_2 = P \qquad (2.1a)$$

$$m_2\ddot{x}_2 + c\dot{x}_2 + k_2x_2 - c\dot{x}_1 - k_2x_1 = 0 \qquad (2.1b)$$

$$\left|\frac{X_1}{P}\right|^2 = (k_2-\omega^2 m_2)^2/\{[(k_2-\omega^2 m_1)(k_2-\omega^2 m_2)-\omega^2 m_2 k_2]^2+ \omega^2 c^2[k_1-\omega^2(m_1+m_2)]^2\} \quad (2.2)$$

The transfer function can be nondimensionalized as

$$\left|\frac{X_1}{\Delta_{ST}}\right|^2 = [4\mu^2\gamma^2+(\gamma^2-\sigma^2)^2]/\{[\beta\sigma^2\gamma^2-(\gamma^2-1)(\gamma^2-\delta^2)]^2+ 4\mu^2\gamma^2[\gamma^2(1+\beta)-1]^2\} \quad (2.3)$$

where the notation of Reference 12 has been used:

Δ_{ST}	$= P/k_1$	STRUCTURE'S STATIC DEFLECTION	(2.4a)
p_0	$= (k_1/m_1)^{1/2}$	DECOUPLED STRUCTURAL FREQUENCY	(2.4b)
p_a	$= (k_2/m_2)^{1/2}$	DECOUPLED ABSORBER FREQUENCY	(2.4c)
δ	$= p_a/p_0$	ABSORBER/STRUCTURE FREQUENCY RATIO	(2.4d)
γ	$= \omega/p_0$	NONDIMENSIONAL FOURIER FREQUENCY RATIO	(2.4e)
β	$= m_2/m_1$	ABSORBER/STRUCTURE MASS RATIO	(2.4f)
μ	$= c/(2m_2p_0)$	NONDIMENSIONAL DAMPING	(2.4g)
S	$= s/p_0$	NONDIMENSIONAL LAPLACE OPERATOR	(2.4h)

The characteristic equation for the poles of Eq. 2.3 is given by

$$s^4 + 2\mu(1+\beta)s^3 + (1+\delta^2(1+\beta))s^2 + 2\mu s + \delta^2 \quad . \quad (2.5)$$

where the two natural frequencies of the structure/absorber system

in the absence of a damper are

$$\gamma_1^2, \gamma_2^2 = \frac{1}{2}(\delta^2(1+\beta)+1) \mp \frac{1}{2}[(\delta^2(1+\beta)+1)^2 - 4\delta^2]^{1/2} \qquad (2.6)$$

Figure 2.3 shows the magnitude of the response X_1 to the disturbance P versus the disturbance frequency for the arbitrary case where the mass ratio (β) is 0.02 (i.e. the actuator is 2% of the structure's modal mass), the frequency ratio (δ) is 1.0 (i.e. the actuator in isolation has the same frequency as the structure in isolation) and the damper strength is as indicated.

There are three nondimensional absorber parameters in the design problem: β the mass ratio, δ the frequency ratio and μ the damper value. For now, it will be assumed that β is fixed and the other two parameters can be varied to achieve the best steady-state performance. Figure 2.3 includes several important features of a passive absorber system with a fixed mass ratio β. First, for any value of the frequency ratio δ there exist two frequencies, indicated by points S and T, where the response magnitude is independent of the passive damping in the system. Second, for this value of δ, there are two limiting cases of the transfer function: no damper ($\mu = 0$) and large damper ($\mu \to \infty$). If the damper is removed ($\mu = 0$), there are two unbounded resonant peaks in the transfer function at the frequencies given by the nondimensional frequency ratios γ_1 and γ_2 (Eq. 2.6). The corresponding transfer function for this undamped case is

$$\frac{X_1}{\Delta_{ST}} = \frac{\gamma^2 - \delta^2}{\beta\delta^2\gamma^2 - (\gamma^2-1)(\gamma^2-\delta^2)} \tag{2.7}$$

In the other limiting case, an infinitely strong damper ($\mu \to \infty$), there is a transfer function with one unbounded resonant peak

$$\left|\frac{X_1}{\Delta_{ST}}\right| = \left| \frac{1}{(1+\beta)\gamma^2 - 1} \right| \tag{2.8}$$

Since all choices of damper (μ) between the limiting cases yield a system with bounded response (Fig. 2.3), it is clear that the absorber components can be selected to yield a system with a minimum, maximum system response.

The criterion for optimal steady-state response of a system with a passive vibration absorber leads to a minimax solution (i.e. minimizing the maximum system response). The magnitudes of the transfer function, at the two resonances (Eq. 2.3), are equated and minimized. As an example, the curve labled $\mu = 0.1$ in Fig. 2.3 illustrates the situation where, for a given a mass ratio (β) of 0.02 and a frequency ratio δ of 1.0, system damping is maximized because resonant magnitude is minimized. However, if there is a free choice of the frequency ratio δ, further reductions in the peak resonant amplitude might be obtained. The procedure outlined below derives this minimax response based on free choice of μ and δ for a fixed β.

The first step of the procedure for maximizing the system damping is to adjust the spring of the passive damper (adjusting the frequency ratio δ) to equate the magnitudes of the transfer

function at points S and T (i.e. at the points common to all transfer functions). Once equated, damping is added through the adjustable viscous damper (μ) until the peak resonant response corresponds to the magnitude of the transfer function indicated by points S and T. At this magnitude, the maximum response is at a minimum and the minimax criterion is satisfied. The frequency ratio is adjusted first because the tuned damper value μ_{OPT} depends on the frequency ratio. The relation which determines frequencies which are common to the two transfer functions (denoted by γ_S and γ_T) can be found by equating the transfer functions for the limiting cases of $\mu = 0$ and $\mu \to \infty$ (Eqs. 2.7 and 2.8),

$$\gamma^4 - 2\left[\frac{1 + \delta^2(1+\beta)}{2 + \beta}\right]\gamma^2 + \frac{2\delta^2}{2 + \beta} = 0 \qquad (2.9)$$

This relationship can be solved for γ_S and γ_T. Then, the objective is to find the frequency ratio (δ) which makes the magnitudes of the transfer function at the frequencies γ_S and γ_T, equal. By evaluating Eq. 2.8, at γ_S and γ_T, and equating, we get

$$\gamma_S^2 + \gamma_T^2 = \frac{2}{1 + \beta} \qquad (2.10a)$$

where the magnitudes are related by

$$\left.\frac{X_1}{\Delta_{ST}}\right|_S = -\left.\frac{X_1}{\Delta_{ST}}\right|_T \qquad (2.10b)$$

Since the solution of Eq. 2.9 is of the form

$$\gamma^4 - (\gamma_S^2 + \gamma_T^2)\gamma^2 + \gamma_S^2\gamma_T^2 = 0 \tag{2.11}$$

equating the γ^2 coefficient in Eq. 2.9 to the right hand side of Eq. 2.10a gives

$$\frac{2}{1+\beta} = \frac{2}{2+\beta}(1 + \delta^2(1+\beta)) \tag{2.12}$$

which can be reduced to yield the expression for the optimal actuator-to-modal frequency ratio (δ_{OPT}),

$$\delta_{OPT} = \frac{1}{1+\beta} \tag{2.13}$$

The frequencies associated with points S and T are found by placing Eq. 2.13 into Eq. 2.9 to get

$$\gamma_{S,T}^2 = \frac{1}{1+\beta}\left[1 \mp \sqrt{\frac{\beta}{2+\beta}}\right] \tag{2.14}$$

The magnitude of the transfer function associated with points S and T is found from Eq. 2.8 as

$$\left|\frac{X_1}{\Delta_{ST}}\right|_{S,T} = \left|\sqrt{\frac{2+\beta}{\beta}}\right| \tag{2.15}$$

This gives the minimum, maximum magnitudes of the transfer function using a passively tuned vibration absorber for a fixed

mass ratio β. As an example, for a system with a mass ratio of β = 0.02, the optimal frequency ratio δ, from Eq. 2.13, is 0.98. The plot of magnitude of response versus frequency for this system is shown in Fig. 2.4.

Now that the optimal frequency ratio has been found, the optimal value for the nondimensionalized damping (μ) is found by solving Eq. 2.3 for μ^2 and substituting for δ from Eq. 2.13, γ_S and γ_T from Eq. 2.14 and using X_1/Δ_{ST} from Eq. 2.15. This gives an expres in the general form

$$\mu^2_{OPT} = \frac{N - Q(\ X_1/\Delta_{ST}\ )^2}{P(\ X_1/\Delta_{ST}\ )^2 - M} \tag{2.16a}$$

where

$$M = \frac{4\left[\ 1 + \sqrt{\frac{\beta}{2+\beta}}\ \right]}{1+\beta} \tag{2.16b}$$

$$N = \left[\frac{\beta + (1+\beta)\sqrt{\frac{\beta}{2+\beta}}}{(1+\beta)^2}\right]^2 \tag{2.16c}$$

$$P = \frac{4\beta\left[1 + \sqrt{\frac{\beta}{2+\beta}}\ \right]}{(1+\beta)^2(2+\beta)} \tag{2.16d}$$

$$Q = \left[\frac{\beta\left[(2+\beta)\sqrt{\frac{\beta}{2+\beta}} + 1 + \beta\right]}{(1+\beta)^2(2+\beta)}\right]^2 \tag{2.16e}$$

which is indeterminant because both the numerator and denominator vanish at both γ_S and γ_T. Therefore, the optimal nondimensional damper value is found by taking the limit as the frequency approaches either γ_S or γ_T. An approximate optimal value of μ can actually be found by considering a value of γ_S or γ_T slightly shifted from the value given in Eq. 2.14. For the example of a mass ratio $\beta = 0.02$, the optimal frequency ratio is found from Eq. 2.13 as $\delta = 0.98$ and the optimal nondimensionalized damping is found from Eq. 2.16a as $\mu = 0.086$. The corresponding response of the structural mass is shown, in Fig. 2.4, by the curve labled with this optimal value of μ. This curve represents the optimal steady-state response, based on the criterion of minimizing the maximum value of the transfer function.

Figure 2.5 and Table 2.1 give some insight into this tuning scheme. Figure 2.5 is a plot of the natural modal frequencies of the system versus the frequency ratio (δ) for a mass ratio of $\beta = 0.02$. The vertical line is located at the optimal frequency ratio (δ_{OPT}), as calculated from Eq. 2.13. As seen in the figure, the optimal solution is that frequency ratio (δ) that places the natural modal frequencies as close together as possible. This allows the greatest absorber/structure interaction and maximized motion across the passive damper.

Table 2.1 lists eigenvectors which show the motion of the two masses for several values of frequency ratio (δ). For high values of δ (10.00), relative motion (the difference between the motions of the masses) is almost zero in the low mode. For low values of

δ (0.10), relative motion in the high mode is reduced. Note that all values of δ yield some relative motion and corresponding damping in the high mode. Since overall damper effectiveness is maximized by maximizing the relative motion between the two masses on average in all modes, the best choice is if the absorber frequency is made close to but lower than the decoupled structure's modal frequency. In this way the relative motion across the damper in the two modes is approximately equal.

Thus far an algorithm has been determined for finding the optimal frequency ratio (δ) and optimal nondimensional damper (μ) given a fixed mass ratio. No criterion has been set for determining the best mass ratio (β). As seen in Figure 2.4, the minimum achievable value of the maximum amplitude is set by the frequency separation, subject to the constraint that the magnitudes at points S and T be equal. By comparing the maximum response for larger mass ratios (β = 0.2 in Fig. 2.6) with that for the smaller mass ratios (β = 0.02 in Fig. 2.4) it is clear that a larger mass ratio is advantageous. Eq. 2.15 gives the relationship between mass ratio and minimum, maximum magnitude of the transfer function. While steady-state response improves with larger mass ratios, overall system mass also increases. If an optimal mass ratio (β) is desired, the choice of β must be determined through a systems analysis involving a tradeoff between total system mass and damper performance.

2.1.2 POLE PLACEMENT DESIGN CRITERION

A different insight into the effectiveness of a passive vibration absorber can be gained by examining the location of the poles in the S-plane of the one DOF structure plus absorber system. This S-plane interpretation gives a better understanding of the transient characteristics. As previously stated, the optimal pole placement design usually calls for placing the poles as far to the left as possible in the S-plane, thereby decreasing the system response time.

Figure 2.7 shows the upper half of the S-plane representation of the poles of this one DOF structure plus absorber system, plotted for the case of optimal frequency ratio (δ_{OPT}) (derived from Eq. 2.13) as the value of nondimensional damping μ is increased. As the damper strength increases the system poles move to the left, pass through the poles corresponding to μ_{OPT}, approach, meet (equal damping ratios) and split. Point A corresponds to the value of μ which yields the case where the poles are the farthest left. This value of μ is designated μ_{OPT-PP} for optimal pole placement damping.

The optimal damping value (μ_{OPT-PP}) for the pole placement design can be derived. By manipulating the characteristic equation (Eq. 2.5), the S-plane coordinates and nondimensional damping of the optimal pole placement solution can be determined. At point A of Fig. 2.7, the roots of Eq. 2.5 must be double pairs of complex conjugate poles. Substituting the optimal frequency ratio (δ_{OPT}) from Eq. 2.13 into Eq. 2.5, and equating the pairs of

roots, four equations arise from equating coefficients

$$2\mu(1 + \beta) = -4a \tag{2.17a}$$

$$\frac{2 + \beta}{1 + \beta} = 6a^2 + 2b^2 \tag{2.17b}$$

$$2\mu = -4a(a^2 + b^2) \tag{2.17c}$$

$$\frac{1}{1 + \beta} = a^2 + b^2 \tag{2.17d}$$

where the S-plane pole locations are $S = a \pm bi$. Since 2.17c and 2.17d can be combined to form 2.17a, there are three independent equations with which to solve for the real part (a), the imaginary part (b) of the pole location and the nondimensional damping (μ) in terms of the mass ratio (β). Solving Eqs. 2.17 yields

$$\mu^2_{OPT\text{-}PP} = \frac{\beta}{(1 + \beta)^3} \tag{2.18a}$$

$$a\Big|_A = -0.5\sqrt{\frac{\beta}{1 + \beta}} = Re(S) \tag{2.18b}$$

$$b\Big|_A = \pm 0.5\sqrt{\frac{4 - \beta}{1 + \beta}} = Im(S) \tag{2.18c}$$

For the same example computed in the last section, that of a mass ratio of 0.02, the optimal value of the nondimensional damper is

$\mu_{OPT-PP} = 0.137$.

In this derivation of μ_{OPT-PP}, we have assumed that Eq. 2.13 provides the optimal value of δ even though it was defined based on the steady-state criterion. The rationale for this choice of $\delta = \delta_{OPT}$ is that this is the exact value of the frequency ratio which causes the two branches of the root locus (Fig. 2.7) to exactly converge at point A. Therefore, the damping of each of the two poles will be identical, and maximized.

As in the steady-state design procedure, guidance is available in choosing δ and μ, but not the mass ratio β. Again it is clear that a larger mass ratio gives a more damped system (contrast Eqs. 2.18b and 2.15), and so again, a systems analysis must be performed to determine the optimal mass ratio.

It is now instructive to compare the steady-state responses and transient responses of the two optimal damper cases. Figure 2.8a compares the steady-state responses of the optimal steady-state (μ_{OPT}) and pole placement (μ_{OPT-PP}) designs for a mass ratio of $\beta = 0.02$. Note that, as would be expected, the optimal steady-state design exhibits better steady-state behavior. This is because the peak responses of the two modes in the optimal pole placement design overlay. Figure 2.8b shows the transient responses of these two solutions. The steady-state solution also exhibits slightly better transient behavior due to the destructive interference of the two modes, which appears as a beating. Though the two design procedures result in similar vibration absorber parameters, and the two solutions exhibit very similar behavior, the performance of the steady-state design is slightly preferable.

Thus far, tuning rules have been developed for the first two cases of vibration absorber optimization. For the steady-state case, the following steps are followed:

1. Choose the mass ratio (β) through a tradeoff between mass and performance, as dictated by Eq. 2.15.
2. Determine the frequency ratio (δ_{OPT}) using Eq. 2.13.
3. Determine nondimensional damping (μ_{OPT}) through Eq. 2.16.

For the pole placement case, the following steps are followed:

1. The value of the mass ratio (β) is determined through a tradeoff between mass and performance, as dictated by Eq. 2.18b.
2. The frequency ratio (δ_{OPT}) is determined by Eq. 2.13.
3. The nondimensional damping (μ_{OPT-PP}) is found through Eq. 2.18a.

2.1.3 WEIGHTED QUADRATIC COST DESIGN CRITERION

A third possible design criterion involves selecting absorber parameters which cause the system response to minimize a weighted quadratic cost function of the states. The first section of Appendix A details this analysis, which yields the set of optimal spring and damper parameters, again for a predetermined absorber-to-structure mass ratio. The resulting set of optimal absorber parameters closely matches those derived by the previous two criteria. Thus all three cases, though approaching the absorber tuning problem from three distinct definitions of optimal performance, result in similar absorber designs. In fact, considering the accuracy to which the absorber parameters can be physically adjusted, these three solutions might be considered identical.

Up to this point, the interaction of the passive vibration absorber has been studied with a plant with only a single degree of freedom. Yet realistic structures have higher order dynamics. Therefore, the next step is to derive tuning rules for selecting absorber parameters which best introduce damping into higher order structural models. Due to the similarity between the three design cases presented in damping the single degree of freedom structure, only the steady-state design solution will be extended in Section 2.2 to the damping of multiple DOF structures. By introducing and tuning a vibration absorber to a structural model containing two modes, rules can be derived which allow the extrapolation of the solution derived in this section to the passive damping of higher

order structural models.

2.2 TUNING A SINGLE DOF PASSIVE VIBRATION ABSORBER TO A TWO DOF STRUCTURAL MODEL

The two degree of freedom (DOF) system, analyzed in the previous section, represents the simplest model describing the interaction between a vibration absorber and a structure. A more accurate structural model would include many modes, but this model could not be dealt with as completely as the low order model. The simplest model which includes an absorber and more than one structural mode is a three DOF model in which the structure is represented by two modes, or masses, and the absorber by one. This section studies tuning of a vibration absorber in a three DOF model. With this information, the tuning rules for achieving maximum system damping can be extrapolated to higher order, more realistic structural models.

As shown in Figure 2.9, the two mode structure has been modeled using two lumped masses (M_o) and two interconnecting springs (K_o). In this section, two approaches will be taken in devising tuning rules for this system. In the first approach, the selection of the absorber spring (K_3) will be set based upon the structure's lower modal mass in a fashion similar to that which resulted in Eq. 2.13. Then, the damper (C) will be adjusted to determine its effect on both the lower and the higher structural modes. Secondly, the absorber will be tuned to the higher mode and the same process repeated to determine the effect of the damper on both modes. These two analyses will be compared and the

best approach determined. Again, the control force (F_E) is ignored and the analysis is performed assuming a fixed absorber/structure mass ratio.

The procedure presented here is similar to that followed in section 2.1.1 for steady-state optimization. Again, sinusoidal disturbances and motion are assumed. Nondimensionalizing the equations of motion

$$m_o\ddot{x}_1 + 2k_o x_1 - k_o x_2 = 0 \tag{2.19a}$$

$$m_o\ddot{x}_2 + c\dot{x}_3 + (k_o + k_3)x_2 - k_o x_1 - c\dot{x}_3 - k_3 x_3 = P \tag{2.19b}$$

$$m_3\ddot{x}_3 + c\dot{x}_3 - c\dot{x}_2 + k_3 x_3 - k_3 x_2 = 0 \tag{2.19c}$$

results in the transfer function relating the disturbance on the second structural mass (P) to the motion of that mass (Fig. 2.9)

$$\left|\frac{X_2}{\Delta_{ST}}\right| = 0.25(\gamma^2-2)^2[(\gamma^2-\delta^2)^2+4\gamma^2\mu^2] \;/\; \{[\delta^2- -\gamma^2(1+\delta^2(3+2\beta))+\gamma^4(3+\delta^2(1+\beta))-\gamma^6]^2+ 4\gamma^2\mu^2[1-\gamma^2(3+2\beta)+\gamma^4(1+\beta)]^2\} \tag{2.20}$$

where

$$\Delta_{ST} = 2P/k_o \quad \text{STRUCTURE'S STATIC DEFLECTION} \tag{2.21a}$$

$$p_o = (k_o/m_o)^{1/2} \quad \text{CHARACTERISTIC STRUCTURAL FREQUENCY} \tag{2.21b}$$

$p_3 = (k_3/m_3)$	DECOUPLED ABSORBER FREQUENCY		(2.21c)
$\delta = p_3/p_o$	ABSORBER/STRUCTURE FREQUENCY RATIO		(2.21d)
$\gamma = \omega/p_o$	NONDIMENSIONAL FOURIER FREQUENCY RATIO		(2.21e)
$\beta = m_3/m_o$	ABSORBER/STRUCTURE MASS RATIO		(2.21f)
$\mu = c/(2m_3p_o)$	NONDIMENSIONAL DAMPING		(2.21g)
$z = x/\Delta_{ST}$	NONDIMENSIONAL DISPLACEMENT		(2.21h)

The choice of having the force (P) act on the second mass is arbitrary since its location only affects the zeros of the system. The system poles which most directly affect resonant amplitudes are solely a function of the homogeneous dynamics.

The following analysis assumes that if the 'absorber mode' (i.e. that mode which exhibits most of the absorber motion) is placed near, in frequency, to a structural mode, the interaction between these two modes in the vicinity of their resonances can be treated similarly to the two DOF analysis previously presented. If this assumption is correct, the relations previously presented can be readily applied to this three DOF system. Therefore, the tuning rules developed for a single structural mass will be applied to the structural model with two degrees of freedom and the resulting response of the full three degree of freedom (DOF) system will be evaluated. If these rules provide an optimal steady-state solution for the three DOF model, using the minimax criterion, then it will be assumed that they can be used to design passive absorbers for higher order structural systems.

In the two DOF problem, the passive absorber components were tuned to the inner mass (M_1 in Fig. 2.2) using Eqs. 2.13 and 2.16. For the three DOF case, the absorber will be tuned to the modal mass, first of the lower and then of the higher structural mode.

The first step is to determine the modal characteristics of the structural system when the absorber is removed or absent. Eliminating the absorber parameters from Eqs. 2.19b and 2.19c gives the nondimensional equations of motion for the two DOF structural model as

$$\begin{bmatrix} 1 & 0 \\ 0 & 1 \end{bmatrix} \begin{Bmatrix} \ddot{z}_1 \\ \ddot{z}_2 \end{Bmatrix} + p_o^2 \begin{bmatrix} 2 & -1 \\ -1 & 1 \end{bmatrix} \begin{Bmatrix} z_1 \\ z_2 \end{Bmatrix} = \begin{Bmatrix} 0 \\ 0.5 \end{Bmatrix} p_o^2 \qquad (2.22)$$

The corresponding eigenvectors and frequencies are

$$\Psi_1^T = \begin{bmatrix} 1 & \dfrac{1}{1-\gamma_1^2} \end{bmatrix} = [1 \quad 1.618] \qquad \gamma_1 = 0.618 \qquad (2.23a)$$

$$\Psi_2^T = \begin{bmatrix} 1 & \dfrac{1}{1-\gamma_2^2} \end{bmatrix} = [1 \quad -0.618] \qquad \gamma_2 = 1.618 \qquad (2.23b)$$

The modal masses, as perceived from the actuator attachment point, are found by normalizing Eqs. 2.23a and 2.23b to achieve a displacement of unity for the outer mass. By assembling the eigenvector matrix and performing the following operation, the modal masses are

$$\left[\backslash M \backslash\right] = [\Psi_1 : \Psi_2]^T \left[\backslash m \backslash\right] [\Psi_1 : \Psi_2] \equiv \begin{bmatrix} \beta_1 & 0 \\ 0 & \beta_2 \end{bmatrix} = \begin{bmatrix} \dfrac{M_1}{m_o} & 0 \\ 0 & \dfrac{M_2}{m_o} \end{bmatrix}$$

$$= \begin{bmatrix} 1.382 & 0 \\ 0 & 3.618 \end{bmatrix} \tag{2.24}$$

where β_n is the ratio of modal mass to the reference mass (M_o).

Now that the modal frequencies and masses have been determined, the tuning rules developed in Section 2.1.1 can be applied. At this point, it is convenient to define two new variables: the ratio of actuator-to-modal frequency (δ_{*n}) and the ratio of actuator-to-modal mass (β_{*n}); as

$$\delta_{*n} = p_a/\gamma_n \tag{2.25a}$$

$$\beta_{*n} = m_3/M_n = \beta/\beta_n \tag{2.25b}$$

Note that three mass ratios have been defined. As in Section 2.1, β is defined as the ratio of absorber mass to the mass of one structural element shown in Figure 2.9 (i.e. $\beta = M_3/M_o$). β_n, defined in Equation 2.24, represents the ratio between the modal masses of the two degree of freedom structure and the mass of a structural element (M_o). The third mass ratio β_{*n} is the indexed ratio of absorber mass to the modal mass of the structure (Eq. 2.25b). The same variable suffixes have been used for the frequency ratios.

In the selection of the optimal absorber parameters these ratios, with respect to the modal frequency and mass (δ_{*n} and β_{*n}), will be used in lieu of the ratios to the physical frequency and mass used in Section 2.1. As in the two DOF analysis, let the optimal δ_{*n} be defined with respect to the modal mass ratio

$$\delta_{*n_{OPT}} = \frac{1}{1 + \beta_{*n}} \tag{2.26}$$

Then, the optimal value of the frequency ratio (δ), defined in Eq. 2.21d, is related to $\delta_{*n_{OPT}}$ by

$$\delta_{OPT} = \frac{p_a}{p_o} = \frac{p_a}{p_n}\frac{p_n}{p_o} = \delta_{*n_{OPT}}\gamma_n \tag{2.27}$$

As a numerical example, assume that the mass ratio $\beta_{*n} = 0.02$ for both the low and high modes. This can not be the case if the same absorber mass is used, but this assumption makes this problem similar to the numerical cases presented in Section 2.1. Table 2.2 lists the values for the various nondimensional parameters used in this example. The first column corresponds to the tuning of the actuator to the low frequency structural mode, and the second column corresponds to the higher mode. The next step is to verify that the absorber parameters derived by application of these rules achieve a nearly optimal steady-state response for the full three DOF system.

Recall the absorber frequency can be tuned to either the frequency of the lower or the higher structural mode. Up to this point the rule for deriving the optimal damper value has not been extended to the case of the multiple DOF structural model (Figure 2.9). Fig. 2.10 illustrates the frequency transfer function, or the response to broad band disturbance, of the three DOF system

when the absorber frequency is tuned to the frequency of the lower structural mode according to Equation 2.26. Two curves are shown in Figure 2.10. For Curve 1, the damper has been set to optimally damp the lower mode, using the rule for optimal damper selection given by Eq. 2.16 in Section 2.1.1. This damper value equates the amplitude of the actuator and structural response of the lower mode. This validates the assumption that the tuning law for a one DOF structure governing absorber frequency and damping can be applied to this two DOF structure, provided reasonable separation in structural frequencies exists. However, further examination of Curve 1 of Fig. 2.10 reveals that while the two resonant peaks in the vicinity of the lower mode have been equalized, the peak of the higher frequency structural mode is four times greater in magnitude. Since the addition of more damping will decrease the response of this higher mode, the generalized minimax criterion has not yet been satisfied.

Curve 2 in Fig. 2.10 shows the transfer function for the system with approximately three times more damper strength than that given in Curve 1. Notice that the maximum response of the upper mode has decreased at the cost of increasing the response of the lower mode. However, the minimax criterion has been satisfied in that any change in damper setting from this value will increase the maximum response. Thus, in order to achieve minimum system response, the damper value must be increased from the optimal two DOF value (Curve 1) to the value that equates all of the maximum response magnitudes (Curve 2). This passive absorber configuration gives the optimal steady-state solution for the

three DOF system, in the case in which the absorber has been tuned to the lower mode.

A similar analysis can be performed in which the objective is to tune the absorber to the higher structural mode using the frequency ratio derived from the simple two DOF approach. Curve 1 of Figure 2.11a, b and c shows the frequency response for the case in which the absorber damper has been optimally adjusted for the higher structural mode only. Note that while the high mode has a peak magnitude on the order of unity, the low mode peak magnitude exceeds 1000. Curve 2 shows the minimum low mode magnitude achievable through damper adjustment. The maximum amplitude of the low mode has been reduced to about 500, at the cost of increasing the maximum response of the high mode to 15. The significant result of this case is that no damper adjustment can be made which equates all of the peak magnitudes. Therefore, structural modes lower, in frequency, than the mode to which the absorber is tuned exhibit relatively small levels of damping. This result can be explained using the modal characteristics of the system.

An eigenvector argument, which is valid for small damping, can be used to illustrate the lack of damper effectiveness in modes lower in frequency than the mode to which the absorber is tuned. Figure 2.12 shows the directions of motion for the possible modes of the system. Table 2.3 lists eigenvectors for various frequency ratios (δ) with the motion of the absorber mass normalized to unity. Together, this figure and table illustrate how the absorber and structure interact.

Several important features can be seen in Fig. 2.12. The first column, containing models of two DOF, lumped mass systems, illustrates the relative directions of motion between the two masses for the two structural modes when the absorber has been removed. Columns 2 and 3 represent the three modes which exist with the absorber in place. The absorber in Column 2 is modeled with a frequency just below that of the lowest structural mode (a more flexible absorber) whereas column three shows the eigenvectors for the case where the absorber is tuned to the higher structural mode (a stiff absorber). Since the modal damping is dependent on the relative motion between the outer two masses, a flexible absorber guarentees significant damping in system modes 2 and 3 due to opposing motion between the outer two masses in these modes. The system response corresponding to a stiff absorber only exhibits opposing motion between the outer two masses in the highest mode. In fact, the stiffer the absorber (larger δ), the less the relative motion and damping in the lower two modes.

Table 2.3 verifies this argument. This table lists the modal frequencies and eigenvectors for various values of the frequency ratio δ. The eigenvector of Mass 3 corresponds to the absorber's motion. The lowest mode exhibits its largest relative motion for small values of frequency ratio (δ). As the frequency ratio is increased, relative motion between the outer two masses in the lowest mode decreases and damper effectiveness is lost. Damper effectiveness is also significantly reduced in the second mode at high frequency ratios. The third mode always exhibits opposing

motion between the outer two masses and as a result, damped behavior. Therefore, to most effectively introduce damping into a structural system using a passive vibration absorber, the absorber should be tuned to the lowest mode of interest.

When designing an absorber to damp several modes of a multiple DOF system, tune the absorber frequency, using Eqs. 2.26 and 2.27, to the lowest critical mode. This might be the lowest system mode, the lowest uncontrolled mode, or the lowest frequency mode which can be most affected at a particular location. When adjusting the absorber damper, only the tuned mode, and those of higher frequency, can be significantly damped. In other words, when attempting to passively damp several modes, tune to the lowest and adjust the damper for the desired response of it and the higher modes.

The results of these first two sections can be summarized as follows. Thus far, three passive tuning rules have been derived for the two DOF model. First, Eqs. 2.13 and 2.16 size the absorber spring and damper for optimal steady-state response based on a minimax criterion. For the optimal pole placement response, Eqs. 2.13, 2.18a, and 2.18b are used. Thirdly, a weighted quadratic cost of state is minimized by the procedure discussed in Appendix A. The three DOF problem allows the extrapolation of the steady-state tuning rules to higher order models. The next phase of investigation involves the introduction of a control force into the absorber, transforming it from a passive absorber into a control actuator with passive dynamics.

2.3 SINGLE STRUCTURAL DOF WITH A SINGLE DOF ACTIVE CONTROL ACTUATOR

Now that the rules for tuning a passive absorber to one and two DOF structural models have been derived, rules for tuning actuators, whose passive components resemble vibration absorbers, will be derived. The purpose of this actuator is to provide efficient active control of the original one DOF structure (Fig. 2.2) using state-dependent feedback (i.e. F_E included). In this section the passive actuator design best suited for an active feedback controller is determined. It is assumed that the control system designer has the freedom to select the passive actuator characteristics, and therefore the actuator components can be selected in such a way as to best make use of the control effort available to achieve a certain system performance. In designing the passive aspects of an actuator, two approaches are possible: the passive components can be designed first, then the active gains determined (sequential design); or the passive components and active gains can be determined simultaneously. The matrix presented in Table 2.4 summarizes the design cases analyzed in this chapter. The first row of cases, consisting of the design of passive vibration absorbers using the steady-state, pole placement and minimum quadratic cost formulations, was presented in Section 2.1. The middle row includes cases of sequential designs in which the passive actuator characteristics have been designed using one of the techniques in Section 2.1 and optimal active feedback gains

were derived using the Linear Quadratic Regulator (LQR) formulation. The third row involves the simultaneous optimization of the passive actuator components and active feedback gains. The objectives of this section are threefold: to determine the passive components of the control actuator that maximizes the benefits of the available control effort; to determine whether the passive and active portions can be derived sequentially rather than simultaneously; and determine if the passive components of the optimal actuator resemble the components of the optimal passive vibration absorber.

It should first be determined whether or not, for this simple structure, active control provides any performance improvements not achievable through passive means. A spring/damper is effective because it exerts equal and opposite forces on the two masses, between which it is attached, proportional to their relative motion. For this reason, the stiffness and damping matrices are symmetric in the passive case. This corresponds to self-adjoint system matrices. Self-adjointness does not necessarily exist in the active case. Because of this, active damping provides more versatility in dynamic design in that nonsymmetric state feedback terms can be added to the system matrices. From another viewpoint, it can be shown that the linear time-invariant system, shown in Fig. 2.2, is fully controllable. This means that the system poles can be arbitrarily placed through full state feedback gain selection. Arbitrary pole placement is not achievable using only passive components capable of functioning in the space environment. The procedure followed in

this section determines the effects and benefits of these feedback terms.

Feedback is introduced through the control force labeled F_E in Figure 2.2. In this analysis, the control force F_E is determined through full state feedback

$$F_E = -F_1 x_1 - F_2 x_2 - F_3 \dot{x}_1 - F_4 \dot{x}_2 = -[F]\{x\} \tag{2.28}$$

Since this force is motion-dependent, the action of the control force produces homogeneous terms which can be moved to the left hand side of the governing equations of motion

$$\begin{bmatrix} m_1 & 0 \\ 0 & m_2 \end{bmatrix} \begin{Bmatrix} \ddot{x}_1 \\ \ddot{x}_2 \end{Bmatrix} + \begin{bmatrix} c-F_3 & -c-F_4 \\ c+F_3 & c+F_4 \end{bmatrix} \begin{Bmatrix} \dot{x}_1 \\ \dot{x}_2 \end{Bmatrix} + \begin{bmatrix} k_1+k_2-F_1 & -k_2-F_2 \\ -k_2+F_1 & k_2+F_2 \end{bmatrix} = \begin{Bmatrix} P \\ 0 \end{Bmatrix} \tag{2.29}$$

Notice the nonsymmetric contributions of the feedback. The new nondimensional transfer function is given by

$$\left|\frac{X_1}{\Delta_{ST}}\right|^2 = \{(\delta^2-\xi^2-\gamma^2)^2 + 4\gamma^2(\mu+\rho)^2\} / \{\gamma^4 - \gamma^2(\delta^2+\xi^2+\beta(\delta^2-\alpha^2)+1)+\delta^2+\xi^2]^2 + 4\gamma^2[\mu+\rho+\beta(\mu-\eta))]^2\} \tag{2.30}$$

where, in addition to the terms defined in Eqs. 2.4a through 2.4g, there are

$\eta = F_3/(2m_2p_o)$ STRUCTURE'S RATE FEEDBACK GAIN (2.31a)

$\rho = F_4/(2m_2p_o)$ ABSORBER'S RATE FEEDBACK GAIN (2.31b)

$\alpha^2 = F_1/(m_2p_o^2)$ STRUCTURE'S POSITION FEEDBACK GAIN (2.31c)

$\xi^2 = F_2/(m_2p_o^2)$ ABSORBER'S POSITION FEEDBACK GAIN (2.31d)

These relations are used in the subsequent control analysis.

The procedure followed in Appendix A uses LQR design techniques first to optimize the passive absorber design (as already discussed in Section 2.1.3) and secondly to optimize the active feedback gains and passive actuator components both sequentially and simultaneously. These passive actuator components are then compared to the passive components derived for the vibration absorber in Sections 2.1.1, 2.1.2 and 2.1.3.

Appendix A and Reference 10 give the theory and analysis involved in the LQR technique. In the simultaneous formulation, the passive actuator parameters and active feedback gains are simultaneously optimized based on the minimization of a consistent quadratic state plus control effort cost function. The following is a list of the main conclusions drawn in Appendix A.

1. This formulation yields an antisymmetric active control gain matrix. There is no symmetric part in the gain matrix since all symmetric terms are realized through the passive parameters whose existance is not penalized in the cost function.
2. The passive components in the simultaneous design are similar to the components of the passive vibration absorber designs. The sequential and simultaneous design of the passive components and active feedback gains

give the same design.

3. The optimal active feedback gains may be determined assuming that the passive components of the actuator are the same as the optimal passive absorber and these gains may be superimposed upon the passive vibration absorber design to create the optimal active control actuator. In other words, the simultaneous optimization of passive components and active gains is not necessary.

Figure 2.13 compares the responses of the system in Fig. 2.2 subjected to a broad band disturbance for a variety of design cases. A mass ratio of $\beta = 0.1$ was used for comparison with the results of Appendix A and Reference 14. The design cases corresponding to the response curves in this figure are listed below:

A - Optimal passive steady-state response from Section 2.1.1. (Row 1, column 1 in Table 2.4.)

B - Optimal pole placement response from Section 2.1.2. (Row 1, column 2 in Table 2.4.)

C - Response of passive system optimized using a weighted quadratic cost function of the states (Section 2.1.3). (Row 1, column 3 in Table 2.4.)

D1- Response of passive design from A with the superposition of optimal active control based on a minimum quadratic cost of displacement, velocity and active control effort. (Row 2, column 1 in Table 2.4.)

D2- Response of passive design from A with the superposition of optimal active control based on a minimum quadratic cost of displacement and active control effort (i.e. same system as in case D1 but with the velocity penalty removed. (Row 2, column 1 in Table 2.4.)

E1- Response of the passive component of the simultaneous optimization detailed in Appendix A. The active feedback terms have been excluded. (Row 3, column 3 in Table 2.4.)

E2- Response of system that has undergone simultaneous optimization using displacement, velocity and control effort penalties in the quadratic cost function. Same as curve E1 but with active feedback included. (Row 3, column 3 in Table 2.4.)

As seen in curves A, B, C and E1 of Fig. 2.13, the passive absorber and passive component of the active actuator are roughly equivalent. In addition, whether the passive actuator parameters and active feedback gains are optimized simultaneously (Curve E2) or optimal feedback gains are superimposed on the passive steady-state design (Curves D1 and D2), the closed-loop responses are roughly equivalent. Therefore, the optimal active feedback gains and optimal passive actuator components can be superimposed to yield the optimal control actuator. This allows the passive actuator components to be selected using the rules derived in the vibration absorber analysis (Sections 2.1 and 2.2). It should be noted that these conclusions are only rigorously valid for collocated feedback control using the actuator states and the collocated (actuator mounting point) beam states.

It must be emphasized that the vibration absorber and simultaneous LQR techniques differ in their definitions of optimal and in their design techniques. Yet, the behavior of the resulting systems are roughly the same for a mass ratio of 0.1, which represents a practical case in which the mass of the actuator is only a small fraction (10%) of the total system mass.

Additional insight can be gained into the behavior of the LQR design formulation by analyzing the root locus of the optimized system pole locations as the mass ratio (β) is varied. Figure 2.14 shows the root locus for the design cases listed. The optimal steady-state vibration absorber poles (Section 2.1.1, Case A) are in the proximity of the LQR passive design poles (Section

2.1.3, Case C) for low mass ratios (β = 0.01 to β = 0.1). But, for high mass ratios, the LQR passive poles approach the poles of the system whose active and passive portions were designed simultaneously (Case E for β > 0.75). This implies that for a given amount of control effort available the active aspects of the actuator become less important at high mass ratios where the damping achievable through passive tuning is significant.

2.4 CONCLUSIONS

The original goals of this investigation have been achieved and they are summarized here along with the tuning rules. Three definitions of optimal passive design were derived and their resulting solutions, compared. The steady-state solution equalizes and minimizes peak magnitudes of the modal response. The pole placement solution places the system poles as far left in the S-plane as possible. The weighted quadratic cost solution minimizes the cost of the system subjected to a set of quadratic state penalties. All three techniques resulted in almost identical vibration absorber configurations.

The optimal passive, steady-state solution was derived for two and three DOF systems. The solution methods were found to be similar for each case. The method calls for passively tuning to the lowest of a set of 'critical' modes and adjusting the damper setting for the desired response. 'Critical' modes are defined as the lowest modes, those outside the bandwidth of the active

controller or those most effectively damped at that absorber's location.

The steady-state passive design and the passive component of the LQR design were compared and were in rough agreement for small values of mass ratio (β). Therefore, the LQR active feedback gains are superimposable with the vibration absorber design allowing the passive and active designs to be performed sequentially: passive followed by active design. A practical advantage is realized from the superposition of the optimal active and passive designs. In the event of a failure of an active component, the structure still exhibits maximum passively damped behavior.

The typical design steps for an inertial control actuator are listed below. An actuator model, as seen in Fig. 2.1, is assumed.

1. Select the actuator-to-modal mass ratio using a tradeoff between mass and performance.
   A. For steady-state response, Eq. 2.15 determines performance.
   B. For pole placement, Eq. 2.18b determines performance.
2. Determine actuator stiffness using Eq. 2.26.
3. Determine actuator damping using either Eq. 2.16 or Eq. 2.18a. The optimal damper value will exceed these values in the multimode case.
4. Determine a suitable quadratic cost index for the required system performance and calculate the optimal LQR feedback gains (Appendix A).

3.0 CONTROL PROCESSOR ARCHITECTURE

The processor is that control system component that is used to implement the closed-loop compensation. These compensation alogrithms can be realized through analog circuitry or digital hardware and software, or a hybrid of the two. Though analog computers are able to track and process higher frequency signals, without discretization effects such as aliasing, analog compensation is not as versatile as digital compensation. Algorithms can be more easily altered if implemented in software, and in addition, digital compensation reduces the problems of component drift and noise which are common among analog components. Digital realization also enables compensation of low frequency signals for which analog circuits often contain unreliable, high drift elements. For these reasons, a digital control implementation was chosen.

Controller bandwidth is the limitation encountered when using a digital computer to implement control algorithms. Controller bandwidth is directly related to controller sample rate, which is defined as the number of times the control algorithm is repeated per second. The higher the control rate, the larger the achievable bandwidth since the Nyquist frequency, one half the sample frequency, effectively marks the high frequency limit of the controller.

Structures are dynamic systems of almost infinite order and the objective of this research is to devise high authority, high

bandwidth controllers for these structures. As the bandwidth of a structural compensator is increased, not only must the cycle time of the fixed number of calculations in the digital processor be reduced, but the order of the estimator model (and therefore the number of calculations per cycle) must be increased to reflect the increase in bandwidth. Due to the limited speed of a given processor and the virtually unlimited number of structural modes some method is needed to increase the effective control rate.

Several options are viable for increasing the controller bandwidth. First, as advances are made in digital technology, faster processors can be acquired. Secondly, parallel processing can be used to perform simultaneous operations in parallel hardware. Finally, distribution of the processing task among several processors enables faster processing of system states which increases the bandwidth of the controller. If this distribution of tasks is done in a hierarchic sense to reflect structural behavior, further benefits may occur.

This chapter discusses the advantages of applying distributed multiprocessor control to modify elastic structural behavior. As advances are made in the first two technological areas, faster and more parallel processors, they can be readily incorporated into this distributed hardware format which represents a long term processing solution. Section 3.1 presents a proposed microprocessor architecture based upon distributed processing and control hierarchy. Section 3.2 details two digital hardware configurations which support this architectural format. The present, first generation processor system and planned expansion

to the second generation system are detailed in Sections 3.3 and 3.4, respectively.

3.1 ARCHITECTURE FOR A DISTRIBUTED HIERARCHY OF CONTROL

The processor architecture discussed in this section centers around two important principles which potentially enhance the performance of high speed digital control. These principles are distributed processing and hierarchy of control. Distributed processing allows simple multiplication of data throughput capacity. Since the processing at all localities is performed simultaneously, the achievable control rates are significantly faster than that achievable with control using a single, equivalent processor. This increases both the bandwidth of the controller and the number of structural modes that can be controlled. But, there are many options for distribution of processing. Parallel processing is, in a sense, a scheme of distributed processing, as are dynamic task allocation schemes. One potentially useful distribution scheme is coupled to the concept of hierarchic control.

Control hierarchy can be used to reduce the order of the structural model required in each processor. In such a scheme, each processor is responsible for controlling a particular set of modes or range of wavelengths. The command signal sent to any given actuator is the sum of command signals from the set of processors whose combined model fully represents the controlled

modes of the structure. Figure 3.1 illustrates the processor network for distributed, hierarchic control. Distributed processing increases control speed by reducing the number of sensors and actuators for which each of the lowest level processors is responsible. Hierarchic processing reduces the number of modes or range of wavelengths for which each processor is responsible. Both principles tend to distribute the processing task, increase the control rate, and expand the controller's bandwidth.

In the following discussion, several terms are used which require definition. The terms 'master' and 'slave' refer to any pair of processors which interact directly with each other. The master processor maintains some level of authority or control over its respective slave(s) in the areas of control synchronization and data transfer. The terms '*local*', '*component*' and 'global' refer to the levels of hierarchic processing illustrated in Fig. 3.1. The local processors interact most closely with the structure through sensor data retrieval and processing and the issuance of actuator commands. A component level processor interacts with several local level processors (its slaves). A global processor is in the highest level and interacts with several component level processors in a master/slave arrangement. Interaction between a component and local level processor is a second example of master/slave interaction.

With each processor controlling a certain set of modes at a particular location, the idea of hierarchic control naturally follows. Assign to the zero or local level processor (Fig. 3.1)

the highest frequency modes or waves which lie within its bandwidth. This processing level has the highest bandwidth because most of the processing load is distributed throughout the higher levels. Space these processors, and their corresponding actuators, along the length of the structure as is appropriate. This processing level would typically perform local, collocated state feedback using high speed digital hardware. In this situation, each processor obtains information about a small portion of the structure and controls these high frequency, short wavelength modes over a limited section of the structural domain.

At this point a one or component level processor is assigned to preside over several adjacent zero level units which are its slave processors. By obtaining all of the sensor data from its distributed zero level units, the one level processor can observe longer wavelength vibrations better than its associated zero level units because it possesses sensor information over a larger portion of the structure. This enables the component level processor to perform feedback between multiple sensors and actuators at different locations (noncollocated feedback). This processor task versus level is illustrated in Fig. 3.2.

If the lower frequency, longer wavelength modes are considered the most critical modes to control (i.e. most sensitive to a performance index and most easy to excite), the advantage of this distributed arrangement is obvious. The component level can process more information on the lower frequency, more critical modes at a slower speed since these lower modes lie within the bandwidth of processors with slower control rates. If need be,

more component levels may be added in a pyramid fashion. The highest, global level of processing would perform the highest level of control on the lowest structural modes and have coprocessors to perform such tasks as component failure detection, control reconfiguration and system identification. Figures 3.3a and 3.3b show two possible control authority arrangements in the frequency domain for these three levels of processing.

This scheme provides several advantages over single processor control. First, portions of the processing task can be performed simultaneously allowing the control of higher freqency modes due to the increase in controller bandwidth. Secondly, control activation can parallel the construction phase in a building block fashion. As the structure becomes larger, additional processors ar levels may be added. Thirdly, local level processors manipulate a small amount of information on a small portion of the structure enabling them to work at high speeds. Higher level units process more information on the more critical modes without reducing the bandwidth of the entire control system.

There remain a number of important issues: The applicability; appropriateness or effectiveness of such a concept; the design and analysis scheme for such a distributed hierarchy; and its implementation in hardware. The former two issues are the subject of Reference 14. The following sections discuss how this architecture can be implemented in hardware and Appendix B discusses how structural models influence the distribution of control tasks in a hierarchic controller.

3.2 COMPATIBLE HARDWARE DESIGN OPTIONS

Several hardware configurations can be used to interface processors in a distributed and hierarchic architecture. Two configurations will be discussed here: a single bus and a multibus system. A single bus system could support all of the control processors on the same bus. A 'housekeeping' processor would be used to synchronize the data transfer between control processors on adjacent levels. In Figure 3.4, data transfer between processors G and C1, or between C2 and L2,1, constitutes communication between master and slave. A second approach would allow each level of processing to communicate directly with adjacent levels in a multibus system (Fig. 3.5). This configuration will be refered to as multibus and resembles a pyramidal communications network. The merits of each arrangement will be discussed, followed by a discussion of the designs chosen for the first and second generation control experiment.

In the single bus system, interprocessor communication takes place through shared memory space. In other words, there exists a section of memory which can be accessed by two different CPU's. All memory in the single bus system is addressable by the housekeeping processor while different portions of that same memory are accessible by each of the other processors. The control processors cannot address each other's memory space directly. Thus, the housekeeper is required to handle synchronization, avoid bus contention and perform data transmission.

A typical interrupt routine for this single bus system is shown in Fig. 3.6. The local level and housekeeping processors cycle through their respective interrupt handlers faster than the higher levels. The local level processors retrieve sensor information via analog-to-digital converters and place this information in memory. Every n local interrupts the housekeeper passes this information to the appropriate master processors on the component level. The same is done for the global level every nxm local interrupts. In each case, n and m are positive integers whose values depend on the relative control rates of the component and global levels. Control commands are processed by all levels and placed in the common memory. After the appropriate number of local interrupts, the housekeeper sums and passes the commands from the higher levels to the appropriate local level processors which create the actuator commands through digital-to-analog converters. The control commands issued by the local levels occur more often than those issued by the higher levels. This causes the lower levels to have higher control rates and corresponding bandwidth. The programmable clocks keep all of the processors synchronized.

This scheme has two important attributes. First, the housekeeper has the ability to monitor the performance of all of the processors. Secondly, the local level processors issue control commands at much higher rates than the higher levels.

This configuration has two major drawbacks. First, the number of control processors is limited by the amount of memory addressable by the housekeeper. Secondly, the rate of data

transmission is reduced because all communication is performed over a single bus.

The multibus approach allows data transmission to be performed directly by the processors involved. This eliminates the extra step of transfering data to the housekeeper. In this design the lower levels are interfaced to the higher levels through multiple ports and utilize shared memory for communication (Fig. 3.5).

Sensor information is passed to higher levels in a fashion resembling a communication pyramid while control commands are passed down to the local level. The typical interrupt sequence is illustrated in Fig. 3.7. Data acquisition is performed on the local level as is command output. Sensor information is pushed up the pyramid and made available to the higher levels. The higher processors issue commands based on the available information at rates inversely proportional to the respective level. In other words, the higher the level, the more processed information and the longer the processing delay resulting in slower control rates. Commands from each level are then passed back down through the pyramid, summed with lower level commands and issued to the actuators from the zero, or local level.

The multibus approach eliminates some of the limitations encountered with the single bus configuration. This scheme is not limited by the amount of memory addressable by the global processor. More information can be passed at a time because several busses are available. Because of more efficient communication and limitless expandability, the multibus

configuration is used in the experimental setup.

3.3 PRESENT PROCESSING CAPABILITY

The initial objective of the microprocessor development program was to implement the processors for one element, i.e. for one component and several local processors (Fig. 3.2). The present digital hardware therefore consists of three processors and support peripherals. A component and local level are achieved through one master and two slave processors, respectively, which communicate through shared memory space on the slave boards (Fig. 3.8). The master contains an INTEL 8088 CPU which performs sixteen bit operations, synchronized by a five megahertz system clock, and an 8087 NDP, numeric data processor. The CPU board is a model 8759 built by JF Microsystems. Each Ziatech ZT8830 slave board contains an INTEL 8088 CPU. Both slave and master memory is addressable by the master across an eight bit STD bus. But, each slave can only address its respective memory. In the shared memory space, memory access is performed through bus arbitration to avoid bus contention. Support peripherals include analog-to-digital and digital-to-analog conversion boards for the master (Analog Devices: RTI-1260 and RTI-1262, respectively) and an Intel iSBX-311 Multimodule analog input board for each slave. This system is housed in a Labtech 70 built by Laboratory Technologies, Inc. and runs Fortran 86 and Assembler 86.

As will be discussed in the next chapter, four actuators were

built and each outfitted with three collocated sensors. This arrangement calls for processing twelve measurements and producing four command signals. To achieve this capability, each slave was equiped with eight A/D channels and the master was equiped with four A/D and four D/A channels. This configuration deviates slightly from that detailed in the previous section in that the all D/A functions take place on the component level through the master processor. This temporary deviation from the planned implementation was made due to the initial difficulty of providing for D/A capability at the local slave processor level.

The interrupt sequence used in the control experiments is displayed in Fig. 3.9. The interrupt cycle starts with a clock interrupt on the master board which causes the instruction pointer to exit keyboard communications and execute the master's interrupt handler. The first operation of the master interrupt handler is to interrupt both slave boards by setting a flag in the maskable interrupt control address on each slave board. This address is located in the shared memory space. The slaves digitize the sensor signals, pass some of the digitized information to the master, process the remaining information and then pass the resulting command data to the master. Then the slaves are idle until the next interrupt from the master. After initiating the slaves, the master processes the first set of incoming data, reads the second set of slave data, D/A's the actuator command signals and returns to its interrupted routine which performs keyboard communications and monitors the interrupt clock. This cycle repeats every five milliseconds resulting in a two hundred hertz

control rate. The second generation system is presently under development and will provide greater processing power and better resemble the multibus system of Fig. 3.5.

3.4 SECOND GENERATION PROCESSING NETWORK

In the second generation arrangement, several new features will be added to the original experimental hardware. A new processing level is being introduced in addition to a second level of communication links, or busses. Each current slave processor will also gain a high speed floating point processor (MATH) and additional D/A capability. In Figure 3.10, the master now represents a global level processor with the capability of communication with the keyboard and the three component level processors (Slaves C, D and E). The three component level processors now contain A/D, D/A and floating point math capabilities. These processors can communicate with the global processor and the local level processors; denoted by SPH in Figure 3.10. The local level processors (SPH) correspond to signal processing hardware which perform real-time, high speed signal processing on various sensor signals.

This new system will contain one global, three component and three local level processors resulting in seven processors operating simultaneously. A total of fourty channels of A/D, twenty-eight channels of D/A and four independent communication busses will be available for control purposes. This hardware

implementation more closely resembles the distributed, hierarchic processing of Fig. 3.5 in that: the local level processors operate at rates much higher than the component or global levels; each component level processor can monitor up to four actuators within its domain; and digital communication flows from level to level in the processing pyramid.

4.0 EXPERIMENTAL HARDWARE AND SOFTWARE DESIGN

This chapter discusses the design considerations involved in the construction of both the experimental test bed and the various active control components. A schematic of the experimental hardware is shown in Fig. 4.1. First, the selection of the test article, or model space structure, will be discussed. This will be followed by a discussion of the design issues dealt with during actuator construction and sensor selection. Finally, the development of digital and analog signal processing is presented. In each case, component development is guided by the desire to develop a robust controller using components that are capable of functioning in the space environment (space-realizable). In addition, the experimental test bed is designed with enough versatility to support numerous types of control experiments.

4.1 TEST ARTICLE

A free-free beam was selected as the first test article. These boundary conditions provide the most realistic model of a free floating space structure. A uniform beam was chosen as a test article because it has a linear response and can be easily modeled. A twenty-four foot brass beam was suspended from cables arranged in a swinging parallelogram fashion (Fig. 4.2). This parallelogram suspension helps to suppress torsional response in

the beam which may arise from gravity moment couples created by the motion of the beam and actuators. Except for the suspension cables and power cords, this test article is free of the laboratory frame and is considered a realistic representation of a large flexible space structure.

The desire was to design a test article whose standing and propagating wave behavior were distinguishable to the control processor. Table 4.1 lists the first sixteen experimentally determined modal frequencies of this beam along with its geometric and material properties. The parameters of this beam were chosen for several reasons. The beam was made very long and flexible to test the frequency range of the actuators and controller and to provide a test article representative of a space structure. For a standing wave controller the beam dimensions were chosen to result in many closely spaced modes at low frequencies.

For a propagating wave controller, this beam provides seemingly finite wave propagation speeds, phase velocities and energy transport speeds, or group velocities. With a processor control rate of two hundred hertz, waves associated with the first ten modes can be observed over one hundred times during a single traversal of the beam. Depending on the wave speeds and the closed-loop damping in the system, vibrational motion may be better modelled as propagating wave behavior. The theory behind the wave mechanics based controller will be discussed briefly in Appendix B and may be implemented in later tests. The next step is to outfit this structure with the controller components: its actuators; sensors; and signal processing equipment.

4.2 ACTUATOR IMPLEMENTATION

From amongst the four types of space-realizable actuators: linear momentum exchange devices; angular momentum storage devices (CMG's); relative motion devices (hydraulic actuators); and expelled mass momentum devices (thrusters); the linear momentum devices were chosen for development. These devices were modeled and optimized for this application in Chapter 2, but there remains the issue of hardware implementation. The objective of the implementation is to create a proof-mass actuator capable of producing smooth and authoritative command forces or moments on the structure while also incorporating adjustable passive properties.

Several types of inertial actuators have been developed at M.I.T.; all having DC motors as their electromechanical driving elements. Translating proof-mass actuators, resembling audio speakers or solenoids, have been built. Here the motor is a translating DC motor with field coils or permanent magnets. These devices proved to be conceptually simple but their translating suspensions introduced considerable friction and stiction problems. Rack and pinion devices incorporate a rotational DC motor and a linearly translating mass, but the rack and pinion introduce backlash problems. The lowest friction and sturdiest suspension proved to be a pivoting, proof-mass arrangment. In this design, a direct current motor rotates a reaction arm. This device produces a torque, if the center of mass (CM) of the arm is placed at the pivot. If the CM is offset from the pivot, a force

proportional to commanded motor torque is produced for small arm angle motion. This pivoting configuration was chosen for experimental development.

Four pivoting, proof-mass actuators were built each capable of generating control forces on the beam of up to 3 Nts. Figure 4.3 shows a typical actuator, shown in both the force and torque configuration. This actuator design resembles a device developed at Lockheed Missiles and Space Company (Reference 1). Several improvements have been made over the original Lockheed design. M.I.T.'s actuators are built from stock components including samerium cobalt, permanent magnet motors. The same actuator can be adjusted to produce either torque or force, based on the arrangement of the masses on the reaction arm. Adjustable passive components were added to the devices to alter the passive dynamics of the actuator as discussed in Chapter 2. The appropriate sensors were added to obtain full measurements of the actuator states, in order to provide full actuator observability and compensation for the active actuator dynamics.

The conceptual actuator models developed in Chapter 2 can be directly applied to this pivoting, proof-mass actuator when it is used either in the torque or force configurations. Fig. 4.4a shows the model of the torque configured actuator (i.e. the CM of the arm is located at the pivot). In this case a pure torque is applied to the beam and the model of Chapter 2 can be applied with just a change in notation. The following are the governing equations of motion for the model shown in Fig. 4.4a, based upon Eq. 2.1.

$$I_o\ddot{\theta}_o + C\dot{\theta}_o + K_o\theta_o - C\dot{\theta}_1 - K_o\theta_1 = -\tau \qquad (4.1a)$$

$$I_1\ddot{\theta}_1 + C\dot{\theta}_1 + (K_1+K_o)\theta_1 - C\dot{\theta}_o - K_o\theta_o = \tau_P + \tau \qquad (4.1b)$$

where

I_o Rotary inertia about the center of mass of the pivoting arm.

I_1 Rotary inertia of the beam mode.

C Rotary damping of actuator.

K_o Rotary stiffness of actuator.

K_1 Rotary stiffness of beam mode.

τ Control torque.

τ_P Disturbance torque.

The optimal frequency ratio, from the analysis in Section 2.1.1 using the two step minimax criterion, is

$$\delta_{OPT} = \frac{1}{1+\beta} = \left[\frac{K_o/I_o}{K_1/I_1}\right]^{1/2}\Bigg|_{OPT} \qquad (4.2a)$$

$$\beta = I_o/I_1 \qquad (4.2b)$$

Figure 4.4b shows the model of the actuator in force configuration (i.e. the CM of the arm is offset from the pivot by the length b). The following are the relations corresponding to

the force configuration, based again on Eqs. 2.1 and 2.13.

$$(I_o+mb^2)\ddot{\Theta} + C\dot{\Theta} + K\Theta + mb\ddot{X}_1 = \tau \tag{4.3a}$$

$$(M_1+m)\ddot{X}_1 + K_1X_1 + mb\ddot{\Theta} = P \tag{4.3b}$$

$$\delta_{OPT} = \sqrt{\frac{1 + (1-\rho)\beta}{1 + \beta}} \tag{4.4a}$$

$$\rho = \frac{mb^2}{I_c + mb^2} \tag{4.4b}$$

The new parameters for this model are listed below.

- I_o Rotary inertia about the center of mass of the pivoting arm.
- b Location of the center of mass with respect to the pivot.
- m Mass of pivoting arm. $m = m_o + m_1$
- C Actuator damper.
- K Actuator stiffness.
- τ Actuator's motor torque. Control torque.
- M_1 Modal mass of structure.

In the force configuration, the variable ρ accounts for the ratio of offset inertia to total inertia. Notice the similarity to Eq. 2.13 for values of ρ approaching unity.

Table 4.2 lists the actuator specifications and components as built. The only actuator component that is not space-realizable is the adjustable air damper. This is presently being replaced by an adjustable electromagnetic device.

The permanent field magnet, DC motors of these pivoting, proof-mass actuators have their armature windings driven by current amplifiers. Current amplifiers output a current that is proportional to, and in phase with, the input voltage signal supplied by the control processors. Since motor torque is proportional to, and in phase with, armature current, the current amplifiers allow the control designer to ignore the electrodynamics of the motor coils. Thus, the electromagnetic, proof-mass actuator coupled to a current source provides a simple, easily modeled, space-realizable actuator.

4.3 SENSOR IMPLEMENTATION

The actuators and beam are equiped with the necessary sensors for making state measurements of the system. Note that the states include the states of the beam and the relative motion between the actuators and beam. This state information can be obtained in two ways. First, a state estimator can be used to transform a required minimum set of measurements into estimates of all of the states of the system. This is done by using a plant model in the control processor to relate sensor measurements to state variables. Secondly, the test article can be outfitted with a

sufficient number of sensors to sense all of its states directly and these state measurements can be used to perform state feedback control. In the interest of implementing a simple robust controller in the first set of control experiments, the latter approach was chosen and simple collocated state feedback was used.

The state measurements necessary to provide full state, output feedback for this beam/actuator system are the velocity and position of the actuator relative to the beam and the absolute velocity and position of the beam at each actuator location. To maintain a space-realizable test bed, only relative and inertial motion sensors were considered. The measurement of the relative motion between the actuator and the beam was straight forward. Tachometers and potentiometers are mounted on the actuator to provide measurements of the relative rotational velocity and position with respect to the beam. Analog sensors were chosen to enhance low level measurements of actuator motion associated with low level vibrations. This avoids the loss in resolution encountered with discrete measurement devices. The major difficulty in state measurement stems from obtaining the beam states in absolute coordinates in a way other than measuring against the reference frame of the laboratory. Inertial measurements would preserve the space-realizable nature of the experiment.

Inertial piezoresistive accelerometers, whose frequency response is constant from zero frequency to 2 KHz, were used to sense the inertial acceleration of the beam. The control processors were used to obtain velocity and position estimates

through a stabilized double integration algorithm. This is done without the use of a system model and will be discussed in Section 4.4. Table 4.3 lists the specifications for each of these sensors.

The final sensor configuration called for three sensors (tachometer, potentiometer and accelerometer) at each actuator location. This provides four collocated state measurements, after double integrating the accelerometer signal, for use in generating a full collocated state feedback control command for each actuator.

4.4 SIGNAL PROCESSING IMPLEMENTATION

The digital control processors generate control commands based upon the measured sensor data. In the initial set of experiments, the processor performed two functions: the stable double integration of the accelerometer to yield the beam states; and the computation of force feedback commands from the measured actuator states and integrated beam states. This section will describe the processing algorithms implemented in the processors in the initial experiments.

To obtain beam state information (i.e. velocity and position) from a measured acceleration signal, two temperal integrations are required. The beam response, as measured by the accelerometers, contains the true acceleration signal as well as two noise components. The first noise component can be modeled as a zero

mean, broad band measurement noise. Such noise is limited to band limited white noise after passing through analog, low pass, antialiasing filters (Fig. 4.1) and diminishes in importance after integration. The second noise component consists of nonzero mean DC offsets in the sensors and slow signal drift due to sensor heating or deterioration. Since the first integral of nonzero mean offsets is linear in time, and the second integral is second order in time, their presence will destabilize an exact integration of the beam acceleration. A minor loop stabilization technique is required to keep the displacement and velocity integrals within the computer's digital-to-analog converter windows (-5 to +5 volts) and avoid actuator saturation.

This stabilization of the integration can be achieved by output (i.e. displacement and velocity) feedback and can be implemented in either analog hardware or digital hardware or software. Digital feedback stabilization is useful when working at these low beam frequencies where analog components become unreliable. Reference 10 discusses the derivation of appropriate state feedback algorithms for discrete control.

Fig. 4.5a shows the open loop system representing the simple double integration which must be stabilized. The state space representation of the governing equations and output of a double integrator are

$$\begin{bmatrix} \dot{x} \\ \ddot{x} \end{bmatrix} = \begin{bmatrix} 0 & 1 \\ 0 & 0 \end{bmatrix} \begin{bmatrix} x \\ \dot{x} \end{bmatrix} + \begin{bmatrix} 0 \\ 1 \end{bmatrix} u \qquad (4.5a)$$

$$(y) = \begin{bmatrix} x \\ \dot{x} \end{bmatrix} = \begin{bmatrix} 1 & 0 \\ 0 & 1 \end{bmatrix} \begin{bmatrix} x \\ \dot{x} \end{bmatrix} \tag{4.5b}$$

where u is the system input, the accelerometer signal, and y is the output, the position and velocity signals. Using any of the techniques for transforming a continuous representation into a discrete time representation (e.g. matrix exponential: Reference 10) gives the discrete time equations

$$\begin{bmatrix} \tilde{x} \\ \dot{\tilde{x}} \end{bmatrix}_{i+1} = \begin{bmatrix} 1 & T \\ 0 & 1 \end{bmatrix} \begin{bmatrix} \tilde{x} \\ \dot{\tilde{x}} \end{bmatrix}_i + \begin{bmatrix} T^2/2 \\ T \end{bmatrix} \tilde{u}_i \tag{4.6a}$$

$$(\tilde{y})_i = \begin{bmatrix} 1 & T-\delta \\ 0 & 1 \end{bmatrix} \begin{bmatrix} \tilde{x} \\ \dot{\tilde{x}} \end{bmatrix} + \begin{bmatrix} (T-\delta)^2/2 \\ T-\delta \end{bmatrix} \tilde{u}_i \tag{4.6b}$$

The sample period is T, the processing delay is δ and state feedback is implemented through

$$\tilde{u}_i = -[F_1 \; F_2] \begin{bmatrix} \tilde{x} \\ \dot{\tilde{x}} \end{bmatrix}_i + \ddot{\tilde{x}}_i \tag{4.7}$$

This arrangement is illustrated in Fig. 4.5b.

The closed-loop characteristic equation of the double integrator is

$$z^2 + (T(0.5TF_1 + F_2) - 2)z + T(0.5TF_1 - F_2) + 1 \tag{4.8}$$

where 'z' is the discrete Laplace operator. This second order characteristic equation can be altered to meet the objective of providing stable integrations of the frequencies of interest while rejecting the nonzero mean noise. The solution is to perform high pass filtering at low frequencies and integrations at the higher frequencies of interest, in a closed-loop fashion. The resulting frequency transfer functions are shown in Fig. 4.6.

For a second order system the corner frequency and damping ratio, characterizing the performance of the filter-to-integrator transition zone, can be defined. These characteristics determine the s-plane poles which, after being converted to z-plane poles through Eq. 4.9, determine the desired roots of Eq. 4.8.

$$z = e^{sT} \tag{4.9}$$

Assuming a sample period of T = 0.005 sec, a negligible processing delay, a corner frequency of 1.0 rad/sec and a damping ratio of 0.7071, the algorithm for the stabilized double integrator is

$$\begin{bmatrix} \tilde{x} \\ \dot{\tilde{x}} \end{bmatrix} = \begin{bmatrix} 0.99999 & 0.00498 \\ -0.00498 & 0.99294 \end{bmatrix} \begin{bmatrix} \hat{x} \\ \dot{\hat{x}} \end{bmatrix} + \begin{bmatrix} 0.0000125 \\ 0.005 \end{bmatrix} \ddot{\tilde{x}}_i \tag{4.10}$$

These parameters were chosen because this is the fastest sample period presently achievable, the stabilization corner frequency is half the frequency of the lowest mode of interest (allowing proper integration of this lowest mode) and this damping ratio provides minimum overshoot. For a negligible processing delay, the output

equation is identical to the state equation. Therefore, only the state equation is computed by the processor and the velocity and position values are output from this integration computation during each interval.

Fig. 4.6 shows the frequency response of this double integration algorithm (Eq. 4.10). Low frequency components of the accelerometer signal are filtered out of the velocity output term and appear in the position output term, multiplied by a constant. The presence of this low frequency component in the position output term is undesirable. Therefore a single pole, high pass digital filter, given in Equations 4.11a and 4.11b, is used to filter the position term after the integration routine. This removes the nonzero mean, low frequency error in the position estimate.

$$x_i = z_i + \tilde{x}_i \tag{4.11a}$$

$$z_{i+1} = 0.99843\, z_i - 0.00157\, \tilde{x}_i \tag{4.11b}$$

This algorithm, Eqs. 4.10 and 4.11, yields a low frequency range in which filtering of the various input and output terms takes place, a middle frequency range in which the integrations of the accelerometer signals take place and a high frequency range in which the Nyquist Frequency correspondes to a system zero due to the aliasing caused by digitization of the accelerometer signal. The total configuration of the integration process, consisting of the analog antialiasing filter, A/D and digital integrator, is

shown in Fig. 4.7. The accelerometer signal is low pass filtered, integrated twice and the estimated position signal is high pass filtered.

Figure 4.8 gives the frequency response in magnitude and phase for the estimated velocity and position signals. At low frequencies, the signals are filtered to eliminate nonzero mean noise. The transition region exhibits the response near the selectable poles of the system. The integrating regions contain the frequencies corresponding to the beam modes of interest. The highest corner frequency corresponds to the filtering of the zero mean noise by the antialiasing filter and aliasing effects introduced by the discretization of the accelerometer signal. In the current implementation, the poles are located at 1.0 Hz, for the integrator and high pass filter routines, and at 700 Hz, for the low pass, antialiasing filters. They are, of course, adjustable for easy manipulation of corner frequencies, putting the frequencies of the state signals of interest in the integrating regions.

As a final task of the processor, these estimated beam states are combined with the measured actuator states to generate the full collocated state feedback command to each actuator. The computational task is evenly distributed among the three processors. This arrangment deviates slightly from the original plan for hierarchic control, as discussed in Section 3.3. The master, or component processor digitizes and double integrates two accelerometer signals. Each of the two slave, or local processors digitizes five signals (including one accelerometer signal),

performs one double integration, multiplies states by gains and passes the information to the master. Then the master converts the four command signals to analog signals via its D/A. This routine is repeated every 5 msec, yielding a 200 Hz sample and control rate for a twelve sensor, four actuator system being processed on three commercially available microprocessors.

The final hardware components in the overall control system are the analog signal processing equipment shown in Fig. 4.1 as signal amplifiers and filters. The preprocessor signal processing equipment consists of signal amplifiers, for boosting sensor signal levels followed by low pass, antialiasing filters; just discussed. Table 4.4 lists the specifications of the amplifiers and filters. Antialiasing filters prevent the occurance of low frequencies which result from digital misrepresentation of high frequency signals. These filters are second order Sallen and Key circuits. After the command signals are digitally processed, they pass from the D/A through low pass, smoothing filters. This smooths the two hundred hertz step generated by the D/A. If not filtered, this 200 Hz step component causes the actuators, and high frequency beam modes, to buzz. These analog command signals then pass to the current amplifiers to drive the actuators.

These hardware and software components comprise the closed loop controller. Every feature is space-realizable with only two exceptions. First, the air dampers are not functional in space and are being replaced by passive electrodynamic dampers. Secondly, current amplifier power is not generated or dissipated locally. This, of course, could be done with appropriate space

based power generating equipment.

With this controller hardware, several tests were performed to demonstrate the use of some collocated state feedback techniques and verify that this equipment functions properly. These experiments will be described in the next chapter.

5.0 CONTROL EXPERIMENTS

A preliminary set of simple collocated state feedback experiments was deemed essential to verify that the closed-loop controller functions properly. The overall goals of the experiments detailed in this chapter were twofold: to verify the controllability of structural modes using an inertially actuated, space-realizable control system; and to establish the functionality of the versatile testbed upon which future testing of the full hierarchic controller can be performed.

These tests had several specific objectives. First, they were used to identify any necessary hardware changes. This includes evaluation of the digital processing performance, analog signal processing equipment and sensor performance. Secondly, the experiments established the degree to which the actuators can be tuned, according to the rules derived in Chapter 2. Third, the test would serve as a verification of the controllability of structural modes using inertial actuation and collocated state feedback. Lastly, these experiments help identify some of the experimentally encountered limitations involved in state feedback, structural control.

Four series of tests were planned to achieve these specific objectives. The tests were chosen in a sequence that would first demonstrate the effectiveness of strictly active and then strictly passive damping and, then demonstrate the effectiveness of a combination of both damping techniques. In the conduct of each

test, any limitations on the system's performance were noted and appropriate solutions or explanations are presented.

The first experiment tests a single input, single output (SISO) active controller. In this test, one actuator was used to control structural modes using only collocated structural rate in the feedback loop. The second test improves on this technique by adding collocated actuator rate to the feedback loop. In the second test, two actuators were used to control several modes, each using both collocated structural and actuator rate measurements. Thirdly, the passive components of the actuators were tuned to different modes following the tuned vibration absorber methods detailed in Chapter 2, and the performance of the passive system was evaluated. Lastly, both active and passive techniques were employed to damp the same structural modes.

In the following section, the preliminary design of the experiment is detailed (Section 5.1). Sections 5.2 through 5.5 present the experimental results. In each of these sections, the expected results, actual results and degree of achievement, or the limitations encountered, are discussed.

5.1 DESIGN CONSIDERATIONS FOR EXPERIMENTAL PHASE

There are several questions bearing on the experimental design that must be addressed by analysis prior to testing. These questions are concerned with how the controller hardware should be arranged with regard to the test structure and what stability

limitations can be expected during testing. The four such questions discussed in this section are:

- Under what hardware and configuration conditions are the beam modes controllable (i.e. arbitrary pole placement through feedback selection given a linear, time-invariant system)?
- What are the primary energy dissipation mechanisms in this system?
- Where, on the beam, should the four actuators be placed in order that maximum control performance is achieved?
- What stability limitations exist when using only beam state feedback (i.e. not compensating for actuator dynamics)?

An understanding of the answers to these questions helps determine an appropriate sequence of experiments.

The question of prime importance is that of controllability. The dynamics of the beam will be modeled as a single structural mode. Can a SISO controller, using an inertial actuator and a collocated beam rate measurement, exert control to the extent that there is an increase in that mode's structural damping? Furthermore, does full collocated state feedback (including actuator states) provide the system with the capability to perform arbitrary pole placement?

The question of controllability is answered by examining the 'Controllability Matrix' (Reference 10). If the matrix has full rank and the system is linear and time-invariant, the system is fully controllable and the closed-loop poles may be arbitrarily placed through the feedback of all of the system states. If the determinant of this matrix is nonzero, for a single input system, it is of full rank.

In order to examine the controllability, the system matrices

for a pivoting, proof-mass actuator, coupled to a structural mode, must be derived in appropriate form. The reaction equations of motion for a pivoting proof-mass actuator, used as a force actuator coupled to a single structural mode, are repeated from Chapter 4 as

$$(I_o+mb^2)\ddot{\theta} + C\dot{\theta} + K\theta + mbX_1 = \tau \tag{5.1a}$$

$$(M_1+m)\ddot{X}_1 + C_1\dot{X}_1 + K_1X_1 + mb\ddot{\theta} = P \tag{5.1b}$$

Equivalent viscous structural damping (C_1) is introduced to determine its effect on controllability. Since pole placement represents only homogeneous dynamics, P can be set to zero. The control torque (τ) is a function of state variables and is therefore homogeneous. Transforming these equations into state variable form,

$$\dot{z} = Az + Bu \tag{5.2a}$$

$$\begin{bmatrix} \dot{X}_1 \\ \dot{\theta} \\ \ddot{X}_1 \\ \ddot{\theta} \end{bmatrix} = \begin{bmatrix} 0 & 0 & 1 & 0 \\ 0 & 0 & 0 & 1 \\ \frac{IK_1}{a} & \frac{-mbK}{a} & \frac{C_1T}{a} & \frac{-mbC}{a} \\ \frac{-mbK_1}{a} & \frac{K(M_1+m)}{a} & \frac{-mbC_1}{a} & \frac{C(M_1+m)}{a} \end{bmatrix} \begin{bmatrix} X_1 \\ \theta \\ \dot{X}_1 \\ \dot{\theta} \end{bmatrix} + \begin{bmatrix} 0 \\ 0 \\ \frac{mb}{a} \\ \frac{-(M_1+m)}{a} \end{bmatrix} \tau \tag{5.2b}$$

yields the Fundamental Matrix (A) and the Control Effectiveness Matrix (B) where

$$a = m^2 b^2 - I(M_1+m) \tag{5.2c}$$

$$I = I_o + mb^2 \tag{5.2d}$$

The controllability matrix is defined as

$$[P] = \begin{bmatrix} | & | & | & & | \\ B & AB & A^2B & \cdots & A^{n-1}B \\ | & | & | & & | \end{bmatrix} \tag{5.3}$$

A linear, time-invariant system (LTI), as defined in Eq. 5.2a, is controllable if and only if the columns of P span the dimension of the state space representation (i.e. the determinant of P is nonzero for this single input system). The determinant of P is

$$\det(P) = (mbT/a^2)^2 \tag{5.4}$$

Thus, the following conclusions can be made for a single DOF damped structural mode acted on by a pivoted, proof-mass actuator. To be controllable, the structural mode must be elastic ($T > 0$), a reaction mass must exist ($m > 0$) and that mass must be offset from the pivot to generate force ($b \neq 0$). The denominator (a) requires that I, M, m and b be finite. The latter is a trivial result in that the beam's modal mass must not be immovable and the actuator components must allow it to pivot. No restrictions are placed on actuator stiffness and damping or on passive modal damping in the beam.

Since this single structural mode is controllable, even in the absence of passive energy dissipation mechanisms, a mechanism associated with the active actuator must exist which enables dissipation to be introduced.

To identify the source of dissipation, examine the work balance at the actuator. The work performed on a system equals that system's change in energy. The work on the structure's modal mass 'M' is

$$\text{Work} = \int F dx = \int mb^2 \ddot{\theta} \, d\theta \tag{5.5}$$

The work is done as a result of relative motion between the pivoting part of the actuator and structure. This relative motion causes the motor coils to travel through the magnetic field of the permanent magnet thus generating a back EMF proportional to the relative velocity ($\dot{\theta}$).

In steady-state oscillatory motion, the product of this voltage and the motor's command current gives the power transmitted to the system as

$$P = V \cdot I \cdot \cos\varphi \tag{5.6}$$

If the phase (φ) between voltage and current is other than 90° or 270°, some energy is supplied to, or drained from, the structural system. Thus, the presence of the actuator effects a change in system damping by this energy transfer process. When increasing the damping in the system, the controller acts as a generator

converting mechanical energy into electricity which is eventually dissipated through heat. If the phase is exactly 90° or 270°, no energy transfer occurs and the system experiences only a change in stiffness.

Since the work on the structure is equal to the integral of force times the structural displacement, the structure must exhibit motion at the actuator location in order to effect energy transfer. The structural modal mass must therefore be finite; the same requirement derived to insure controllability. Since apparant modal mass is determined through Eq. 5.7, where the mode shape (Ψ) is normalized to the position where the modal mass is desired (actuator location), if the actuator is placed at a node, Ψ cannot be normalized to that location and 'M ' is infinite.

$$M_i = \int_0^L m(x)\, \Psi_i^2(x)\, dx \qquad (5.7)$$

This line of reasoning raises the question of allowable and optimal actuator placement. Clearly, Eq. 5.7 suggests the actuator should not be placed at a node. To maximize the work done on the structure, the force from the actuator should be exerted through the greatest displacement. Since the mode shape Ψ represents the open-loop, spacial variation of displacement of the mode, this function might be used to determine the most effective actuation locations. More rigorous solutions to optimal actuator placement are discussed in Reference 11 and alternative placement criteria are presented in Reference 13. For a single mode, the

actuator would clearly be placed at the location of maximum modal displacement. For multiple mode control, both the sum and product of the squares of the modes might be considered. Figure 5.1a shows the sum of the mode shapes squared for a uniform free-free beam, defined by

$$(1) = \Sigma_{i=1} \psi_i^2 \tag{5.8}$$

and Fig. 5.1b shows the product of the mode shapes squared, defined by

$$(2) = \Pi_{i=1} \psi_i^2 \tag{5.9}$$

Figure 5.1a indicates positions on the beam where displacement is at a minimum and maximum for the combined motion of the modes listed. The zero levels in Figure 5.1b indicate positions on the beam where at least one mode is uncontrollable. Note the relative difficulty in locating actuators for control of the higher modes. For an unrestrained free-free beam, both criteria indicate that for all modes the tip is the best place to locate an actuator, so two of the four actuators will be placed at the tips. Other relative maxima in the actuator effectiveness curves for the higher modes occur at approximately the 0.08 and 0.25 length fractions from the tip. For these experiments, the remaining two force actuators are placed at a quarter of the length in from each tip. The actuator locations are indicated by asterisks at the bottom of Figures 5.1a and 5.1b.

AD-A169 928 DEVELOPMENT OF FINITE ACTIVE CONTROL ELEMENTS FOR LARGE FLEXIBLE SPACE ST.. (U) MASSACHUSETTS INST OF TECH CAMBRIDGE MA SPACE SYSTEMS LAB D W MILLER ET AL. 2/3

UNCLASSIFIED 02 JUN 85 MIT-SSL-6-85 AFOSR-TR-86-0480 F/G 20/11 NL

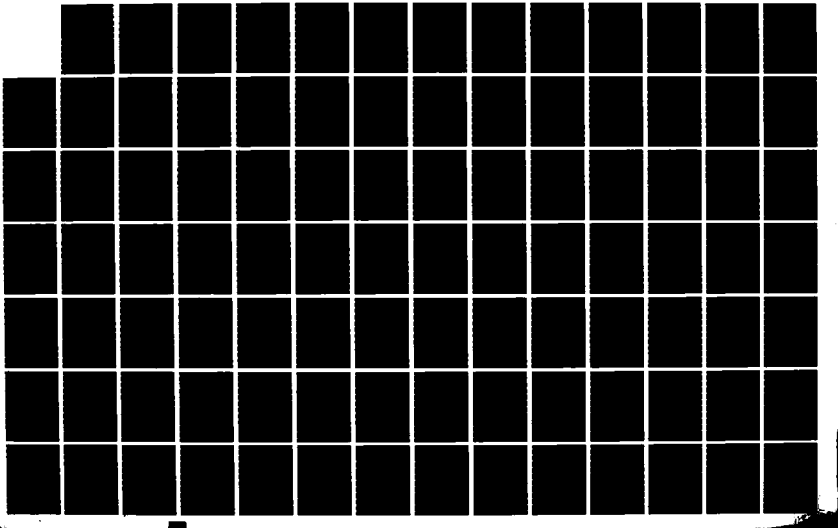

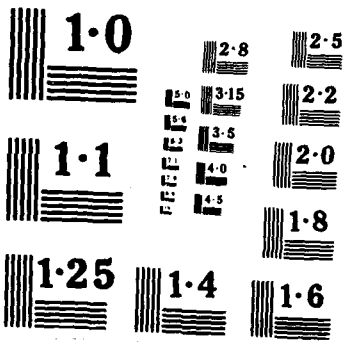
1·0
1·1
1·25
1·4
1·6
1·8
2·0
2·2
2·5
2·8
3·15
3·5
4·0
4·5

Once a controllable system is built and actuators are placed, an investigation can be made into stability limits for various state feedback methods. Several assumptions are made for this analysis. First, these stability limitations will only be derived for a single actuator controlling a single mode using collocated beam and actuator states. Secondly, state estimator dynamics are not considered since states are assumed to be measured directly. Finally, the actuator is assumed to have a frequency that is much lower than the frequency of the mode of interest. In other words, it is a 'weak' actuator not tuned to the frequency of the mode of interest. The model shown in Fig. 2.2 is used. The feedback laws that will be investigated are of the form

$$\tau = -F_1 X_1 - F_2 \Theta - F_3 \dot{X}_1 - F_4 \dot{\Theta} \qquad (5.10)$$

where X_1 and $\dot{X}_1$ are the beam states and Θ and $\dot{\Theta}$ are the actuator states. The discussion will be limited to the rate feedback terms, F_3 and F_4 (i.e. $F_1 = F_2 = 0$).

The most obvious approach to increasing the beam damping is to feed the actuator the collocated velocity of the beam. As seen in the root locus of Figure 5.2a for increasing beam rate feedback, this introduces damping into the high, predominantly beam mode while destabilizing the lower, actuator mode. The opposite is true when only absolute actuator rate is fed back (i.e. the upper beam mode is destabilized and the actuator mode becomes damped). If relative actuator rate is fed back, the system responds as if a passive damper was placed between the beam

and actuator. Thus in the absence of passive damping, feedback of either the absolute beam or absolute actuator rate alone is destabilizing.

Two options are therefore available to stabilize the actuator/beam system. First, if passive damping is present in the actuator, both the lower and upper modes are initially damped as shown by the locations of the open-loop poles in Figure 5.2b. Upon feeding back small amounts of beam rate, the low (actuator) mode will be destabilized, but still have net positive stability due to the passive damping. With further increases in beam rate feedback, the system will become unstable (point B). An experiment based on this single rate feedback will be discussed in Section 5.2. As a second approach, both beam and actuator rate can be fed back, in effect compensating for actuator dynamics. Actuator rate feedback stabilizes the dynamics of the actuator which were destabilized by the use of beam rate feedback, as shown in Fig. 5.2c. Therefore, a combination of both beam and actuator velocity feedback is needed to maintain system stability while generating significant increases in beam damping.

With the four actuators placed at the tips and the quarter length locations, a test was performed using one of these four distinct SISO controllers to demonstrate the stability limitation inherent in single collocated beam rate measurement feedback. The actuator dynamics are compensated through active means in the MISO tests discussed in Section 5.3.

5.2 SINGLE INPUT, SINGLE OUTPUT (SISO) COLLOCATED CONTROLLER

The first test involved controlling individual beam modes by feeding back, to one tip actuator, the corresponding collocated beam velocity. This test was performed to investigate the onset of the instability discussed in the previous section. The tuned frequency of the force actuator was set well below the frequency of the seventh mode. This situation in which the actuator frequency is much less than the beam frequency will hereafter be refered to as a 'weak' actuator case. The closed-loop dynamics of the seventh mode were chosen for investigation so as not to require the weak actuator frequency to be set so low that friction effects in the mechanism dominate its behavior.

As discussed above in Section 5.1, increasing beam rate feedback should monotonically increase the damping in the higher, beam mode and destabilize the lower, actuator mode. At sufficiently high gains, the feedback will overcome the passive damping in the low mode and an instability should appear. This test was run at various negative beam velocity feedback gains. Figure 5.3 shows the time response of the beam acceleration as a result of an initial displacement. The gain is set to that value which first exhibited the low mode instability. In this plot of the accelerometer response, the lightly damped 5.2 Hz beam response initially decays. The very slightly unstable lower mode, which primarily contains actuator motion, eventually drives the beam unstable. This verifies the trend of the root locus analysis performed in Section 5.1 for feedback of beam rate only.

The factor that limited the achievable damping in this single rate feedback case was the occurance of this instability. This can be corrected in two ways: a passive damper can be mounted on the actuator to stabilize the low, 'actuator' mode, or actuator rate feedback can be introduced through feedback of the actuator tachometer signal. The latter method was chosen and a second set of tests was performed.

5.3 MULTIPLE INPUT, SINGLE OUTPUT (MISO) CONTROLLER

The next set of tests used collocated beam and actuator rate feedback to stabilize the low mode instability and thus enable higher levels of active beam mode damping. In these tests, two force actuators were used; one at each end of the beam. Note that although a total of eight state variables were available, beam and actuator rate and position at each tip, each actuator was only fed back its two collocated state measurements. Thus, two independent MISO processors were used. Again, 'weak' actuators were used to control individual beam modes.

Results of tests run on modes seven through fourteen are summarized in Table 5.1. These modes were chosen for investigation since their frequencies were high enough that the actuator friction was again not dominant, and due to a signal-to-noise difficulty in the accelerometer which will be discussed below. Figures 5.4a through 5.11b show the open-loop, free decays and closed-loop, controlled decays of these modes.

Table 5.1 lists the open and closed-loop frequencies and damping ratios, measured using logarithmic decrement methods, for each mode. Figures 5.12a and 5.12b show the results of a frequency sweep of the uncontrolled and controlled beam, respectively. The sweeps were performed at constant feedback gains. These results show, on the average, a factor of 4 to 6 decrease in the forced vibration response of the beam. This is in substantial agreement with the data taken from the transient responses which show an average improvement in damping ratio (ζ) of 7.25.

Two major difficulties arose in these tests. First, at high feedback gains, a system mode at 42 Hz. was driven unstable. With the computers sampling two hundred times a second, 42 Hz. lies near the frequency where the processors must be considered as discrete time controllers. Furthermore, phase shifts due to filter rolloffs also occur in this frequency range causing a further reduction in phase margin (see Table 4.4).

The second difficulty prevented the control of the first six beam modes. At these modal frequencies, the accelerometer signal contained too low of a signal-to-noise ratio. In order to maintain a constant level of accelerometer signal in low modes, the displacement must increase by the square of the frequency ratio between the higher and lower modes. Shaker power and suspension limitations prevented such large amplitude motions of these lower modes. In addition, the actuator frequency of the 'weak' actuator was in close proximity to the modal frequencies of these lower modes. This would require a more complicated state feedback algorithm employing additional displacement feedback.

5.4 TESTS USING PASSIVE VIBRATION ABSORBERS

As described in Chapter 2, passive damping of the beam can be augmented by adding spring-mass-damper passive vibration absorbers. The proof-mass actuators were designed with variable springs and dampers so that they could also fulfill this function. Each actuator was equiped with a variable spring and adjustable damper to allow passive tuning. Tuning refers to the adjustment of passive absorber parameters to achieve some desired system performance. In these tests, absorbers were tuned to various individual beam modes. The performance of the absorbers was assessed in free decay tests and in steady-state sine sweep tests. This section discusses the expected and actual test results along with the probable causes of disagreement and the limitations encountered.

The seventh, eighth and nineth modes of the beam were damped using passive vibration absorbers (Table 4.1). These modes were selected to enable a comparison with results from the active control tests presented in Section 5.3. The first step involves determining the achievable amount of damping using a single absorber tuned to a single mode. From the analysis of Chapter 2, predictions can be made as to the best theoretically achievable performance. The dynamic magnification factor for the magnitude of the beam response at resonance, as a function of modal damping ratio and static response, is

$$\frac{X_1}{\Delta_{ST}} = \frac{1}{2\zeta} \tag{5.11}$$

Equation 2.15, repeated below, presents this same magnification factor as a function of absorber-to-modal mass ratio (β) for the optimally tuned absorber.

$$\frac{X_1}{\Delta_{ST}} = \sqrt{\frac{2+\beta_{*n}}{\beta_{*n}}} \tag{2.15}$$

For these passive tuning techniques, these two equations can be combined to predict the highest achievable modal damping ratio for an otherwise undamped beam

$$\zeta_{OPT} = \frac{1}{2}\sqrt{\frac{\beta}{2+\beta}} \tag{5.12}$$

The model of the pivoted, proof-mass actuator must be put in terms of the vibration absorber of Chapter 2. For this purpose, the absorber arms are assumed massless (I = 0) and the fraction of the absorber mass associated with the nonpivoting base is added to the modal mass of the beam. For the modes tested, Table 5.2 lists the absorber position on the beam, effective modal mass, mass ratio (β), optimal frequency ratio (δ_{OPT}) and predicted maximum modal damping ratio. In each case, the proof mass is 0.165 kg.

An attempt was made to experimentally tune the absorbers to the values shown in Table 5.2, but this attempt encountered certain limitations. In tuning each individual absorber to a

particular mode, a two step iteration was repeated until the best results were obtained. The tuning process started with a 'weak' absorber (low absorber/beam frequency ratio δ). For this weak absorber spring, the damper was adjusted to yield the highest achievable modal damping ratio. Figure 5.13a shows the achieved damping in the eighth mode for such a weak actuator (i.e. for a frequency ratio of δ = 2.8 Hz/8.711 Hz = 0.387). In this case, a tip absorber was tuned to the eighth mode. The next step was to increase the frequency ratio and readjust the damper. This two step iteration was repeated until maximum damping was obtained. Table 5.3 lists the intermediate results of this tuning process (i.e. the largest damping ratios achieved at each frequency ratio for tuning one tip absorber to the eighth mode). The free vibration decays are shown in the corresponding figures.

The two other absorbers, located at the one quarter length and at the other tip, were individually tuned to modes seven and nine, respectively. The achieved modal damping values, for each individual absorber acting alone, are listed in Table 5.4 and Figures 5.14 and 5.15 show the modal free decays. Figure 5.16 shows a frequency sweep through modes seven, eight and nine with one absorber tuned to each mode. This can be compared to Fig. 5.12a for the baseline, open-loop beam response and to Fig. 5.12b for the closed-loop actively controlled beam response. By comparing the analytic predictions of Table 5.2 and the measured results of Table 5.4, it is clear that overall, the tuned absorbers were able to achieve about 40% of the analytically predicted level. Mode eight was as high as 84% while mode nine

was the lowest at 34%.

Unmodeled friction present in the absorbers, the proximity of the absorber to beam nodes and the difficulty of tuning the absorbers close to resonance presented the major problems in performing this portion of the experiment. The effects of friction were twofold. As the frequency ratio was increased towards the optimal, defined in Eq. 2.13, the damper setting needed to create the optimal results decreased (Fig. 5.17a). Above a frequency ratio of $\delta = 0.9$, the damping associated with the friction in the absorber mechanism was greater than that needed to yield the maximum amount of beam damping. The horizontal lines represent the minimum achievable damper levels. These levels are set by the amount of friction in the absorbers. The equivalent nondimensional damping due to the friction was determined by inferring the necessary nondimensional damping needed to produce the highest beam damping ratios achieved in the experiments. The horizontal lines correspond to the absorber tuned to the eighth and nineth modes. Figure 5.17b shows that up to this friction limit, the experimentally achieved damping is in fairly close agreement with the analytic prediction. Discrepencies are due to measurement errors and the fact that the beam possesses some level of material and aerodynamic damping. To compensate for the latter, the open-loop damping ratio from Table 5.1 was added to the analytic prediction curve. Figure 5.18 shows the value of the nondimensional damper (μ) and equivalent absorber damper strength ($\mu\beta$) versus mass ratio. These parameters are defined in Eqs. 2.4a through 2.4h. Equivalent damper strength

increases with mass ratio. This indicates that the absorber dampers are more easily tuned at high mass ratios. For the low mass ratios used in the experiment, as δ approached δ_{OPT} the damping required fell below the minimum set by friction and the experimental results and analytic predictions departed.

Fig. 5.15 shows the free vibration decay for the case where the damping in the vibration absorber is in fact dominated by the friction. The linear decay of the response shown is characteristic of friction damping. A second noticable feature of the frictional damping, as opposed to linear viscous damping, is that at low vibration levels, the friction would seize the motion of the absorber. This eliminates motion across the damper and therefore stops any further damping of the beam motion (Fig. 5.13d). These difficulties can be reduced through the use of a lower friction suspension. However, since all rotational mechanisms contain some friction, this represents a lower limit of the motion amplitude for which such absorber designs are useful.

The proximity of beam nodes to the absorber locations strongly affect the amount of achievable damping (Reference 11). When absorbers are located other than at the tip, the apparant modal mass of the beam is greater causing smaller absorber-to-beam modal mass ratios for a fixed absorber mass. The smaller the mass ratio, the lower the modal damping achievable (Eq. 5.12). A second effect occurs due to the change in the open-loop beam dynamics caused by the addition of the absorber mass. When the concentrated mass of the absorber is added to a beam, nodes in proximity to that mass are drawn towards it causing a reduction in

modal amplitude at the location of the absorber, and a subsequent further increase in the apparant modal mass. For these two reasons, actuators and absorbers, which were placed in the interior of the beam, were less effective than those that were placed at the tips. The former is due to the fundamental physics of the mode shape while the latter can be diminished by reducing the nonpivoting mass of the absorbers, or by using rotational torque absorbers. These arguements as to why absorbers have diminished effectiveness are equally applicable to the selection of locations for active control actuators, which also rely on local beam motion to be effective (Reference 11).

The third difficulty encountered in the experimental implementation of the absorbers stems from the fact that tuned absorbers are very close in frequency to the beam mode. This, along with the fact that the optimal damper setting required (as the frequency ratio δ approaches optimal) decreases, causes absorber motion to become extremely large. In many cases, this response violates small angle approximations in the analysis. Furthermore, the physical constraints of small angle absorber motion are encountered and absorber saturation occurs. Increasing the offset inertia (mb) of the absorber will lower this response amplitude to some extent.

5.5 DAMPING USING ACTIVE ACTUATORS AND VIBRATION ABSORBERS

A final test was performed using a combination of both active feedback and passively tuned absorbers. In this experiment, the actuators located one quarter of the length in from the ends of the beam were tuned to the ninth mode as passive vibration absorbers. At the same time, 'weak' actuators, located at the tips of the beam, were used to actively control the same mode. Figure 5.19d shows the time response results to initial displacement of this configuration. Figures 5.19a, 5.19b and 5.19c are nineth mode free decays for the open-loop, actively controlled and passively damped systems repeated from the previous figures for comparison.

As these two forms of damping were used simultaneously, the problems associated with each were compounded. Limited response amplitude due to insufficient excitation and actuator stiction, prevented accurate analysis of the overall effectiveness of this combined damping scheme. The initial response in Fig. 5.19a is well over an order of magnitude larger than that in Fig. 5.19d. In actuality, the beam has become too heavily damped for the exciting shaker to create a significantly large response displacement. In other words, the beam has become so damped that its response is within the measurement noise and the deadband of the absorbers.

6.0 CONCLUSIONS

The work presented represents the present state of development of the finite element controller. The following is a summary of the goals achieved in this phase of research and the experiments planned for the immediate future.

Throughout this phase of research, all components of the active control system were chosen based upon the criterion that they be capable, in principle, of functioning in the space environment. Several types of electromagnetic actuators were designed and built. Each is capable of inducing force or torque on a structure through acceleration of captive masses. By operating on inertial principles, these devices function independent of the laboratory (earth) frame. Inertial and relative sensors were used to eliminate the need for state measurements relative to the laboratory reference. These space-realizable components were used to control the elastic behavior of a quasi free-free beam.

Active control actuators were built with variable passive dampers and springs to incorporate into these devices the passive damping characteristics typical of passive vibration absorbers. Optimal tuning laws were developed to provide maximum passive damping in a single beam mode and several beam modes. In the latter case, to introduce maximum damping into several modes, the stiffness of the actuator should be tuned to the lowest frequency mode and the actuator damper adjusted for desired response.

Two optimizations were used to design the actuators. First, a sequential optimization was performed which used the vibration absorber tuning laws to maximize passive damping followed by a Linear Quadratic Regulator optimization to select the active feedback gains. Secondly, a simultaneous optimization was performed which used the LQR formulation to derive gains for various passive actuator configurations and an iterative search was used to determine which combined set of passive and active actuator characteristics minimized the quadratic state and control effort cost of the system. Both the sequential and simultaneous optimizations resulted in similar actuator designs implying that the vibration absorber tuning laws can be used to select the passive characteristics of the optimal active control actuator. Finally, optimal actuation locations were determined and simple collocated feedback, distributed control was performed.

An experimental test-bed was designed, for this portion of the research, which exhibits many of the detrimental characteristics of large, flexible space structures. The highly flexible free-free beam possesses a low wave propagation to computation speed ratio in addition to low frequency, large amplitude vibrations. The geometric dimensions resulted in low frequency, closely spaced modes. Yet, the beam has linear properties which were beneficial in developing this first phase of tests.

The combined use and interaction of two zero level and a one level processor was demonstrated in the framework of a finite control element. A robust collocated controller was demonstrated

which performed independently of a system model. Theoretically, vibration absorber damping should achieve 5% critical damping through the addition of 0.5% beam mass. Experimentally, 4.2% critical damping was achieved through the addition of 2.3% of the beam mass. The active control actuators, without vibration absorber characteristics, achieved 2% to 3% critical damping. These actuators, along with the two zero level processors and one component level processor, comprize the present state of the finite control element.

There are three sets of experiments planned for the near future. The first set involves improving the performance of the tests detailed in Chapter 5. This includes improving on some of the techniques used in signal processing, measurement feedback and beam excitation and solving some of the control and friction limitations encountered.

The second set of tests will use the feedback of more collocated, state information to more actuators. In these tests, the actuators will also be tuned as passive vibration absorbers. The microprocessor hardware will be expanded to include seven processors distributed on three levels of control. Tests will be performed which include free decays, frequency sweeps, impact testing and multimode control.

The third set of tests will attempt to exploit the wave propagation behavior of the beam. Controllers will be devised to simulate elastic and viscous foundations to generate propagation cutoff frequencies and damped behavior. The transmissivity and reflectivity of the beam will be passively and actively altered.

Finally, disturbance rejection schemes may be employed to suppress propagating behavior.

Thus far, this research has demonstrated the feasibility of incorporating machine intelligence into the design of space structures. Currently available technology has been used effectively in a space-realizable experiment. Though passive techniques currently exhibit the same performance as active feedback, the problems experienced in the active tests are surmountable. Active control still provides a versatility in design not available through passive methods. Inevitably, the optimal form of structural static and dynamic control will be achieved through a combination of various techniques of which active control will be the most innovative.

REFERENCES

1. Aubrun, J.N., Breakwell, J.A., Gupta, N.K., Lyons, M.G., Marguiles, G., ACOSS FIVE (Active Control of Space Structures) PHASE 1A, Lockheed Missiles & Space Co., Inc., Mar. 80 - Sept. 81.

2. Aubrun, J. N., Marguiles, G., "Low-Authority Control Synthesis for Large Space Structures," Lockheed Palo Alto Research Laboratory, Contract Report on Contract NAS1-14887, May 1982.

3. Bathe, K., *Finite Element Procedures in Engineering Analysis*, Prentice-Hall, Inc., New Jersey, 1982.

4. Carignan, C.R., "Filter Failure Detection for Systems with Large Space Structure Dynamics," S.M. Thesis, M.I.T., 1982.

5. von Flotow, A. H.,"Disturbance Propagation in Structural Networks: Control of Large Space Structures," Ph.D Thesis, Dept. of Aeronautics and Astronautics, Stanford, CA., June 1984.

6. Graff, K. F., Wave Motion in Elastic Solids, Ohio State University Press, 1975.

7. Gupta, N. K., Lyons, M. G., Aubrun, J. N., Marguiles, G., "Modeling, Control and System Identification Methods for Flexible Structures," AGARDograph no. 260.

8. Hertz, T.J., "The Effect of Scale on the Dynamics of Flexible Space Structures," E.A.A. Thesis, M.I.T., 1983.

9. Juang, J.,"Optimal Design of a Passive Vibration Absorber for a Truss Beam," J. Guidance, Control and Dynamics, Nov.-Dec. 1984, p. 733.

10. Kwakernaak , H., Sivan, R., Linear Optimal Control Systems, Wiley-Interscience, New York, 1972.

11. Mills, R. A.,"Active Vibration Control of a Cantilevered Beam: A Study of Control Actuators," 34th Congress International Astronautical Federation, Budapest, Hungary, Oct. 1983.

12. Timoshenko, S., Young, D.H. and Weaver, W. Jr., Vibration Problems in Engineering, Fourth Edition, John Wiley and Sons, New York, 1974.

13. Vander Velde, W. E. and Carignan, C. R.,"Number and Placement of Control System Components Considering Possible Failures," J. Guidance, Control and Dynamics, Nov.-Dec. 1984, p. 703.

14. Ward, B., "Finite Control Elements for a Hierarchic Controller," S.M. Thesis M.I.T., June 1985.

A.0 APPENDIX A: OPTIMIZING THE PASSIVE PARAMETERS OF PASSIVE VIBRATION ABSORBERS AND ACTIVE CONTROL ACTUATORS

This appendix addresses selection of optimal spring and damper values for inertial-reaction devices. Two device types are considered: a strictly passive inertial-reaction vibration absorber, and an active control actuator, which contains passive elements implementing feedback control. The optimal values for the passive components are determined for both devices when mounted to one and two degree of freedom structures.

Three optimizations can be performed. First the passive components of the vibration absorber can be determined based upon the minimization of a weighted quadratic cost. This cost is the temporal integral of state penalties times the response of the system (Case C of Table 2.4). The second optimization involves the simultaneous design of the passive actuator components and active feedback gains using Linear Quadratic Regulator Theory to determine the gains for each set passive actuator components and performing a search through component sets to determine which control actuator components and gains minimize a given cost (Case E of Table 2.4). The third case involves using LQR theory to sequentially derive a set of feedback gains for the optimal passive design developed in Section 2.1.1 (Case D of Table 2.4). The passive and active portions of each design can then be compered. Section A.1 presents the system models used in this analysis. Section A.2 presents parameter optimization using a

quadratic cost, and Section A.3 details the results and conclusions.

A.1 SYSTEM MODELS

Linear models were used for both the control actuator and the passive vibration absorber paralleling those used in Chapter 2. The passive absorber model is shown in Figure A.1a and the control actuator model is shown in Figure A.1b. The actuator or passive absorber was mounted to two separate spring and mass structures. The first structure was a spring-mass oscillator that had a single mode of vibration. The second structure was a spring-mass-spring-mass oscillator with two vibration modes. The frequency ratio between the low and high vibration modes of the second structure was 2.618. This ratio was thought to be small enough to represent two adjacent modes. The mounting location on the single mode structure for the actuator or passive absorber was at the mass (Figure A.2a). The actuator or passive absorber was mounted to the two DOF structure at both the outer mass (Figure A.2b) and at the inner mass (Figure A.2c). Both mounting locations were considered because of different modal influence levels at the two masses. The influence is greater on the low mode at the outer mass and the influence is greater on the high mode at the inner mass. For ease of reference, the systems in Figures A.2a, A.2b, and A.2c will be referred to as System 1, System 20 (outside mount), and System 2I (inside mount),

respectively. System numbers may have a postscript indicating the type of vibration damper being used. A postscript of "a" specifies an active control actuator and a postscript "p" specifies a passive absorber.

The state differential equation describing the motion of System 1 is

$$\dot{x} = Ax + Bu \tag{A.1}$$

where

$$x = \begin{bmatrix} x_1 & x_2 & \dot{x}_1 & \dot{x}_2 \end{bmatrix}^T \tag{A.2}$$

$$A = \begin{bmatrix} 0 & 0 & 1 & 0 \\ 0 & 0 & 0 & 1 \\ -(K+k)/M & k/M & -c/M & c/M \\ k/m & -k/m & c/m & -c/m \end{bmatrix} \tag{A.3}$$

$$B = \begin{bmatrix} 0 & 0 & -1/M & 1/m \end{bmatrix}^T \tag{A.4}$$

and

$$u = 0 \quad \{\text{for passive absorber}\} \tag{A.5a}$$

$$u = -Fx \ \{\text{for active actuator}\}. \tag{A.5b}$$

$$F = \begin{bmatrix} F_1 & F_2 & F_3 & F_4 \end{bmatrix} \tag{A.6}$$

where F are the optimal regulator gains. The following

substitutions were made to Equations A.1 through A.6

$p_o = K/M$ DECOUPLED STRUCTURAL FREQUENCY (A.7a)

$p_a = k/m$ DECOUPLED ABSORBER FREQUENCY (A.7b)

$\delta = p_a/p_o$ ABSORBER/STRUCTURE FREQUENCY RATIO (A.7c)

$\mu = c/(2mp_o)$ NONDIMENSIONAL DAMPING (A.7d)

$\beta = m/M$ ABSORBER/STRUCTURE MASS RATIO (A.7e)

$\Delta = 1/K$ STRUCTURE'S STATIC DEFLECTION (A.7f)

$z(n) = q(n)/\Delta$ NONDIMENSIONAL POSITION (A.7g)

$\dot{z}(n) = \dot{q}(n)/\Delta p_o$ NONDIMENSIONAL VELOCITY (A.7h)

$\ddot{z}(n) = \ddot{q}(n)/\Delta p_o^2$ NONDIMENSIONAL ACCELERATION (A.7i)

$u' = u/(M\Delta p_o^2)$ NONDIMENSIONAL CONTROL FORCE (A.7j)

The resulting demensionless state equations are

$$\dot{z} = A'z + B'u' \tag{A.8}$$

$$z = [\ z_1 \quad z_2 \quad \dot{z}_1 \quad \dot{z}_2\ ]^T \tag{A.9}$$

$u' = 0$ {passive absorber} (A.10a)

$u' = -F'z$ {active actuator} (A.10b)

where

$$A' = \begin{bmatrix} 0 & 0 & 1 & 0 \\ 0 & 0 & 0 & 1 \\ -(1+\beta\delta^2) & \beta\delta^2 & -2\beta\mu & 2\beta\mu \\ \delta^2 & -\delta^2 & 2\mu & -2\mu \end{bmatrix} \qquad (A.11)$$

$$B' = \begin{bmatrix} 0 & 0 & 2\mu & \beta^{-1} \end{bmatrix}^T \qquad (A.12)$$

$$F' = \begin{bmatrix} F'_1 & F'_2 & F'_3 & F'_4 \end{bmatrix}$$
$$= \begin{bmatrix} F_1/K & F_2/K & F_3/Kp_o & F_4/Kp_o \end{bmatrix} \qquad (A.13)$$

where F are the nondimensional optimal regulator gains.

Now the fundamental matrix A' (Equation A.11) and control effectiveness matrix B' (Equation A.12) are functions of dimensionless quantities δ, μ, and β, which represent spring, damper, and mass values of the absorber or actuator. For this investigation the absorber/structural mass ratio β was set to 0.05 and δ and μ were left as the free variables to be used in the optimization. At this β value the absorber mass is much lighter than the structure but large enough to assure noticeable damping in the systems. Substituting the value of $\beta = 0.05$ into Equations A.11 and A.12 yield

$$A' = \begin{bmatrix} 0 & 0 & 1 & 0 \\ 0 & 0 & 0 & 1 \\ -(1+\delta^2/20) & \beta\delta^2 & -2\beta\mu & 2\beta\mu \\ \delta^2 & -\delta^2 & 2\mu & -2\mu \end{bmatrix} \qquad (A.14)$$

$$B' = \begin{bmatrix} 0 & 0 & -1 & 20 \end{bmatrix}^T \qquad (A.15)$$

which is the final nondimensional form of the equations for System 1.

Nondimensionalizing the state equation for System 20 and System 2I and substituting $\beta = 0.05$ yields the following state and control effectiveness matrices:

System 20:

$$A' = \begin{bmatrix} 0 & 0 & 0 & 1 & 0 & 0 \\ 0 & 0 & 0 & 0 & 1 & 0 \\ 0 & 0 & 0 & 0 & 0 & 1 \\ -2 & 1 & 0 & 0 & 0 & 0 \\ 0 & -(1+\delta^2/20) & \delta^2/20 & 0 & -\mu/10 & \mu/10 \\ 0 & \delta^2 & -\delta^2 & 0 & 2\mu & -2\mu \end{bmatrix} \qquad (A.16)$$

$$B' = \begin{bmatrix} 0 & 0 & 0 & 0 & -1 & 20 \end{bmatrix}^T \qquad (A.17)$$

System 2I:

$$A' = \begin{bmatrix} 0 & 0 & 0 & 1 & 0 & 0 \\ 0 & 0 & 0 & 0 & 1 & 0 \\ 0 & 0 & 0 & 0 & 0 & 1 \\ -(2+\delta^2/20) & 1 & \delta^2/20 & -\mu/10 & 0 & \mu/10 \\ 1 & -1 & 0 & 0 & 0 & 0 \\ \delta^2 & 0 & -\delta^2 & 2\mu & 0 & -2\mu \end{bmatrix} \qquad (A.18)$$

$$B' = \begin{bmatrix} 0 & 0 & 0 & -1 & 0 & 20 \end{bmatrix}^T \qquad (A.19)$$

A.2 QUADRATIC COST OPTIMIZATION OF PARAMETERS

Values for the frequency ratio and nondimensional damper will be derived in this section for the models developed in the previous section. The values which minimize a cost based on system response will be chosen as the optimal absorber component settings. In order to evaluate the effectiveness of a particular selection of δ and μ (spring and damper parameters) for a vibration damper design, a technique is needed to analyze the structure plus damper system performance. A commonly accepted method of measuring performance is the quadratic cost of bringing the system to rest from a perturbed state. The quadratic cost is defined by

$$J = \int_{t_o}^{\infty} [z^T W_{zz} z + 2z^T W_{zu} u + u^T W_{uu} u] \, dt \qquad (A.20)$$

where

W_{zz} = state penalty matrix

W_{zu} = cross cost penalty matrix

W_{uu} = control penalty matrix

Optimal full state feedback control (optimal regulator theory) is based on minimization of the cost represented by Eq. A.20. Thus by using the cost formulation to select the passive device parameters, the active feedback gains and passive parameters could

be optimized in a consistent manner. Now this cost formulation will be used to simultaneously optimize both the passive parameters and active gains of the active actuator, then secondly to optimize the passive parameters of the vibration absorber.

Simultaneous optimization of the active actuator parameters for Systems 1a, 20a, and 21a involved an iterative procedure. The iteration had two steps. In the first step a value was selected for δ and μ, and the gain matrix F' for optimal state feedback control was calculated for these fixed values of δ and μ. The feedback gain matrix F' was actually calculated for a discrete time version of the System Equations 9 and 10b. In order that the discrete time feedback gain matrix closely match the continuous time matrix F', a period of $0.01\omega_o$ seconds was used for equation discretization. The second step was to calculate the quadratic cost for a given initial condition using

$$J = z_o^T P z_o \qquad (A.21)$$

P = Riccati solution matrix

z_o = initial condition

The Riccati solution matrix is a output of step one, the feedback optimization step, while the initial condition was a predetermined vector value. This quadratic cost calculation was tabulated. This procedure was repeated over a range of δ and a range of μ and the parameter value pair that resulted in the lowest quadratic cost was defined to be the optimal passive parameter values.

Parameter optimization for the passive absorber parameters in Systems 1p, 20p, and 21p followed the same process as the above actuator parameter optimization described above. Unlike the actuators, passive dampers do not have to go through feedback optimization. Yet the simplest method for calculating quadratic cost was from the Riccati solution matrix (Equation A.21). To take advantage of this fact the control effectiveness matrix B' (Equation A.17 or A.19) was set to zero. With the system unaffected by control action, the optimal feedback gain matrix F' becomes zero, satisfying Equation A.10a. The Riccati solution matrix will still be generated so the quadratic cost could be calculated as before (Eq. A.20). Again, the quadratic costs were tabulated for a range of values for both δ and μ and the value pair that resulted in the lowest cost was defined to be the optimal.

Two important factors in the quadratic optimization process need further discussion: the weighting matrices that were used in the quadratic cost equation (Equation A.20); and the initial conditions used in cost calculations (Equation A.21).

The criteria used to determine the values for the three weighting matricies were as follows. First, for all three systems the energy storage components of the structure were penalized equally. For System 1 the structural energy Es is

$$E_s = Mv_1^2/2 + Kx_1^2/2 \qquad (A.22)$$

Nondimensionalizing Equation A.22 by Equations A.7a-j results in

$$E_s' = (\dot{z}_1^2 + z_1^2)/2 \tag{A.23}$$

$$E_s' = E_s/K \tag{A.24}$$

The structural energy for Systems 20 and 2I in demensional and nondimensional forms are

$$E_s = Mv_1^2/2 + Mv_2^2/2 + Kx_1^2/2 + K(x_2 - x_1)^2/2 \tag{A.25}$$

$$E_s' = (2z_1^2 + z_2^2 - 2z_1z_2 + z_1^2 + z_2^2)/2 \tag{A.26}$$

The coefficients in Equation A.23 (System 1) or in Equation A.26 (Systems 20 and 2I) were incorporated into the state penalty matrix. To avoid extra restrictions in selection of optimal passive parameters or feedback gains, the energy in the vibration damper was not penalized. This is reasonable only if the resulting damper design does not have zero spring and damper values or exhibit extreme resonant peaks. The cross cost state-control penalty matrix was set to zero. Lastly, requirements had to be balanced in the selection of the control penalty had to balance two conflicting desires. On one hand the control penalty should be low enough to allow significant control levels that will, presumably, affect optimal passive parameter selections. On the other hand the control penalty should be high enough to keep control forces small compaired to structural forces (a practical limit for space applications).

The penalty matrices that were used to satisfy the above criteria were

System 1,

$$W_{zz} = \begin{bmatrix} 1 & 0 & 0 & 0 \\ 0 & 0 & 0 & 0 \\ 0 & 0 & 1 & 0 \\ 0 & 0 & 0 & 0 \end{bmatrix} \tag{A.27}$$

$$W_{zu} = [\ 0 \quad 0 \quad 0 \quad 0\ ]^T \tag{A.28}$$

$$W_{uu} = [\ 100\ ] \tag{A.29}$$

System 20 & 21,

$$W_{zz} = \begin{bmatrix} 2 & -1 & 0 & 0 & 0 & 0 \\ 1 & 1 & 0 & 0 & 0 & 0 \\ 0 & 0 & 1 & 0 & 0 & 0 \\ 0 & 0 & 0 & 1 & 0 & 0 \\ 0 & 0 & 0 & 0 & 0 & 0 \\ 0 & 0 & 0 & 0 & 0 & 0 \end{bmatrix} \tag{A.30}$$

$$W_{zu} = [\ 0 \quad 0 \quad 0 \quad 0 \quad 0 \quad 0\ ]^T \tag{A.31}$$

$$W_{uu} = [\ 100\ ] \tag{A.32}$$

(In addition to the above state weighting matrix for Systems 20 and 21 a state weighting matrix with 1, 2, 1, 1 in the first four diagonal elements and 0 elsewhere was also used. The results using either state weighting matrix were very similar so the results of this latter case will not be presented.)

The second factor which requires consideration is the choice of initial conditions. Passive parameters were optimized for the systems under several sets of initial conditions. The initial conditions were all chosen to represent an impulsive energy imparted to the structure when it was at rest. The initial state vector therefore had zero positions and nonzero velocities. The impulse was assumed to have excited only homogeneous structural modes and not the vibration absorber. Table A.1 lists the ten parameter optimization runs that were done and their corresponding initial condition sets. For optimizations 1 and 2 the single structure mass had an initial velocity and all other states were zero. For optimizations 3 through 10 three types of initial conditions were used. The initial energy for optimizations 3 and 4 was in the low frequency mode of the structure. Similarly, the initial energy was in the high frequency mode of the structure for runs 5 and 6. For optimizations 7 through 10 the initial condition was the sum of the previous two initial conditions resulting in equal energy in both structural modes.

A.3 RESULTS AND EVALUATION

Following the procedure outlined in the previous section, optimal values of the passive parameters were determined using an iterative search procedure. The optimal passive parameter values were selected after generating tables of quadratic cost versus values of δ (spring) and μ (damper). Initially, "coarse" cost

tables were formed that spanned a wide range of δ and μ. The δ and μ value pair(s) that produced a cost minima in this table was noted. "Fine" cost tables were formed "around" minima over a narrower range of parameter values to determine more accurately the optimal values for δ and μ. Table A.2a is a "coarse" cost table for System 1p, the single degree of freedom passive vibration absorber only case (optimization 1 in Table A.1), with one minimum at a δ and μ of 0.968 and 0.106. Table A.2b is a "fine" cost table for the same system where the final optimal parameter selection for δ and μ is 0.970 and 0.107 respectively. Similar "coarse" (Tables A.4-13) and "fine" (Tables A.14-23) cost tables were formed for all the optimizations in Table A.1. Only one minimum was found for each optimization. The results of the optimizations are summarized in Table A.3. The optimal values of δ and the damping ratio μ/δ are recorded next to the system and initial condition they were optimized for. Table A.3 is split in two so the results for passive absorbers and active actuators can be compared side by side. The initial condition column of Table A.3 has three symbols: "1", for initial energy in the low stuctural mode only, "H", for initial energy in the high structural mode only, and "=", for initial energy equally distributed between both modes.

The passive component selections for the optimal actuator and passive damper designs have some interesting trends. The resulting natural frequency, $p_a = \delta p_o$ was always near a mode frequency of the structure. The natural frequency for both damper types in System 1 is just below the structural frequency ω_o.

System 20 has two structural modes; a low frequency mode at $0.618\omega_o$ and a high frequency mode at $1.62\omega_o$. When initial energy was only in the low mode the natural frequencies for both actuator and passive damper were just below the low mode frequency. Likewise, the natural frequencys were just below the high mode frequency for initial energy in the high mode only. The similarity between this low or high mode tuning and the tuning in System 1 was probably due to the small damper to structural mass ratio β. This mass ratio keeped the coupling between the two structural vibration modes in System 20 and 21 low. The trend of the damping ratio μ/δ was toward light damping when the initial energy was in one structural mode. The net result of these component selections are vibration dampers that were resonant at a frequency near the structural mode with contained the initial system energy.

Actuator and passive damper designs that resulted from optimizations with equal initial energies in both structural modes had somewhat different characteristics. The natural frequencies of both devices were near the low frequency structural mode. For both systems 20p and 21p the passive absorber Systems 20p and 21p the natural frequencies were close to, but above, the low frequency mode. The natural frequencies of the two actuators were below the low modal frequency but above the natural frequency of the atuator optimized with just low mode initial energy. The more noticable effect of optimizing with both modes initially excited is the substantial increase in the required damping ratios. Also note the difference in damping ratios between System 20p and

System 21p. This difference was the most dramatic effect of different damper mounting locations.

After the ten passive parameter optimizations (see Table A.1) were completed the pole locations for the resulting closed-loop systems were calculated. The pole locations were originally calculated in the Z-plane from the discrete time system equations. The Z-plane poles were translated into S-plane poles by the equation

$$S = \ln(z)/T \tag{A.33}$$

Because of the short sample period of $0.01\omega_o$ sec., these pole locations should not differ appreciably from poles calculated from the continuous time system.

Five additional actuator systems were designed using a sequential design procedure. First the optimal passive parameters were determined. Then with the spring and damper parameters δ and μ constrained to optimal passive absorber values, optimal regulator feedback gains were calculated. This will be refered to as the sequential or suboptimal active actuator design. The closed-loop poles were then calculated as they were for the optimal active actuator and optimal passive absorber systems.

The closed-loop poles for the optimal passive absorber, optimal active actuator, and corresponding suboptimal actuator systems of each row in Table A.3 are plotted in Figures A.3 to A.7. For instance, Figure A.3 shows the pole locations for System 1 (first row of Table A.3) with either an optimal active actuator,

an optimal passive absorber, or a suboptimal actuator with δ and μ constrained to 0.970 and 0.107 (see Table A.2b). It is interesting to observe the closed-loop pole locations of the optimal and suboptimal actuator systems. When the initial energy of the structure is in one mode, the pole locations for both optimal and suboptimal actuator systems are nearly the same (Figures A.3, A.4 and A.5). Similar results are evident for two of the poles of systems 20a and 21a when optimizations were done with both strucural modes having equal initial energies (Figures A.6 and A.7). The one pole that was significantly different in the two actuator systems is dominated by motion of the actuators.

A.4 CONCLUSION

Two important insights can be drawn from these results. First, actuator design might be done sequentially by optimizing the passive components and then optimizing the feedback control law. The differences in system performance between sequential and parallel optimization of passive parameters and control (as judged by pole locations) appear to be small. Second, passive parameters might be selected to damp the lowest mode of significant influence at the damper mounting point. Improving damping over higher modes is achieved by larger damping ratios with the same natural frequency. If both these insights prove correct, a damper design procedure could be fairly straightforward.

B.0 APPENDIX B: INFORMATION TRANSPORT IN STRUCTURES

Explicitly or implicitly, all active control schemes require an accurate plant model to assure effective high authority control. When using classical or output feedback, this model is used implicitly, in that it was necessary for the design of the compensation. In estimator based control, the model is used not only in design, but is explicitly used in the real-time processing. When attempting to devise algorithms for controlling flexible structures, several difficulties arise in the implementation of these control techniques. These difficulties stem from the large number of degrees of freedom exhibited by elastic systems.

For practical purposes, an elastic structure is a complex dynamic system of almost infinite order. The demand created by traditional approaches to high authority control challenge the modeling of this complex, infinite order system in two ways. First, the process requires a system model which includes many degrees of freedom. Secondly, the accuracy of the model must be very good, even in higher order modes. For these reasons, this chapter investigates alternative methods by which the structure can be modeled accurately without the use of high order models.

Specifically, attention will be focused on the transport of information in structures. The two questions that will be addressed are: over what regions of a structure is the information that a force has been applied instantaneously transmitted (i.e.

what is the instantaneous local sphere of influence of a force) and secondly; once that force has established a displacement disturbance; over what range is that disturbance eventually transported in a damped structure.

This chapter contains two discussions of structural modeling to address these two questions of instantaneous and eventual information transport. The first is a discretized elasticity model which would lead to a traditional standing mode model. The second is a travelling wave or wave propagation treatment.

Several options are available to discretize the elastic behavior of a structure. If the structure is sufficiently simple to describe exactly with a partial differential equation then exact flexibility and stiffness influence coefficients can be derived. Alternatively, finite difference operators can be used to discretize the partial differential equation. If the structure is sufficiently complex, finite elements, which exactly or approximately model the behavior of the structure in a piecewise manner, can be employed to discretize the structure. Using the example of a simple uniform beam, these three approaches will be used to delineate the sphere of influence of static, elastic structures.

The second model formulation is related to the propagating transportation of information in a structure. Structural response can be treated in a standing wave fashion, where the lag between disturbance and response is infinitesimal, or treated using a wave propagation approach. The factor that determines which approach is more applicable is the relative propagation to decay times of

the disturbance. In other words, are the group velocities slow enough, or the structure large enough, that the controller can dissipate the propagating waves before they reflect and reinforce (or constructively interfere) to generate a standing wave motion?

The motivation for studying the information transport arguments is to understand the analytic structural mechanics basis for spacially discretizing the control problem into actively controlled elements or components, much like the structural analysis problem is discretized into finite elements. If the control of large, flexible structures can be performed using an assemblage of controlled elements, several advantageous features would result. First, the controller would exhibit robust behavior because the complex system model would simply be a combination of many simpler, theoretically more accurate models which reflect the principles involved in basic, local structural behavior. Secondly, implementation of the structural controller could parallel the construction of the space structure in a building block fashion. Thirdly, the real-time computational task would be significantly reduced since the control response can be computed on either a local or component level, and a higher or global level, and the matrices involved in the global level would be expected to be sparse.

B.1 DISCRETIZATION OF LOCAL ELASTIC BEHAVIOR

In considering the extent of instantaneous transport of information in a discretized structure, one could consider coupling in the three structural dynamic matrices. However, it is well known in finite element modeling that simple diagonal, lumped mass models give results comparable to more fully populated, consistant mass matrices. Furthermore, from first principles, it is the localized inertia which effects the dynamics of a structure. Thus, if the generalized coordinates are chosen in an appropriate way, the coupling in a structure can be largely eliminated from the mass matrix. Since the coupling in the structural damping matrix is a reflection of that in the stiffness matrix, a study of the real stiffness matrix will be sufficient to identify the sphere of influence and coupling patterns present in a structure.

In studying this coupling, finite elements, finite differences and flexibility influence coefficients will be examined. See Reference 3 for basic theory behind finite element analysis. The governing equation for the static response of a structure, using any of these discretization methods, is

$$\{q\} = [C]\{Q\} \tag{B.1a}$$

$$\{Q\} = [K]\{q\} \tag{B.1b}$$

In these matrix equations, C is the flexibility matrix, K is the

stiffness matrix, q is the generalized displacement vector and Q is the generalized force vector. When using a discrete method, the structure is conceptually divided into segments, areas or elements whose boundaries occur at nodes. The generalized displacements and forces are defined to occur at these nodes (Fig. B.1). The fineness of the discretization and the number of allowable nodal displacements determine the number of degrees of freedom and therefore the order of the matrices in Eqs. B.1.

This stiffness matrix can be constructed using several methods. Construction by flexibility influence coefficients, finite difference operators and finite elements will be discussed. The characteristics of each formulation will be compared and the implication on information transport, analyzed.

The flexibility influence coefficient matrix is formed for a constrained structure by combining vectors which contain the displacements at all of the i^{th} locations due to a unit load at the j^{th} location. By computing the vector for a load at each j^{th} location, a populated flexibility matrix results. The flexibility influence coefficient matrix will, in general, be fully populated, because all i^{th} locations displace when a force is placed at any j^{th} location. However, the flexibility matrix is not the appropriate representation of the structure's elasticity to consider when addressing the assessment of spheres of influence for the control problem. The control problem is not posed as: given a force at A, how will it affect the structure. Rather, the control problem is posed as: given a required response at B, what forces must be applied to achieve it. This more closely parallels

the function of the stiffness influence coefficient matrix.

The stiffness matrix is the inverse of the flexibility matrix. Eq. B.2 gives the Bernoulli Euler differential equation governing static, elastic beam bending where F(x) is the distributed force, w is the transverse displacement, E is the modulus of elasticity and I is the bending moment of inertia.

$$F(x) = \frac{d^2}{dx^2}\left[EI(x) \frac{d^2 w(x)}{dx^2} \right] \tag{B.2}$$

Using this governing differential equation, the stiffness matrix, derived by inversion of the flexibility matrix for a uniform clamped-clamped beam with nine internal translational degrees of freedom (ten "elements") is

$$[K] = \begin{bmatrix} \cdots & 0.344 & -0.092 & 0.025 & -0.007 & 0.002 \\ \cdots & 1.206 & 0.323 & -0.087 & 0.023 & -0.007 \\ \cdots & 4.478 & -1.200 & 0.322 & -0.087 & 0.025 \\ \cdots & -10.708 & 4.477 & -1.200 & 0.323 & -0.092 \\ & 14.354 & -10.708 & 4.478 & -1.206 & 0.344 \\ & & 14.355 & -10.714 & 4.500 & -1.286 \\ & & & 14.377 & -10.794 & 4.798 \\ & & \text{SYMM} & & 14.675 & -11.907 \\ & & & & & 18.831 \end{bmatrix} \tag{B.3}$$

A moderately large number of "elements" was chosen to reduce the effect of boundary conditions at the internal nodes. This influence coefficient method yields an exact discrete solution, within the limitations of beam theory, but is restricted to simple structures.

Finite diffence operators provide an alternative approach to approximate discretization of the governing differential equation

(Eq. B.2). Assuming constant EI, finite difference operators can be used to approximate the fourth derivative spatial dependence of transverse displacement. The lowest order difference operator for this equation is second order accurate

$$\frac{d^4w(x)}{dx^4} = q_{-2} - 4.0q_{-1} + 6.0q_o - 4.0q_1 + q_2 \qquad (B.4)$$

where the q's are the w(x) displacements at the nodes. Table B.1 lists appropriate fourth order operators of increasing truncation orders and illustrates the relative magnitude of the terms in each. These FD operators are approximate discrete representations of the fourth derivative using displacements at internal locations. The effects of boundary conditions are not yet included. A portion of a resulting stiffness matrix, using the second order accurate FD operator, is

$$[K] = \frac{EI}{l^3}\begin{bmatrix} \vdots & & & & & & \vdots & \\ \cdots -4 & 6 & -4 & 1 & 0 & 0 & 0 & \cdots \\ 1 & -4 & 6 & -4 & 1 & 0 & 0 & \\ 0 & 1 & -4 & 6 & -4 & 1 & 0 & \\ 0 & 0 & 1 & -4 & 6 & -4 & 1 & \\ 0 & 0 & 0 & 1 & -4 & 6 & -4 & \\ 0 & 0 & 0 & 0 & 1 & -4 & 6 & \\ \cdots 0 & 0 & 0 & 0 & 0 & 1 & -4 & \cdots \\ \vdots & & & & & & \vdots & \end{bmatrix} \qquad (B.5)$$

Note that the exact stiffness matrix (Eq. B.3), although diagonally dominant, is fully populated. The approximate stiffness matrix is banded. Thus, for identical discretization mesh sizes, stiffness matrices derived using FD operators, because

of their sparseness, require less computation for inversion than those derived using flexibility influence coefficient methods. But, the FD operators do not provide the same degree of accuracy.

In both the stiffness influence coefficients and finite difference operator formulations, the relative magnitudes of the stiffness matrix entries in a given column indicate several important trends. Recall that a column of the stiffness matrix is the set of forces necessary to create a unit displacement at the diagonal, and zeroes elsewhere. Fig. B.2a compares the distribution of magnitude of the terms in one column in the interior of the stiffness matrix derived using fourth derivative spatial finite difference operators of different truncation errors. The entries are shown with reference to the diagonal entry. Fig. B.2b overlays the central column of the stiffness matrix, derived using flexibility influence coefficients (Eq. B.3), with a sixth order accurate, fourth derivative finite difference operator.

In each curve of both figures (Figs. B.2a and B.2b), the symbols indicate the relative elastic influence of a force at each nodal location on the location represented on the diagonal. The influence of the two adjacent forces is obviously important. At a position three node points away, the influence of a force is less than ten percent of the influence of a force at the diagonal position. At a position five node points away, the influence of a force is almost insignificant. This rolloff is a measure of the relative effectiveness of noncollocated forces in influencing static, elastic behavior.

Thus, the following observations can be made on the bandedness of the stiffness matrix when transverse displacements are the only deflections represented:

A. When the elasticity is represented exactly (by stiffness influence coefficients) the stiffness matrix is not banded, but is diagonally dominant. At least two off diagonal terms must be maintained, but certainly not more than four or five, in any truncation.
B. When the elasticity is represented approximately (by FD approximations to the governing differential equation) the stiffness matrix is banded. The width of the band depends on the order of the FD approximation. At a minimum, a second order accurate approximation is necessary (two off diagonal terms). Rarely in finite difference calculation is more than a fourth order accurate scheme (three off diagonal terms) used.

A third approach to the discretization of Eq. B.2 uses finite elements. A two node finite element is show in Fig. B.3. For a uniform beam, the static equations of Bernoulli Euler beam theory can be satisfied on the interior of the element by a third order polynomials used as interpolation functions for this element. Thus, this formulation is exact and is the same as would result by using flexibility influence coefficients if translations and rotations were the generalized displacements. The corresponding element stiffness matrix is

$$\begin{bmatrix} Q_1 \\ Q_2 \\ Q_3 \\ Q_4 \end{bmatrix} = \frac{EI}{L^3} \begin{bmatrix} 12 & 6L & -12 & 6L \\ 6L & 4L^2 & -6L & 2L^2 \\ -12 & -6L & 12 & -6L \\ 6L & 2L^2 & -6L & 4L^2 \end{bmatrix} \begin{bmatrix} q_1 \\ q_2 \\ q_3 \\ q_4 \end{bmatrix} = [K]_{ele}\{q\} \qquad (B.6)$$

Assembling these elements, as shown in Fig. B.1, yields the highly banded stiffness matrix

$$[K] = \frac{EI}{L^3}\begin{bmatrix} 12 & 6L & -12 & 6L & 0 & 0 & 0 \cdots \\ 6L & 4L^2 & -6L & 2L^2 & 0 & 0 & 0 \\ -12 & -6L & 24 & 0 & -12 & 6L & 0 \\ 6L & 2L^2 & 0 & 8L^2 & -6L & 2L^2 & 0 \\ 0 & 0 & -12 & -6L & 24 & 0 & -12 \\ 0 & 0 & 6L & 2L^2 & 0 & 8L^2 & -6L \\ 0 & 0 & 0 & 0 & -12 & -6L & 24 \cdots \\ \vdots & & & & & \vdots & \end{bmatrix} \qquad (B.7)$$

The reason the finite element stiffness matrix, which is exact in this case, is strictly banded, as opposed to the exact stiffness influence coefficient matrix which is only diagonally dominant, is that the FE formulation includes rotational degrees of freedom at the nodes. The terms in a column of the stiffness influence coefficient matrix are the forces required, at each location, to create a unit displacement at the i^{th} location and zero displacement at all other nodal locations. Figure B.4 graphically represents the distribution of nodal forces. At all nodes other than that exhibiting unit displacement, displacement is zero but slope is nonzero. Thus, the vector is fully populated.

Figure B.5a and B.5b illustrate the same situation for the finite element formulation with generalized nodal displacements of displacement and rotation and generalized nodal forces of force and torque. By the definition of the columns of a stiffness matrix, displacement and rotation are zero at locations adjacent to the unit displacement position. In a flexural structure, if the displacement and slope are zero at the adjacent node, the structure is stress free beyond these adjacent locations and the

corresponding stiffness terms are zero. Therefore, if a certain nodal static shape is desired between a pair of nodes, an exact formulation, which includes only translational displacements, requires that the structure be influenced at all nodal locations. However, with a formulation that includes both translational displacements and rotations, the availability of control forces and torques reduces the required actuation effort to the node of interest and the two adjacent nodes. The following observation can therefore be made on the bandedness of the stiffness matrix when transverse displacements and rotations are the deflections represented:

C. Even when the elasticity is represented exactly, the stiffness matrix is banded.

There are certain implications of the effect of this bandedness on controller formulations. Collocated control uses sensors to create control commands for actuators located at the same position. In other words, local information is used locally. The argument above regarding the bandedness can be interpreted in the following way: the further away an actuator is from a particular location, the less ability it has in influencing elastic behavior at that location. Thus, a slight generalization of collocated control to include feedback amongst adjacent nodes may be a natural way of dividing the control problem.

B.2 WAVE PROPAGATION MODEL FORMULATION

An understanding of wave propogation models can provide further insight which may be exploitable in the formulation of a structural controller. A wave propogation model is simply an alternate view of a standing wave representation. If the transverse motion of a beam is characterized by an isolated wave packet propagating with some finite phase velocity, sensors on those segments of the beam not moving need not be monitored. The existance of an isolated wave packet is particularly noticeable during the early stages of the generation of standing wave motion. A discussion of wave propagation can be found in Reference 6 and wave propagation applied to the modeling and control of large space structures can be found in Reference 5.

Both standing and propagating wave formulations are obtained from the same mathematical model of the structure. The equation governing the transverse motion of a thin Bernoulli Euler beam is

$$\frac{d^4w}{dx^4} + \frac{1}{a^2}\frac{d^2w}{dx^2} = \frac{1}{m(x)}F(x,t) \qquad \text{(B.8a)}$$

where

$$a^2 = \frac{EI(x)}{m(x)} \qquad \text{(B.8b)}$$

For the homogeneous case an allowable solution, corresponding to rightward and leftward travelling waves, is

$$w(x,t) = A\,[\,\sin(kx-\omega t) + \sin(kx+\omega t)\,] \qquad \text{(B.9a)}$$

Through angle summation identities, Eq. B.9a can be transformed into Eq. B.9b which gives the separation of variable solution typical of standing wave motion.

$$w(x,t) = 2\,A \sin kx \cos\omega t \qquad \text{(B.9b)}$$

For further analysis, the more generalized Timoshenko beam model is used. Eqs. B.10a and B.10b are the governing equations where G and κ are the shear modulus and shape factor, respectively.

$$\rho A \frac{\partial^2 w}{\partial t^2} = \kappa GA \left[\frac{\partial^2 w}{\partial x^2} - \frac{\partial \varphi}{\partial x} \right] \qquad \text{(B.10a)}$$

$$\rho I \frac{\partial^2 \varphi}{\partial t^2} = EI \frac{\partial^2 \varphi}{\partial x^2} + \kappa GA \left[\frac{\partial w}{\partial x} - \varphi \right] \qquad \text{(B.10b)}$$

The section coordinates are transverse displacement (w) and cross sectional rotation (φ). Several interesting conclusions can be drawn from the analysis of propagating disturbances in a damped Timoshenko beam presented in Reference 8.

In the analysis performed in Reference 8, damping is modeled as complex extension and shear modulus:

$$E = E(1 + i\gamma) \qquad \text{(B.11a)}$$

$$G = G(1 + i\gamma) \tag{B.11b}$$

The damping contribution from extensional and shear effects is assumed identical and small. With the introduction of damping, a characteristic length for dissipation can be defined which corresponds to the length over which a wave has traveled when its amplitude has decayed to about 37% (1/e) of the original amplitude (i.e. the length traveled in one damping time constant). This dissipation characteristic length, as a function of wavelength and beam damping at resonance, is

$$L = \frac{\lambda}{4\pi\varsigma}\left[\sqrt{1 + 4\varsigma^2} + 1\right] \approx \frac{\lambda}{2\pi\varsigma} \tag{B.12}$$

where

λ is wavelength

ς is critical damping ratio

Consider the implication of this relationship on the propagation of a disturbance in a damped structure. Immediately after a force impulse is exerted on a structure, waves travel along the structure, reflect and interfere with waves traveling in the opposite direction until a steady-state motion is achieved. If the structure is damped, these waves can be significantly dissipated before a large steady-state motion occurs. Fig. B.6 is a plot of the ratio of the dissipation characteristic length to

wavelength as a function of damping ratio, defined in Eq. B.12. If a particular motion exhibits a damping ratio of $\varsigma = 0.707$ ($\text{Log}(\varsigma) = -0.15$) during free decay, a traveling wave, at the same frequency, will decay to within 37% of its original magnitude in less than 0.31 wavelengths (At this value of damping ratio, Fig. B.6 gives the distance traveled in one time constant to be $L/\lambda = 0.3075$ ($\text{Log}(0.3075) = -0.5122$)). To be less than 5% of original amplitude, the wave must have propagated for three time constants and three dissipation characteristic lengths, or 0.93 wavelengths. Thus, in less than one wavelength, a wave propagating in a structure with $\varsigma = 0.707$ will effectively disappear!

The wavelengths of interest in a free-free beam are those of the free-free normal modes, since their's is the motion which is most easily generated. Fig. B.7 shows the fraction of beam length travelled for a modal wave, starting at one end, to decay to within 5% of its original magnitude (i.e. three dissipation characteristic lengths). These curves are functions of modal damping ratio. Modes 1, 2, 3, 10, 20 and 50 are represented. The portion of a curve below the horizontal reference line (i.e. below $\text{Log}(3L/\text{Beam Length}) = 0.0$) represent damping ratios for which that mode fails to travel one length of the beam before its amplitude has decreased to less than 5% of its original. One length of travel occurs at $\varsigma = 0.955$ for the first mode, $\varsigma = 0.477$ for mode two, $\varsigma = 0.318$ for mode three, 0.095 for mode ten, $\varsigma = 0.047$ for mode twenty and $\varsigma = 0.019$ for mode fifty. It is therefore reasonable to expect that high frequency disturbances will not propagate the length of the structure when a reasonable amount of

passive damping (1-2%) is present. Lower modes may not propagate the length of the structure if higher levels of active damping are present.

Table 2.1: Eigenvectors for Two DOF Model for a Mass Ratio of β = 0.02

Frequency Ratio	Mode Number	Inner Mass	Outer Mass	Relative Motion Across Damper
0.1000	1	1.0	4950.00	4949.00
	2	1.0	- 0.01	1.01
0.9804	1	1.0	8.74	7.74
	2	1.0	- 5.72	6.72
10.0000	1	1.0	1.01	0.01
	2	1.0	-49.51	50.51

Table 2.2: Parameter Values for Tuning to the Low and High Mode of a Two Mode Structural Model

Mode (N)	1	2
$\beta_n = M_n/M_o$	1.3820	3.6180
$\beta = M_3/M_o$	0.0276	0.0724
$\beta_{*n} = M_3/M_n$	0.0200	0.0200
$\delta_{*n_{OPT}}$ Optimal Frequency Ratio Based on β_{*n}	0.9804	0.9804
γ_n Modal Frequency	0.6180	1.6180
δ_{OPT} Optimal Frequency Ratio Based on β	0.6060	1.5863

Table 2.3; Eigenvectors and Frequencies for Different Absorber Frequency Ratios. (Three DOF Model)

Absorber Frequency Ratio	Mode	Modal Frequency	Eigenvector of Mass		
			1	2	3
0.1000	1	0.100	0.0003	0.0006	1.0000
	2	0.618	- 23.0044	- 37.2171	1.0000
	3	1.618	421.9374	-260.8053	1.0000
0.6060	1	0.570	0.0667	0.1150	1.0000
	2	0.857	- 0.1108	- 0.1738	1.0000
	3	1.619	9.8783	- 6.1374	1.0000
1.1000	1	0.609	0.4256	0.6932	1.0000
	2	1.112	- 0.0289	- 0.0221	1.0000
	3	1.623	1.8538	- 1.1780	1.0000
1.6057	1	0.611	0.5257	0.8552	1.0000
	2	1.553	- 0.1582	0.0650	1.0000
	3	1.693	0.1287	- 0.1114	1.0000
2.1000	1	0.611	0.5628	0.9152	1.0000
	2	1.604	- 0.7262	0.4164	1.0000
	3	2.141	0.0153	- 0.0396	1.0000
20.0000	1	0.612	0.6146	0.9991	1.0000
	2	1.612	- 1.6599	0.9935	1.0000
	3	20.275	0.0001	- 0.0277	1.0000

Table 2.4: Actuator Design Cases Studied in Chapter Two and Appendix A.

	Steady State Minimax	Pole Placement	Minimum Quadratic Cost
Passive Vibration Absorber only	Section 2.1.1 (A)	Section 2.1.2 (B)	Section 2.1.3 (C)
Sequential Choice of Passive Actuator Design and Active Feedback Gains *	Section 2.3 (D) (Section 2.1.1 plus Appendix A.2)	not performed	Section 2.3 (Appendix A.2)
Simultaneous Choice of Passive Actuator Design and Active Feedback Gains *	not performed	not performed	Section 2.3 (E) (Section 2.1.3 plus Appendix A.2)

* Feedback gains derived using LQR formulation

Table 4.1; Modal Characteristics of a Free-Free Beam.

E =	15.9×10^{6} lbs/in^{2}	1.090×10^{12} Nt/m	Young's Modulus
I =	0.0009766 in^{4}	4.065×10^{-10} m^{4}	Area Moment of Inertia
m =	0.007329 slugs/in	4.120 kg/m	Mass per Unit Length
l =	288.0 in	7.32 m	Length
b =	4.0 in	0.1016 m	Width
t =	0.125 in	0.003175 m	Thickness
M =	2.10 slugs	30.7 kg	Total Mass

Mode	Modal Frequency w/4 actuators	Modal Mass wo/actuators For Unit Displacement		Group Velocity wo/actuators
#	Experimental (Hz)	At The Tip (Kg)	At The 1/4 Point (kg)	Analytic (m/sec)
1	0.33	7.61	694.81	8.9
2	0.63	7.61	21.02	17.8
3	1.06	7.61	18.99	26.7
4	1.88	7.61	112.96	35.6
5	2.77	7.45	96.91	44.5
6	3.76	7.49	17.39	53.4
7	5.23	7.51	17.54	62.3
8	6.70	7.53	102.33	71.2
9	8.20	7.55	103.31	80.1
10	10.06	7.56	17.74	89.0
11	12.44	7.57	17.72	97.9
12	14.27	7.58	103.51	106.8
13	16.36	7.59	103.61	115.7
14	19.38	7.59	17.77	124.6
15	21.98	7.60	17.78	133.5
16	22.37	7.60	103.83	142.4

Table 4.2; Force Actuator Specifications and Components.

Maximum Actuator Force	3.0 Nts.
Actuator Mass wo/Proof-Mass	0.550 Kg.
Proof-Mass Mass (1)	0.165 Kg.
Arm Length	0.127 m
Motor Resistance	5.000 Ohms
Motor Inductance	1.760 mH
Motor's Peak Amperage	4.920 Amps.
Motor's Peak Voltage	19.10 Volts
Torque Constant	35.70 mN m/Amp
Peak Stall Torque	173.0 mN m
Field Magnet	Samarium-Cobalt
DC Motor	Pittman Corp. Model # 7214
Flexural Spring	Adjustable
Damper Adjustable	Airpot, Inc. Model # S95A1.5Y2
Displacement Transducer	See Table 4.4
Velocity Transducer	See Table 4.4
Current Source	EG&G Torque System 110 Watt Model # PA-223

Table 4.3; Sensor Specifications.

	Accelerometers	Tachometers	Potentiometers
Company:	Endevco	Inland Motor	Maurey
Quantity:	4	4	4
Type:	Piezoresistive	A	25,000 Ohms
Model #:	2262-25	TG-0702	SA 200-M608
Range:	+/- 25 g	+/- 363 rad/sec	+/- 178 Degs
Sensitivity:	27.8 mV/g	0.26 V/rad/sec	0.33 V/Deg
Resonant Frequency:	2.5-2.8 KHz	-	-

Table 4.4: Signal Processing Equipment Specifications.

	Anti-Aliasing Filters	Smoothing Filters	Voltage Amplifiers
Type:	Sallen-key	Sallen-Keye	Instrumentation
Output Voltage Range:	+/- 10 V	+/- 10 V	+/- 10 V
Selectable Gains:	-	-	x 10, 50, 100, 200, Variable
Corner Frequency:	700 Hz	100 Hz	-
Damping Ratio:	0.7071	0.7071	-

Table 5.1; Open and Closed-Loop Characteristics of Controlled Modes.

Mode	Freq (Hz.) O.L.	C.L.	Damping Ratio O.L.	C.L.	Fractional Change In Damping Ratio C.L./O.L.
7	5.2	5.1	.0059	.0185	3.14
8	6.7	6.7	.0024	.0200	8.33
9	8.3	8.2	.0033	.0216	6.55
10	10.3	10.3	.0046	.0165	3.59
11	12.5	12.3	.0025	.0215	8.60
12	14.5	14.5	.0015	.0284	18.90
13	16.5	16.5	.0081	?	?
14	19.8	19.5	.0069	.0113	1.64
Ave:			.0044	.0197	7.25

.0197/0.0044=4.48

O.L. = Open-Loop
C.L. = Closed-Loop

Table 5.2; Analytic Results for Optimally Tuned Vibration Absorber.

Mode	Absorber Position	Effective Modal Mass (Kg.)	Absorber/ Modal Mass Ratio	Calculated Optimal Frequency Ratio (Eq. 2.13)	Calculated Modal Damping Ratio (Eq. 5.12)
7	L/4	18.089	0.009	0.991	0.034
8	TIP	8.081	0.020	0.980	0.050
9	TIP	8.096	0.020	0.980	0.050

Table 5.3; Experimental Vibration Absorber Results for 8th Mode Using a Tip Absorber at Various Frequency Ratios.

Absorber/ Beam Frequency Ratio	Damping Ratio	Fractional Increase in Damping Ratio	Figure
(Baseline)	0.0024	----	5.5a
0.387	0.0031	1.29	5.13a
0.493	0.0082	3.42	5.13b
0.671	0.0117	4.88	5.13c
0.846	0.0300	12.50	5.13d
0.884	0.0420	17.50	5.13e

Table 5.4; Summary of Experimental Vibration Absorber Results for Modes Tested.

Mode	Absorber Position	Frequency Ratio	Untuned Damping Ratio	Tuned Damping Ratio	Fractional Increase in Damping Ratio	Figure
7	L/4	0.859	0.0059	0.0120	2.03	5.14
8	Tip	0.884	0.0024	0.0420	17.50	5.13e
9	Tip	0.864	0.0033	0.0170	5.15	5.15
Ave:			0.0039	0.0237	8.23	

Mode	Ratio of Experimental Damping Ratio to Analytic Damping Ratio
7	0.36
8	0.84
9	0.34
Ave:	0.41

Table A.1: Parameter Optimization: Initial Conditions.

Opt. #	System	Initial Condition (z_o) z_1	$\dot{z}_1$	z_2	$\dot{z}_2$	z_3	$\dot{z}_3$
1	1p	0	1.000	0	0.000	-	-
2	1a	0	1.000	0	0.000	-	-
3	20p	0	1.000	0	1.618	0	0.000
4	20a	0	1.000	0	1.618	0	0.000
5	20p	0	-1.618	0	1.000	0	0.000
6	20a	0	-1.618	0	1.000	0	0.000
7	20p	0	-0.618	0	2.618	0	0.000
8	20a	0	-0.618	0	2.618	0	0.000
9	2Ip	0	-0.618	0	2.618	0	0.000
10	2Ia	0	-0.618	0	2.618	0	0.000

Table A.2: Quadratic Cost Versus Frequency Ratio (δ) and Nondimensional Damper (μ). System 1p with $z = [\ 0.0 \quad 0.0 \quad 1.0 \quad 0.0\ ]^T$

a) δ values	μ values 0.07000	0.08607	0.10580	0.13010	0.16000
0.750	31.650	26.940	23.380	20.820	19.150
0.852	16.730	14.800	13.510	12.790	12.620
0.968	9.654	9.045	8.825*	8.984	9.528
1.100	20.820	18.130	16.210	14.990	14.410
1.250	69.070	57.400	48.140	40.940	35.520

b) δ values	μ values 0.10200	0.10470	0.10740	0.11010	0.11300
0.960	8.867	8.865	8.860	8.863	8.870
0.965	8.847	8.837	8.833	8.836	8.844
0.970	8.837	8.827	8.824*	8.827	8.835
0.975	8.847	8.837	8.833	8.836	8.844
0.980	8.878	8.867	8.862	8.865	8.872

* minimum

Table A.3: Optimal Passive Parameters.

System	Initial Condition	Vibration Damper Type: Passive Absorber δ	Passive Absorber μ/δ	Active Actuator δ	Active Actuator μ/δ
1		0.970	0.1110	0.920	0.0802
20	L	0.605	0.0950	0.540	0.0528
20	H	1.570	0.0573	1.540	0.0377
20		0.690	0.5130	0.576	0.0851
2I		0.630	0.2510	0.602	0.0525

Table A.4: "COARSE" Quadratic Cost Table. Cost Map, System 1p (Passive Vibration Absorber)

Initial State Vector = $[0. \quad 0. \quad 1. \quad 0.]^T$

μ VALS	0.07000	0.08607	0.10580	0.13010	0.16000
δ VALS					
0.7500	31.650	26.940	23.380	20.820	19.150
0.8522	16.730	14.800	13.510	12.790	12.620
0.9682	9.654	9.045	8.825	8.984	9.528
1.1000	20.820	18.130	16.210	14.990	14.410
1.2500	69.070	57.400	48.140	40.940	35.520

Table A.5: "COARSE" Quadratic Cost Table. Cost Map, System 1a (Control Actuator)

Initial State Vector = $[0. \quad 0. \quad 1. \quad 0.]^T$

μ VALS	0.04000	0.05264	0.06928	0.09118	0.12000
δ VALS					
0.7500	7.095	7.056	7.035	7.055	7.151
0.8522	6.283	6.243	6.221	6.244	6.350
0.9682	6.224	6.177	6.145	6.154	6.243
1.1000	7.393	7.340	7.300	7.293	7.355
1.2500	10.370	10.310	10.260	10.230	10.260

Table A.6: "COARSE" Quadratic Cost Table. Cost Map, System 20p (Passive Vibration Absorber)

Initial State Vector = $[0. \quad 0. \quad 0. \quad 1. \quad 1.618 \quad 0.]^T$

μ VALS	0.0330	0.0435	0.0575	0.0758	0.1000
δ VALS					
0.5000	217.80	174.80	145.50	127.40	119.20
0.6300	81.00	71.23	66.96	67.87	74.03
0.7937	828.90	638.70	497.00	393.70	321.30
1.0000	4463.00	3402.00	2588.00	1974.00	1517.00
1.2600	0.170E+05	0.123E+05	9468.00	7205.00	5479.00
1.5870	0.577E+05	0.414E+05	0.297E+05	0.227E+05	0.172E+05
2.0000	0.124E+06	0.104E+06	0.800E+05	0.687E+05	0.511E+05

Table A.7; "COARSE" Quadratic Cost Table. Cost Map, System 20a (Control Actuator)

Initial State Vector = $\{0. \quad 0. \quad 0. \quad 1. \quad 1.618 \quad 0.\}^T$

μ VALS	0.01000	0.01732	0.03000	0.05196	0.90000
δ VALS					
0.5000	32.83	32.70	32.65	33.01	34.81
0.6300	35.14	34.99	34.86	35.02	36.39
0.7937	54.00	53.84	53.67	53.72	54.70
1.0000	103.40	103.20	102.90	102.70	102.90
1.2600	194.00	193.80	193.40	192.90	192.40
1.5870	341.30	341.10	340.60	339.90	339.00
2.0000	575.00	574.70	574.20	573.50	572.60

Table A.8; "COARSE" Quadratic Cost Table. Cost Map, System 20p (Passive Vibration Absorber) Initial Condition Vector

$= \{0. \quad 0. \quad 0. \quad -1.618 \quad 1. \quad 0.\}^T$

μ VALS	0.0300	0.0520	0.0900	0.1559	0.2700
δ VALS					
0.5000	3562.00	2060.00	1201.00	715.60	452.20
0.6300	3114.00	1802.00	1052.00	629.40	402.80
0.7937	2460.00	1427.00	836.00	505.20	331.10
1.0000	1595.00	926.40	547.90	339.00	235.10
1.2600	615.70	363.00	222.70	151.30	126.70
1.5870	68.43	47.08	40.32	46.02	65.96
2.0000	1727.00	1003.00	592.10	364.40	249.70

Table A.9; "COARSE" Quadratic Cost Table. Cost Map, System 20a (Control Actuator) Initial State Vector

$= \{0. \quad 0. \quad 0. \quad -1.618 \quad 1. \quad 0.\}^T$

μ VALS	0.03000	0.05196	0.09000	0.15590	0.27000
δ VALS					
0.5000	87.05	86.44	85.60	84.79	85.19
0.6300	81.47	80.87	80.07	79.37	80.08
0.7937	72.57	72.00	71.29	70.85	72.14
1.0000	58.64	58.16	57.68	57.77	60.22
1.2600	38.62	38.33	38.35	39.63	44.38
1.5870	26.84	26.59	26.79	28.71	35.05
2.0000	61.41	61.01	60.72	61.15	63.93

Table A.10; "COARSE" Quadratic Cost Table. Cost Map, System 20p (Passive Vibration Absorber) Initial State Vector

$= [0. \quad 0. \quad 0. \quad -0.618 \quad 2.618 \quad 0.]^T$

μ VALS	0.1000	0.1732	0.3000	0.5196	0.9000
δ VALS					
0.5000	1208.0	782.8	600.4	603.9	794.8
0.6300	1033.0	681.8	542.0	570.2	774.8
0.7937	1094.0	717.0	562.2	582.1	781.4
1.0000	2045.0	1268.0	879.7	765.4	886.9
1.2600	5748.0	3389.0	2106.0	1473.0	1297.0
1.5870	0.174E+05	9952.0	5883.0	3637.0	2547.0
2.0000	0.520E+05	0.286E+05	0.166E+05	9674.0	5948.0

Table A.11; "COARSE" Quadratic Cost Table. Cost Map, System 20a (Control Actuator) Initial State Vector

$= [0. \quad 0. \quad 0. \quad -0.618 \quad 2.618 \quad 0.]^T$

μ VALS	0.0150	0.0260	0.0450	0.0779	0.1350
δ VALS					
0.5000	121.5	121.1	120.7	121.2	124.6
0.6300	120.6	120.1	119.6	119.7	122.3
0.7937	132.2	131.7	131.2	131.1	133.2
1.0000	168.4	167.8	167.2	166.9	168.2
1.2600	241.2	240.6	239.9	239.3	239.9
1.5870	377.3	376.4	375.7	374.7	374.6
2.0000	636.6	636.0	635.1	634.2	633.3

Table A.12; "COARSE" Quadratic Cost Table. Cost Map, System 21p (Passive Vibration Absorber) Initial State Vector

$= [0. \quad 0. \quad 0. \quad -0.618 \quad 2.618 \quad 0.]^T$

μ VALS	0.0500	0.0866	0.1500	0.2598	0.4500
δ VALS					
0.5000	1218.0	786.3	597.6	594.3	774.6
0.6300	821.8	557.5	465.6	517.9	730.8
0.7937	1800.0	1122.0	791.5	705.9	839.2
1.0000	7477.0	4380.0	2670.0	1787.0	1463.0
1.2600	0.270E+05	0.157E+05	9071.0	5490.0	3588.0
1.5870	0.816E+05	0.486E+05	0.275E+05	0.164E+05	9847.0
2.0000	0.259E+06	0.155E+06	0.804E+05	0.471E+05	0.281E+05

Table A.13; "COARSE" Quadratic Cost Table. Cost Map, System 2Ia (Control Actuator) Initial State Vector $= [0. \quad 0. \quad 0. \quad -0.618 \quad 2.618 \quad 0.]^T$

μ VALS	0.0100	0.0173	0.0300	0.0520	0.0900
δ VALS					
0.5000	99.88	99.62	99.49	100.10	103.30
0.6300	93.58	93.28	93.04	93.44	96.28
0.7937	117.50	117.10	116.80	116.90	118.70
1.0000	192.30	191.90	191.30	190.70	190.70
1.2600	325.80	325.40	324.70	323.70	322.90
1.5870	554.70	554.30	553.60	552.30	551.20
2.0000	952.50	952.00	951.10	949.70	947.70

Table A.14; "FINE" Quadratic Cost Table. Cost Map, System Ip (Passive Vibration Absorber) Initial State Vector $= [0. \quad 0. \quad 1. \quad 0.]^T$

μ VALS	0.1020	0.1046	0.1074	0.1101	0.1130
δ VALS					
0.960	8.876	8.865	8.860	8.863	8.870
0.965	8.847	8.837	8.833	8.836	8.844
0.970	8.837	8.827	8.824	8.827	8.835
0.975	8.847	8.837	8.833	8.836	8.844
0.980	8.878	8.867	8.862	8.865	8.872

Table A.15; "FINE" Quadratic Cost Table. Cost Map, System Ia (Control Actuator) Initial State Vector $= [0. \quad 0. \quad 1. \quad 0.]^T$

μ VALS	0.06800	0.07082	0.07376	0.07681	0.08000
δ VALS					
0.900	6.071	6.070	6.069	6.070	6.072
0.910	6.060	6.059	6.058	6.059	6.061
0.920	6.057	6.055	6.055	6.055	6.057
0.930	6.061	6.059	6.058	6.058	6.060
0.940	6.073	6.071	6.070	6.070	6.071

Table A.16; "FINE" Quadratic Cost Table. Cost Map, System 20p (Passive Vibration Absorber) Initial State Vector = $\{0. \quad 0. \quad 0. \quad 1.0 \quad 1.618 \quad 0.\}^T$

μ VALS	0.05600	0.05674	0.05748	0.05824	0.05900
δ VALS					
0.6025	61.11	61.10	61.09	61.10	61.11
0.6037	61.06	61.05	61.04	61.05	61.06
0.6050	61.05	61.04	61.03	61.04	61.05
0.6062	61.06	61.05	61.04	61.05	61.06
0.6075	61.10	61.09	61.08	61.09	61.10

Table A.17; "FINE" Quadratic Cost Table. Cost Map, System 20a (Control Actuator) Initial State Vector = $\{0. \quad 0. \quad 0. \quad 1. \quad 1.618 \quad 0.\}^T$

μ VALS	0.02200	0.02505	0.02853	0.03249	0.03700
δ VALS					
0.5200	32.24	32.22	32.22	32.23	32.27
0.5297	32.14	32.12	32.11	32.12	32.16
0.5396	32.10	32.08	32.07	32.08	32.11
0.5497	32.14	32.12	32.11	32.11	32.14
0.5600	32.25	32.22	32.21	32.22	32.24

Table A.18; "FINE" Quadratic Cost Table. Cost Map, System 20p (Passive Vibration Absorber) Initial State Vector = $\{0. \quad 0. \quad 0. \quad -1.618 \quad 1. \quad 0.\}^T$

μ VALS	0.08500	0.08740	0.08986	0.09239	0.09500
δ VALS					
1.565	39.85	39.79	39.77	39.78	39.80
1.569	39.77	39.71	39.69	39.71	39.73
1.572	39.76	39.70	39.68	39.70	39.72
1.576	39.82	39.76	39.74	39.75	39.77
1.580	39.94	39.88	39.86	39.87	39.89

Table A.19; "FINE" Quadratic Cost Table. Cost Map, System 20a (Control Actuator) Initial State Vector

$= [0. \quad 0. \quad 0. \quad -1.618 \quad 1. \quad 0.]^T$

μ VALS	0.04500	0.05113	0.05809	0.06601	0.07500
δ VALS					
1.530	26.31	26.27	26.25	26.26	26.32
1.542	26.28	26.24	26.22	26.23	26.28
1.555	26.31	26.27	26.25	26.26	26.31
1.567	26.39	26.35	26.33	26.34	26.38
1.580	26.53	26.49	26.46	26.47	26.52

Table A.20; "FINE" Quadratic Cost Table. Cost Map, System 20p (Passive Vibration Absorber) Initial State Vector

$= [0. \quad 0. \quad 0. \quad -0.618 \quad 2.618 \quad 0.]^T$

μ VALS	0.3300	0.3418	0.3541	0.3668	0.3800
δ VALS					
0.6750	527.9	526.8	526.3	526.5	527.6
0.6824	527.5	526.4	525.9	526.1	527.3
0.6898	527.3	526.2	525.8	525.9	527.1
0.6974	527.3	526.3	525.8	526.0	527.2
0.7050	527.7	526.6	526.1	526.7	527.5

Table A.21; "FINE" Quadratic Cost Table. Cost Map, System 20a (Control Actuator) Initial State Vector

$= [0. \quad 0. \quad 0. \quad -0.618 \quad 2.618 \quad 0.]^T$

μ VALS	0.03000	0.03834	0.04899	0.06260	0.08000
δ VALS					
0.5350	119.6	119.4	119.3	119.4	119.8
0.5551	119.2	119.0	118.9	119.0	119.3
0.5759	119.1	118.9	118.7	118.8	119.1
0.5976	119.3	119.0	118.9	118.8	119.1
0.6200	119.7	119.4	119.2	119.2	119.4

Table A.22: "FINE" Quadratic Cost Table. Cost Map, System 2Ip (Passive Vibration Absorber) Initial State Vector = $[0. \quad 0. \quad 0. \quad -0.618 \quad 2.618 \quad 0.]^T$

μ VALS	0.1450	0.1520	0.1593	0.1670	0.1750
δ VALS					
0.6200	468.3	466.6	465.5	465.7	467.2
0.6249	467.5	465.9	464.8	465.0	466.6
0.6299	467.2	465.6	464.5	464.8	466.3
0.6349	467.4	465.7	464.7	464.9	466.4
0.6400	468.0	466.4	465.3	465.5	467.0

Table A.23: "FINE" Quadratic Cost Table. Cost Map, System 2Ia (Control Actuator) Initial State Vector = $[0. \quad 0. \quad 0. \quad -0.618 \quad 2.618 \quad 0.]^T$

μ VALS	0.02700	0.02921	0.03161	0.03420	0.03700
δ VALS					
0.5900	92.68	92.67	92.67	92.69	92.72
0.5962	92.61	92.59	92.59	92.60	92.63
0.6024	92.58	92.56	92.56	92.57	92.60
0.6087	92.60	92.59	92.58	92.59	92.62
0.6150	92.68	92.66	92.66	92.67	92.69

Table B.1; Fourth Derivative Finite Difference Operators and Relative Magnitudes of Terms in the Operator.

Order	q_{-4}	q_{-3}	q_{-2}	q_{-1}	q_0	q_1	q_2	q_3	q_4
Operator									
2^{nd}	0.0	0.0	1.0	-4.0	6.0	-4.0	1.0	0.0	0.0
4^{th}	0.0	-0.17	2.0	-6.5	9.33	-6.5	2.0	-0.17	0.0
6^{th}	0.03	-0.4	2.82	-8.13	11.38	-8.13	2.82	-0.4	0.03
Relative Magnitude									
2^{nd}			0.17	-0.67	1.0	-0.67	0.17		
4^{th}		0.02	0.21	-0.70	1.0	0.70	0.21	0.02	
6^{th}	0.003	0.04	0.25	-0.71	1.0	0.71	0.25	0.04	0.003

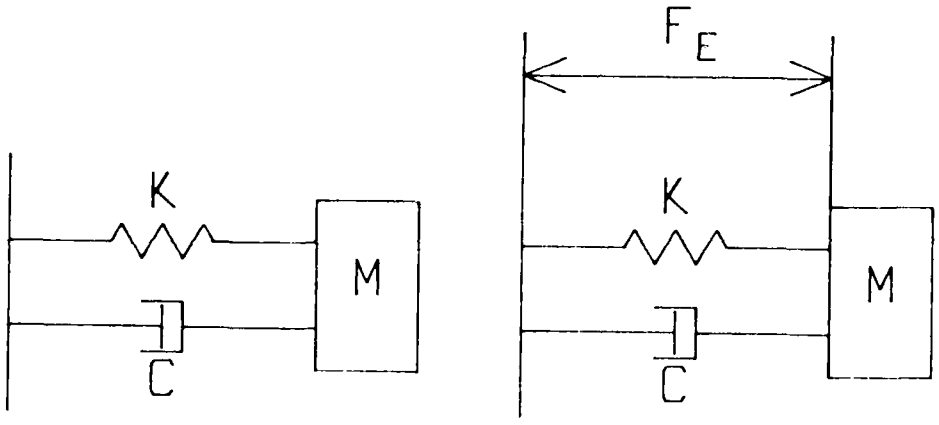

A PASSIVE INERTIAL VIBRATION ABSORBER

B ELECTROMAGNETIC, INERTIAL-REACTION ACTUATOR WITH PASSIVE COMPONENTS

FIG. 2.1: INERTIAL DAMPERS

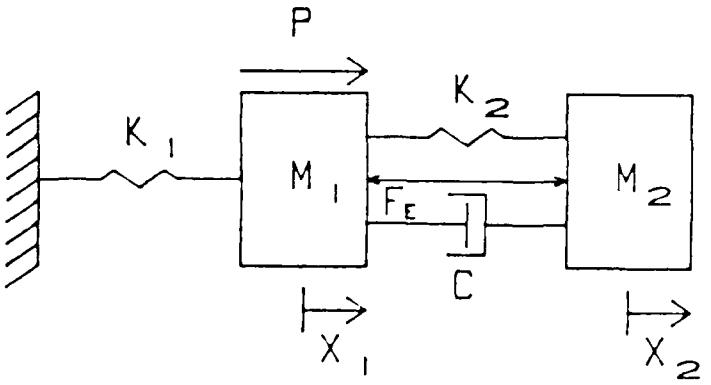

FIG. 2.2: SINGLE DEGREE OF FREEDOM ACTUATOR COUPLED TO A SINGLE DEGREE OF FREEDOM REPRESENTATION OF A STRUCTURAL MODE.

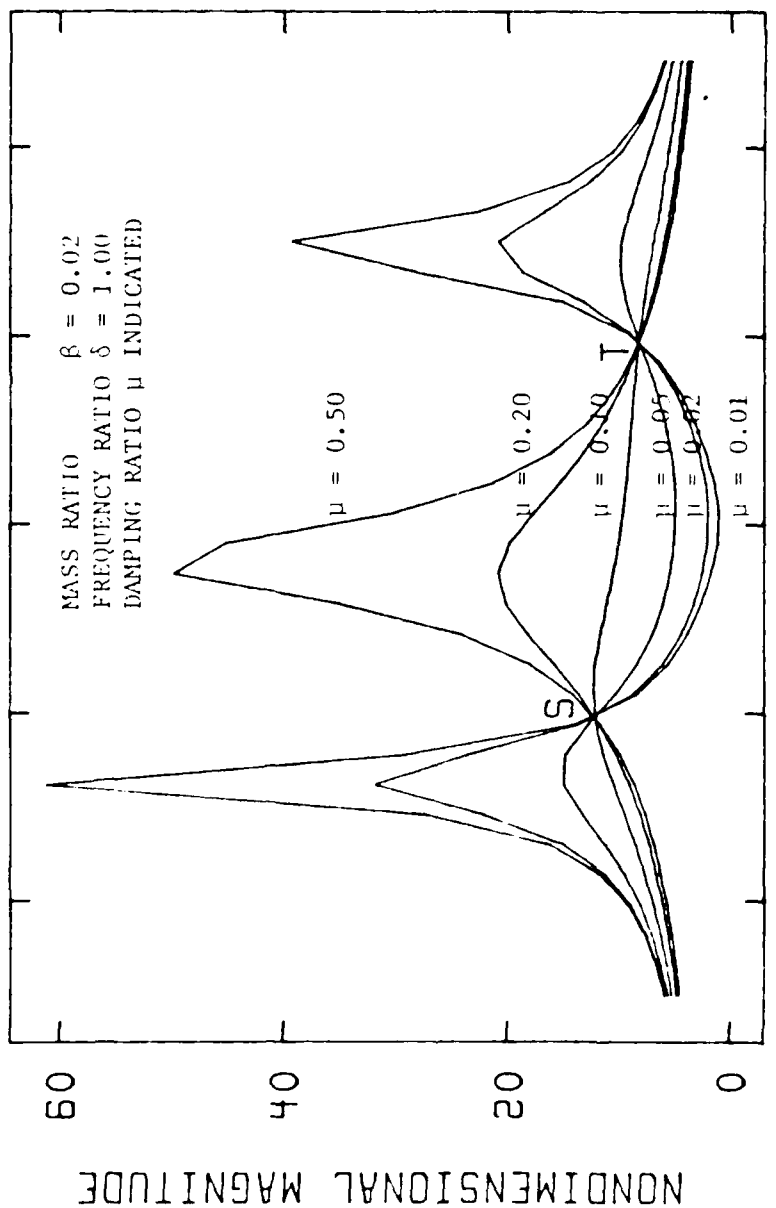

FIG. 2.3: MAGNITUDE OF RESPONSE (X_1/Δ_{ST}) VERSUS NONDIMENSIONAL FREQUENCY (ω/p_0) FOR A TYPICAL VALUE OF MASS AND FREQUENCY RATIO.

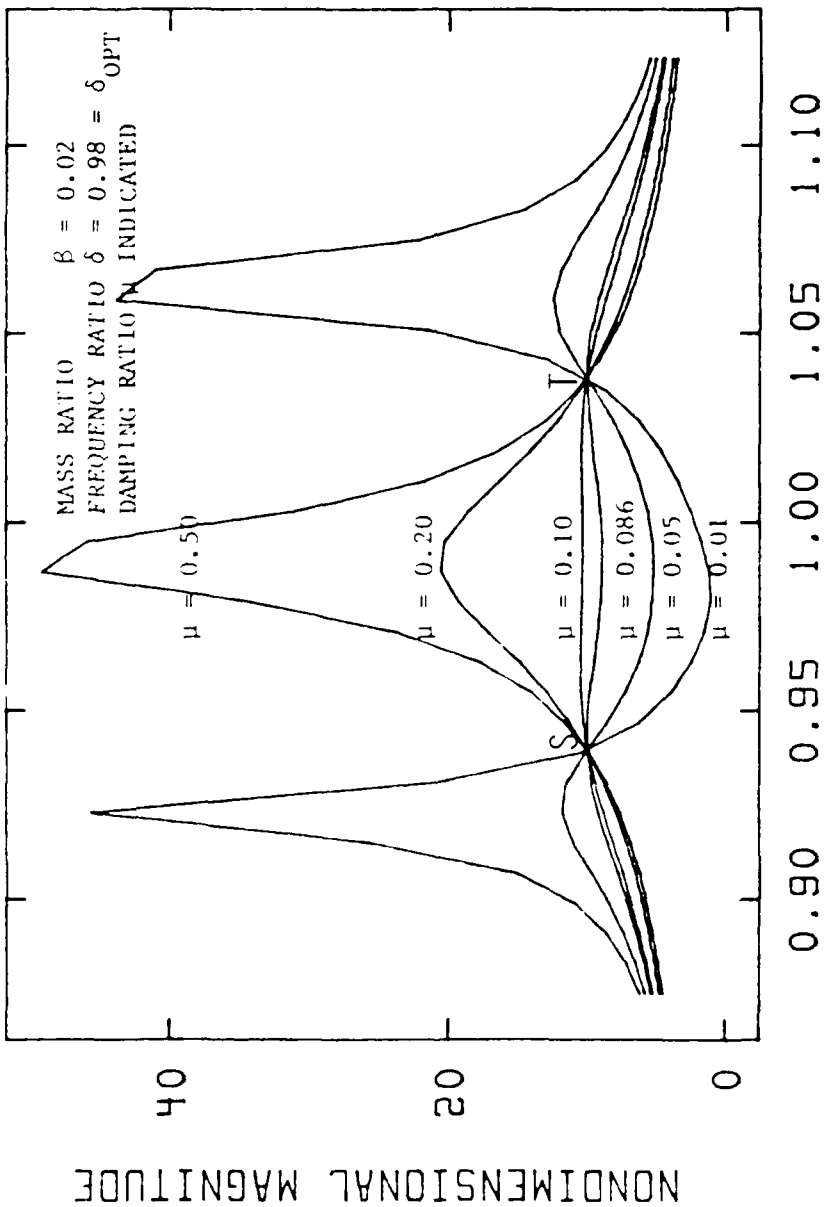

FIG 2.4: MAGNITUDE OF RESPONSE(X_1/Δ_{ST}) VERSUS NONDIMENSIONAL FREQUENCY (ω/p_0) FOR THE OPTIMAL CHOICE OF FREQUENCY RATIO GIVEN A MASS RATIO OF 0.02.

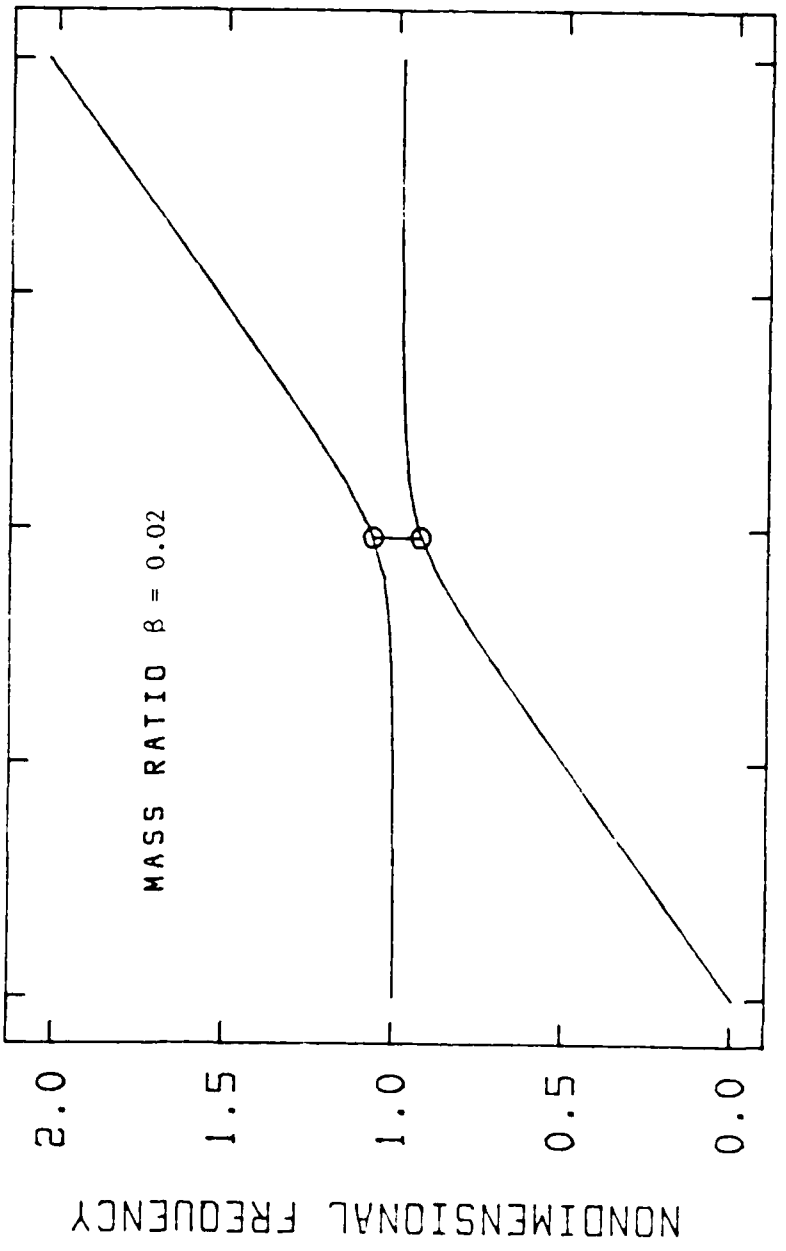

FIG. 2.5: NONDIMENSIONAL NATURAL FREQUENCIES (γ) OF THE TWO SYSTEM MODES AS A FUNCTION OF ABSORBER FREQUENCY RATIO (δ).

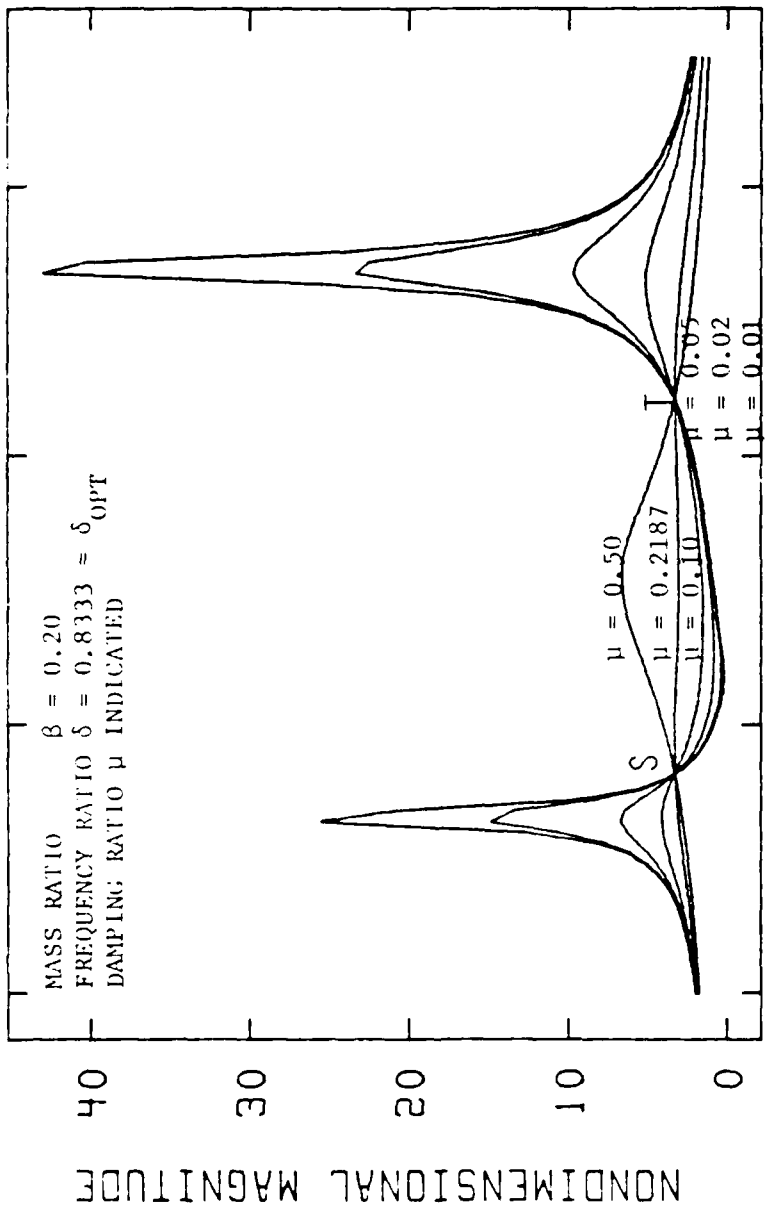

FIG 2.6: MAGNITUDE OF RESPONSE (X_1/Δ_{ST}) VERSUS NONDIMENSIONAL FREQUENCY (ω/p_0) FOR THE[1] Δ_{ST} OPTIMAL CHOICE OF FREQUENCY RATIO GIVEN A MASS RATIO OF 0.2. (COMPARE WITH FIG. 2.4)

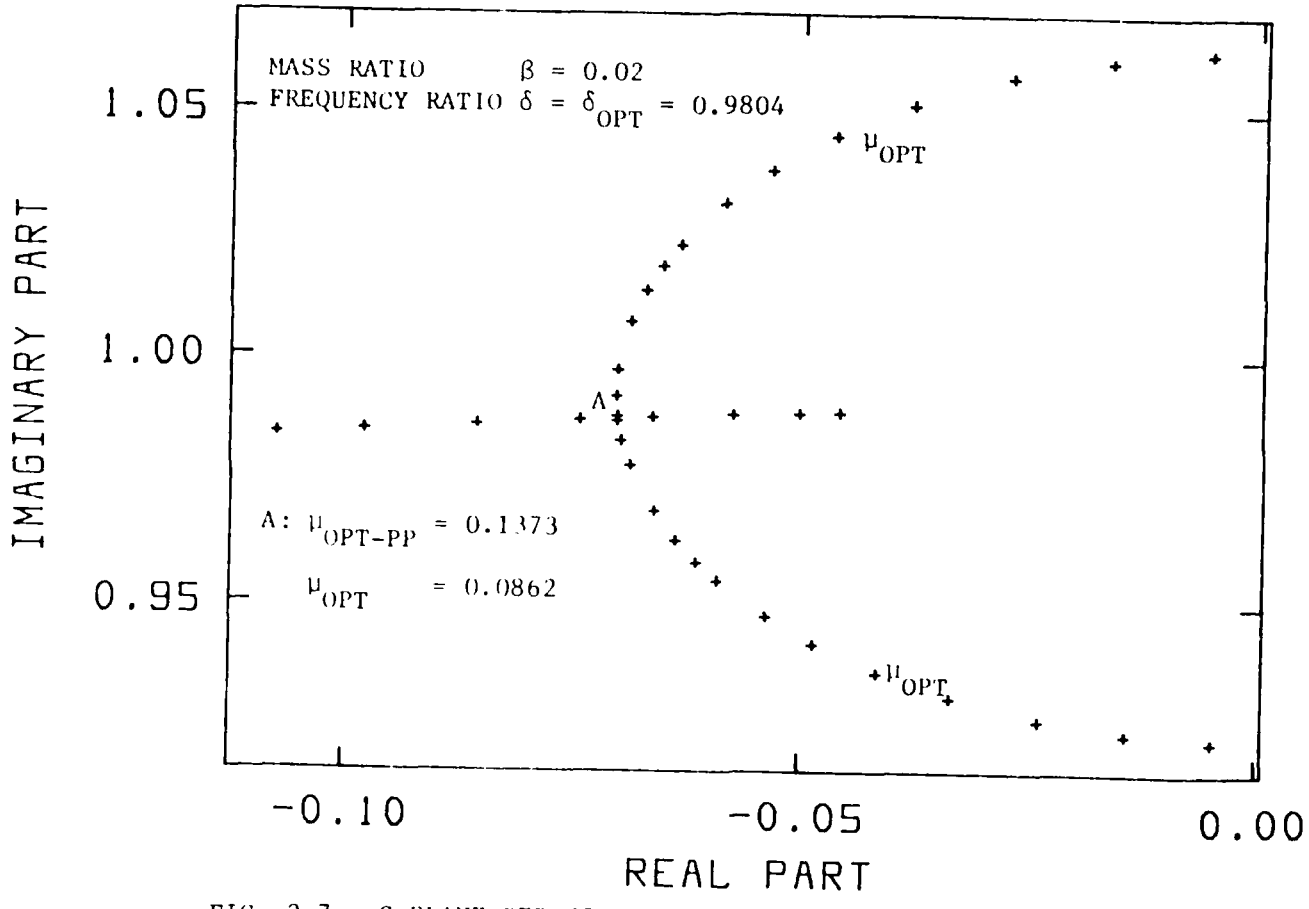

FIG. 2.7: S-PLANE REPRESENTATION OF THE POLES OF THE VIBRATION ABSORBER AS A FUNCTION OF INCREASING DAMPER VALUE.

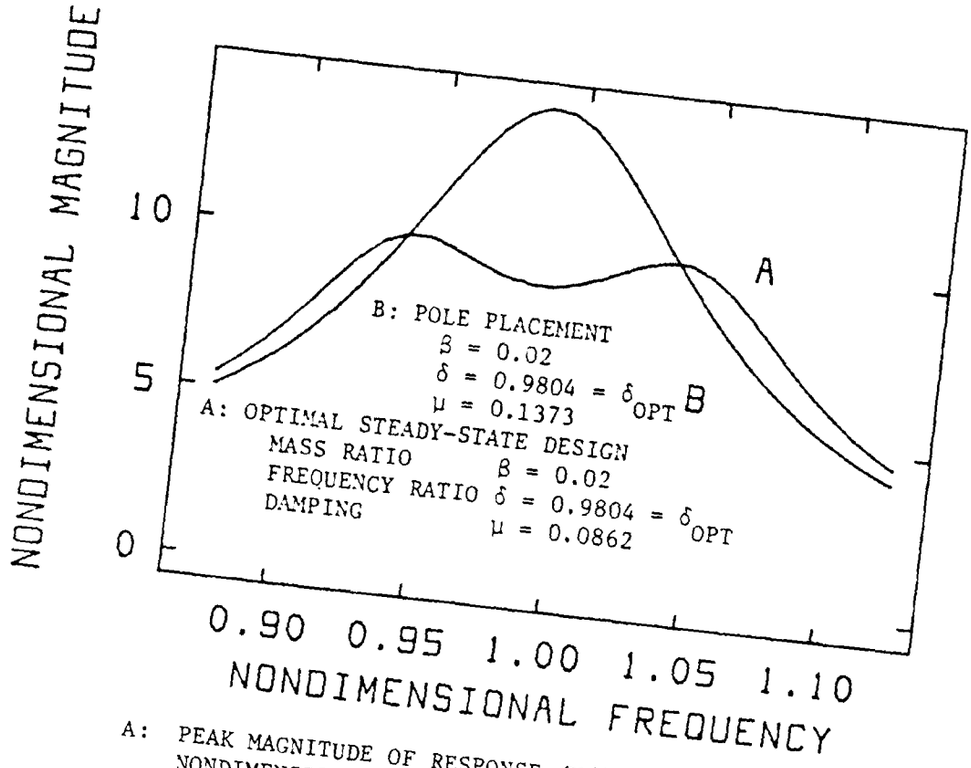

A: PEAK MAGNITUDE OF RESPONSE (X/Δ_{ST}) VERSUS NONDIMENSIONAL FREQUENCY (ω/p_0).

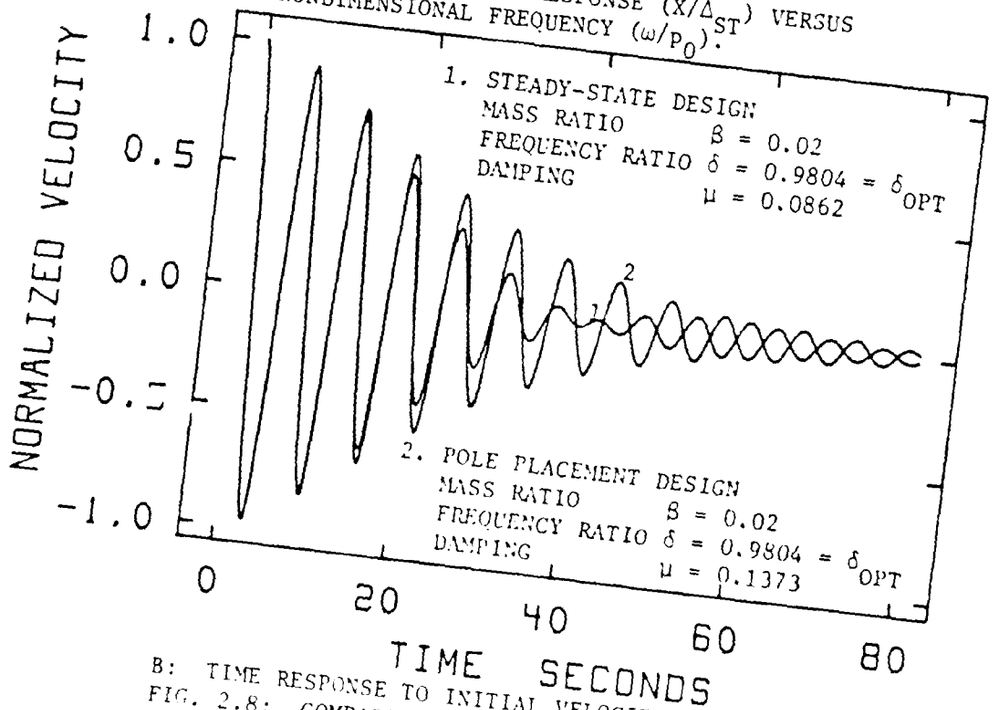

B: TIME RESPONSE TO INITIAL VELOCITY.

FIG. 2.8: COMPARISON OF OPTIMAL STEADY-STATE AND POLE PLACEMENT DESIGN CHARACTERISTICS.

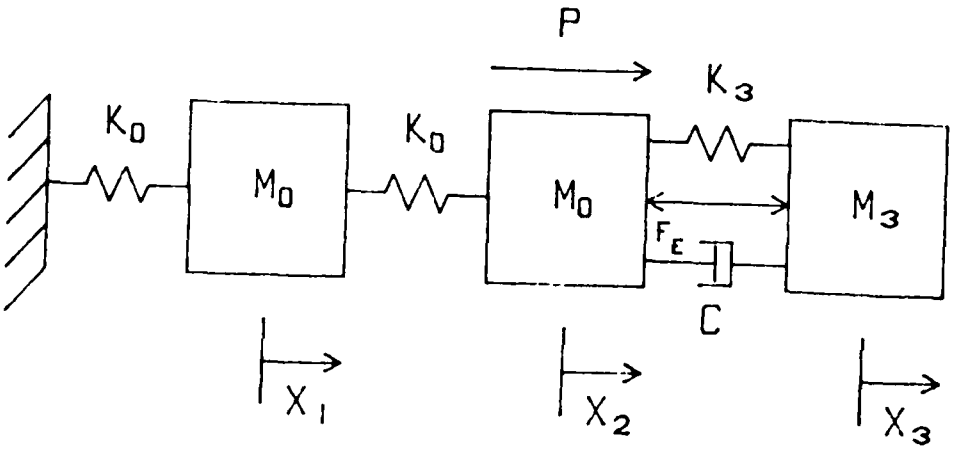

FIG 2.9: SINGLE DOF ACTUATOR COUPLED TO A TWO DOF STRUCTURAL REPRESENTATION.

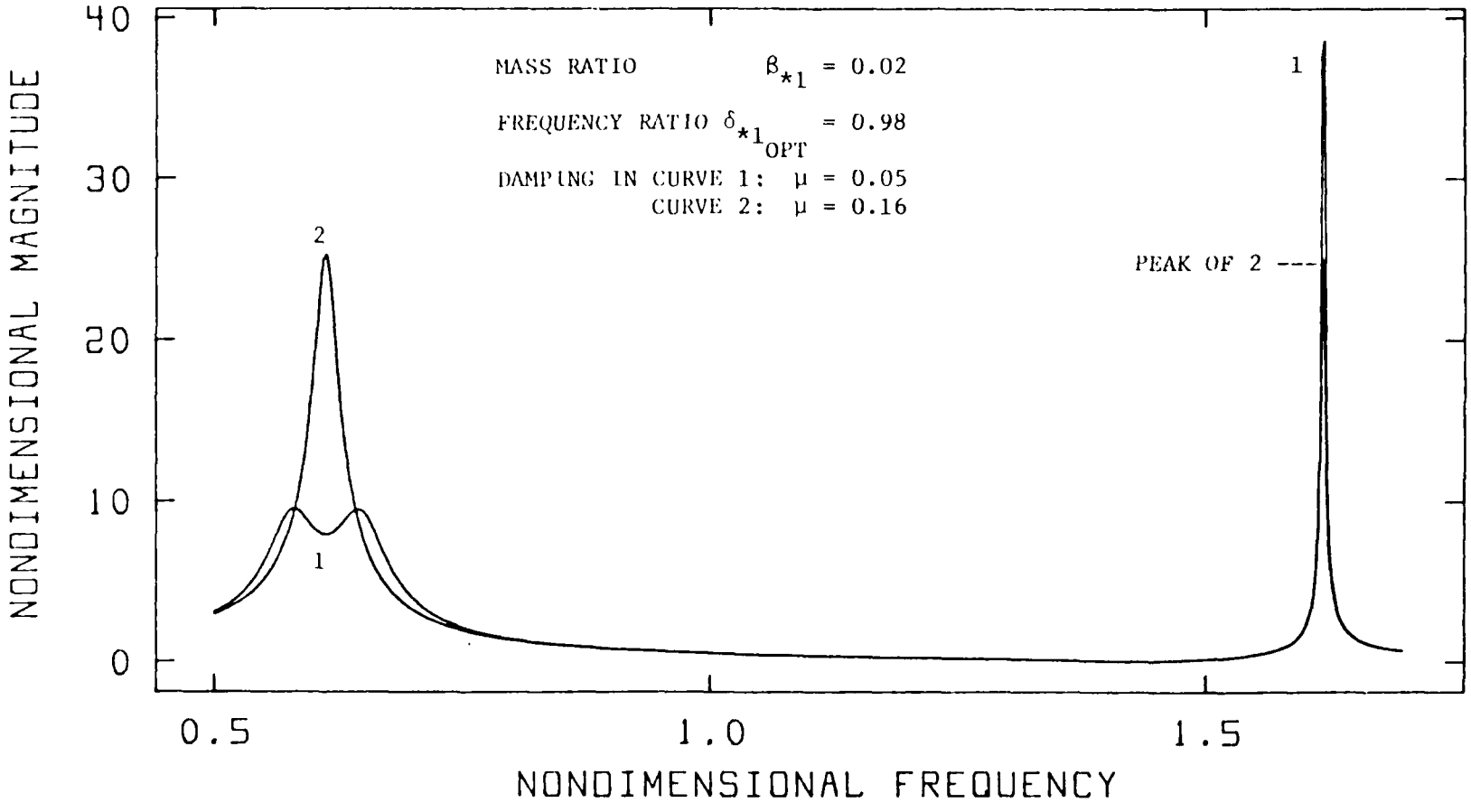

FIG. 2.10: MAGNITUDE OF RESPONSE (X/Δ_{ST}) VERSUS NONDIMENSIONAL FREQUENCY (ω/p_0) FOR AN ABSORBER TUNED TO THE LOWER STRUCTURAL MODE (CURVE 1) AND TUNED TO BOTH MODES (CURVE 2).

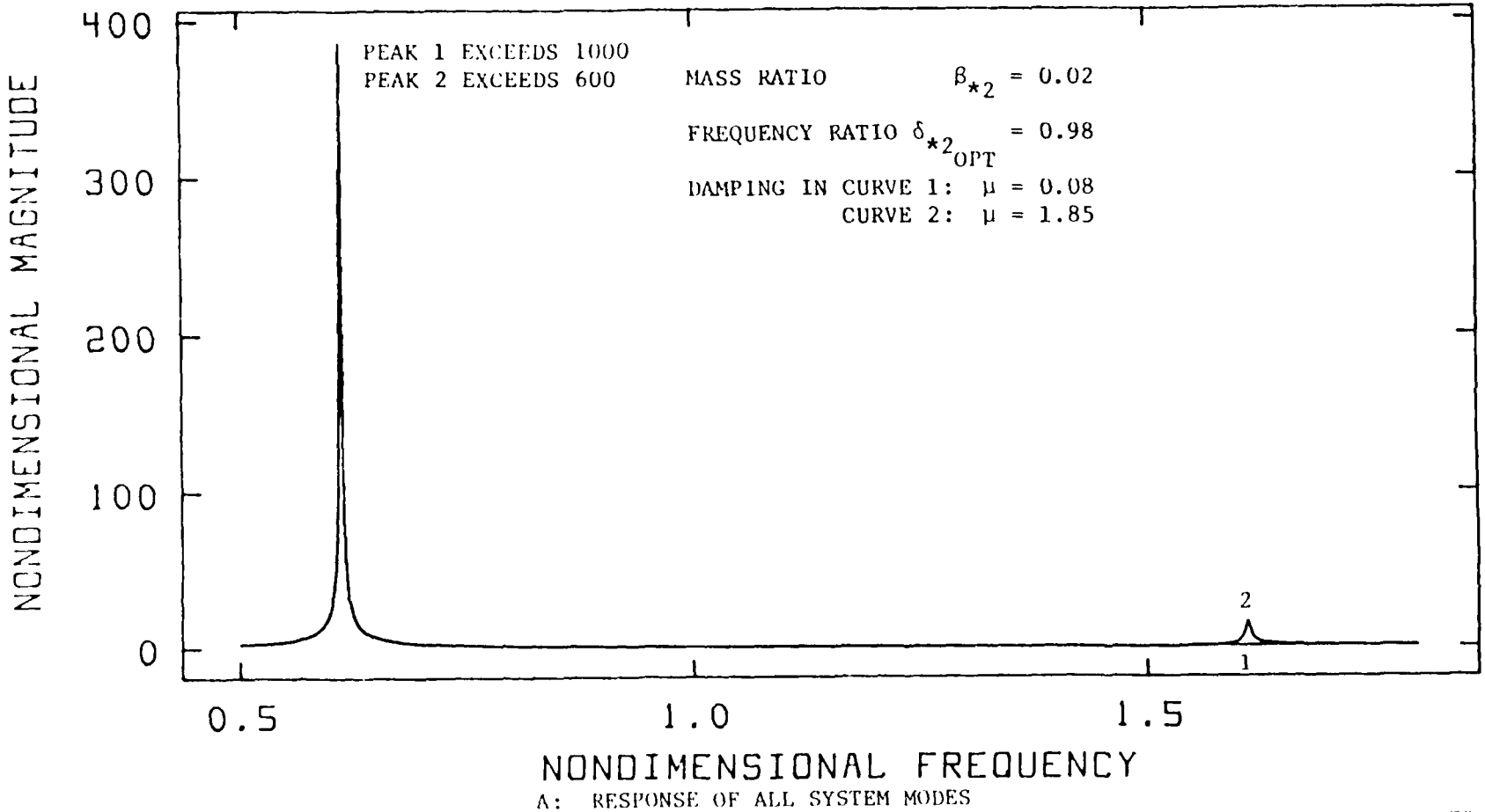

A: RESPONSE OF ALL SYSTEM MODES

FIG. 2.11: MAGNITUDE OF RESPONSE (X/Δ_{ST}) VERSUS NONDIMENSIONAL FREQUENCY (ω/p_0) FOR AN ABSORBER TUNED TO THE HIGHER STRUCTURAL MODE (CURVE 1) AND SOMEWHAT TUNED TO BOTH MODES (CURVE 2).

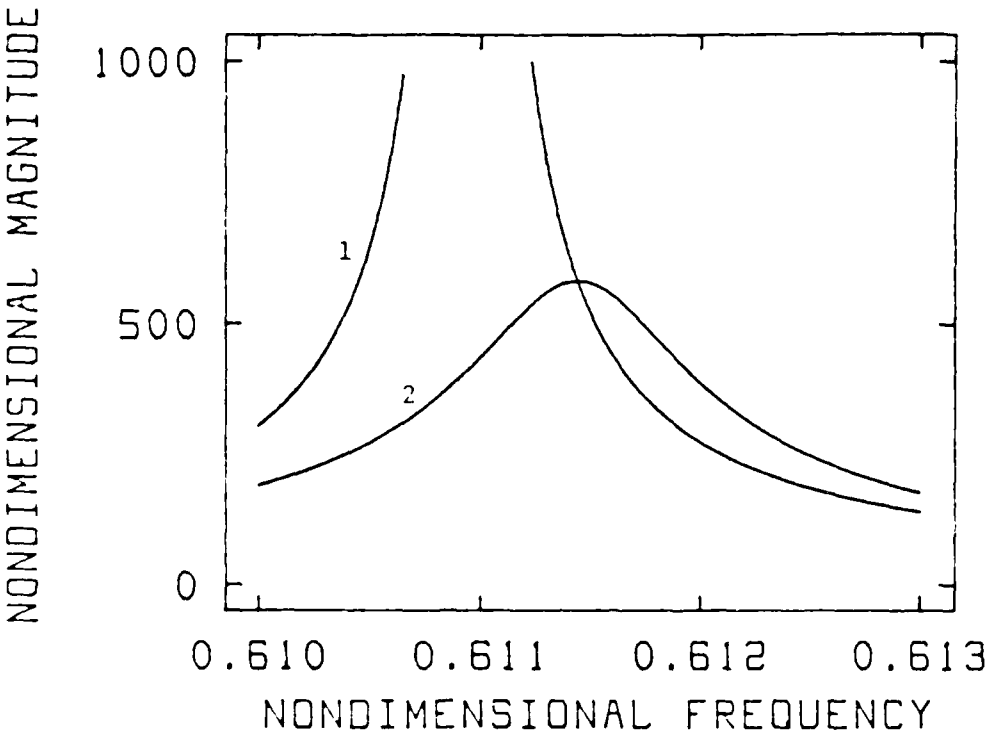

B: DETAIL IN THE VICINITY OF THE LOW MODAL FREQUENCY

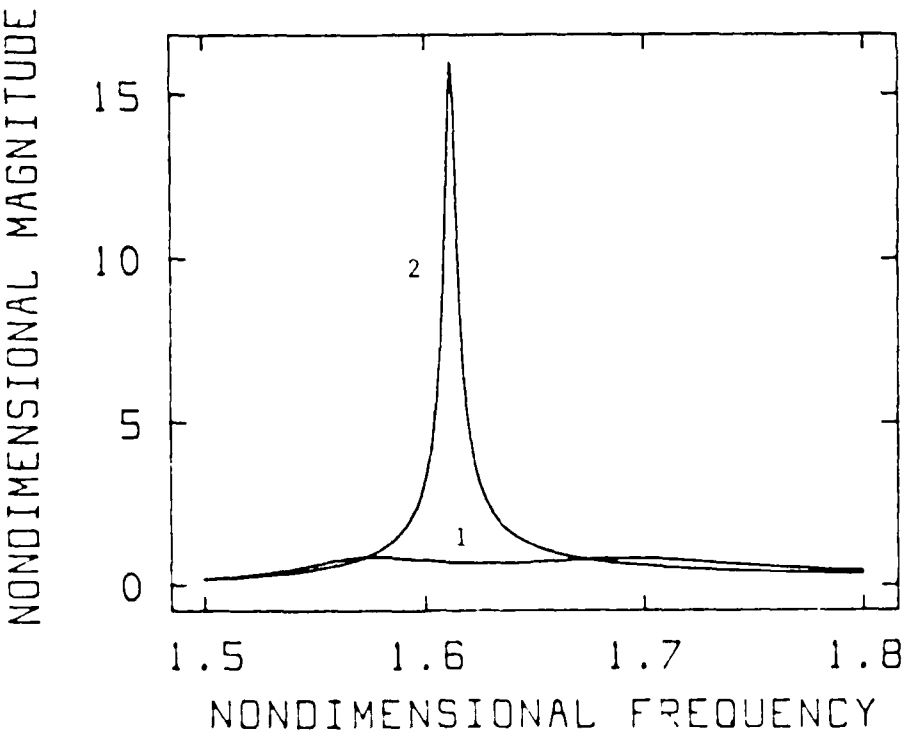

C: DETAIL IN THE VICINITY OF THE HIGHER MODAL FREQUENCY

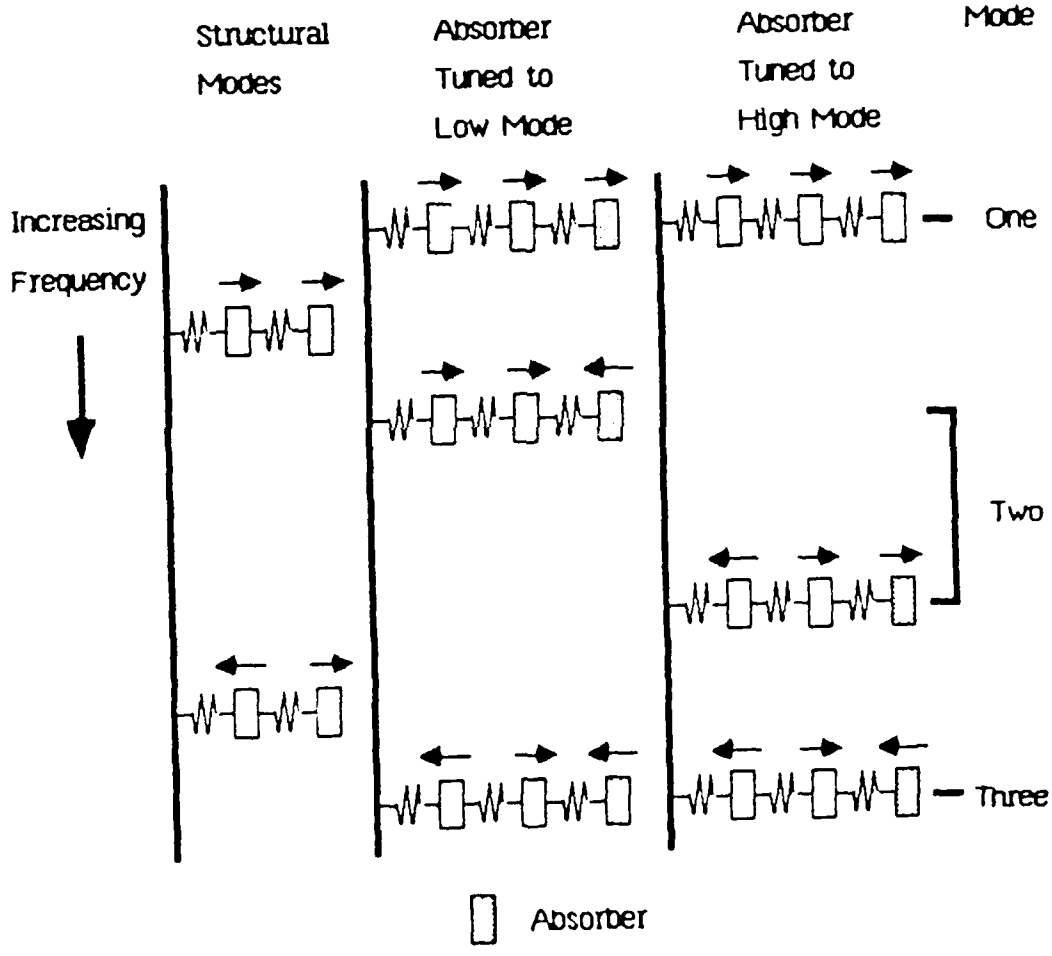

FIG. 2.12: RELATIVE MODAL MOTIONS OF MASS ELEMENTS FOR DIFFERENT STRUCTURE?ABSORBER FREQUENCY RATIOS.

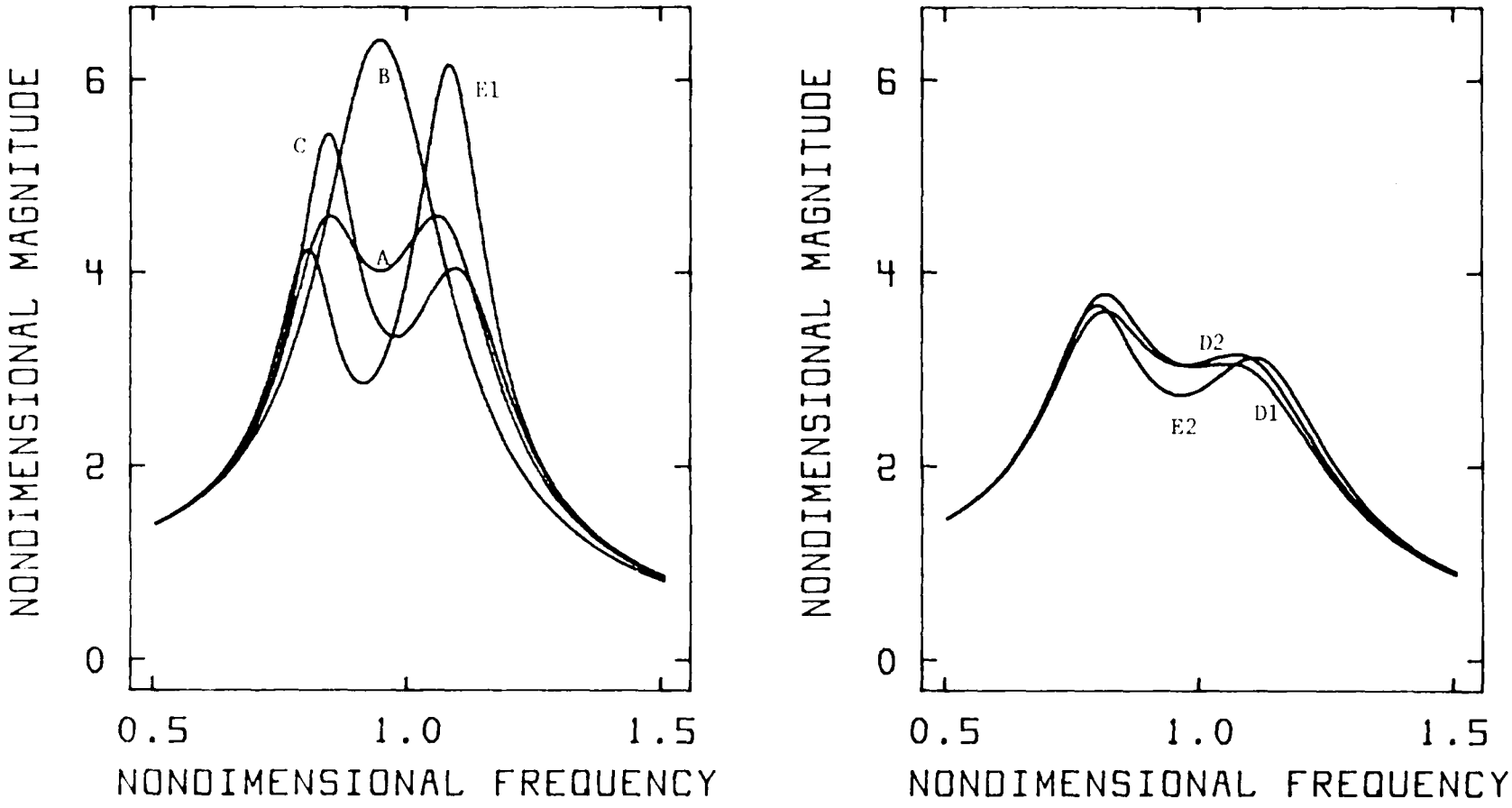

A: PASSIVE COMPONENTS B: ACTIVE COMPONENTS

FIG. 2.13: COMPARISON OF THE FREQUENCY RESPONSE OF SEVERAL OPTIONS OF ACTIVE, PASSIVE AND ACTIVE/PASSIVE, SIMULTANEOUS DESIGN.

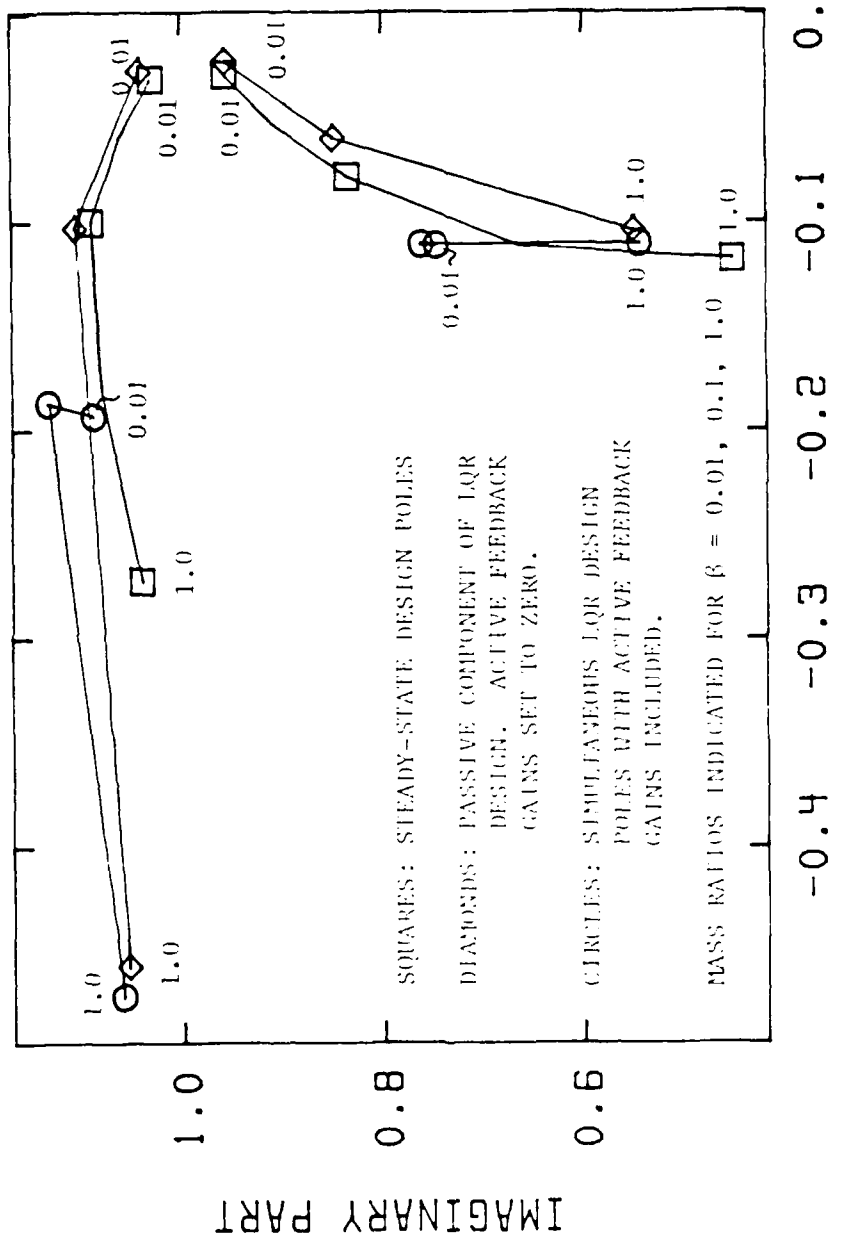

FIG. 2.14: ROOT LOCUS PLOT OF THE SYSTEM POLES FOR VARIOUS MASS RATIOS OBTAINED FROM THE DIFFERENT OPTIMAL FORMULATIONS.

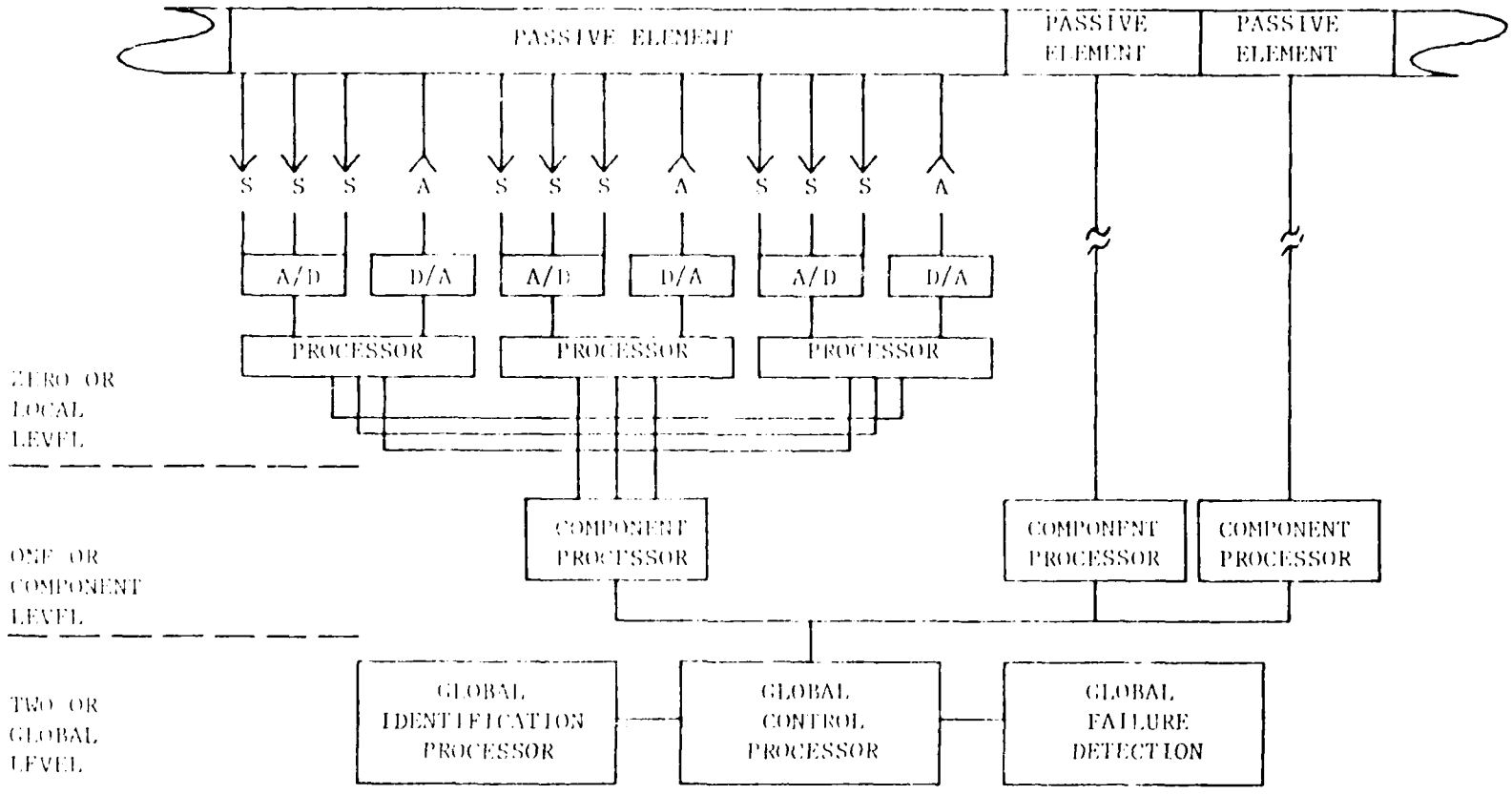

FIG. 3.1: HIERARCHIC PROCESSING NETWORK.

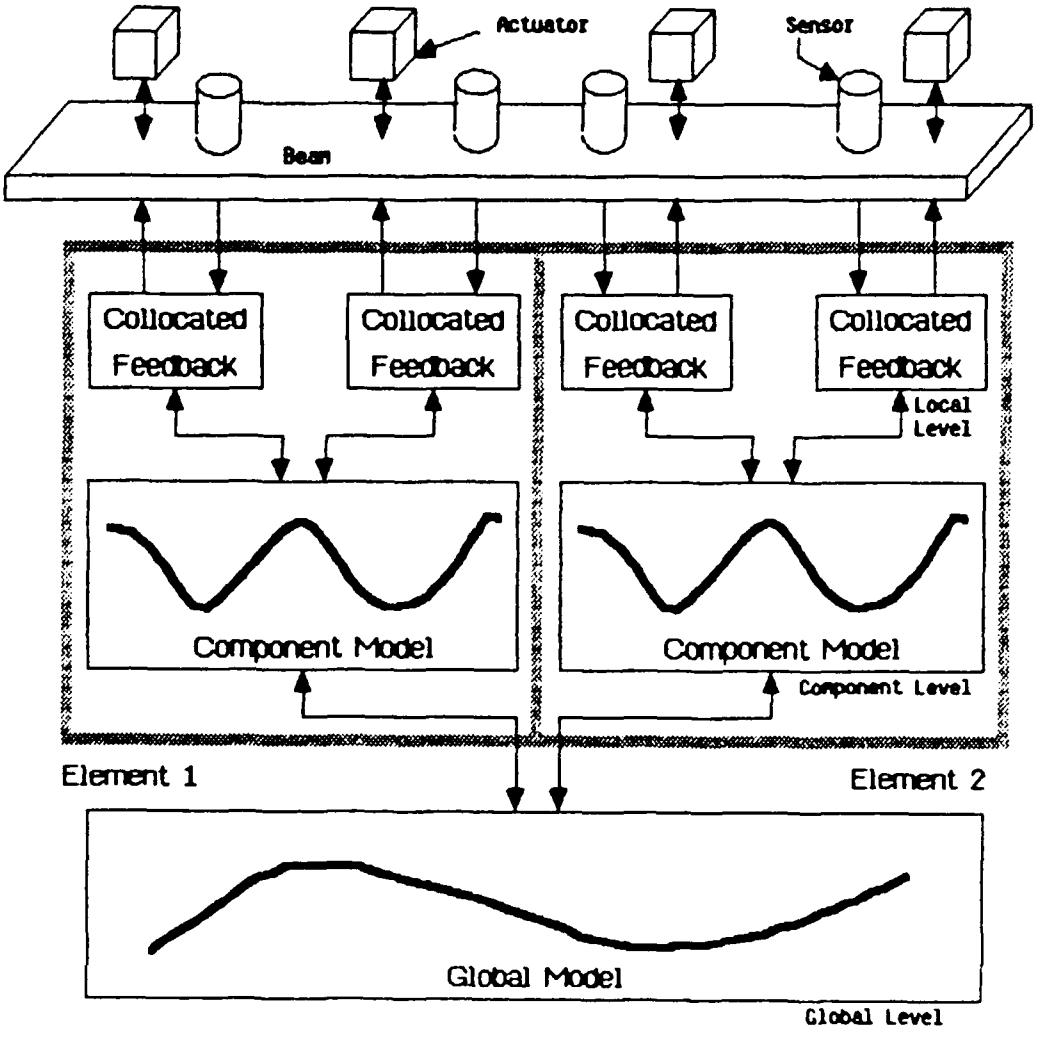

FIG. 3.2: LEVELS OF MODELING AND INFORMATION FEEDBACK IN A DISTRIBUTED, HIERARCHIC CONTROL FORMAT.

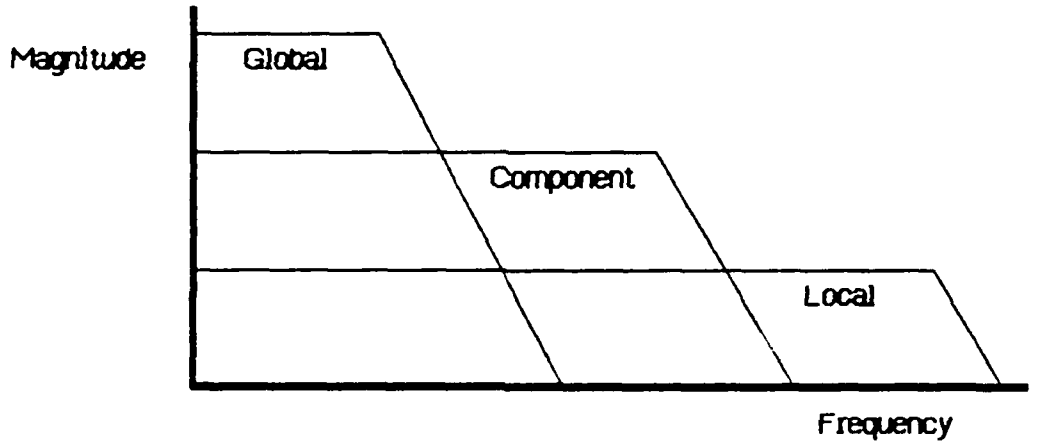

A: CONTROL OPTION PROVIDING EXTENDED BANDWIDTH IN THE LOW AUTHORITY CONTROLLER.

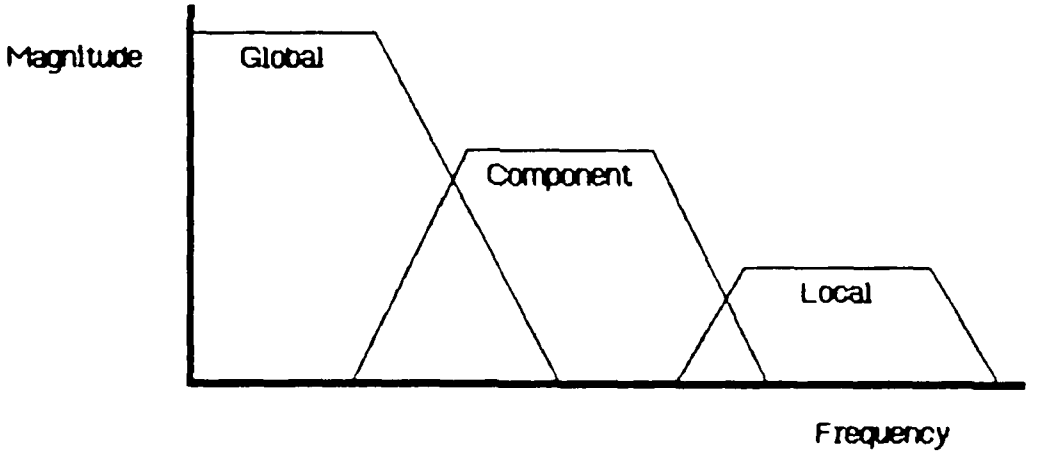

B: OVERLAPPING LOW AND HIGH AUTHORITY CONTROL.

FIG. 3.3: OPTIONS FOR THE SELECTION OF BANDWIDTHS AND INTERACTIONS OF THE VARIOUS LEVELS OF CONTROL.

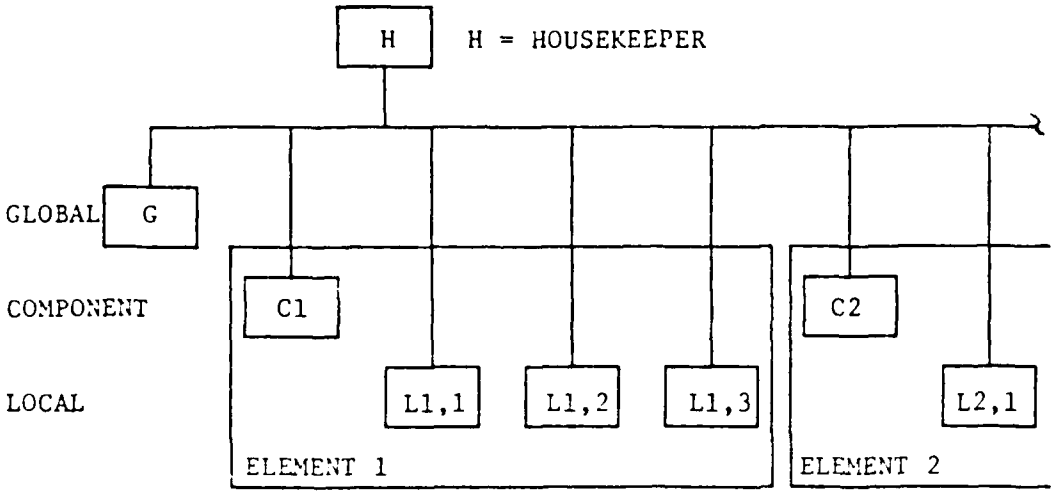

FIG. 3.4: SINGLE BUS HARDWARE ARRANGEMENT FOR MULTIPROCESSOR, HIERARCHIC ARCHITECTURE.

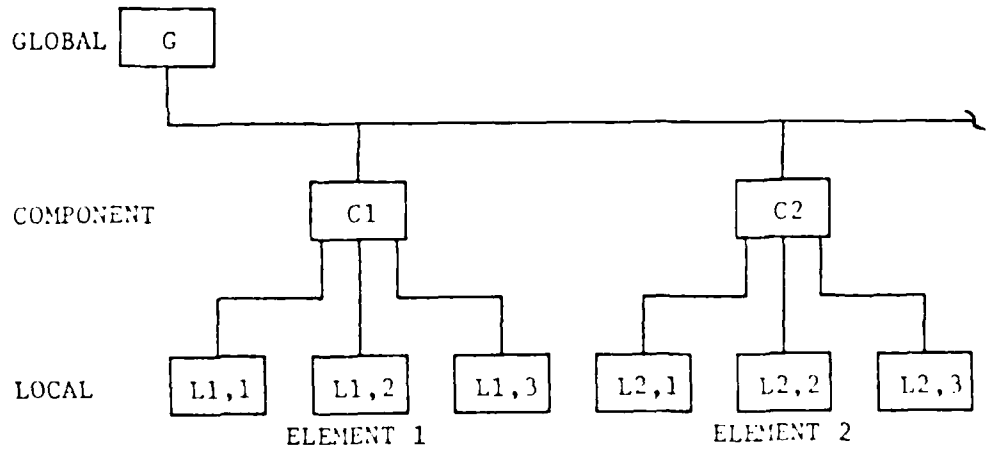

FIG. 3.5: MULTIBUS HARDWARE ARRANGEMENT FOR MULTIPROCESSOR, HIERARCHIC ARCHITECTURE.

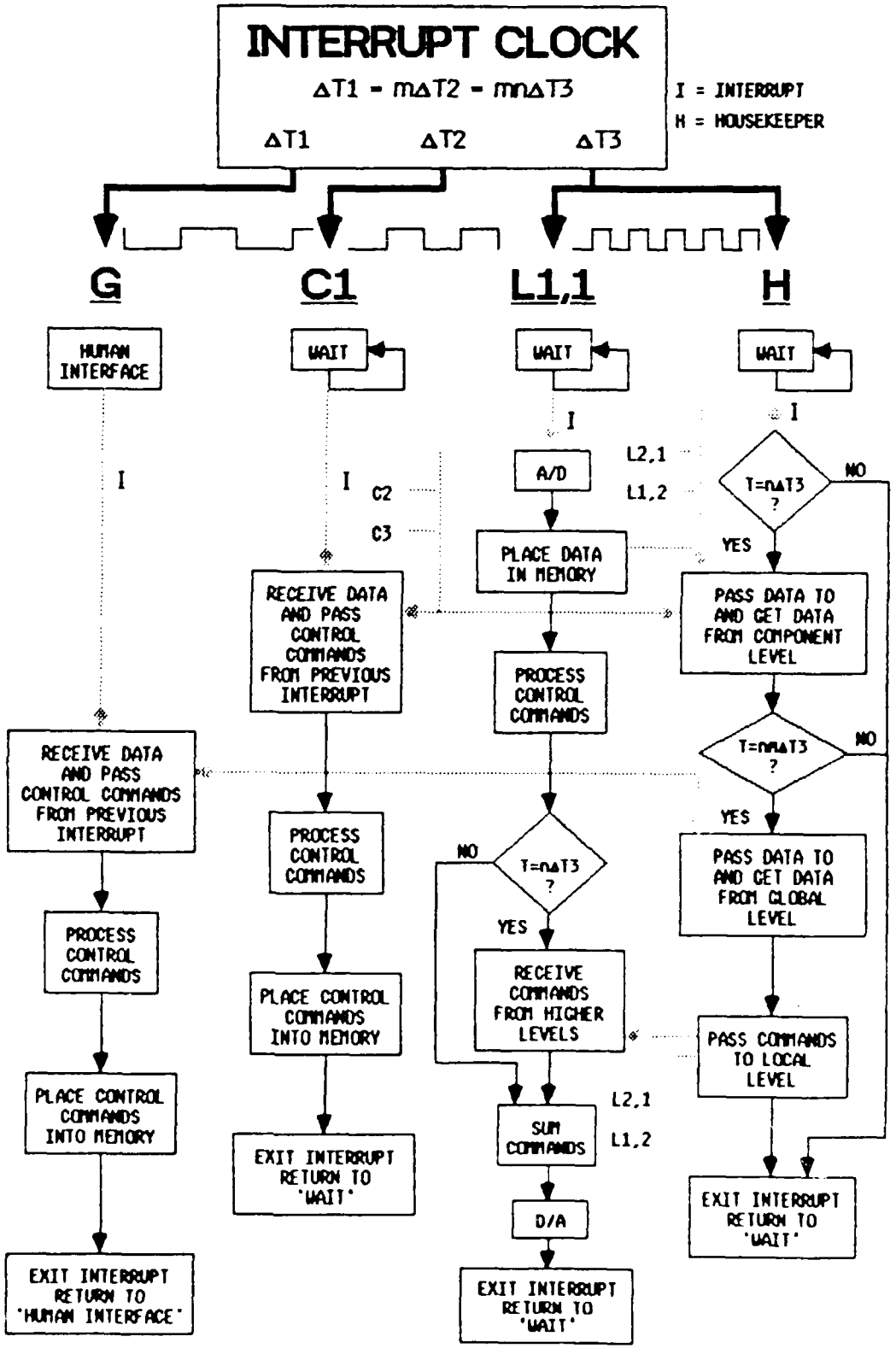

FIG. 3.6: INTERRUPT FLOW CHART FOR SINGLE BUS SYSTEM.

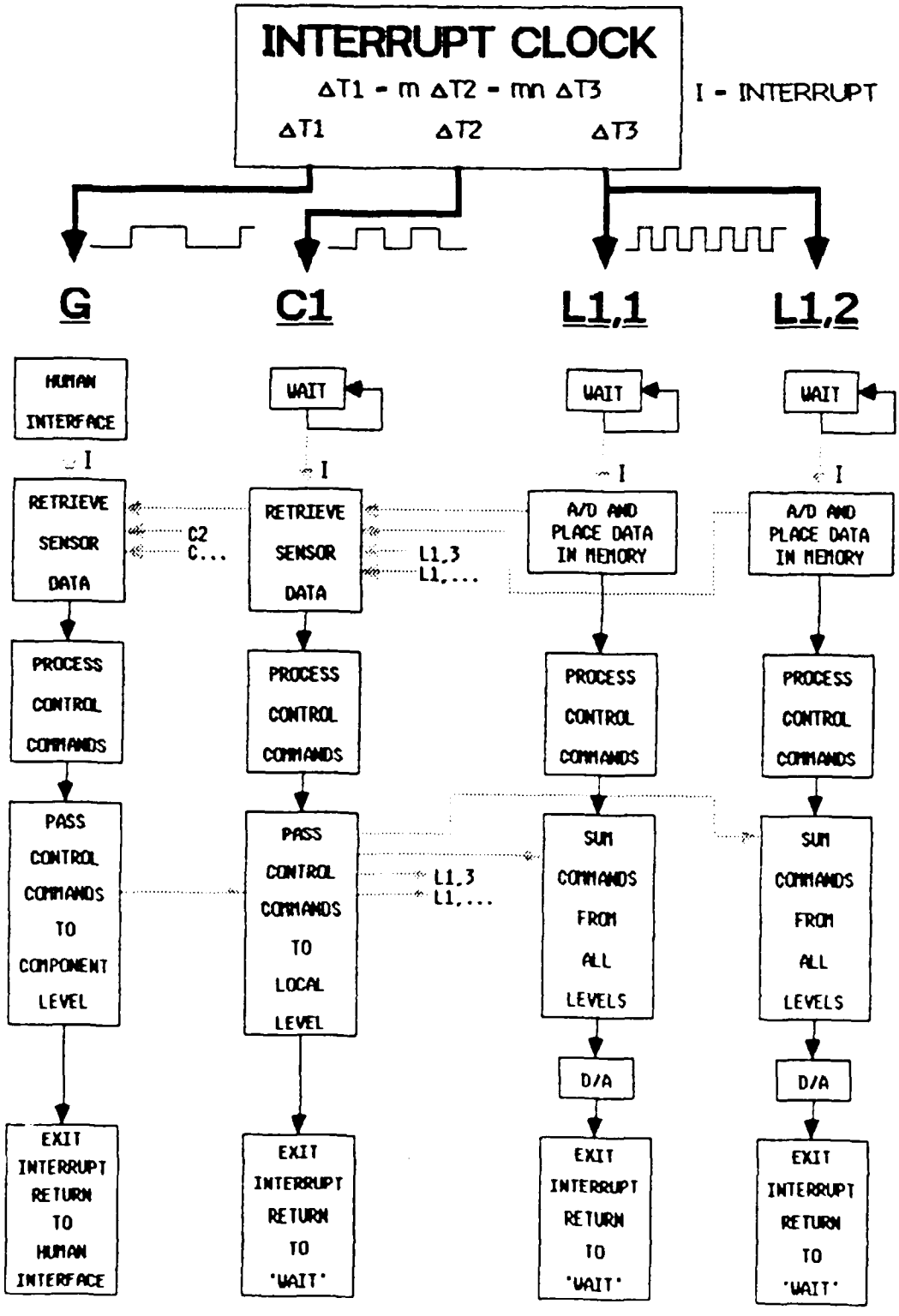

FIG. 3.7: INTERRUPT FLOW CHART FOR MULTIBUS SYSTEM.

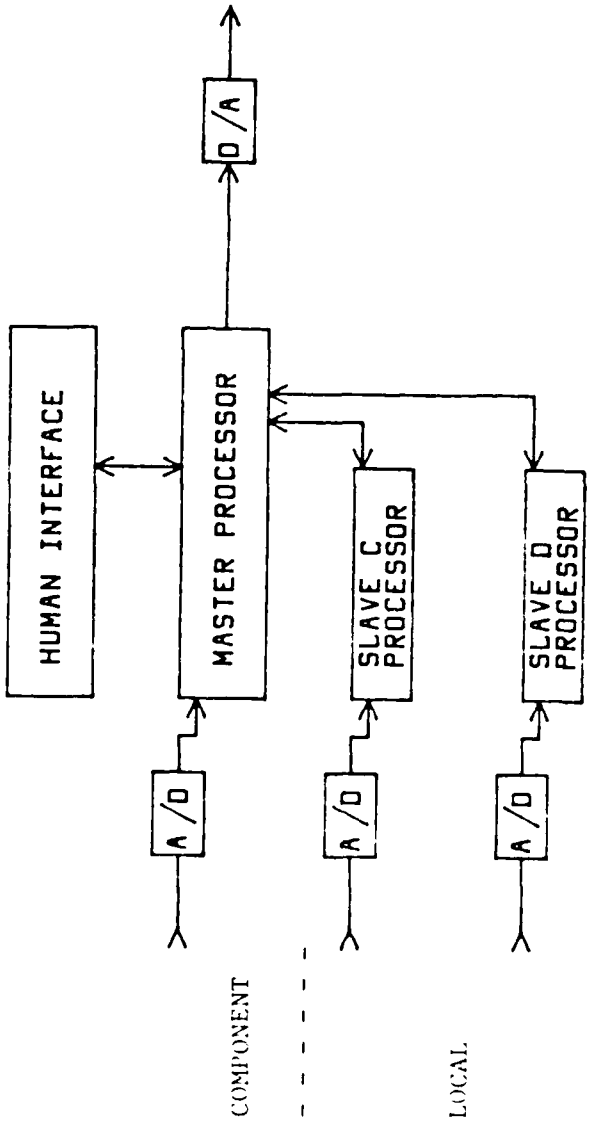

FIG. 3.8: FIRST GENERATION PROCESSING HARDWARE.

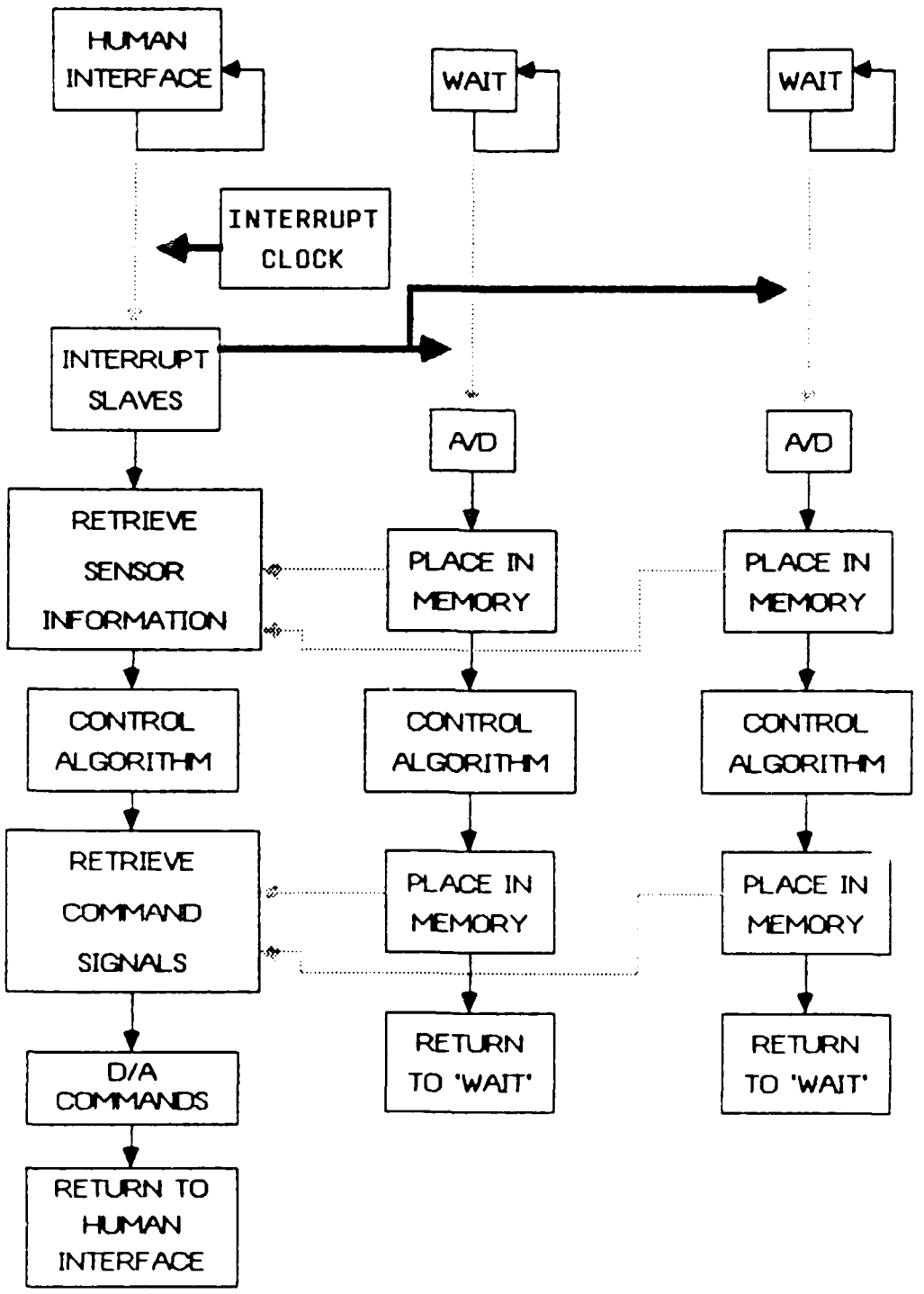

FIG. 3.9: FIRST GENERATION CONTROL SOFTWARE FLOW CHART.

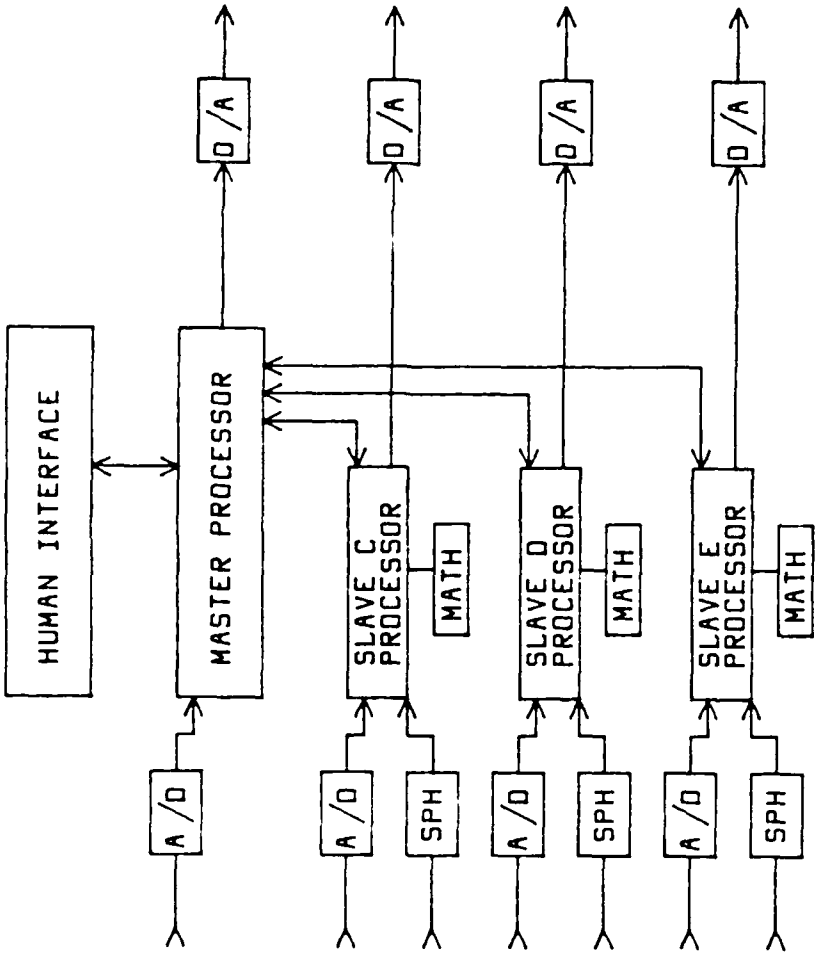

FIG. 3.10: SECOND GENERATION PROCESSING SYSTEM.

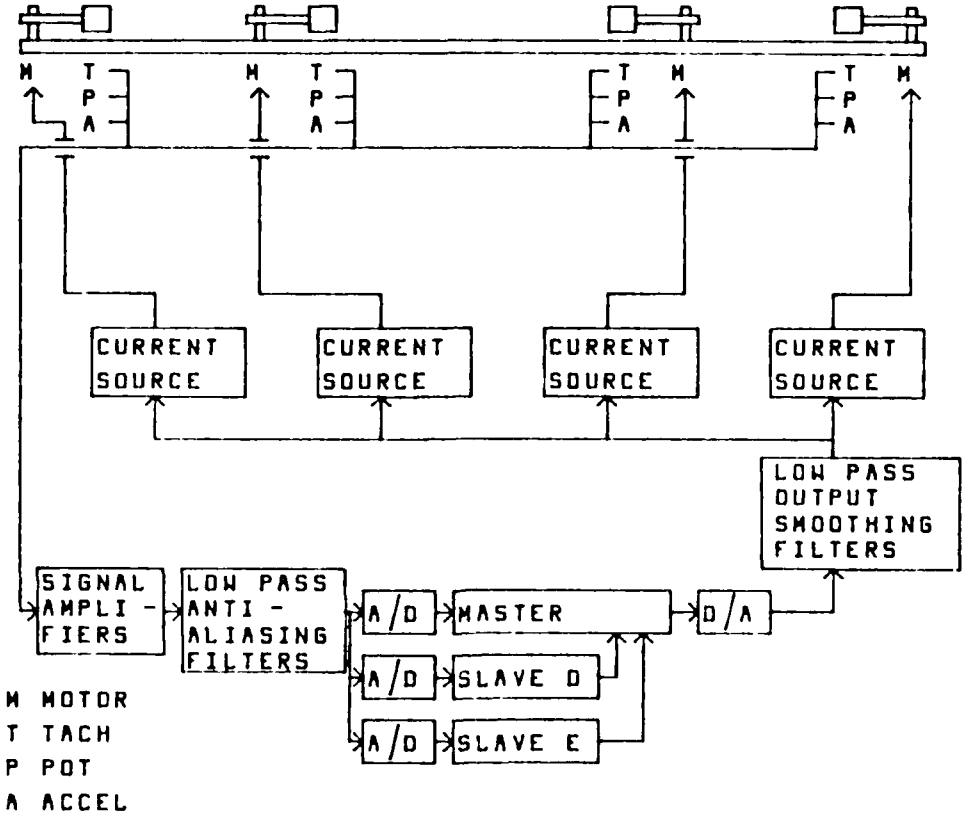

FIG. 4.1: EXPERIMENTAL HARDWARE CONFIGURATION.

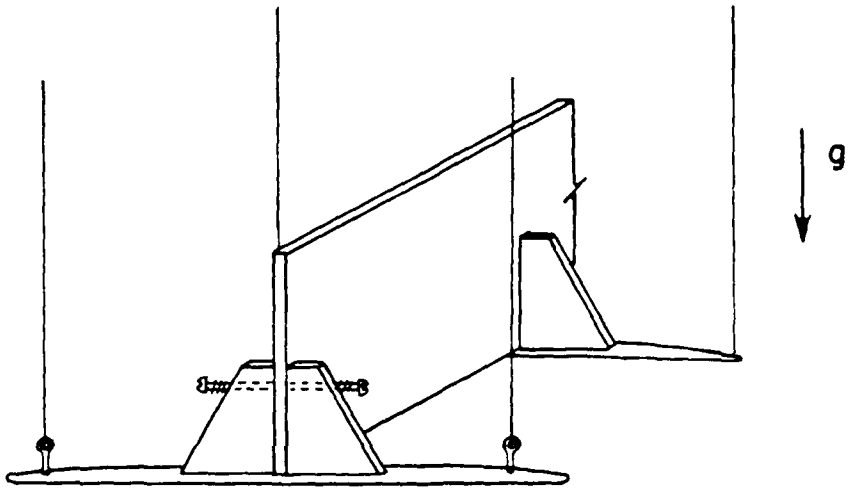

FIG. 4.2: SWINGING PARALLELOGRAM BEAM SUSPENSION.

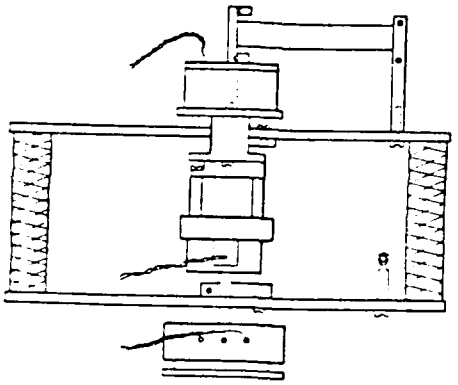

A: TORQUE CONFIGURATION

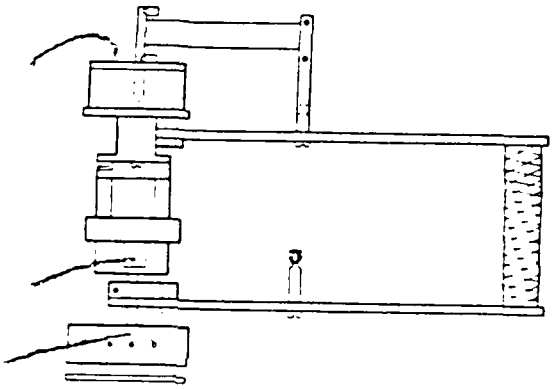

B: FORCE CONFIGURATION

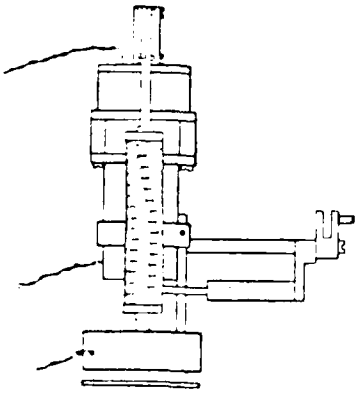

C: SIDE VIEW

FIG. 4.3: ELECTROMAGNETIC, INERTIAL-REACTION ACTUATOR CONFIGURATIONS.

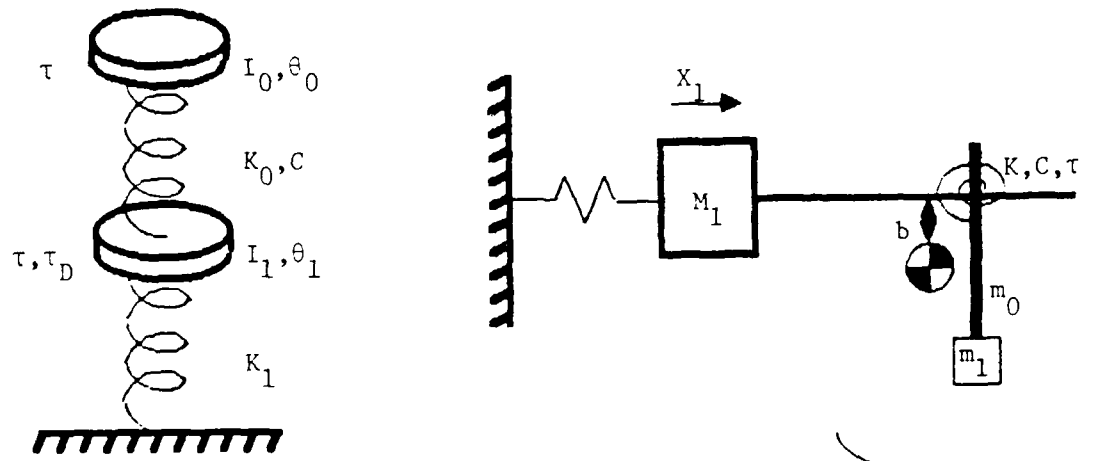

A: MODEL OF A SINGLE DOF TORQUE ACTUATOR CONTROLLING A SINGLE ROTATIONAL MODE OF A STRUCTURE.

B: MODEL OF A SINGLE DOF FORCE ACTUATOR CONTROLLING A SINGLE TRANSLATIONAL MODE OF A STRUCTURE.

FIG. 4.4: MODELS OF ACTUATOR CONFIGURATIONS COUPLED TO A SINGLE DOF STRUCTURAL REPRESENTATION.

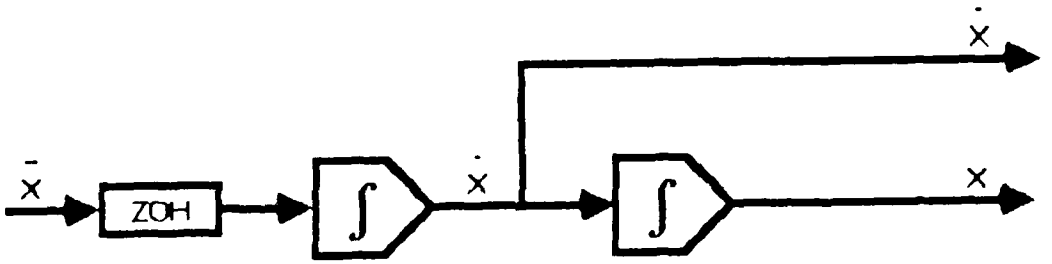

A: OPEN-LOOP CONFIGURATION

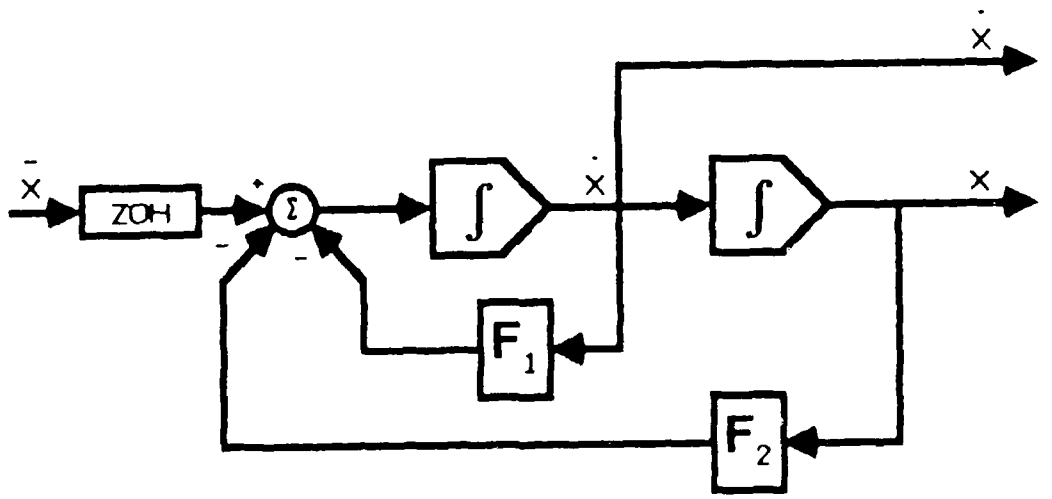

B: CLOSED-LOOP CONFIGURATION

FIG. 4.5: BLOCK DIAGRAM OF A DIGITAL DOUBLE INTEGRATOR.

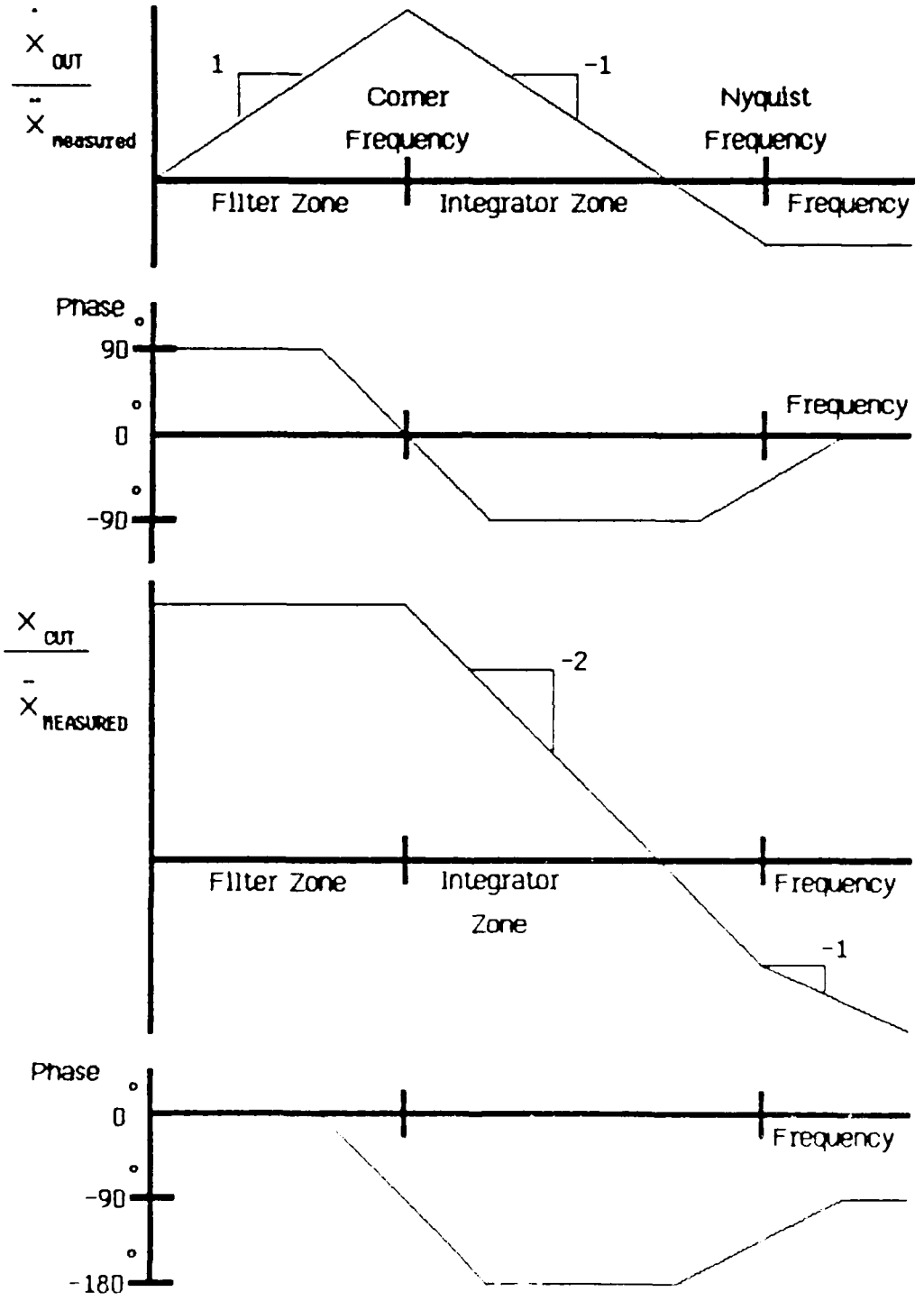

FIG. 4.6: FREQUENCY RESPONSE OF STABILIZED DOUBLE INTEGRATOR.

AD-A169 928 DEVELOPMENT OF FINITE ACTIVE CONTROL ELEMENTS FOR LARGE 3/3
FLEXIBLE SPACE ST.. (U) MASSACHUSETTS INST OF TECH
CAMBRIDGE MA SPACE SYSTEMS LAB D W MILLER ET AL.
UNCLASSIFIED 02 JUN 85 MIT-SSL-6-85 AFOSR-TR-86-0480 F/G 20/11 NL

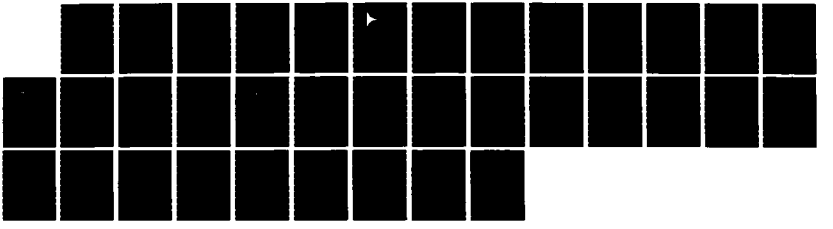

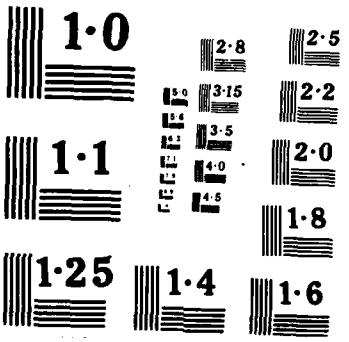
1·0
2·8
2·5
3·15
2·2
1·1
3·5
2·0
4·0
4·5
1·8
1·25
1·4
1·6

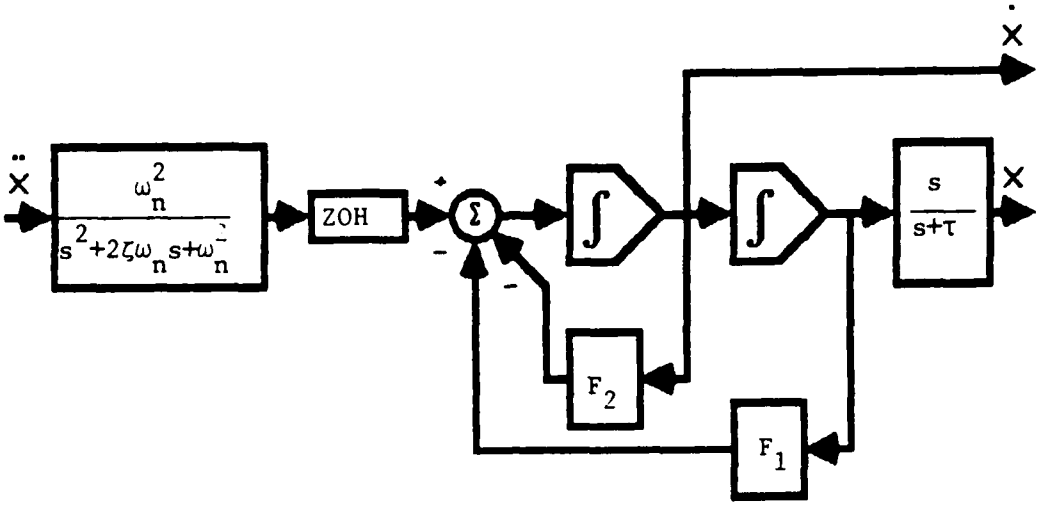

FIG. 4.7: BLOCK DIAGRAM OF TOTAL INTEGRATION AND FILTERING SYSTEM.

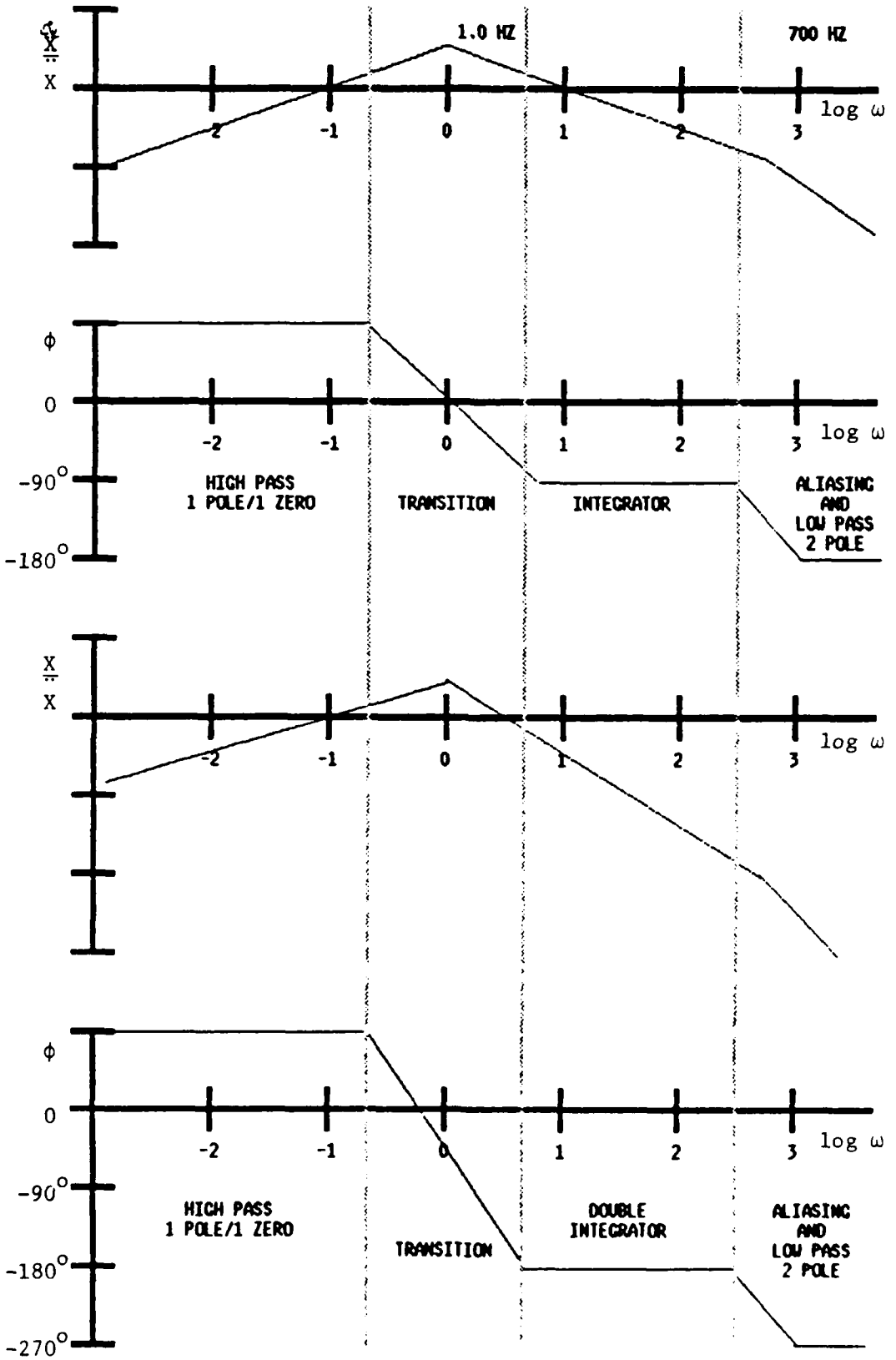

FIG. 4.8: FREQUENCY RESPONSES OF SINGLE AND DOUBLE INTEGRATING AND FILTERING SYSTEMS.

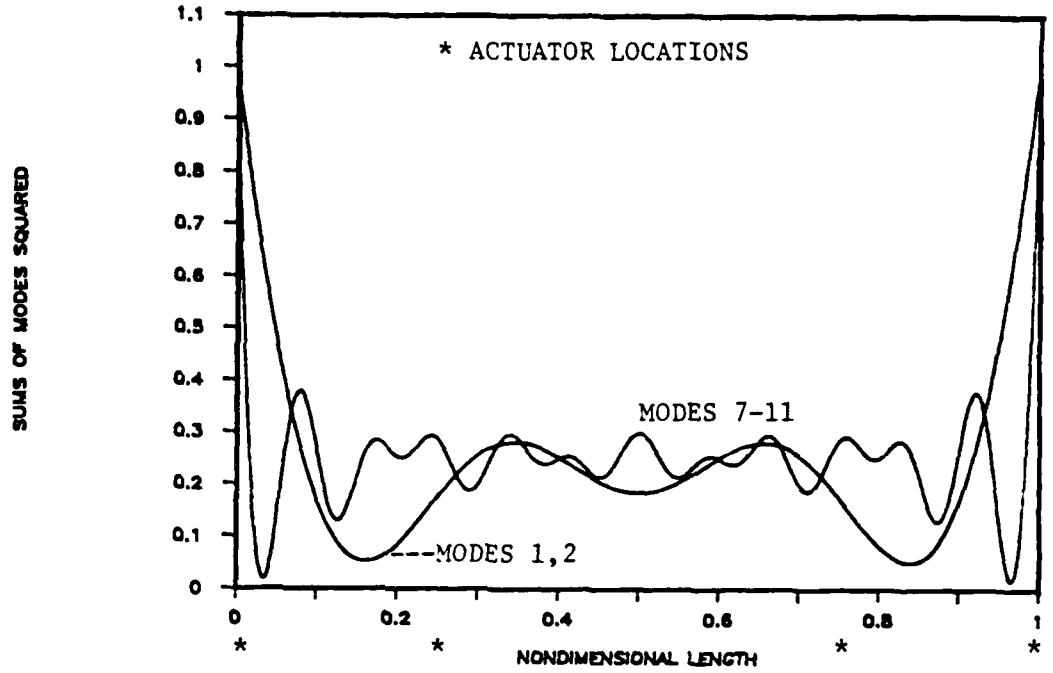

(A)

THE SUM OF THE SQUARES OF THE CONTROLLED MODE SHAPES

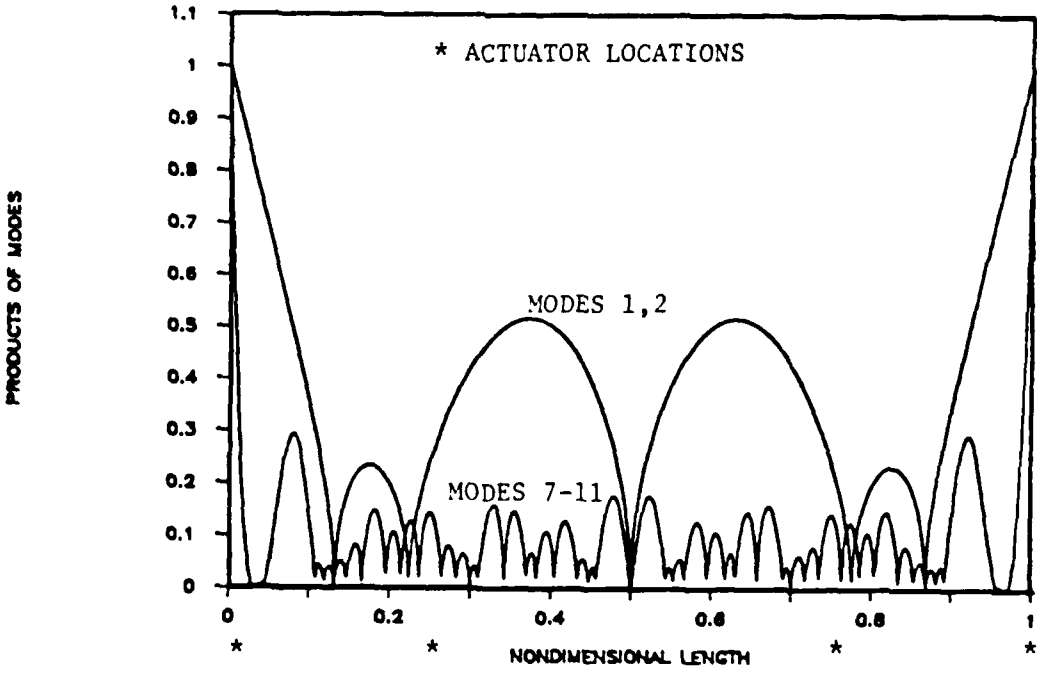

(B)

THE PRODUCT OF THE SQUARES OF THE CONTROLLED MODE SHAPES.

FIG. 5.1: ACTUATOR EFFECTIVENESS AS A FUNCTION OF POSITION ON THE BEAM AS INDICATED BY (A) AND (B).

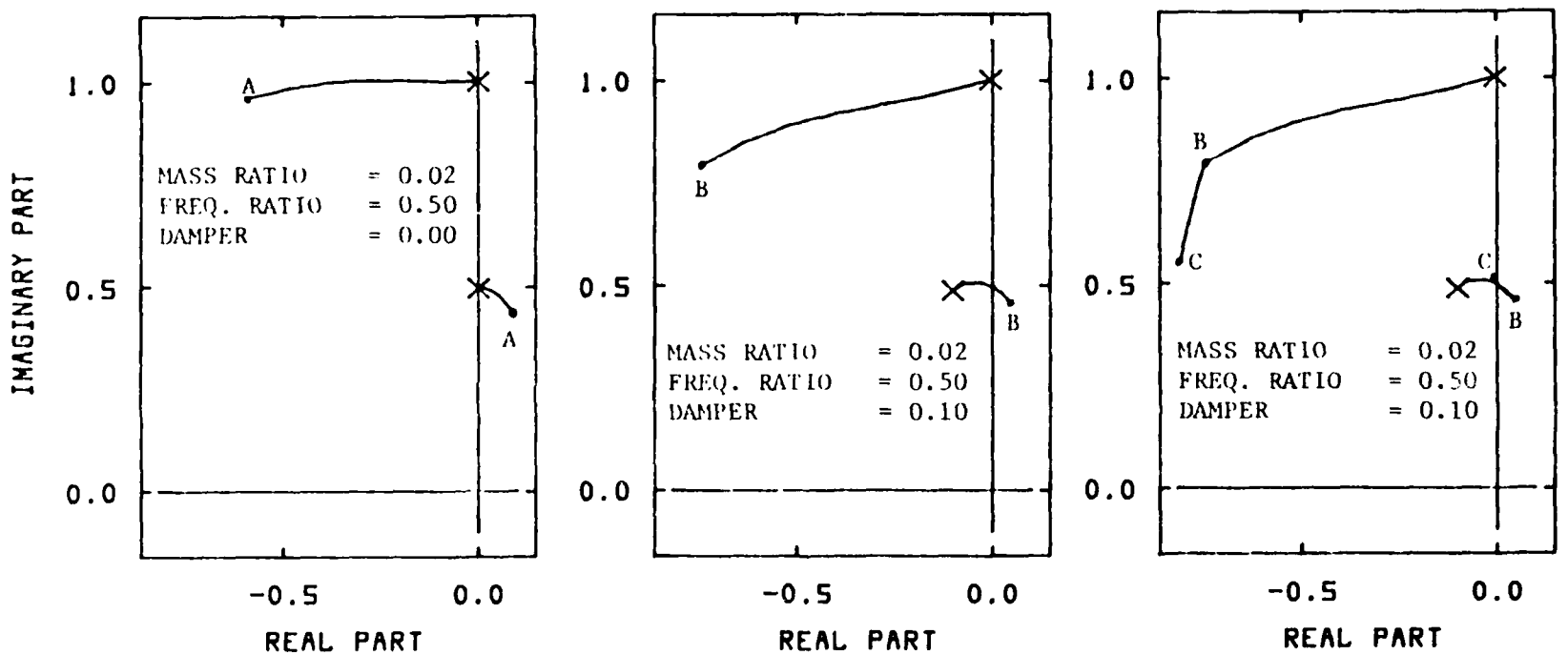

A: PURELY BEAM RATE FEEDBACK WITH NO PASSIVE DAMPER ($\mu = 0$).

B: BEAM RATE FEEDBACK WITH THE PASSIVE ACTUATOR DAMPER INCLUDED ($\mu > 0$).

C: STABILIZATION OF CASE B THROUGH ADDITIONAL ACTUATOR RATE FEEDBACK.

FIG. 5.2: ROOT LOCUS OF THE TWO DOF MODEL WHEN RATE FEEDBACK IS USED.

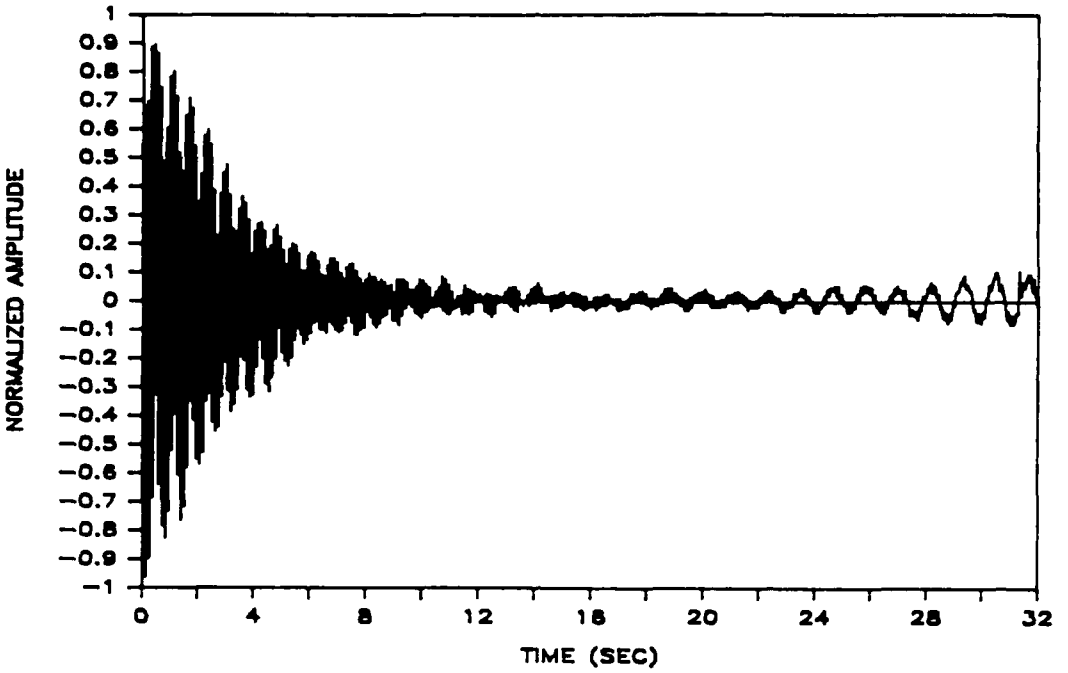

FIG. 5.3: EXPERIMENTAL INSTABILITY INTRODUCED BY HIGH GAIN BEAM RATE FEEDBACK (SEE FIGURE 5.2b).

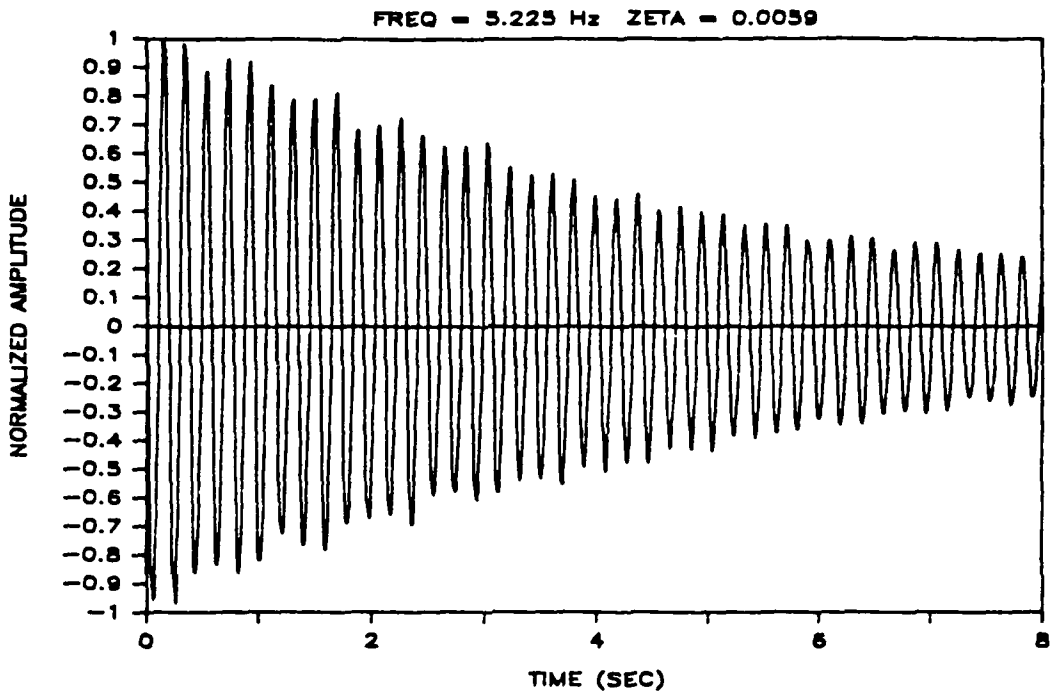

A: OPEN-LOOP

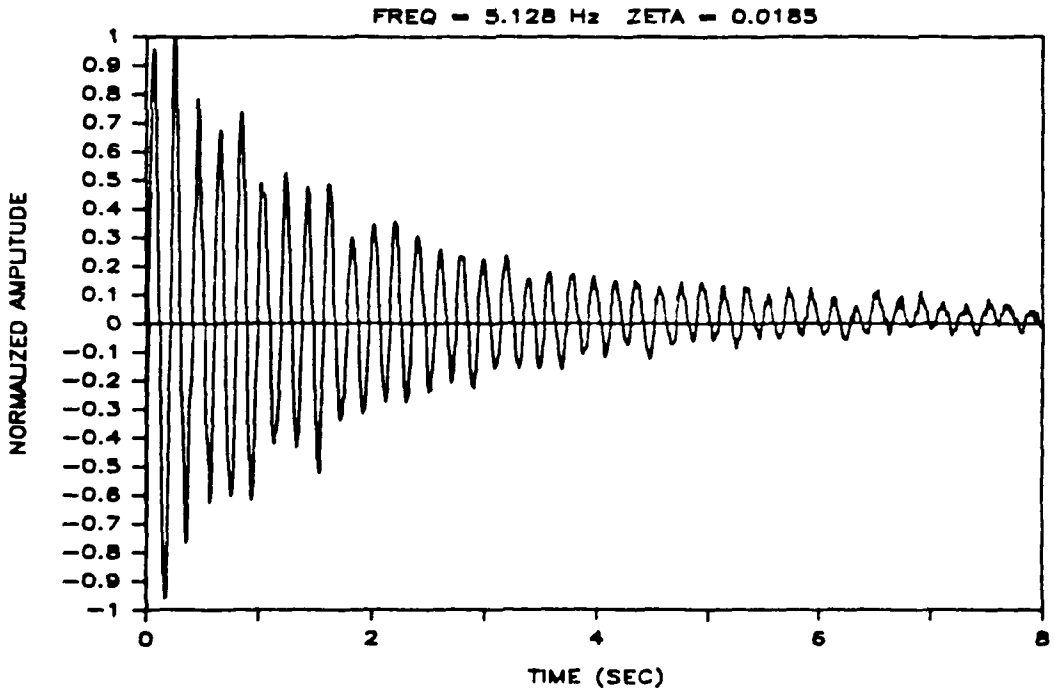

B: CLOSED-LOOP

FIG. 5.4: EXPERIMENTAL TRANSIENT DECAY OF SEVENTH MODE.

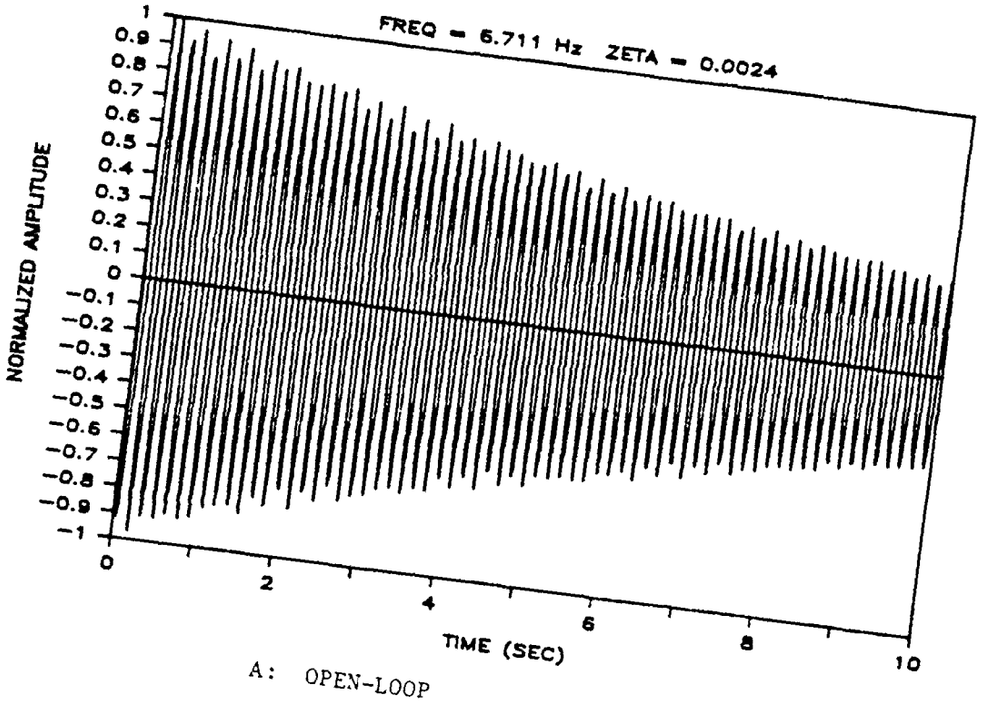

A: OPEN-LOOP

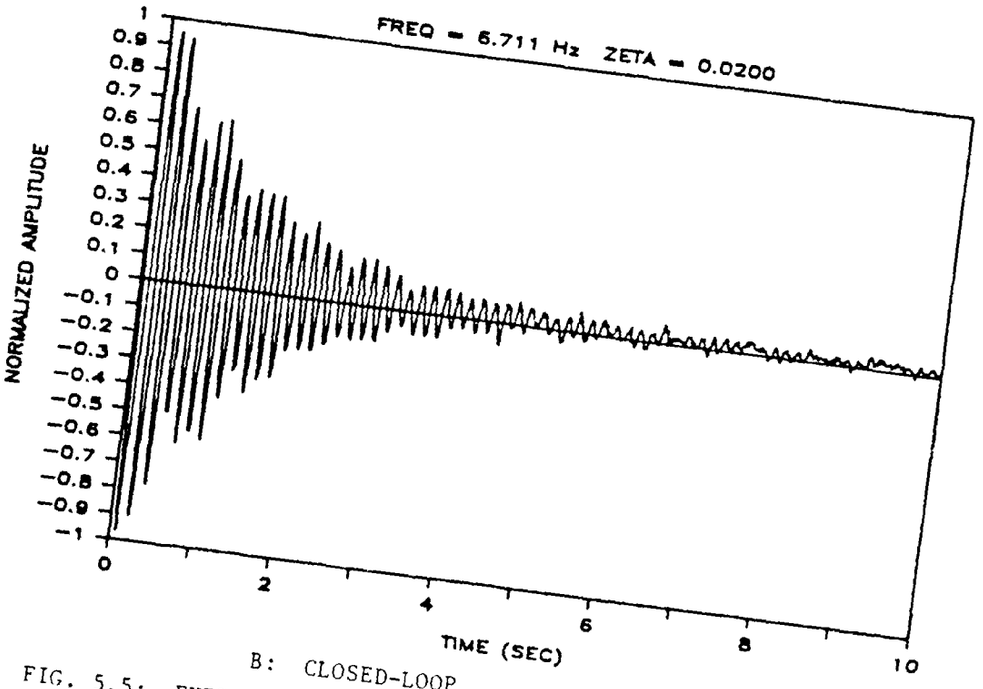

B: CLOSED-LOOP

FIG. 5.5: EXPERIMENTAL TRANSIENT DECAY OF EIGHTH MODE.

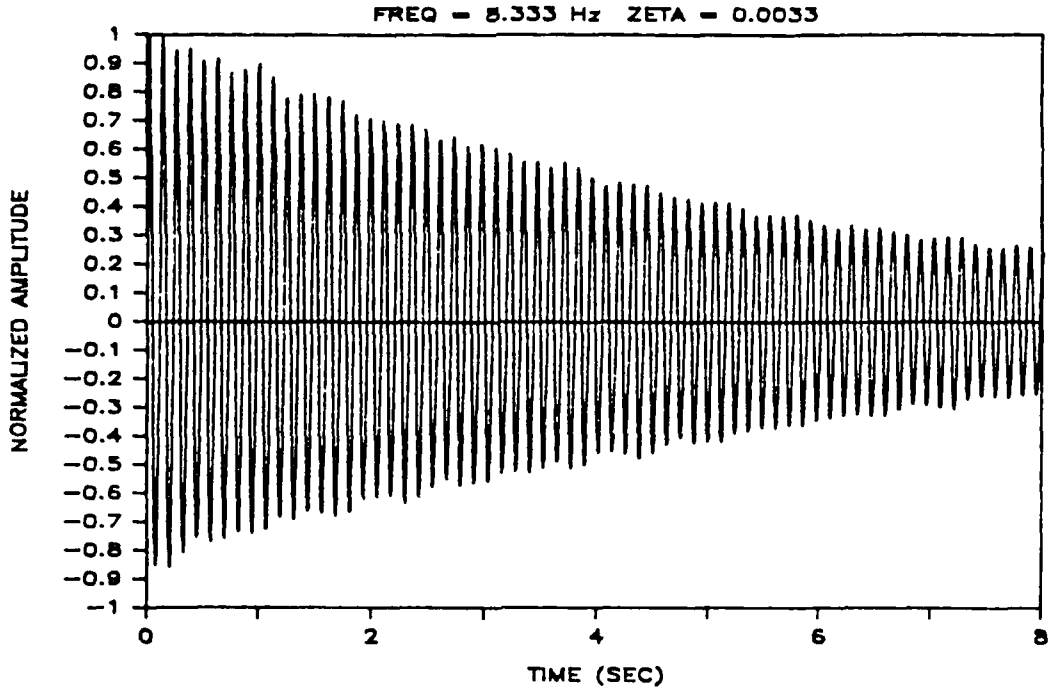

A: OPEN-LOOP

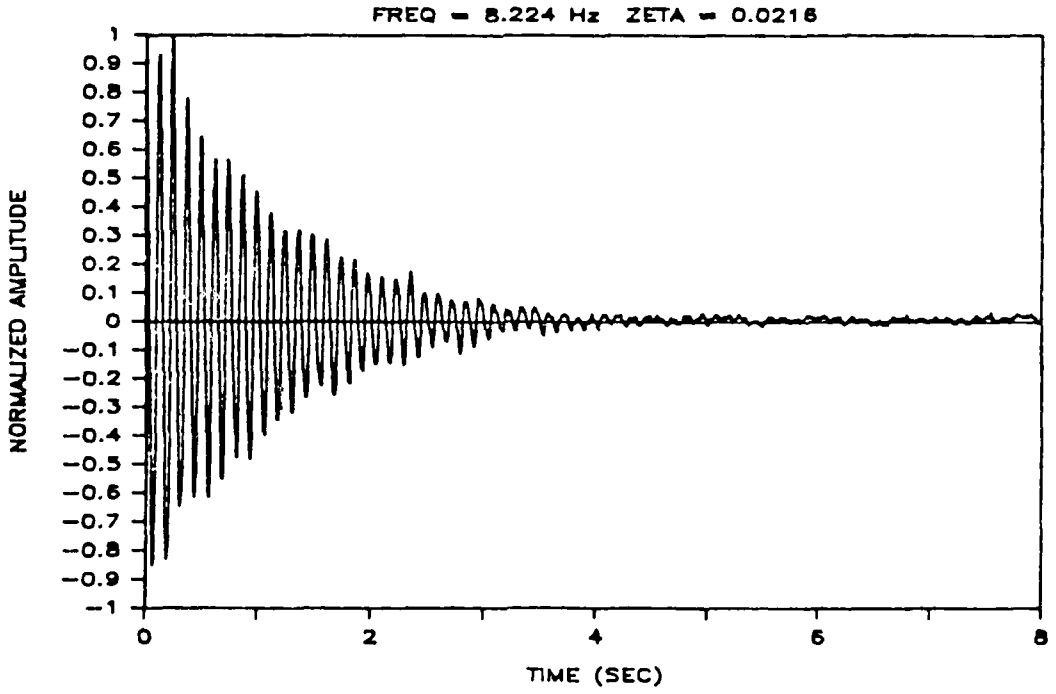

B: CLOSED-LOOP

FIG. 5.6: EXPERIMENTAL TRANSIENT DECAY OF NINTH MODE.

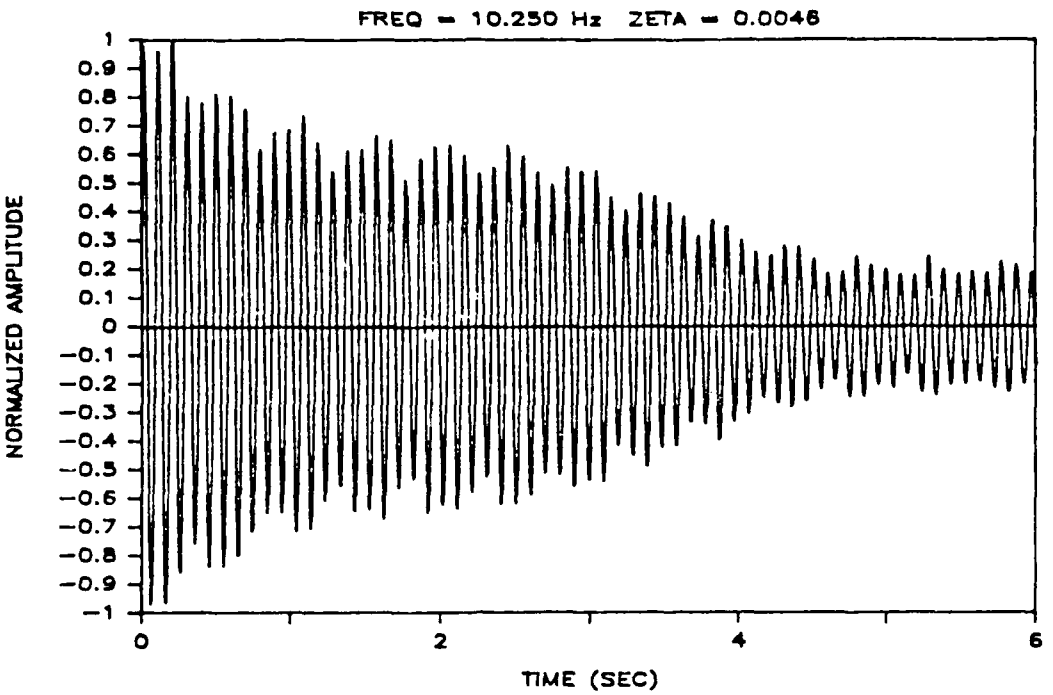

A: OPEN-LOOP

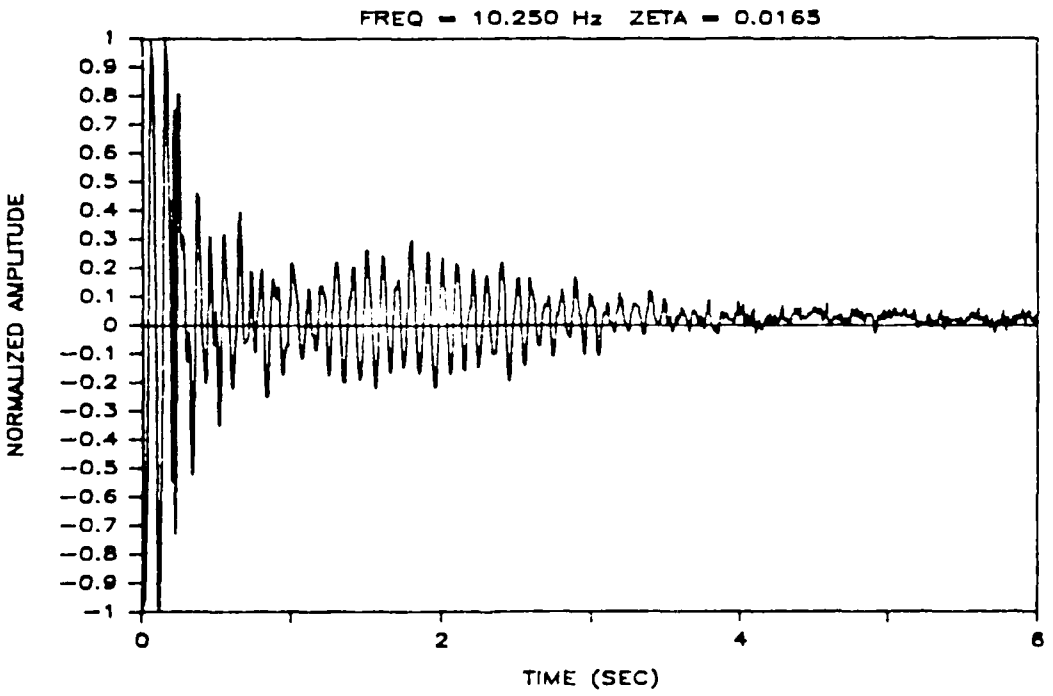

B: CLOSED-LOOP

FIG. 5.7: EXPERIMENTAL TRANSIENT DECAY OF TENTH MODE.

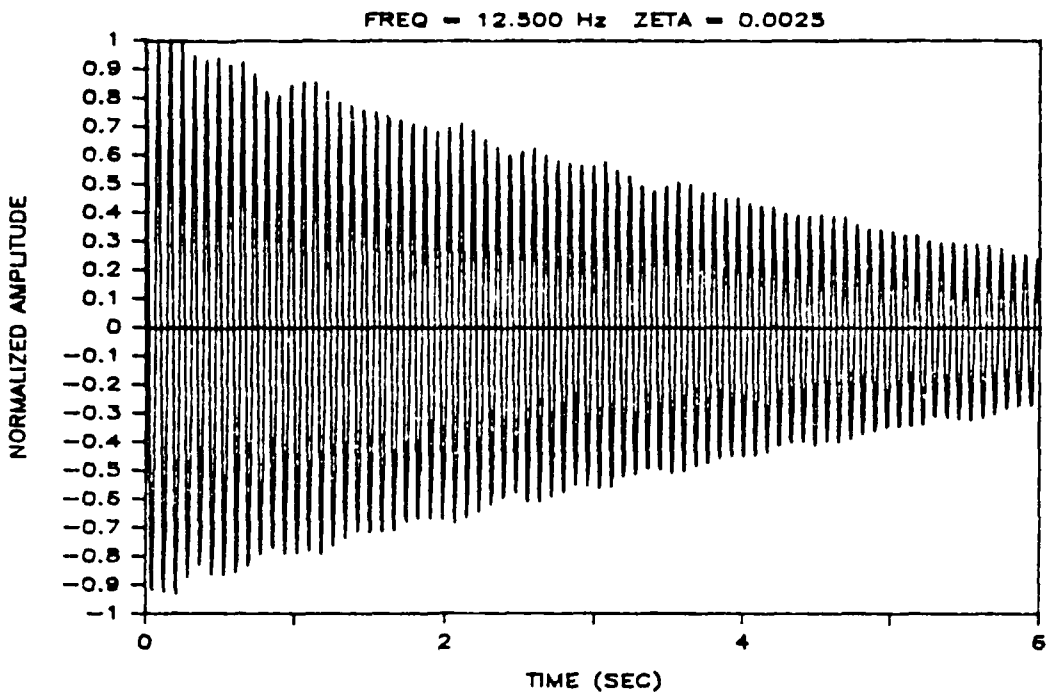

A: OPEN-LOOP

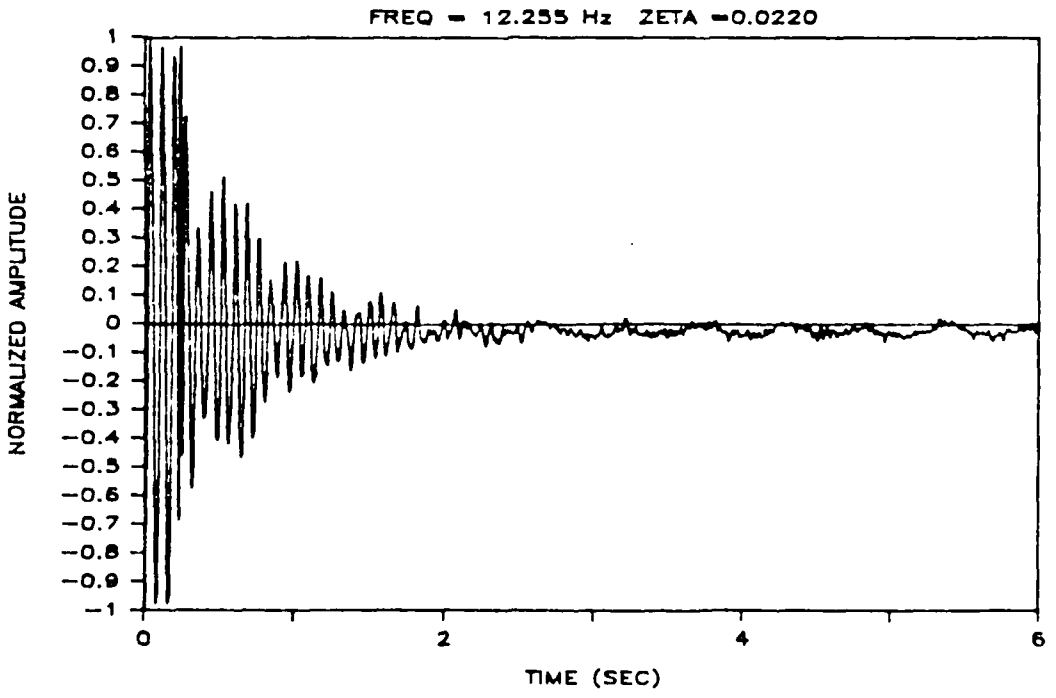

B: CLOSED-LOOP

FIG. 5.8: EXPERIMENTAL TRANSIENT DECAY OF ELEVENTH MODE.

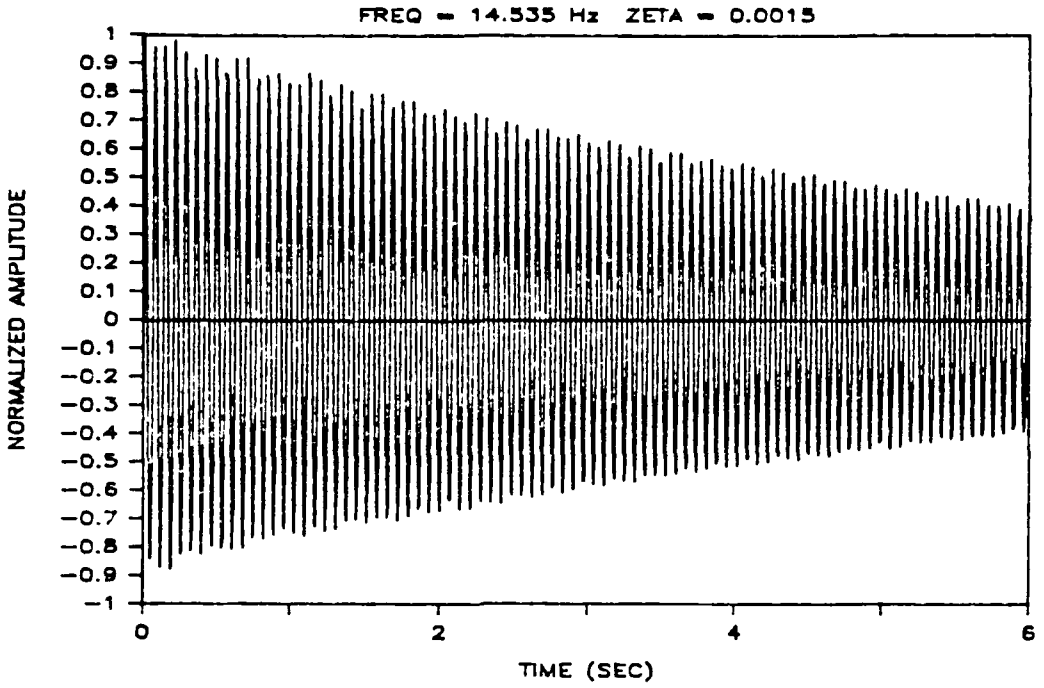

A: OPEN-LOOP

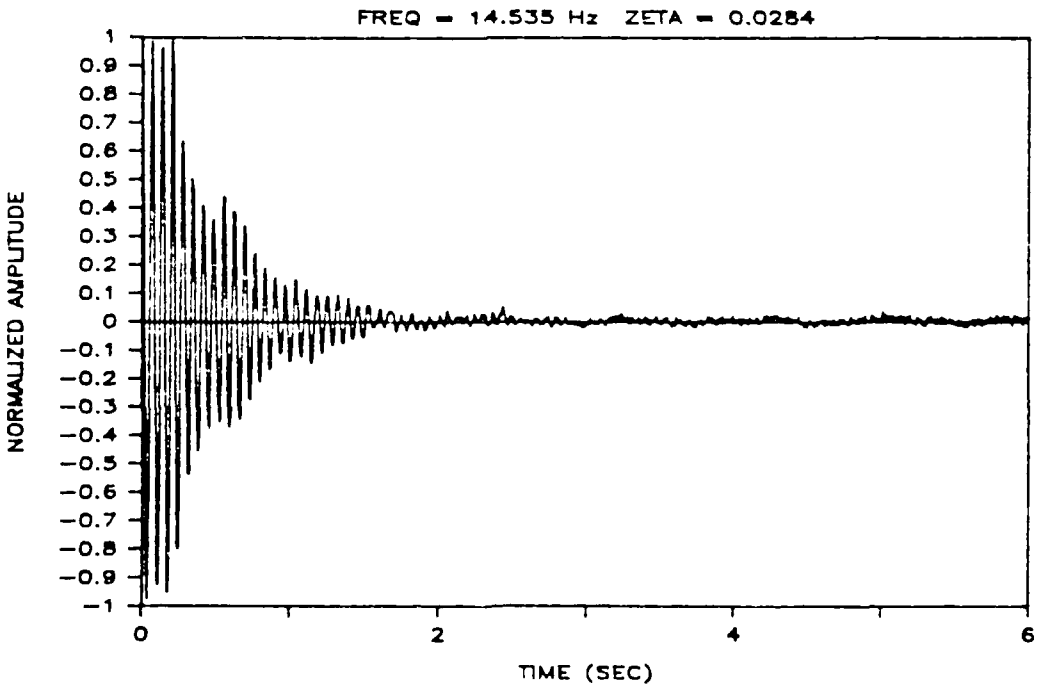

B: CLOSED-LOOP

FIG. 5.9: EXPERIMENTAL TRANSIENT DECAY OF TWELFTH MODE.

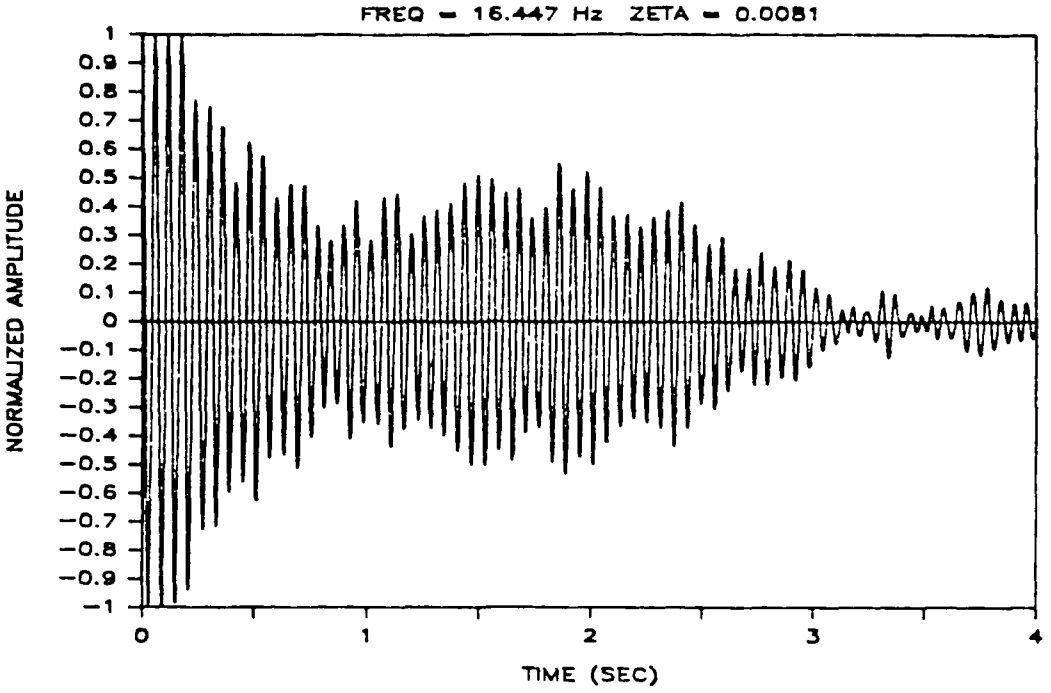

A: OPEN-LOOP

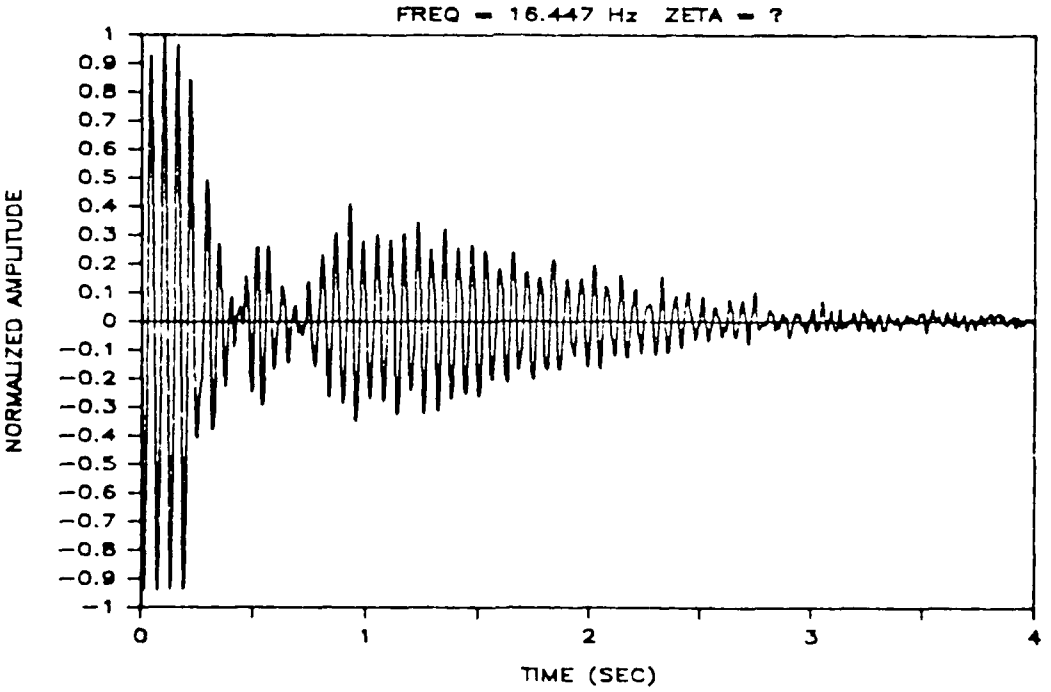

B: CLOSED-LOOP

FIG. 5.10: EXPERIMENTAL TRANSIENT DECAY OF THIRTEENTH MODE.

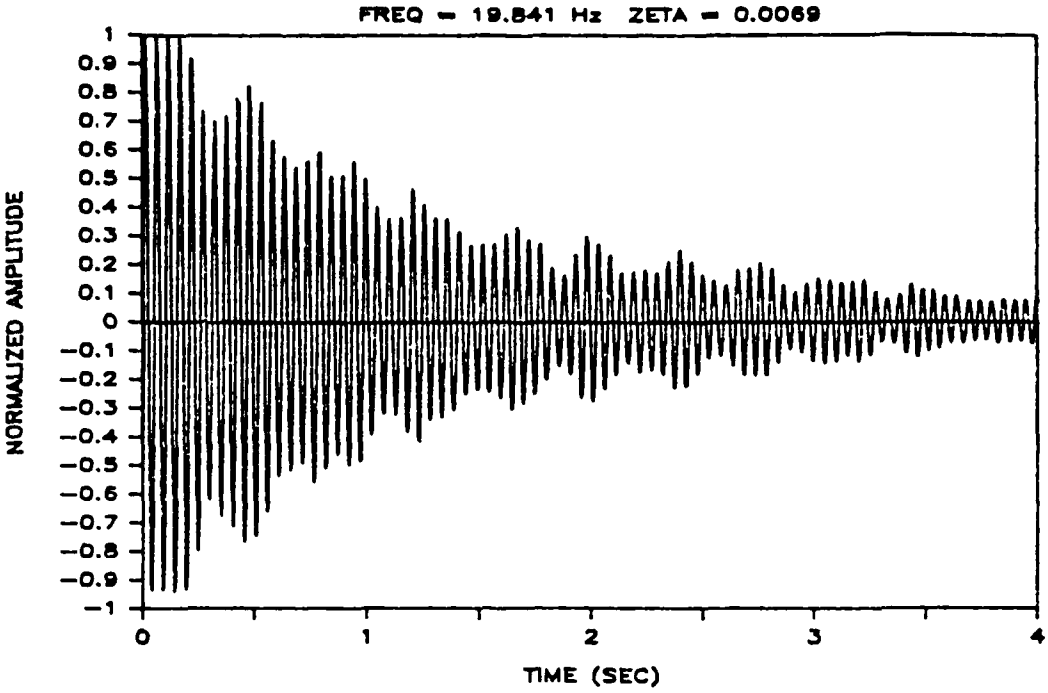

A: OPEN-LOOP

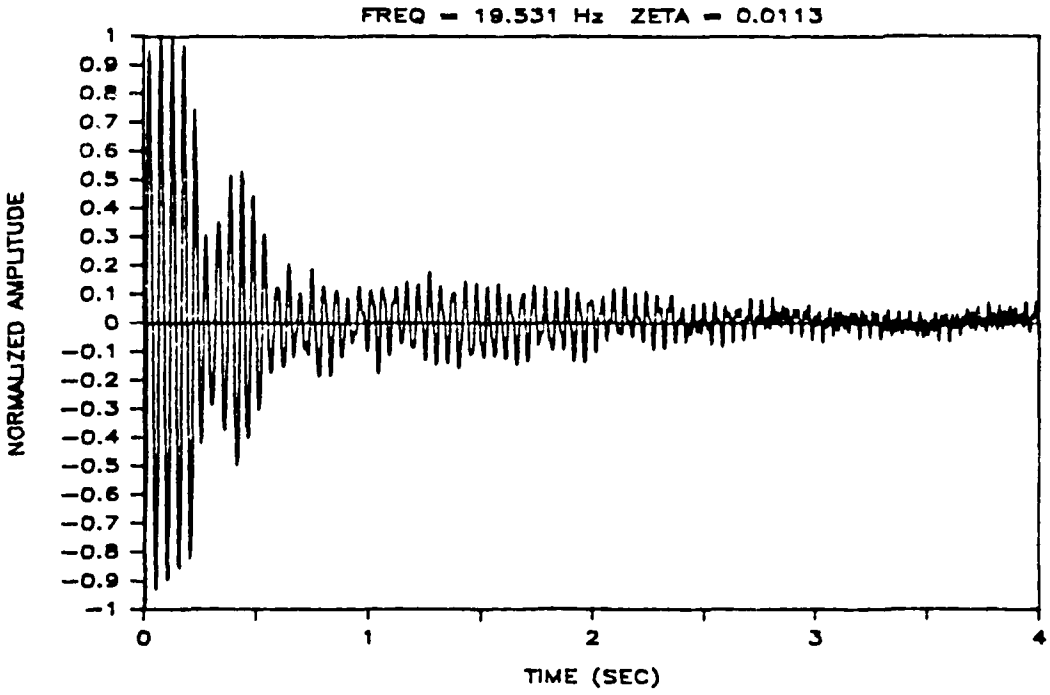

B: CLOSED-LOOP

FIG. 5.11: EXPERIMENTAL TRANSIENT DECAY OF FOURTEENTH MODE.

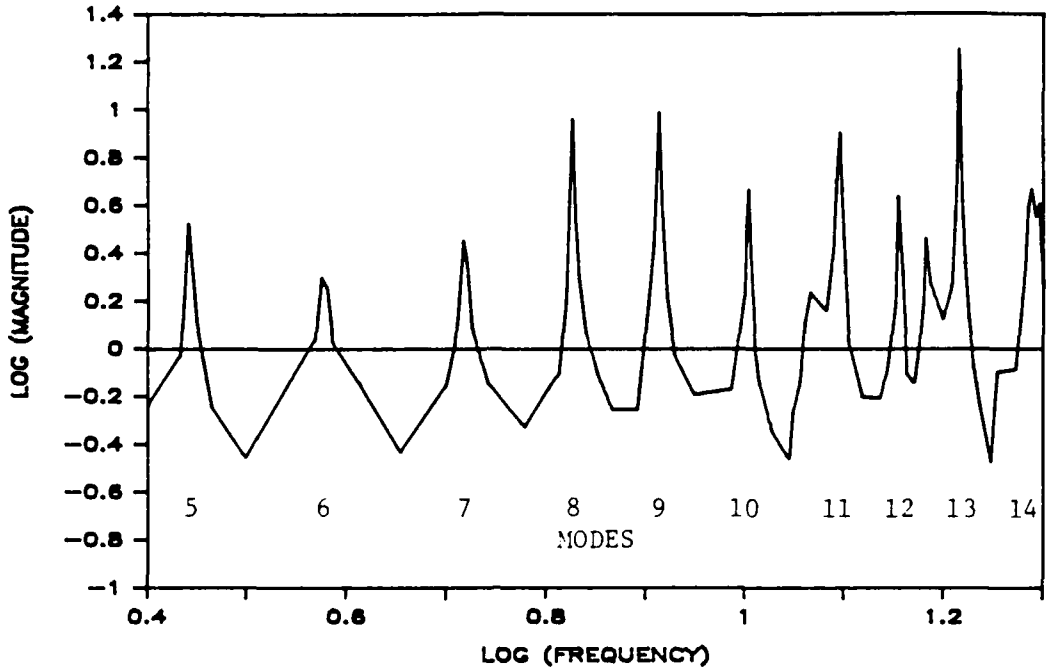

A: OPEN-LOOP

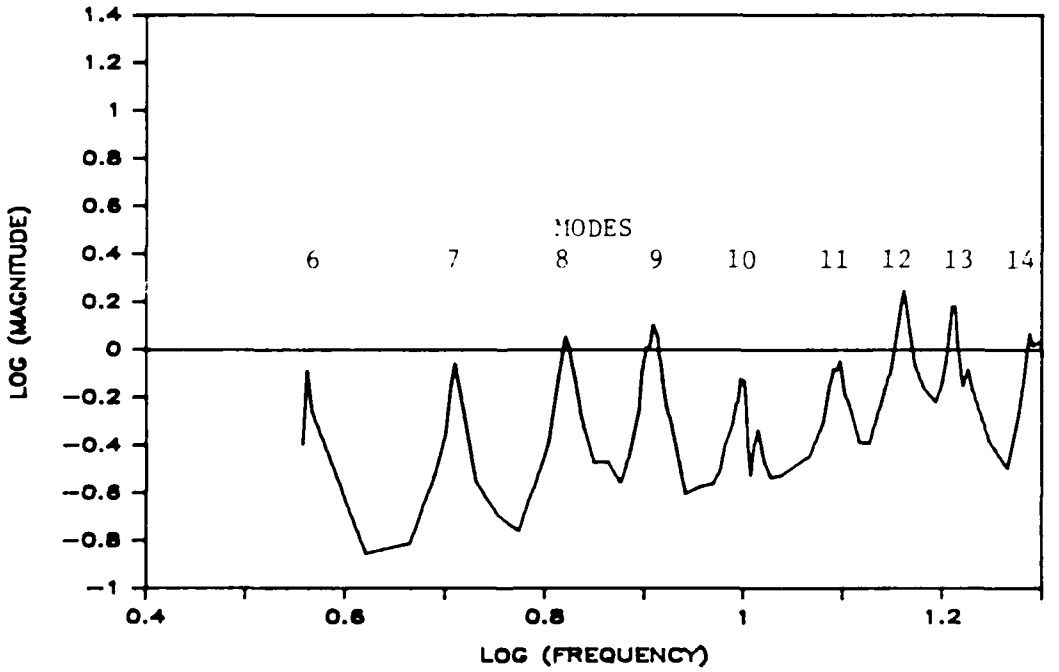

B: CLOSED-LOOP

FIG. 5.12: EXPERIMENTAL FORCED RESPONSE VERSUS SINUSOIDAL EXCITATION FOR OPEN AND CLOSED-LOOP CONTROLLER.

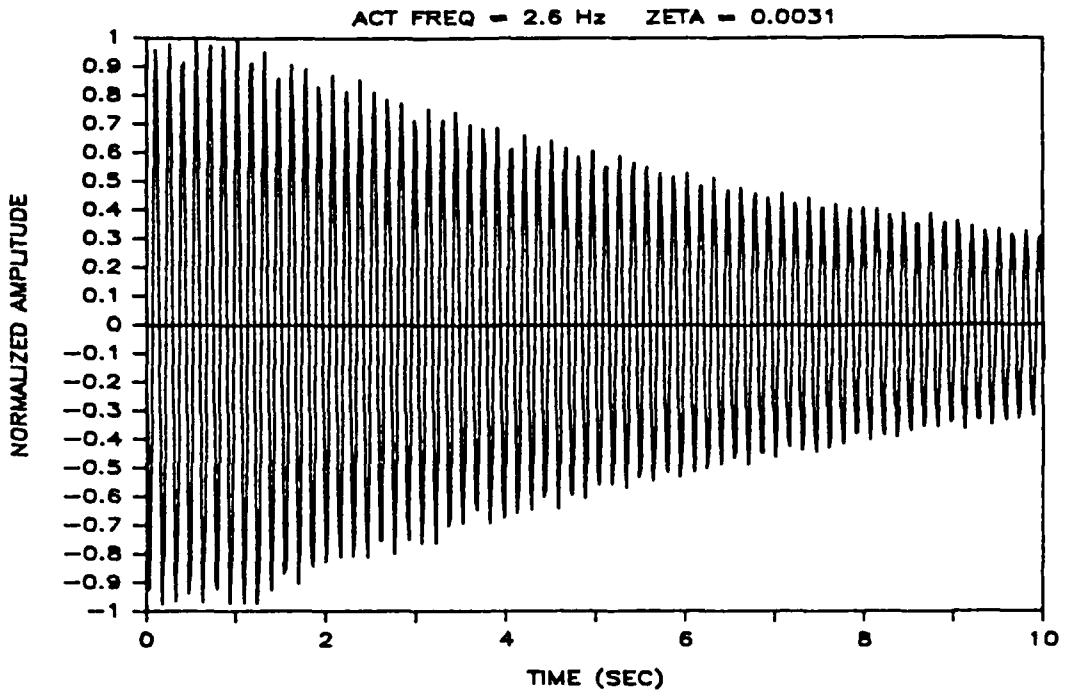

A: ACTUATOR FREQUENCY = 2.60 HZ.

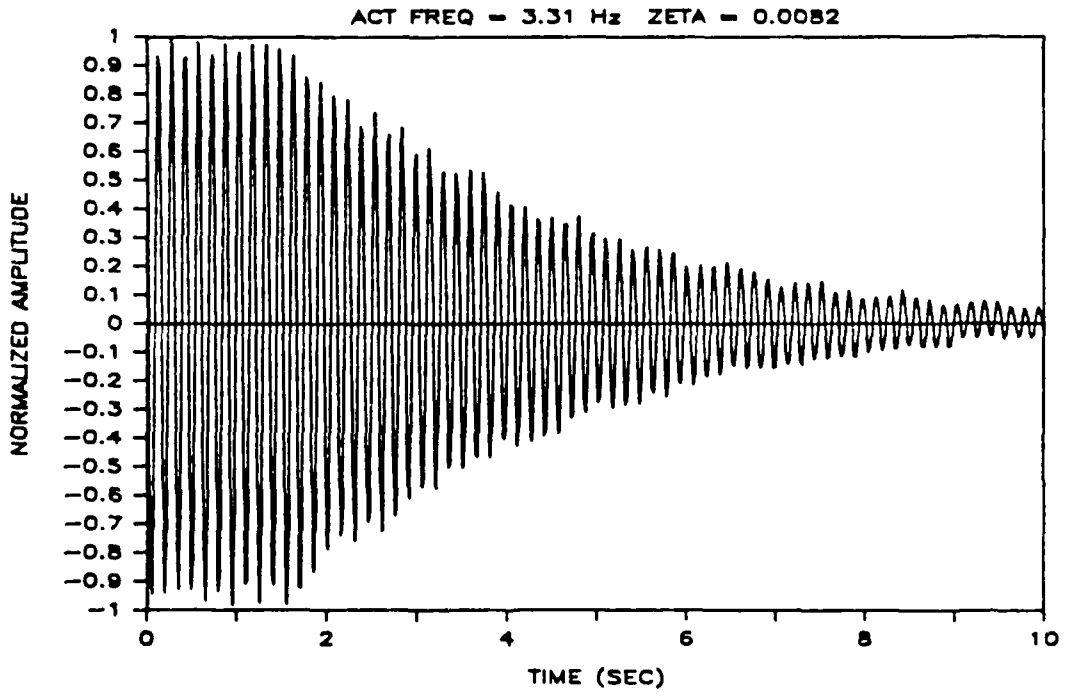

B: ACTUATOR FREQUENCY = 3.31 HZ.

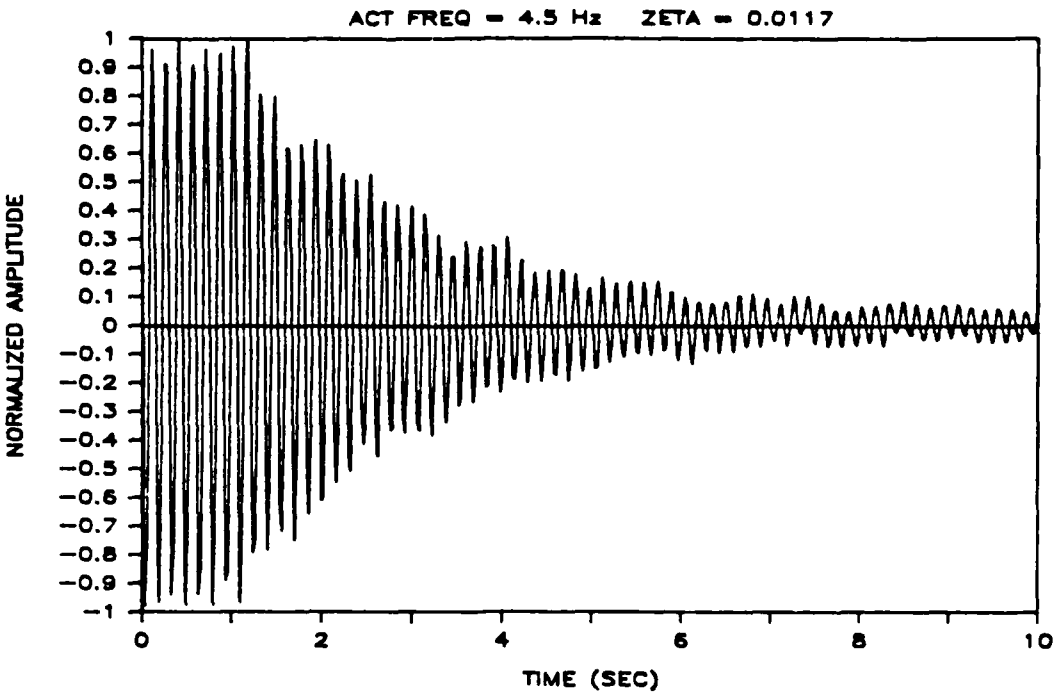

C: ACTUATOR FREQUENCY = 4.50 HZ.

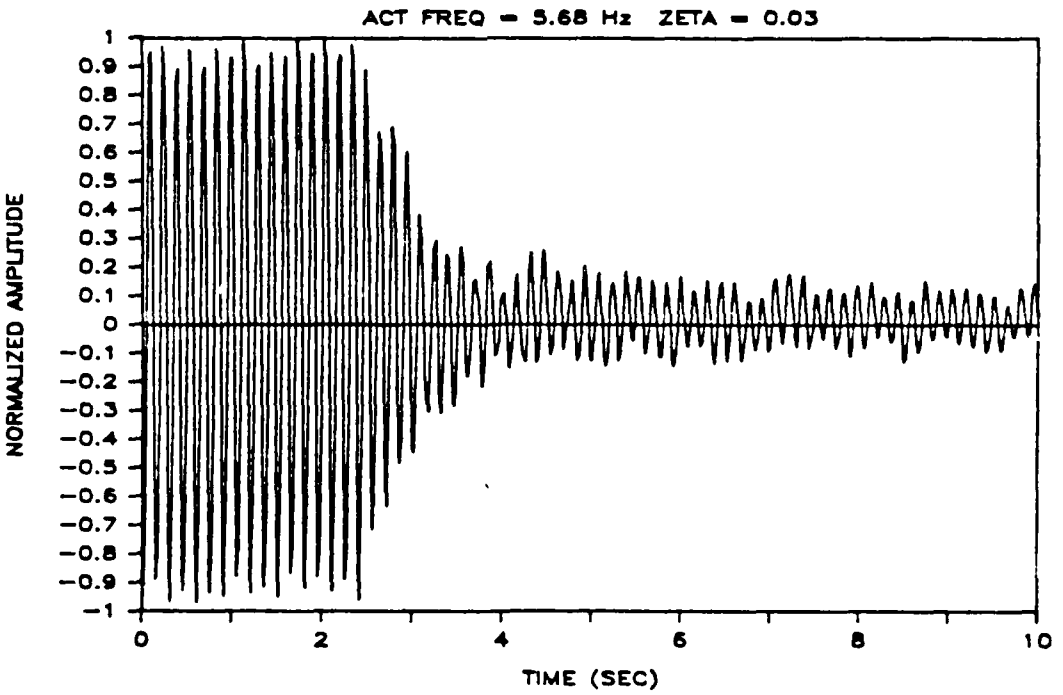

D: ACTUATOR FREQUENCY = 5.68 HZ.

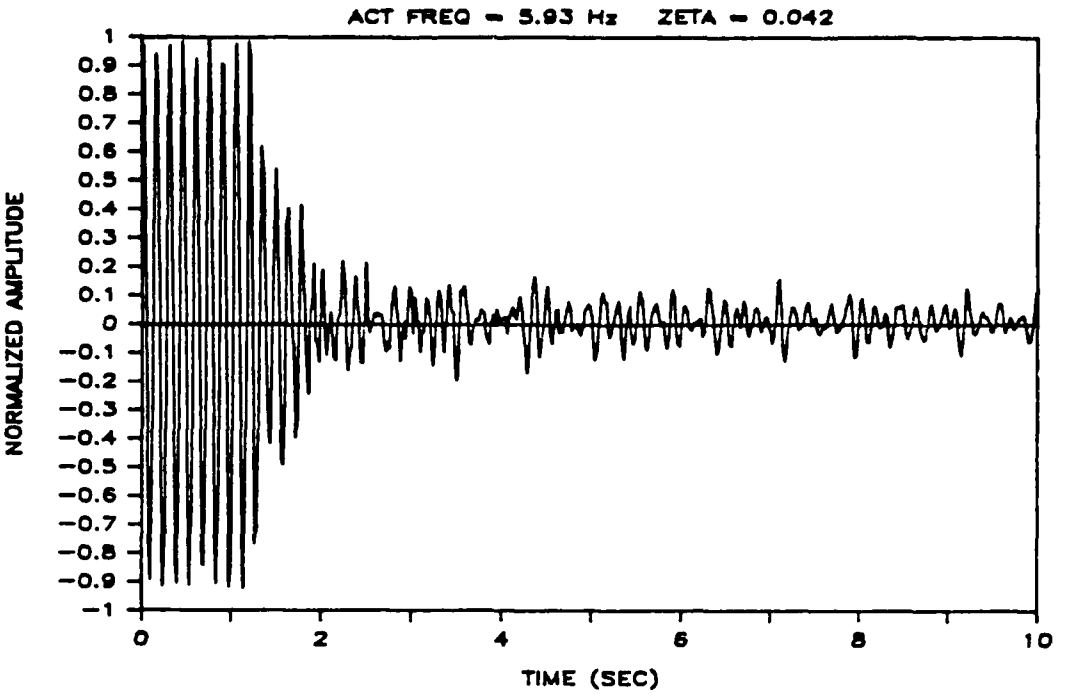

E: ACTUATOR FREQUENCY = 5.93 HZ.

FIG. 5.13: EXPERIMENTAL PASSIVE TUNING OF VIBRATION ABSORBER TO THE EIGHTH MODE.

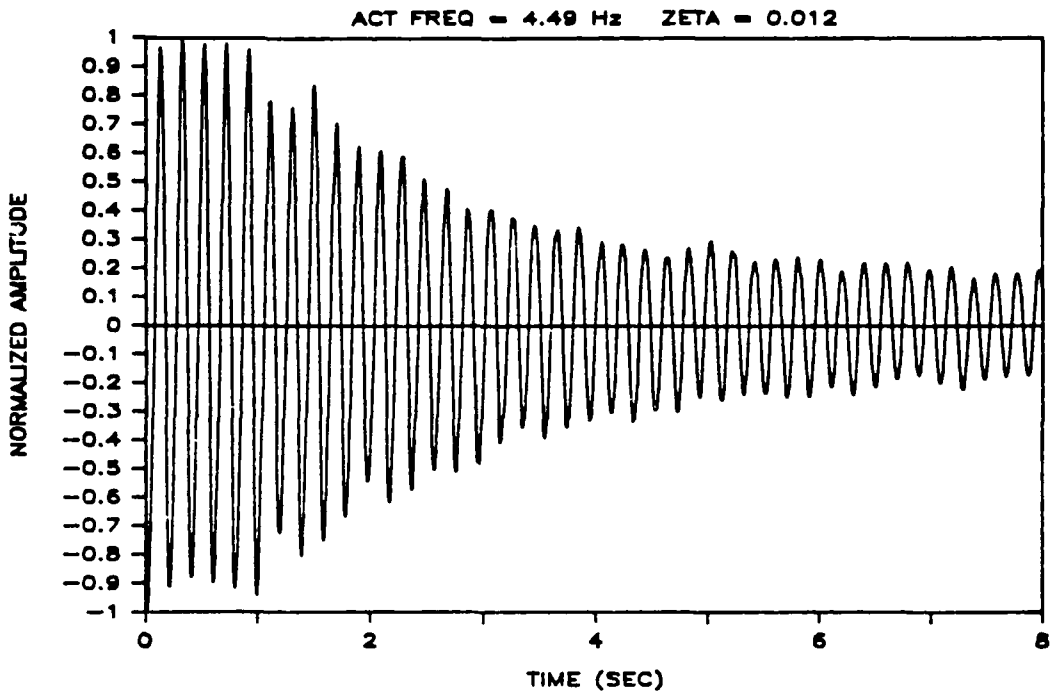

FIG. 5.14: EXPERIMENTAL PASSIVE TUNING TO THE SEVENTH MODE.

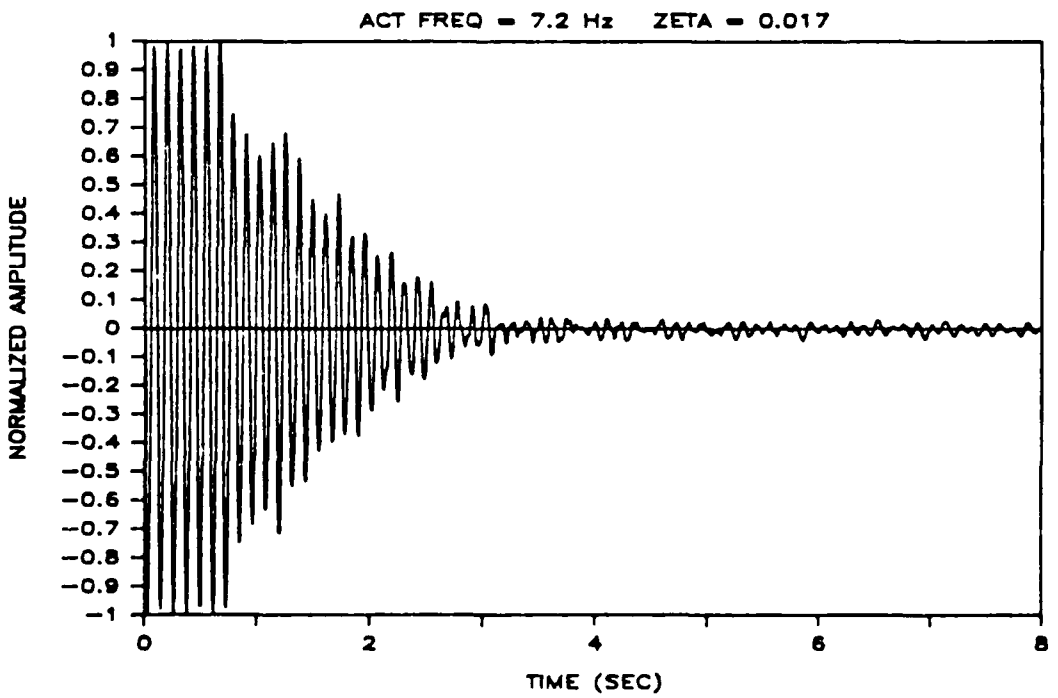

FIG. 5.15: EXPERIMENTAL PASSIVE TUNING TO THE NINTH MODE.

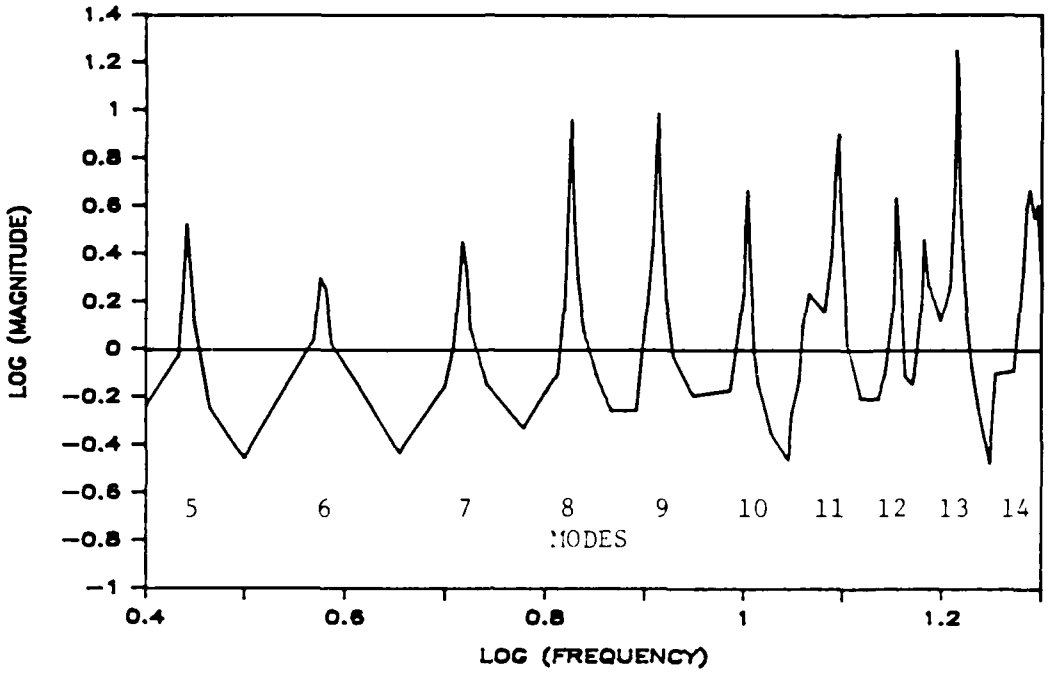

A: OPEN-LOOP

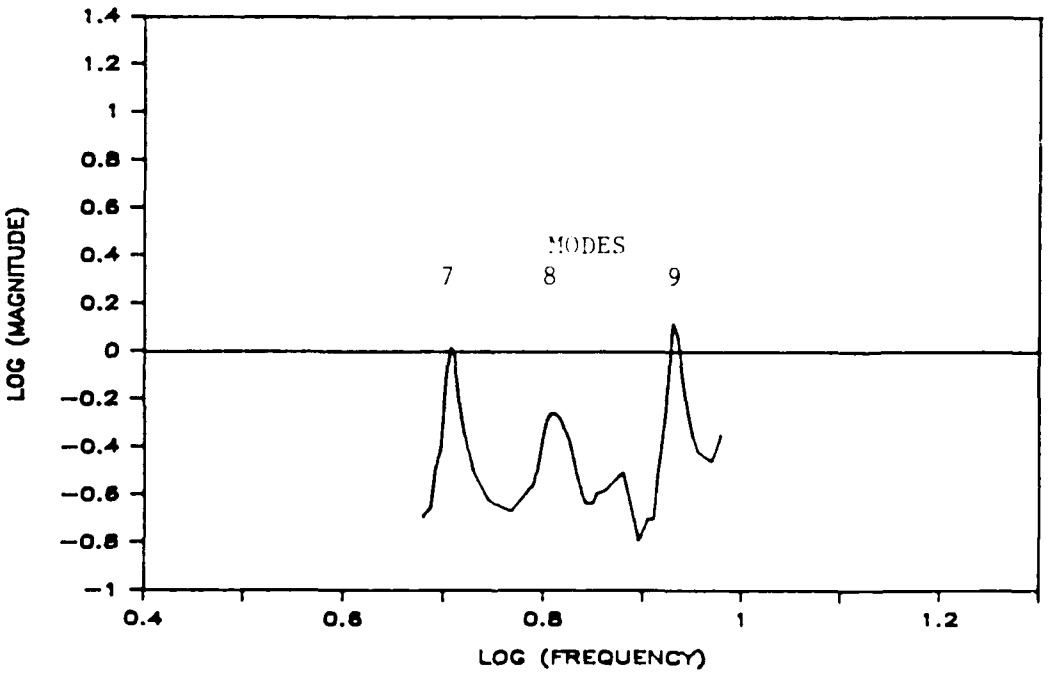

B: CLOSED-LOOP

FIG. 5.16: EXPERIMENTAL FORCED RESPONSE VERSUS SINUSOIDAL EXCITATION FOR UNTUNED AND TUNED ABSORBERS.

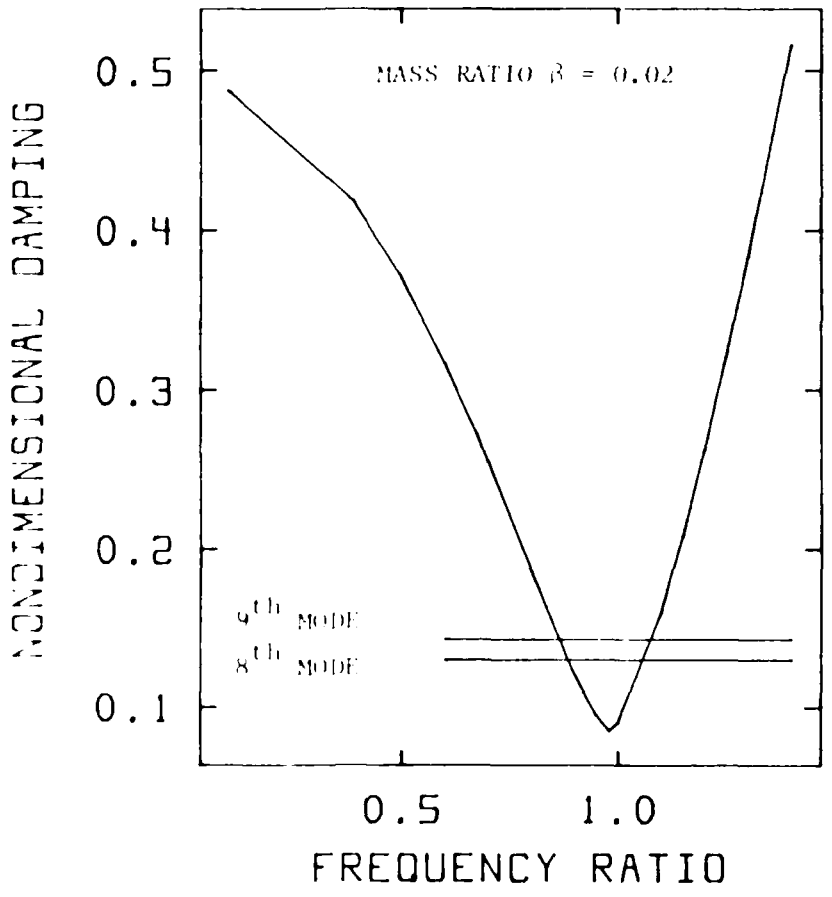

A: MINIMUM ACHIEVED DAMPER SETTINGS NEAR OPTIMAL FREQUENCY RATIOS.

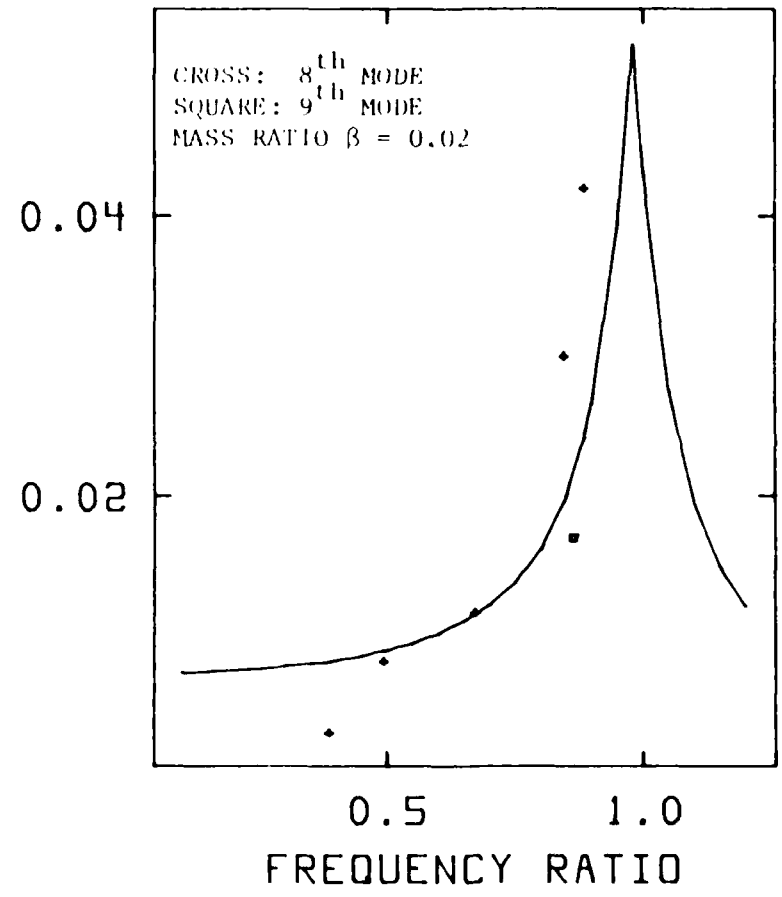

B: COMPARISON OF EXPERIMENTAL AND PREDICTED DAMPING RATIOS.

FIG. 5.17: COMPARISON OF EXPERIMENTAL RESULTS AND THEORETICAL PREDICTIONS.

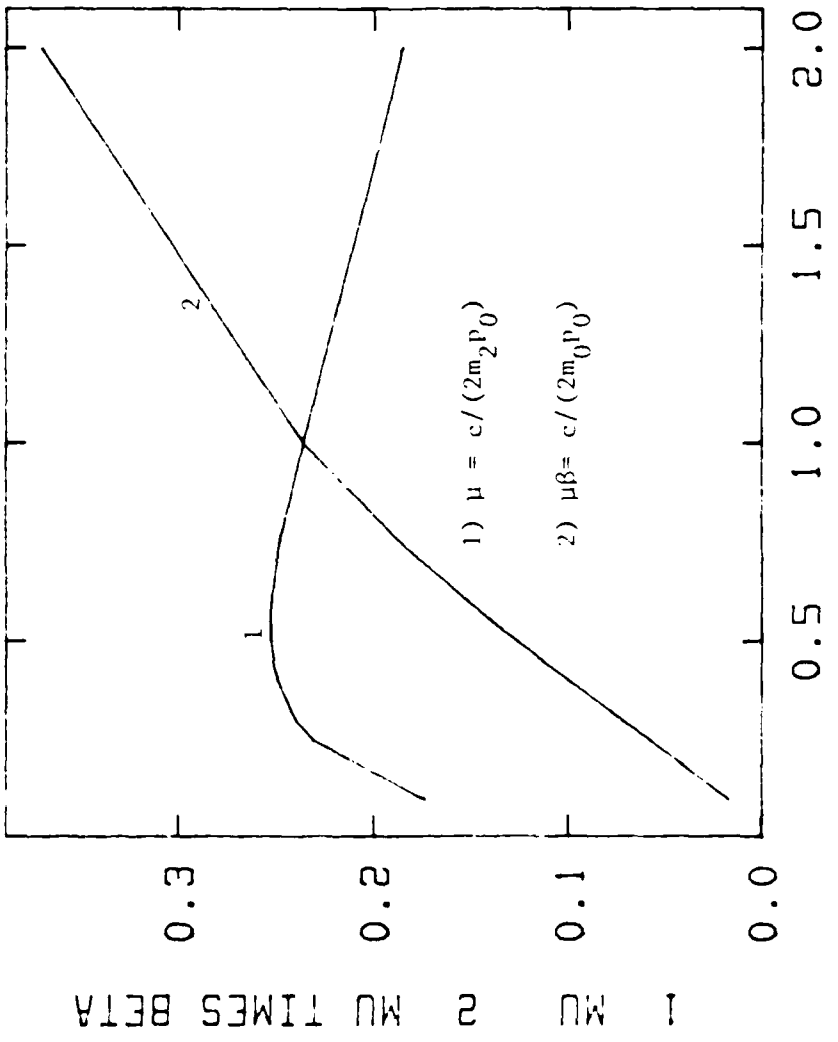

FIG. 5.18: OPTIMAL DAMPER CHARACTERISTICS VERSUS MASS RATIO.

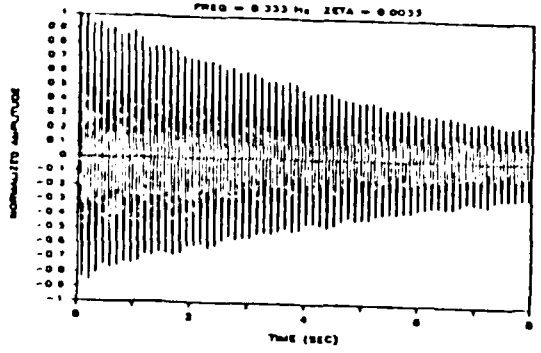

A: FREE DECAY

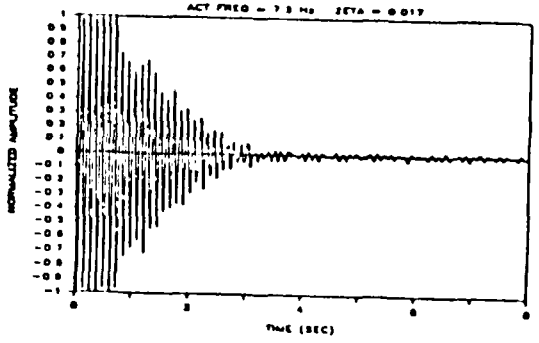

B: PASSIVELY TUNED DECAY

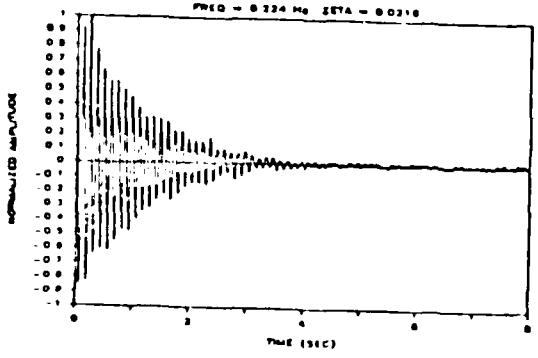

C: ACTIVELY CONTROLLED DECAY

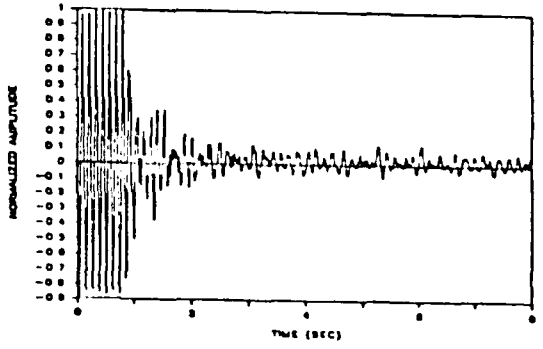

D: ACTIVELY CONTROLLED AND PASSIVELY TUNED DECAY

FIG. 5.19: COMPARISON OF DAMPING TESTS PERFORMED ON THE NINTH MODE.

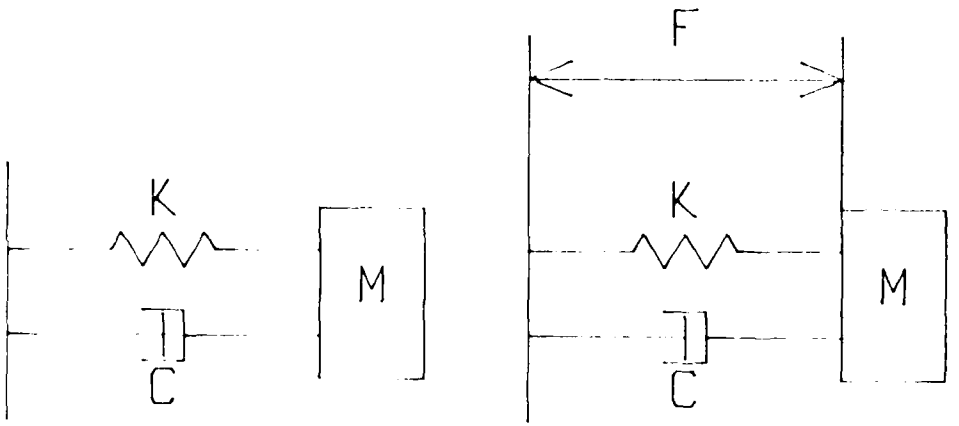

A PASSIVE VIBRATION ABSORBER OR DAMPER

B CONTROL ACTUATOR

FIG. A.1: DAMPER MODELS.

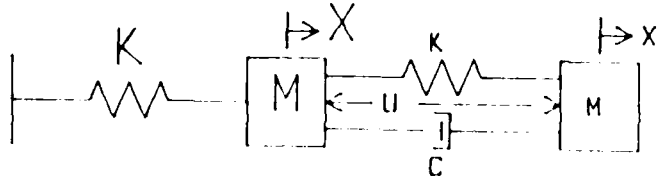

A SYSTEM ONE MODE STRUCTURE WITH DAMPER

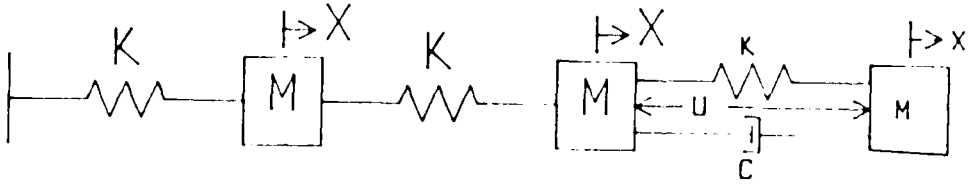

B SYSTEM TWO MODE STRUCTURE WITH DAMPER ON OUTER MASS

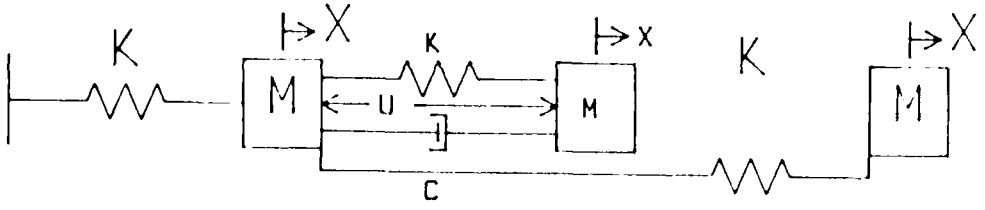

C SYSTEM TWO MODE STRUCTURE WITH DAMPER ON INNER MASS

FIG. A.2: STRUCTURAL REPRESENTATIONS COUPLED TO ONE DOF ABSORBER.

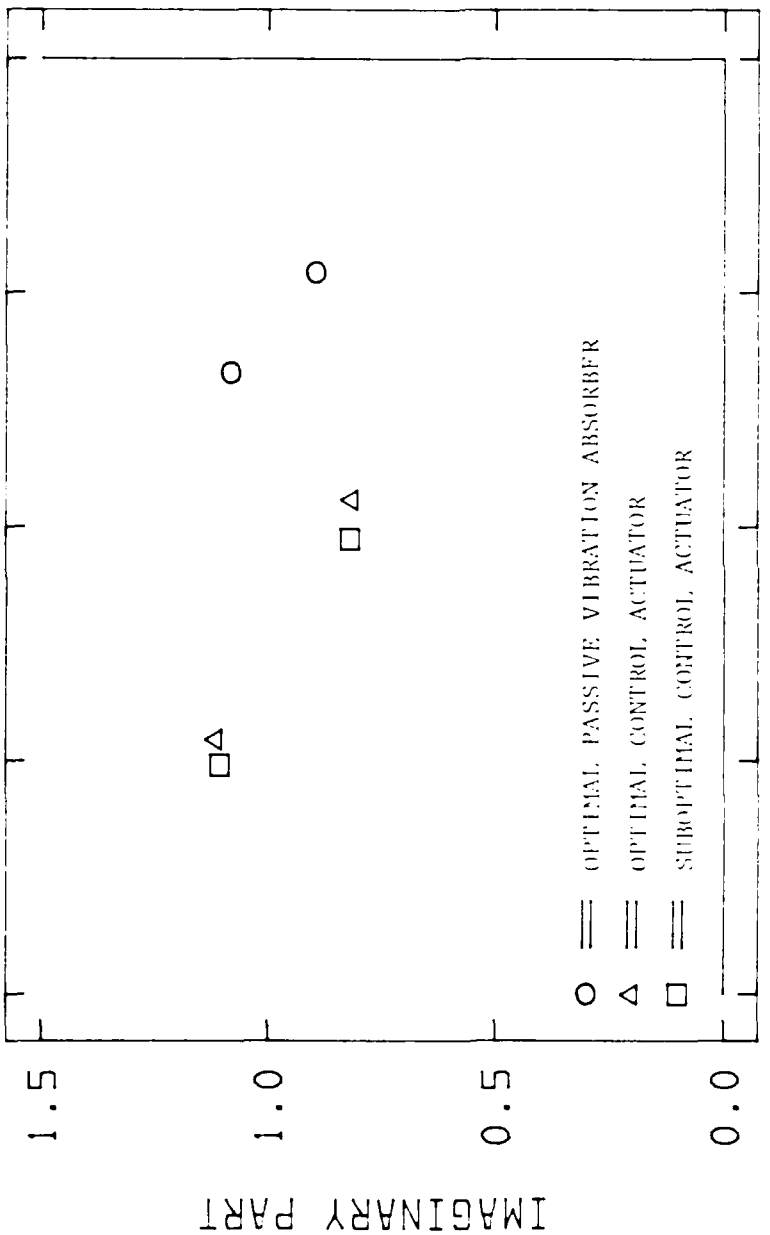

FIG. A.3: CLOSED-LOOP POLES OF SYSTEM 1 OPTIMIZED FOR $Z_0 = [0\ 1\ 0\ 0]^T$.

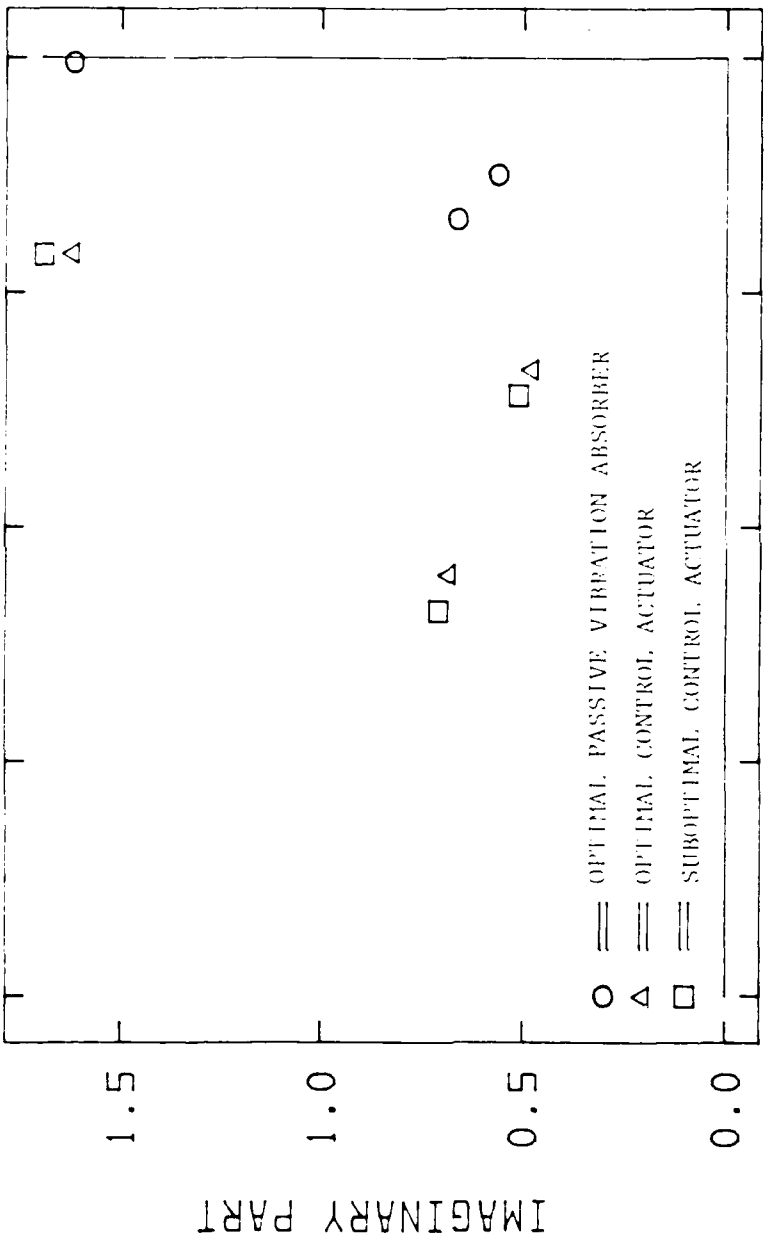

FIG. A.4: CLOSED-LOOP POLES OF SYSTEM 20 OPTIMIZED FOR $z_0 = [0\ 1\ 0\ 1.62\ 0\ 0]^T$.

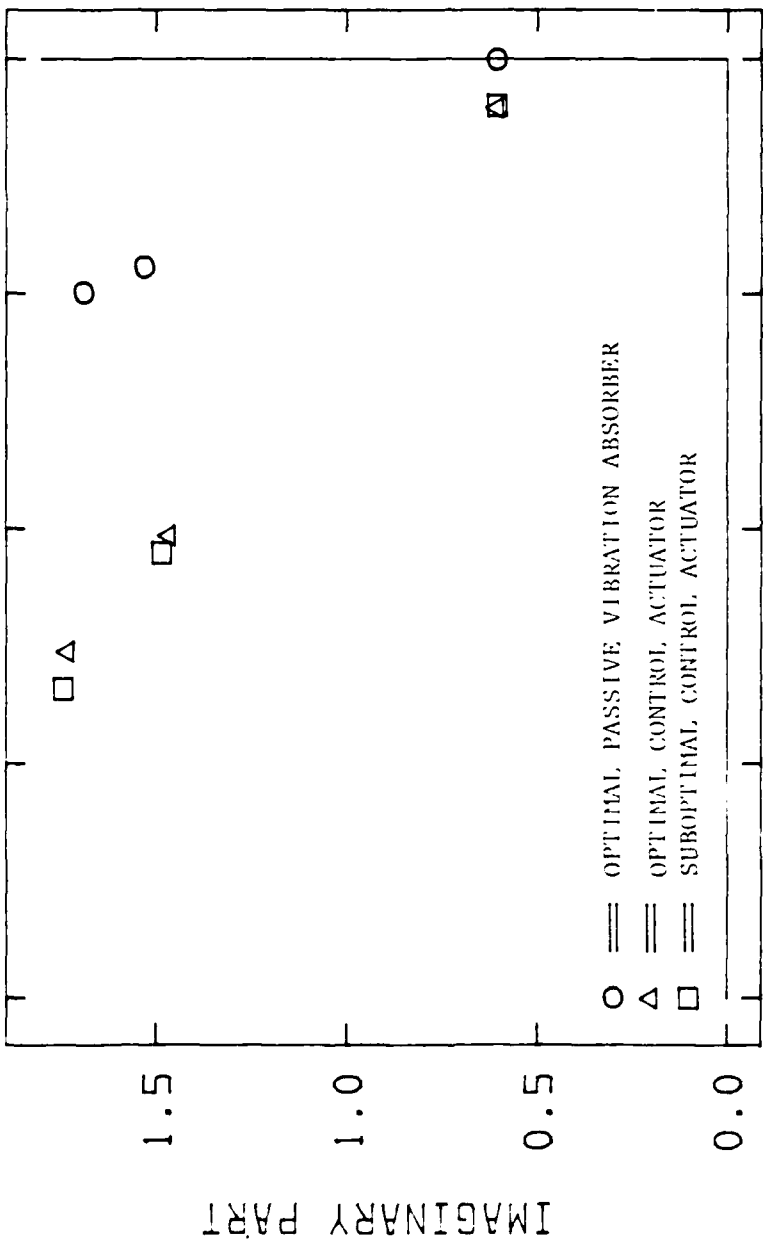

FIG. A.5: CLOSED-LOOP POLES FOR SYSTEM 20 OPTIMIZED FOR $Z_0 = [0\ -1.62\ 0\ 1\ 0\ 0]^T$.

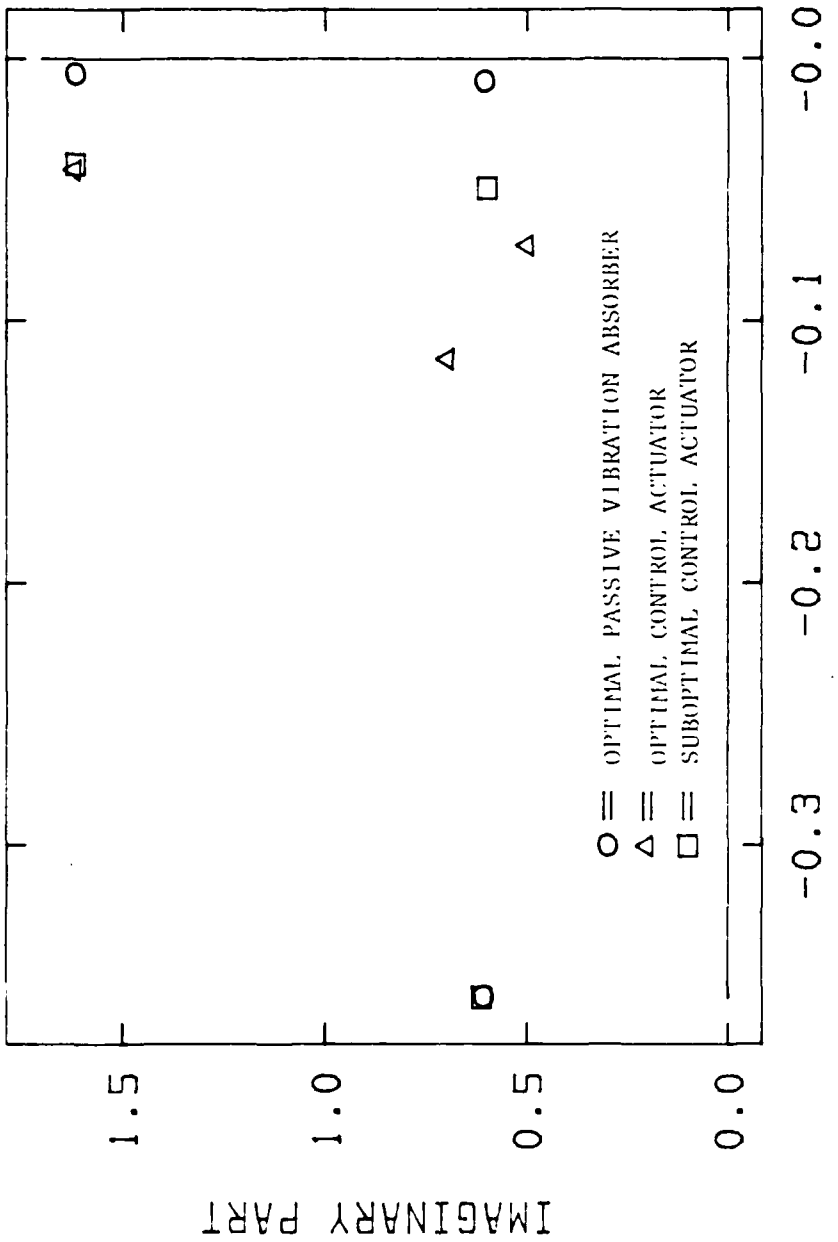

FIG. A.6: CLOSED-LOOP POLES FOR SYSTEM 20 OPTIMIZED FOR $Z_0 = [0\ -0.618\ 0\ 2.62\ 0\ 0]^T$.

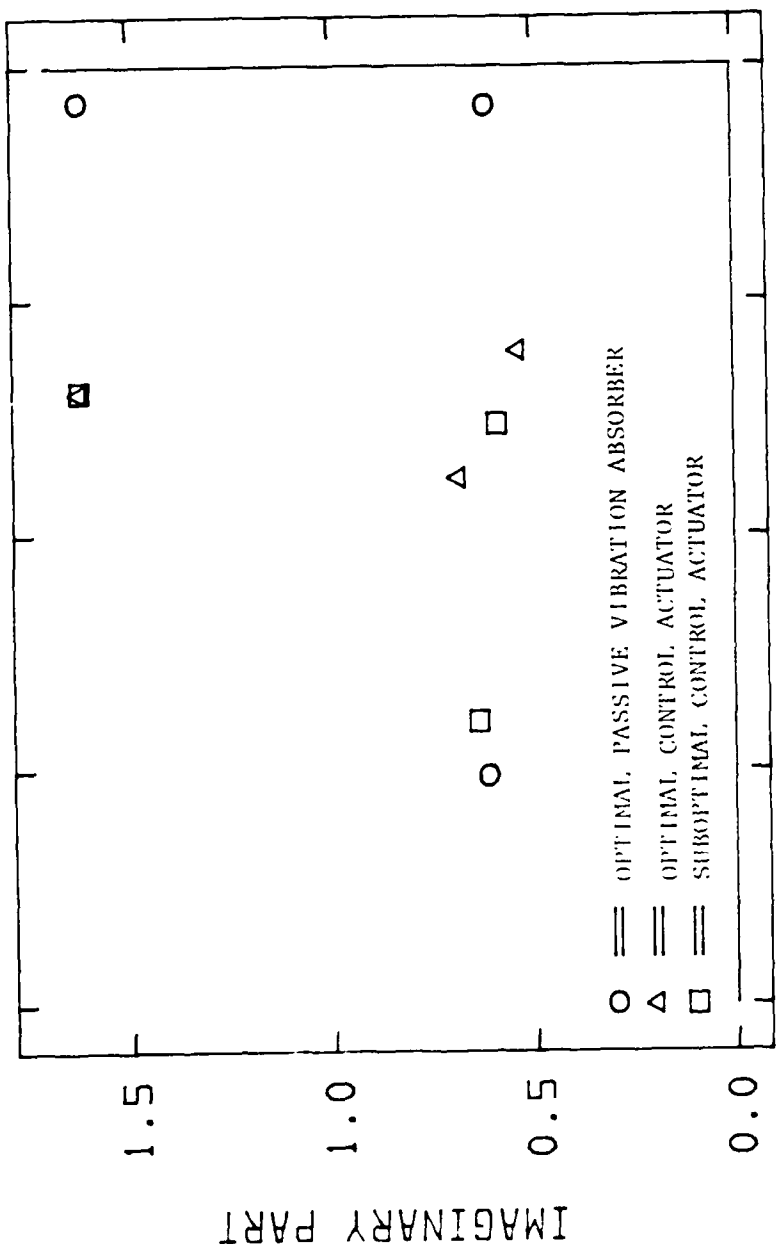

FIG. A.7: CLOSED-LOOP POLES FOR SYSTEM 21 OPTIMIZED FOR $Z_0 = [0\ -0.618\ 0\ 2.62\ 0\ 0]^T$.

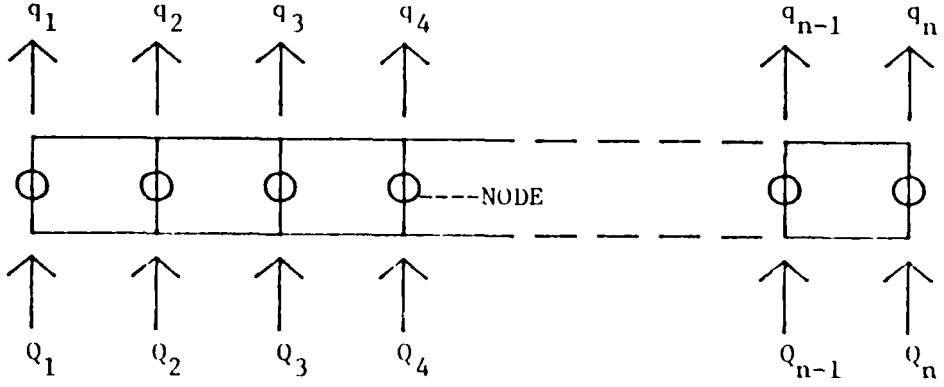

FIG. B.1: STRUCTURAL DISCRETIZATION.

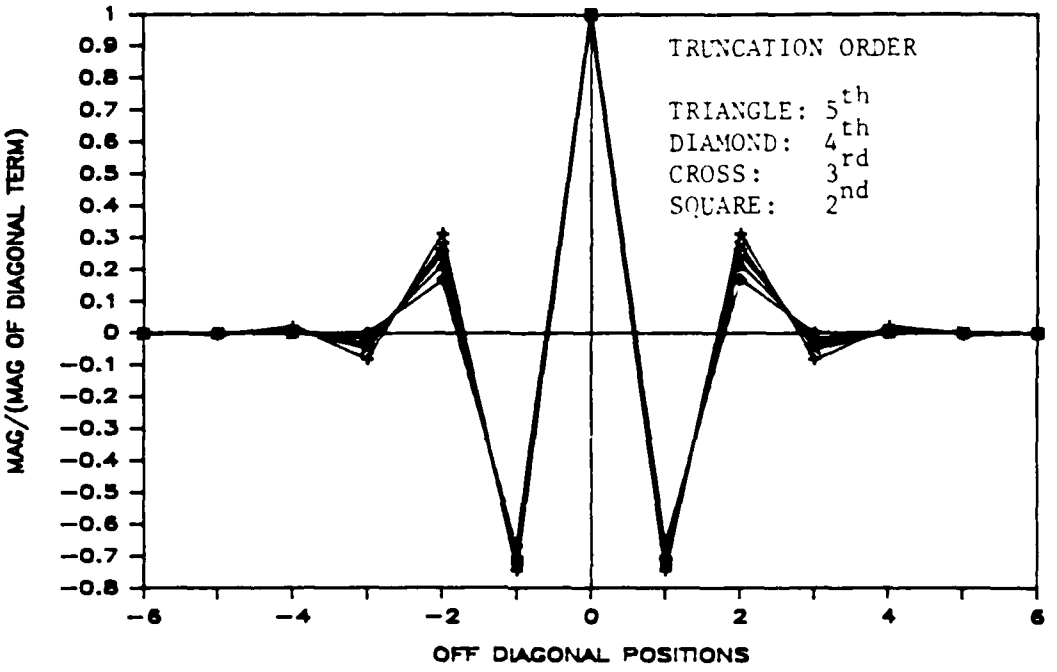

A: BANDEDNESS IN FOURTH DERIVATIVE, FINITE DIFFERENCE OPERATORS.

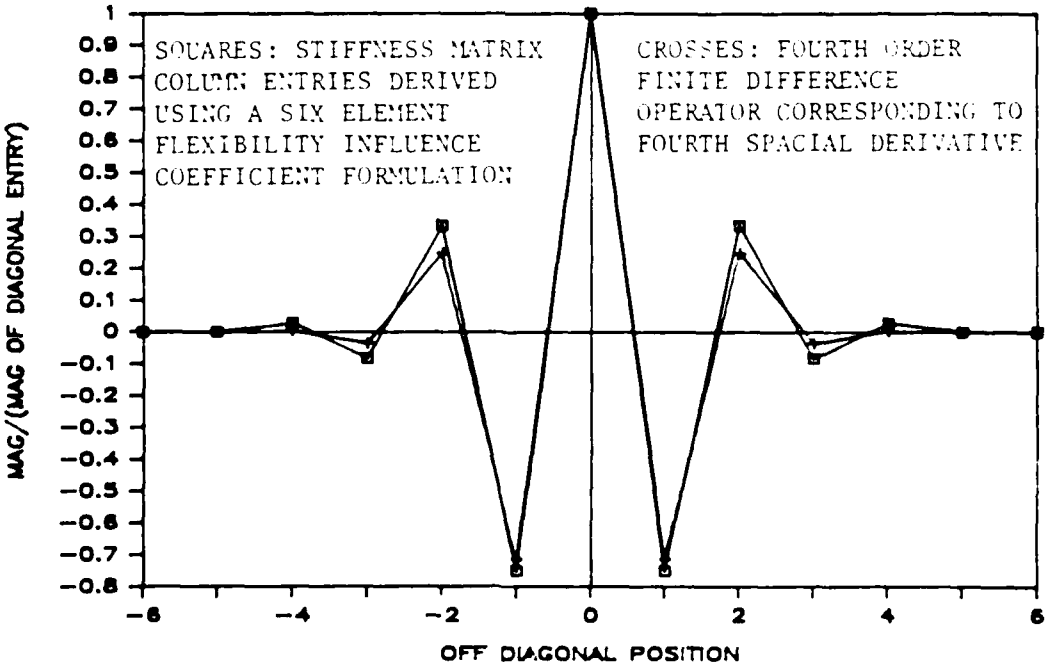

B: COMPARISON OF BANDEDNESS IN FINITE DIFFERENCE OPERATORS AND FLEXIBILITY INFLUENCE COEFFICIENTS.

FIG. B.2: BANDEDNESS IN DISCRETE REPRESENTATIONS OF ELASTIC STRUCTURES.

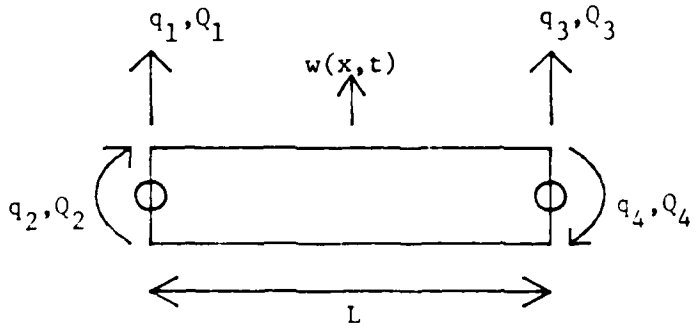

FIG. B.3: A FINITE BEAM ELEMENT.

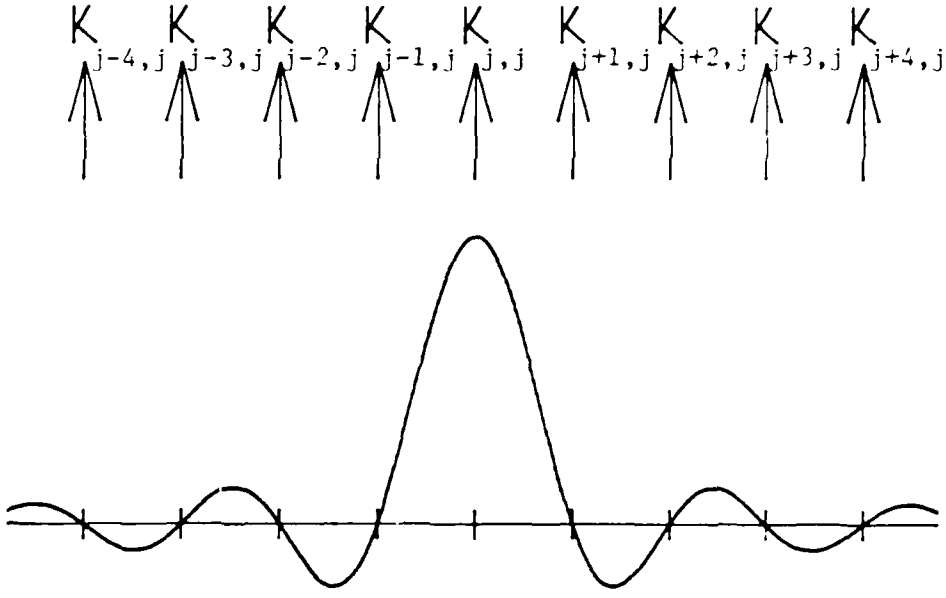

FIG. B.4: STIFFNESS TERMS DERIVED USING A FLEXIBILITY INFLUENCE COEFFICIENT FORMULATION.

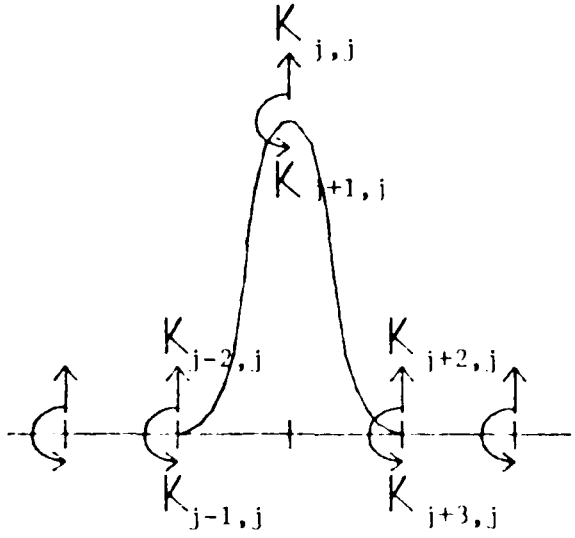

A: ADJACENT TERMS CORRESPONDING TO UNIT DISPLACEMENT.

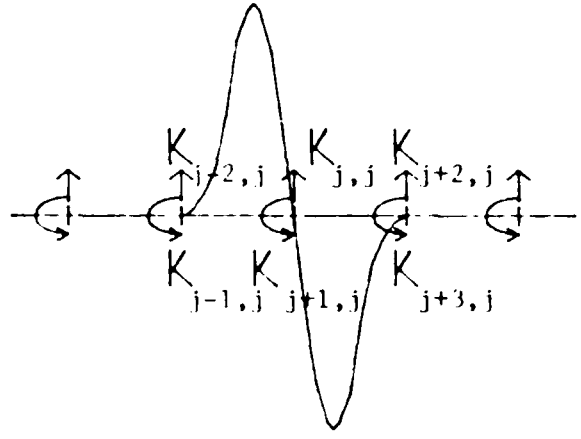

B: ADJACENT TERMS CORRESPONDING TO UNIT ROTATION.

FIG. B.5: BANDEDNESS IN FINITE ELEMENT REPRESENTATION OF STRUCTURAL STIFFNESS AS ILLUSTRATED BY (A) AND (B).

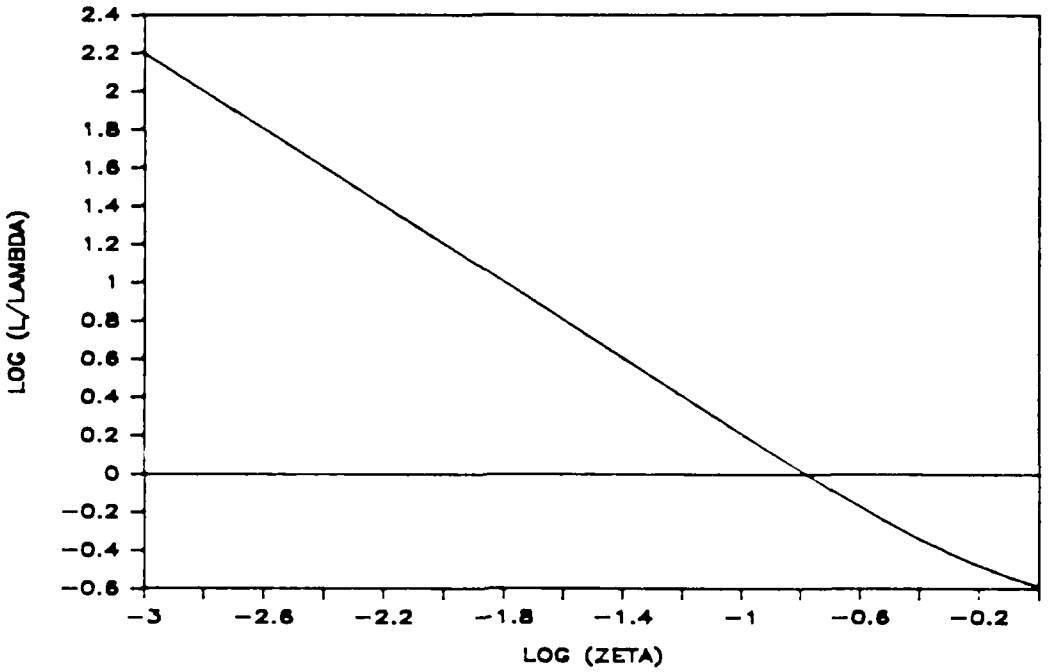

FIG. B.6: CHARACTERISTIC WAVE PROPAGATION LENGTH VERSUS DAMPING.

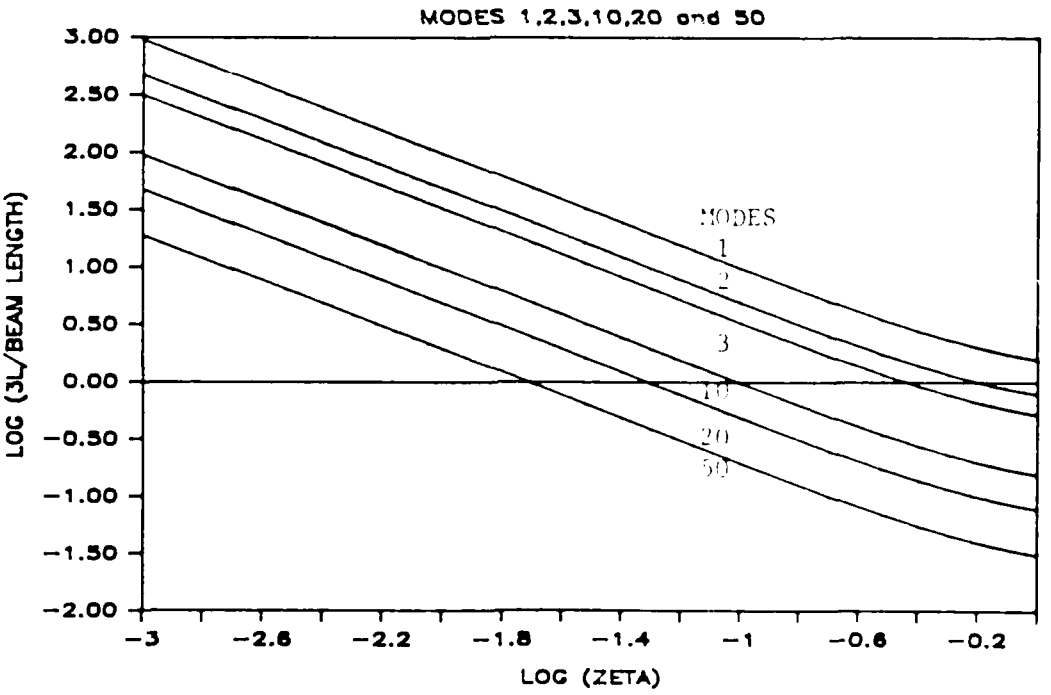

FIG. B.7: RATIO OF CHARACTERISTIC LENGTH OF PROPAGATION AND STRUCTURAL LENGTH VERSUS DAMPING IN STRUCTURAL MODES.

END

DTIC

8-86